Math-for-industry
Education & Research Hub

ISSN2188-1200

平成29年度 九州大学マス・フォア・インダストリ研究所共同利用研究集会(I)

# 結晶の界面、転位、構造の数理

編集：松谷茂樹・佐伯修・中川淳一・田上大助・上坂正晃
Pierluigi Cesana・濵田裕康

九州大学マス・フォア・インダストリ研究所

MI Lecture Note Vol.77 : Kyushu University

# 平成29年度　九州大学マス・フォア・インダストリ研究所
# 共同利用研究集会（I）
# 結晶の界面，転位，構造の数理

編集：松谷茂樹，佐伯修，中川淳一，田上大助，上坂正晃，Pierluigi Cesana，濵田裕康

About MI Lecture Note Series

The Math-for-Industry (MI) Lecture Note Series is the successor to the COE Lecture Notes, which were published for the 21st COE Program "Development of Dynamic Mathematics with High Functionality," sponsored by Japan's Ministry of Education, Culture, Sports, Science and Technology (MEXT) from 2003 to 2007. The MI Lecture Note Series has published the notes of lectures organized under the following two programs: "Training Program for Ph.D. and New Master's Degree in Mathematics as Required by Industry," adopted as a Support Program for Improving Graduate School Education by MEXT from 2007 to 2009; and "Education-and-Research Hub for Mathematics-for-Industry," adopted as a Global COE Program by MEXT from 2008 to 2012.

In accordance with the establishment of the Institute of Mathematics for Industry (IMI) in April 2011 and the authorization of IMI's Joint Research Center for Advanced and Fundamental Mathematics-for-Industry as a MEXT Joint Usage / Research Center in April 2013, hereafter the MI Lecture Notes Series will publish lecture notes and proceedings by worldwide researchers of MI to contribute to the development of MI.

October 2014
Yasuhide Fukumoto
Director
Institute of Mathematics for Industry

# はじめに

本研究集会はIMIの研究集会I「結晶の界面、転位、構造の数理」として2017年8月28日-30日に九州大学西新プラザにおいて催したものである．SGW2015，SGW2016にて新日鐵住金（株）から問題提起された，「結晶構造の秩序乱れの数学的表現」と「金属の結晶粒界エネルギーの異方性の数学的表現」を発展させることとし，2016年9月に実施した研究集会II「結晶のらせん転位の数理」を拡大し，発展させるものとして2016年末より計画され実施された．

結果的には，SGW2014 で取り上げられた「結晶グラフの階層性を利用した結合エネルギーの計算方法」や，本年のSGW2017に取り上げられた「結晶の構造変位後の観測データから変位前の状態を予測する解析方法」に関するものも課題として含めて，本研究集会のテーマとした．

同種の問題は，東京大学大学院数理科学研究科博士課程での社会数理実践研究においても学生が検討を行っており，それらとの交流も図るものとなった．

結晶は特殊ユークリッド変換群 SE(3)の離散部分群の作用で不変な集合として特徴づけられる．2016年9月の研究集会では，らせん転位をこの離散群による対称性の破れとして捉え，代数的な考察による離散幾何の表示とζ関数との関係や，Γ収束によるモデル化に関する話題にフォーカスして議論を行った．

他方，2016年のSGWでの話題である粒界の研究においても，境界条件の下でエネルギー最小を与える状態として，この SE(3)の離散群の，半群を含めた代数的な考察が求められている．特に，近年，界面の形状を直接，電子顕微鏡等で観察することが可能となってきており，離散的，代数的取り扱いとメゾスケールとの関係の解明が求められている．

これらの状況より，本研究集会では

１）結晶の界面に関わる数値解析，非線形時間発展方程式，整数論を援用した離散幾何学などの数学手法に関する知見の共有

２）代数的考察に基づく離散群による対称性の破れを伴う幾何構造の数学的記述に関する知見の共有

３）対称性の破れに対する特異的な摂動を考慮したΓ収束などによるエネルギー論的な数学モデルの構築

４）ナノとミクロの中間を橋渡しするマルチスケール的な数学モデルの構築

５）近年の計測技術の発展による実際の結晶構造に関する知見の共有

を目指し，様々な分野の専門家が集い，議論を行うこととなった．

このような多岐にわたる高度な数学モデルの議論は従来なされてこなかった．しかし，今後，実験技術の急速な発展と，産業界における要求仕様の高度化とにより，そうした数学モデルの必要性が増すものと予想される．我々は，本研究集会をそのモデルケースとして位置づけ，議論を行った．

講演内容の概略を述べると以下のようなものがなされた.

１．界面に関して，数値計算，非線形な時間発展方程式，整数論を援用した離散幾何学など，多岐に亘る視点からの講演があった.

２．Γ収束を利用した転位の解析においては，３つの講演があり，全く異なるアプローチによる様々な階層での解析が可能であることが明らかにされた.

３．幾何学，代数学からのアプローチに関しては，講演も多数あり，３次元空間内の新たな離散幾何や転位の表現，結晶の構造に関する解析が可能となることも示された.

４．数学者が生の実験データに触れることは通常ほとんどないため，実験データに関する講演も設け，現実とモデルとの相違が認識された.

このように本研究集会の趣旨に沿った講演がなされ，異なる分野の研究者同士で素朴な議論を行うことができた.

本研究集会では，１日目にウェルカム・パーティーとしてワン・コイン・パーティーを開催し，2 日目，3 日目には自由に各自の興味あるテーマを議論するためのディスカッション・タイムを設けた．ワン・コイン・パーティーでは一人当たり 500 円でビールなどを飲みながらの議論であったが，それぞれで，異なる分野の研究者がフランクかつ有意義に交流することができた．これにより，2 日目，3 日目のディスカッション・タイムを円滑に推進できた.

これらにより，各研究者の中で，それぞれの研究分野へのフィードバックがかかったものと確信する．今回のテーマではないが，実際，キンク現象に関しては，実験データを再現する新たな解析手法が提案でき，現在，論文化に向けた検討を行っている.

本研究集会の開催により，各分野の専門家が現状とその課題を提示し合い，議論することによって，これらの高度な数学モデルの構築の進展に寄与できたものと考えている.

組織委員：

| | |
|---|---|
| 松谷 茂樹 | 佐世保高専 |
| 佐伯 修 | 九州大学 IMI |
| 中川 淳一 | 新日鐵住金 |
| 田上 大助 | 九州大学 IMI |
| 上坂 正晃 | 北海道大学 |
| Pierluigi Cesana | 九州大学 IMI |
| 濵田 裕康 | 佐世保高専 |

2017 年 12 月

# IMI Workshop I:
# Mathematics in Interface, Dislocation and Structure of Crystals

at Nishijin Plaza, Kyushu University
(Aug 28–30, 2017)

## Program

Aug. 28

| | | |
|---|---|---|
| 13:00-13:05 | Opening | |
| 13:05-13:50 | Junichi Nakagawa (Nippon Steel & Sumitomo Metal Co.) | Algebraic analysis of orientation relationship created by phase transition in crystals |
| 14:10-14:55 | Tomohiro Takaki (Kyoto Inst. of Tech.) | Phase-field simulations of dendrite solidification and grain growth |
| 15:15-16:00 | Karel Svadlenka (Kyoto Univ.) | Numerical analysis of moving interfaces: the level-set and phase-field approaches |
| 16:00-16:30 | Group photo & Tea Time | |
| 16:30-17:15 | Philip Broadbridge (La Trobe Univ./IMI, Kyushu Univ.) | Exact solution of nonlinear boundary value problems for surface diffusion |
| 17:30-19:30 | One-coin party (1F)*) (Discussion, with two beer cans and snacks of one-coin = 500 yen/person) | |

Aug. 29

| | | |
|---|---|---|
| 9:45-10:30 | Kenji Higashida (Nat. Inst. of Tech., Sasebo College) | On observation of dislocations in crystals |
| 10:50-11:35 | Akihiro Nakatani (Osaka Univ.) / Xiao-Wen Lei (Fukui Univ.) | Analysis of stress field of kink boundary based on lattice defect theory |
| 11:55-12:40 | Kazutoshi Inoue (AIMR, Tohoku Univ.) | Structure of tilt grain boundaries from mathematical perspective |
| 12:40-14:10 | Lunch | |
| 14:10-14:40 | FMSP Mathematical Research on Real World Problems, Group G, The University of Tokyo<br>Hokuto Konno (The Univ. of Tokyo), Tsukasa Ishibashi (The Univ. of Tokyo), Sho Ejiri (The Univ. of Tokyo), Junichi Nakagawa (Nippon Steel & Sumitomo Metal Co.), Yasuhiro Wakabayashi (The Univ. of Tokyo) | Lattice defects from monodromy |
| 15:00-15:45 | Shizuo Kaji (Yamaguchi Univ.) | Geometry of closed kinematic chain |
| 15:45-16:10 | Tea Time | |
| 16:10-17:30 | Discussion slot | |
| 18:20-21:00 | Banquet 5,000yen *) | Souen**) |

*) Please let the organizers know if you would like to attend the one-coin party and/or the banquet but have not registered.

**) https://gurunavi.com/en/f429500/rst/

Aug. 30

| | | |
|---|---|---|
| 9:45-10:30 | Patrick van Meurs (Kanazawa Univ) | Discrete-to-continuum limits of moving straight edge dislocations in 2D |
| 10:50-11:35 | Masaaki Uesaka (Hokkaido Univ.) | Anti-plane deformation model of screw dislocation and its related variational problem |
| 11:55-12:40 | Pierluigi Cesana （IMI, Kyushu Univ） | Variational models of lattice defects |
| 12:40-14:10 | Lunch | |
| 14:10-14:30 | Junichi Nakagawa | Sequence representation of graph structure of crystal (Growth) |
| | (Nippon Steel & Sumitomo Metal Co.) | |
| 14:30-14:50 | Tea Time | |
| 14:50-16:55 | Discussion slot | |
| 16:55-17:00 | Closing | |

**On discussion slots:**

**Purpose of discussion slots:** Crucial problems in industry, basically, cannot be solved in the framework of a single mathematical field or a single field in science. They are related to a variety of mathematical fields and wider scientific knowledge. As mentioned above, this conference is arranged so that experts in various fields gather together and discuss problems related to crystals whose origin is in industry. Its prototype is in the style of mathematical studies in industry.

It is expected that participants discuss mathematical problems with those from various fields. It is also expected that the discussions stimulate their own works and generate a new intermediate field of study.

Consequently, there is no rule for discussing problems. Every one will be able to participate in any group to discuss problems with her/his own interest. The one-coin party is also set for similar discussions accompanied with some drinks and snacks.

**Utilities:** We have three rooms including the main room for the discussions. In each room, there are a projector and a white board. You can also use the lobby.

**Report:** There is no duty to report the results of the discussions: however, if you think that your discussions should be shared with others, then we can arrange such occasions in the discussion slots.

Furthermore, we will need to report the discussion slots in the proceedings of this conference later. Therefore, the organizers would appreciate it if you could record briefly the contents of the discussions made during the discussion slots. Thank you.

KYUSHU UNIVERSITY

Institute of Mathematics for Industry
Kyushu University

IMI Joint Research Project in 2017 Workshop (I)

# Mathematics in Interface, Dislocation and Structure of Crystals

**Date :** August 28(Mon) -30(Wed), 2017

**Venue :** Nishijin Plaza, Kyushu University

2-16-23 Nishijin, Sawara-ku, Fukuoka-shi, Fukuoka, JAPAN
http://nishijinplaza.kyushu-u.ac.jp/english/


KYUSHU UNIVERSITY
NISHIJIN PLAZA

**Speakers :** Philip Broadbridge (La Trobe Univ. / IMI, Kyushu Univ.)
Pierluigi Cesana (IMI, Kyushu Univ.)
Kenji Higashida (Nat. Inst. of Tech., Sasebo College)
Kazutoshi Inoue (AIMR, Tohoku Univ.)
Shizuo Kaji (Yamaguchi Univ.)
Xiao-Wen Lei (Fukui Univ.)
Junichi Nakagawa (Nippon Steel & Sumitomo Metal Co.)
Akihiro Nakatani (Osaka Univ.)
Karel Svadlenka (Kyoto Univ.)
Tomohiro Takaki (Kyoto Inst. of Tech.)
Masaaki Uesaka (Hokkaido Univ.)
Patrick van Meurs (Kanazawa Univ.)

■URL ▶ http://www.imi.kyushu-u.ac.jp/eng/events/view/1269

**Organizers :** Pierluigi Cesana (IMI, Kyushu Univ.)
Hiroyasu Hamada (Nat. Inst. of Tech., Sasebo College)
Shigeki Matsutani (Nat. Inst. of Tech., Sasebo College)
Junichi Nakagawa (Nippon Steel & Sumitomo Metal Co.)
Osamu Saeki (IMI, Kyushu Univ.)
Daisuke Tagami (IMI, Kyushu Univ.)
Masaaki Uesaka (Hokkaido Univ.)

■Contact : Institute of Mathematics for Industry, Kyushu University
TEL:+81-(0)92-802-4402 E-mail: kyodo_riyou@imi.kyushu-u.ac.jp

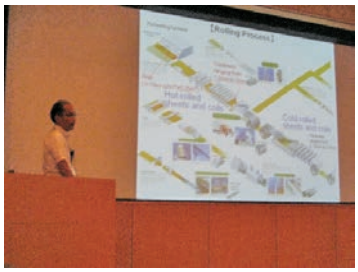
[Rolling Process]

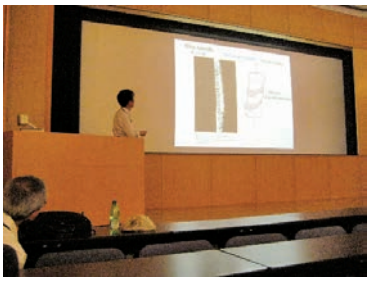


COMMON KEYWORDS
• REPRESENTATION BY GRAPH OF LOCAL
• MONODROMY ON GRAPH
• ENERGY EQUILIBRIUM
• CONFIGURATION SPACE
(REAL ALGEBRAIC GEOMETRY)

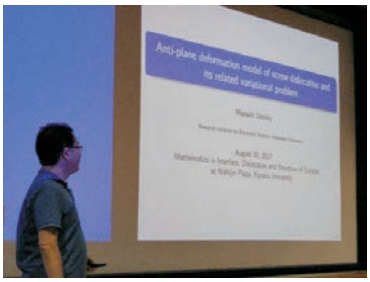
Anti-plane deformation model of screw dislocation and its related variational problem

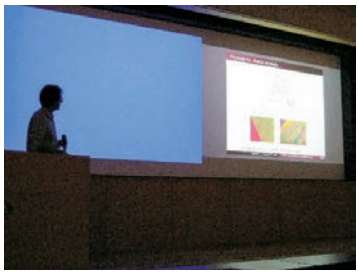


Gaussian Representation of
Graph Structure of Crystal (Growth)















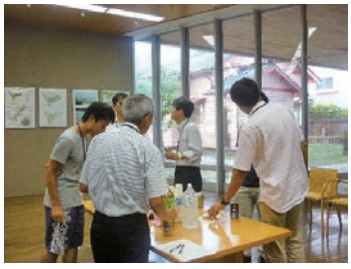




**Contents**

# Algebraic analysis of orientation relationship created by phase transition in crystals

**Junichi Nakagawa**
Nippon Steel & Sumitomo Metal Co.

Polycrystalline materials such as iron acquire their properties from various thermo-mechanical treatments. In many cases, the low temperature behaviors of these materials are sought from high temperature processes, such as re-heating, rolling and cooling, that are followed by phase transitions. The microstructure of polycrystalline materials at low temperatures is an important parameter, and it is greatly involved in plastic deformation. Therefore, the improvement of products designed for a given application requires the formation of an adapted low temperature microstructure, obtained from the high temperature state, which can also be characterized by its microstructure. A grain (for example $\beta$), which is defined by a set of crystals with the same orientation, is transformed into many grains of the same phase (for example $\alpha$) with an orientation relationship. We refer to them as daughter crystals. These daughter crystals ($\alpha$), which have an orientation relationship with the parent crystal ($\beta$), are called variants, and they are algebraically identified with left co-sets. C. Cayron [1] who is a physicist in crystallography dealt with variants using algebraic analysis and proposed a method for reconstructing parent crystals from the observed daughter crystals. Our intention is to redefine the way of describing the method using mathematics and obtain a comprehensible representation mathematically in order to understand Cayron's way of thinking.

## References

[1] C. Cayron, Acta Cryst. A62 (2006) 21-40

Mathematics in Interface, Dislocation and Structure of Crystals

# Algebraic Analysis of Orientation Relationship Created by Phase Transition in Crystals

2017.8.28-8.30
Institute of Mathematics for Industry
Kyusyu University

Nippon Steel & Sumitomo Metal Corporation
Advanced Technology Research Laboratories
Mathematical Science & Technical Research Lab.

**Junichi Nakagawa**



新日鐵住金 NIPPON STEEL & SUMITOMO METAL

## What's Crystal

A crystal is a solid material whose constituents, such as atoms, molecules are arranged in a highly ordered microscopic structure, i.e. semi-product of translation and rotation symmetry, forming a crystal lattice that extends in all directions.

$$\Gamma \cong T \rtimes K$$

In addition, macroscopic single crystals are usually identifiable by their geometrical shape, consisting of faces with specific, characteristic orientations.

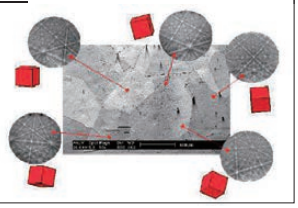



## The 7 Lattice System and The 14 Bravais Lattice

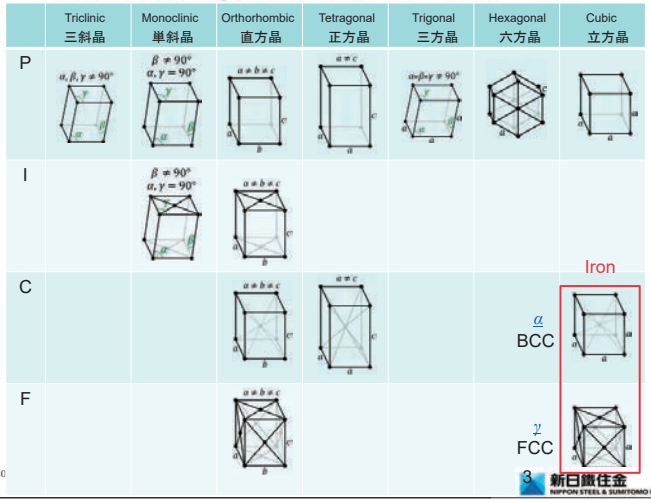




3 新日鐵住金 NIPPON STEEL & SUMITOMO METAL

## Symmetry of Iron Crystal

$$O(3,\mathrm{Z})=\left\{\begin{array}{l} e,a_1,a_1^2,a_1^3,a_2,a_2^2,a_2^3,a_3,a_3^2,a_3^3, \\ d_1,d_1^2,d_2,d_2^2,d_3,d_3^2,d_4,d_4^2, \\ u_1,u_2,u_3,u_4,u_5,u_6, \\ r,ra_1,ra_1^2,ra_1^3,ra_2,ra_2^2,ra_2^3,ra_3,ra_3^2,ra_3^2, \\ rd_1,rd_1^2,rd_2,rd_2^2,rd_3,rd_3^2,rd_4,rd_4^2, \\ ru_1,ru_2,ru_3,ru_4,ru_5,ru_6 \end{array}\right\}$$

$e$: identity matrix $r$: reflection matrix

$a_1^4=e,\ a_2^4=e,\ a_3^4=e,$ 90° rotation matrix <100>

$d_1^3=e,\ d_2^3=e,\ d_3^3=e,\ d_4^3=e,$ 120° rotation <111>

$u_1^2=e,\ u_2^2=e,\ u_3^2=e,\ u_4^2=e,\ u_5^2=e,\ u_6^2=e$ 180° rotation <110>



4 新日鐵住金 NIPPON STEEL & SUMITOMO METAL

## Measurement of Crystal Orientation

### EBSD（Electron Back Scattered Diffraction Pattern）

As these electrons leave the sample, they may exit at the Bragg condition related to the spacing of the periodic atomic lattice planes of the crystalline structure and diffract.

Escaping electrons may exit near to the Bragg angle and diffract to form Kikuchi bands. If the system geometry is well described, it is possible to relate the bands present in the diffraction pattern to the underlying crystal orientation of the material within the electron interaction volume.

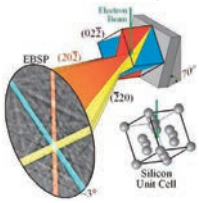


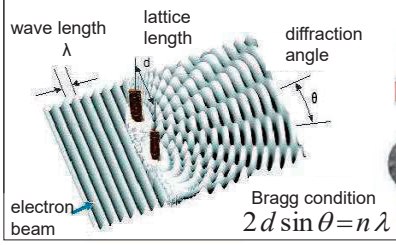


Bragg condition

$$2d\sin\theta=n\lambda$$

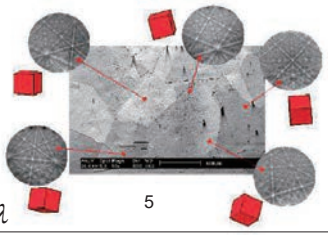

5

## Measurement Data regarding Crystal Orientation

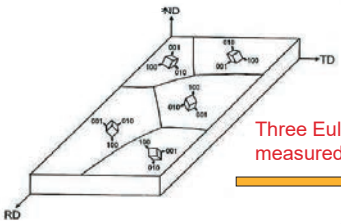


Three Euler angles are measured using EBSD.

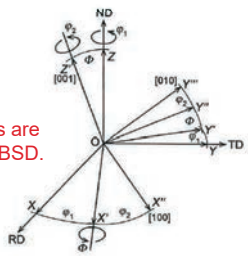


$$R_{\psi_2},\ R_\phi,\ R_{\psi_1}\in SO(3,\mathrm{R})$$

unit vector of crystal coordinate

$$c=R_{\psi_2}\ R_\phi\ R_{\psi_1}\ s$$

unit vector of sample coordinate

$$R_{\psi_1}=\begin{pmatrix}\cos\psi_1 & -\sin\psi_1 & 0\\ \sin\psi_1 & \cos\psi_1 & 0\\ 0 & 0 & 1\end{pmatrix}\quad R_\phi=\begin{pmatrix}1 & 0 & 0\\ 0 & \cos\phi & -\sin\phi\\ 0 & \sin\phi & \cos\phi\end{pmatrix}\quad R_{\psi_2}=\begin{pmatrix}\cos\psi_2 & -\sin\psi_2 & 0\\ \sin\psi_2 & \cos\psi_2 & 0\\ 0 & 0 & 1\end{pmatrix}$$



新日鐵住金 NIPPON STEEL & SUMITOMO METAL

## Objective: Parent Grain Reconstruction for Martensitic Steel

C. Cayron, B. Artaud, L. Briottet,
Reconstruction of parent grains from EBSD data,
Mater. Charact 57 (2006) 386-401.

Observed daughter grains
( $\alpha$: martensitic grains)

BCC

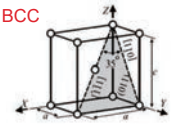

Lattice correspondence
$(x, y, z)_\gamma \rightarrow (X, Y, Z)\alpha$

Reconstructed parent grains
( $\gamma$: austenitic grains)

FCC

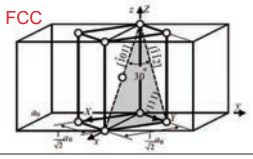

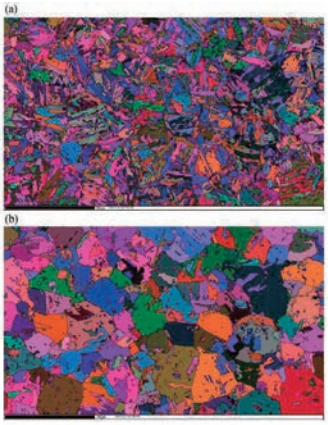


Stable in
Low temperature

$\alpha$

Phase transition with water cooling

$\gamma$

Stable in
high temperature



## Determination of Prior Austenitic Grains Orientation from Martensitic Grains

$g_i, g_j \in O(3,\mathrm{Z})$ — an element of group for cubic lattices, BCC and FCC

$R^\alpha \in SO(3,\mathrm{R})$ — a martensitic grains orientation

$R^\gamma \in SO(3,\mathrm{R})$ — an austenitic grains orientation

$\alpha_k \in V^\gamma$ — an element of variant between austenitic grain (FCC) and martensitic grains (BCC)

$$g_j R^\alpha = \alpha_k g_i R^\gamma$$

$$i, j = 1, \cdots, 48$$

$$\begin{cases} k = 1, \cdots, 12 & \text{NW (Nishiyama-Wasserman) relationship} \\ k = 1, \cdots, 24 & \text{KS (Kurdjumov-Sachs) relationship} \end{cases}$$

$$R^\gamma = (\alpha_k g_i)^{-1} g_j R^\alpha$$

reconstructed orientation

measured data





Y.Gao,, Y. Wang, et al., Group theory description of transformation pathway degeneracy in structual phase transformations, Acta Materialia 109 (2016) 353-363

## Simple Example for Understanding Variants

$$G_\alpha^\alpha = \left\{ \begin{bmatrix} 1 & 0 \\ 0 & 1 \end{bmatrix}, \begin{bmatrix} -1 & 0 \\ 0 & -1 \end{bmatrix}, \begin{bmatrix} 1 & 0 \\ 0 & -1 \end{bmatrix}, \begin{bmatrix} -1 & 0 \\ 0 & 1 \end{bmatrix} \right\} \in O(2,\mathrm{Z})$$

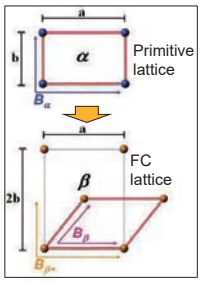


Lattice correspondence $[10]_\alpha \rightarrow [10]_\beta$, $[01]_\alpha \rightarrow 1/2[11]_\beta$

$$G_\alpha^\beta = \begin{bmatrix} 1 & 0.5 \\ 0 & 1 \end{bmatrix}^{-1} G_\alpha^\alpha \begin{bmatrix} 1 & 0.5 \\ 0 & 1 \end{bmatrix}$$

$$= \left\{ \begin{bmatrix} 1 & 0 \\ 0 & 1 \end{bmatrix}, \begin{bmatrix} -1 & 0 \\ 0 & -1 \end{bmatrix}, \begin{bmatrix} 1 & 1 \\ 0 & -1 \end{bmatrix}, \begin{bmatrix} -1 & -1 \\ 0 & 1 \end{bmatrix} \right\} \in GL(2,\mathrm{Z})$$

$$H^{\alpha/\beta} = G_\alpha^\alpha \cap G_\alpha^\beta = \left\{ \begin{bmatrix} 1 & 0 \\ 0 & 1 \end{bmatrix}, \begin{bmatrix} -1 & 0 \\ 0 & -1 \end{bmatrix} \right\}$$

Variants

$$G_\alpha^\beta / H^{\alpha/\beta} = \left\{ \underbrace{\left\{ \begin{bmatrix} 1 & 0 \\ 0 & 1 \end{bmatrix}, \begin{bmatrix} -1 & 0 \\ 0 & -1 \end{bmatrix} \right\}}_{①\ ③}, \underbrace{\left\{ \begin{bmatrix} 1 & 1 \\ 0 & -1 \end{bmatrix}, \begin{bmatrix} -1 & -1 \\ 0 & 1 \end{bmatrix} \right\}}_{④\ ②} \right\}$$

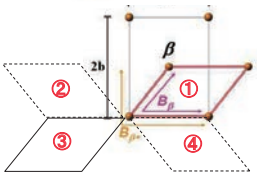

Y.Gao,, Y. Wang, et al., Group theory description of transformation pathway degeneracy in structual phase transformations, Acta Materialia 109 (2016) 353-363

$$G_\alpha^\beta = \left\{ \begin{bmatrix} 1 & 0 \\ 0 & 1 \end{bmatrix}, \begin{bmatrix} -1 & 0 \\ 0 & -1 \end{bmatrix}, \begin{bmatrix} 1 & 1 \\ 0 & -1 \end{bmatrix}, \begin{bmatrix} -1 & -1 \\ 0 & 1 \end{bmatrix} \right\}$$

$$H^{\alpha/\beta} = G_\alpha^\alpha \cap G_\alpha^\beta = \left\{ \begin{bmatrix} 1 & 0 \\ 0 & 1 \end{bmatrix}, \begin{bmatrix} -1 & 0 \\ 0 & -1 \end{bmatrix} \right\}$$

Calculation of left coset

$$\begin{bmatrix} 1 & 0 \\ 0 & 1 \end{bmatrix} H^{\alpha/\beta} = \left\{ \begin{bmatrix} 1 & 0 \\ 0 & 1 \end{bmatrix}\begin{bmatrix} 1 & 0 \\ 0 & 1 \end{bmatrix}, \begin{bmatrix} 1 & 0 \\ 0 & 1 \end{bmatrix}\begin{bmatrix} -1 & 0 \\ 0 & -1 \end{bmatrix} \right\} = \boxed{\left\{ \begin{bmatrix} 1 & 0 \\ 0 & 1 \end{bmatrix}, \begin{bmatrix} -1 & 0 \\ 0 & -1 \end{bmatrix} \right\}}$$

$$\begin{bmatrix} -1 & 0 \\ 0 & -1 \end{bmatrix} H^{\alpha/\beta} = \left\{ \begin{bmatrix} -1 & 0 \\ 0 & -1 \end{bmatrix}\begin{bmatrix} 1 & 0 \\ 0 & 1 \end{bmatrix}, \begin{bmatrix} -1 & 0 \\ 0 & -1 \end{bmatrix}\begin{bmatrix} -1 & 0 \\ 0 & -1 \end{bmatrix} \right\} = \boxed{\left\{ \begin{bmatrix} 1 & 0 \\ 0 & 1 \end{bmatrix}, \begin{bmatrix} -1 & 0 \\ 0 & -1 \end{bmatrix} \right\}}$$

$$\begin{bmatrix} 1 & 1 \\ 0 & -1 \end{bmatrix} H^{\alpha/\beta} = \left\{ \begin{bmatrix} 1 & 1 \\ 0 & -1 \end{bmatrix}\begin{bmatrix} 1 & 0 \\ 0 & 1 \end{bmatrix}, \begin{bmatrix} 1 & 1 \\ 0 & -1 \end{bmatrix}\begin{bmatrix} -1 & 0 \\ 0 & -1 \end{bmatrix} \right\} = \boxed{\left\{ \begin{bmatrix} 1 & 1 \\ 0 & -1 \end{bmatrix}, \begin{bmatrix} -1 & -1 \\ 0 & 1 \end{bmatrix} \right\}}$$

$$\begin{bmatrix} -1 & -1 \\ 0 & 1 \end{bmatrix} H^{\alpha/\beta} = \left\{ \begin{bmatrix} -1 & -1 \\ 0 & 1 \end{bmatrix}\begin{bmatrix} 1 & 0 \\ 0 & 1 \end{bmatrix}, \begin{bmatrix} -1 & -1 \\ 0 & 1 \end{bmatrix}\begin{bmatrix} -1 & 0 \\ 0 & -1 \end{bmatrix} \right\} = \boxed{\left\{ \begin{bmatrix} 1 & 1 \\ 0 & -1 \end{bmatrix}, \begin{bmatrix} -1 & -1 \\ 0 & 1 \end{bmatrix} \right\}}$$

Variants

$$G_\alpha^\beta / H^{\alpha/\beta} = \left\{ \boxed{\left\{ \begin{bmatrix} 1 & 0 \\ 0 & 1 \end{bmatrix}, \begin{bmatrix} -1 & 0 \\ 0 & -1 \end{bmatrix} \right\}}, \boxed{\left\{ \begin{bmatrix} 1 & 1 \\ 0 & -1 \end{bmatrix}, \begin{bmatrix} -1 & -1 \\ 0 & 1 \end{bmatrix} \right\}} \right\}$$





## Study Group Workshop 2017

## Algebraic Analysis of Orientation Relationship Created by Phase Transition in Crystals

九州大学 KYUSHU UNIVERSITY

2017.07.26-07.28

東京大学 THE UNIVERSITY OF TOKYO

2017.07.31-08.01

Junichi Nakagawa* (*Industrial delegate*) Hiroyuki Ochiai** Pierluigi Cesana**
Dimetre Triadis** ∘Ye Yuan** Li Dan† Tokinaga Namba‡ (*Moderator*)
∘ Tatsu-Hiko Miura‡ (*Student moderator*) Lin Dexie‡ Shizuo Kaji⋈

* *Nippon Steel & Sumitomo Metal Corporation* ** *Kyushu University* † *Pusan National University*
‡ *The University of Tokyo* ⋈ *Yamaguchi University*





## Background & Problem

- In crystallography, phase transition of crystals occurs:

| parent crystal | | daughter crystal |
|---|---|---|
| $\gamma$ | $\longrightarrow$ | $\alpha$ |
| (high temperature) | | (low temperature) |

- The orientation of $\gamma$ cannot be measured, so we would like to estimate it from the orientation of $\alpha$ which can be measured.
- Cayron proposes a method to estimate the orientation of the parent crystal based on the group theory:
  - C. Cayron, Acta Cryst. A62 (2006) 21-40.
  - C. Cayron, B. Artaud, L. Briottet, Mater. Charact. 57 (2006) 386-401.
- We are interested in his method since it is related to a kind of inverse problem.
- Our problem in this study group is:
  - To understand mathematically Cayron's way of thinking.
  - To describe his method in mathematically more understandable manner.

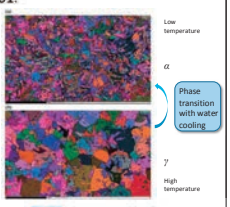

## Notations in Cayron's paper

- Transform matrix from a basis $B_1 \in GL(3,\mathbb{R})$ to $B_2 \in GL(3,\mathbb{R})$: $B_2(B_1)^{-1}$
- A crystal is $\beta := \{a_1 e_1^\beta + a_2 e_2^\beta + a_3 e_3^\beta \mid a_1, a_2, a_3 \in \mathbb{Z}\}$, where
  - $\{e_1^\beta, e_2^\beta, e_3^\beta\}$: (not necessarily orthogonal) basis of $\mathbb{R}^3$,
  - $B_1^\beta := \left\langle e_1^\beta, e_2^\beta, e_3^\beta \right\rangle \in GL(3,\mathbb{R})$, $\mathbf{G}^\beta := \left\{g_i^\beta \in O(3,\mathbb{Z}) \mid g_i^\beta \beta = \beta\right\}$,
  - $\mathbf{B}^\beta := \left\{B_i^\beta := g_i^\beta B_1^\beta \mid g_i^\beta \in \mathbf{G}^\beta\right\}$, $g_{ik}^\beta := g_k^\beta (g_i^\beta)^{-1} = B_k^\beta (B_i^\beta)^{-1} \in \mathbf{G}^\beta$.
- Orientation relationships (OR):
  - For the parent crystal $\beta$ and the daughter crystals $\alpha_i$,
    1. fix a basis $B_1^{\alpha_1} \in GL(3,\mathbb{R})$ of $\alpha_1$ and the set $T_> := B_1^{\alpha_1}$.
    2. for each $i \in \{1, \ldots, |\mathbf{G}^\beta|\}$, define a basis $B_1^{\alpha_i} \in GL(3,\mathbb{R})$ of the crystal $\alpha_i$ by $B_1^{\alpha_i} := T_> g_i^\beta$.





## Variants (Cayron's notation)

- Let $\beta$ and $\alpha_i$ be the parent and daughter crystals.
  - Set $T^{\beta\to\alpha_i} := B_1^{\alpha_i}(B_1^\beta)^{-1}$ (transformation matrix from $B_1^\beta$ to $B_1^{\alpha_i}$).
  - Define an equivalent relationship for $\alpha_i$ by

$$T^{\beta\to\alpha_i} \equiv_I T^{\beta\to\alpha_j} \overset{\text{def}}{\Leftrightarrow} T^{\beta-\alpha_j}(T^{\beta-\alpha_i})^{-1} \in \mathbf{G}^\alpha,$$

    which is equivalent to

$$T^{\beta\to\alpha_i} \equiv_I T^{\beta\to\alpha_j} \overset{\text{def}}{\Leftrightarrow} g_{ij}^\beta \in \mathbf{G}^\beta \cap T_> \mathbf{G}^\alpha T_>^{-1} =: \mathbf{H}^\beta.$$

  - Then we call each equivalence class of $\alpha_i$ an orientation variant.
  - We can identify the variants with elements of $\mathbf{G}^\beta/\mathbf{H}^\beta$ and write

$$\alpha_i = g_i^\beta \mathbf{H}^\beta \ (g_i^\beta \in \mathbf{G}^\beta).$$





## Example: two-dimensional case (1)

[2]

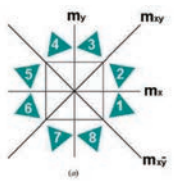


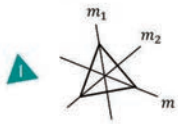


$\mathbf{G}^\beta = \{E, I, m_x^\beta, m_y^\beta, m_{xy}^\beta, m_{x\bar{y}}^\beta, r_{+\pi/2}^\beta, r_{-\pi/2}^\beta\}$

$\mathbf{G}^\alpha = \{E, m_1^\alpha, m_2^\alpha, m_3^\alpha, r_{+\pi/3}^\alpha, r_{-\pi/3}^\alpha\}$

$I = m_x^\beta m_y^\beta = m_y^\beta m_x^\beta$

$r_{+\theta}$: rotation in counter clockwise

$r_{-\theta}$: rotation in clockwise

Since $m_i^\alpha \neq m_x^\beta, m_y^\beta, m_{xy}^\beta, m_{x\bar{y}}^\beta$ for $i = 1,2,3$, we have $\mathbf{H}^\beta = \{E\}$.

$\alpha_1 = \{E\}, \alpha_2 = \left\{m_x^\beta\right\}, \alpha_3 = \left\{r_{+\pi/2}^\beta\right\}, \alpha_4 = \{m_{xy}^\beta\},$

$\alpha_5 = \{I\}, \alpha_6 = \left\{m_y^\beta\right\}, \alpha_7 = \left\{r_{-\pi/2}^\beta\right\}, \alpha_8 = \{\alpha_{x\bar{y}}^\beta\}.$

[2] C. Cayron, "Groupoid of orientational variants." Acta Cryst. A62 (2006) 21-40

## Example: two-dimensional case (2)

[2]

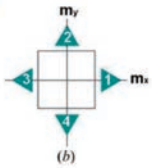


(b)

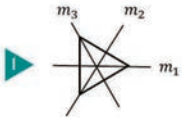


$\mathbf{G}^\beta = \{E, I, m_x^\beta, m_y^\beta, m_{xy}^\beta, m_{x\bar{y}}^\beta, r_{+\pi/2}^\beta, r_{-\pi/2}^\beta\}$ $\quad I = m_x^\beta m_y^\beta = m_y^\beta m_x^\beta$

$\mathbf{G}^\alpha = \{E, m_1^\alpha, m_2^\alpha, m_3^\alpha, r_{+\pi/3}^\alpha, r_{-\pi/3}^\alpha\}$ $\quad r_\theta$: rotation

Since $m_1^\alpha = m_x^\beta$ and $m_i^\alpha \neq m_x^\beta, m_y^\beta, m_{xy}^\beta, m_{x\bar{y}}^\beta$ for $i = 2,3$,

$$\mathbf{H}^\beta = \{E, m_x^\beta\}.$$

Variants are calculated as left co-sets $\alpha_i = g_i \mathbf{H}^\beta$ ($g_i \in \mathbf{G}^\beta$):

$$\alpha_1 = \{E, m_x^\beta\}, \alpha_2 = \{m_{xy}^\beta, r_{+\pi/2}^\beta\},$$
$$\alpha_3 = \{I, m_y^\beta\}, \alpha_4 = \{m_{x\bar{y}}^\beta, r_{-\pi/2}^\beta\}.$$

[2] C. Cayron. "Groupoid of orientational variants." Acta Cryst. A62 (2006) 21-40.





## Redefinition of crystals

- Fix an ambient space $\mathbb{R}^3$ and its standard basis $e_1, e_2, e_3$.
- $GL(3,\mathbb{R}) = \{A \in \mathbb{R}^{3\times 3} \mid \det A \neq 0\}$, $E$ : identity matrix of size 3.
- $Aff(3,\mathbb{R}) = \{A: v \in \mathbb{R}^3 \mapsto \bar{A}v + l \in \mathbb{R}^3 \mid \bar{A} \in GL(3,\mathbb{R}), l \in \mathbb{R}^3\}$.

  We consider $A \in Aff(3,\mathbb{R})$ as a $4 \times 4$ matrix $A = \begin{pmatrix} \bar{A} & l \\ 0 & 1 \end{pmatrix}$.
- $E(3,\mathbb{R}) = \{A \in Aff(3,\mathbb{R}) \mid \bar{A}\bar{A}^T = E\}$.
- A crystal $\beta$ is a triple $(B_1^\beta, L^\beta, \mathbf{G}^\beta)$ consisting of

$$B_1^\beta = \begin{pmatrix} \bar{B}_1^\beta & o^\beta \\ 0 & 1 \end{pmatrix} \in Aff(3,\mathbb{R}) \quad \left(\bar{B}_1^\beta = \left\langle e_1^\beta, e_2^\beta, e_3^\beta \right\rangle \in GL(3,\mathbb{R}), o^\beta \in \mathbb{R}^3\right),$$
$$L^\beta = \{a_1 e_1^{\beta_1} + a_2 e_2^{\beta_2} + a_3 e_3^{\beta_3} + o^\beta \mid a_1, a_2, a_3 \in \mathbb{Z}\},$$
$$\mathbf{G}^\beta = \{g \in E(3,\mathbb{R}) \mid gL^\beta = L^\beta, ge_1^\beta = e_1^\beta\}.$$

(We regard the matrix $B_1^\beta$ as a crystal.)





## Redefinition of variants

- Let $\beta$ and $\alpha$ be given crystals (a parent and a daughter).
- Define the set of externally equivalent crystals (*siblings*) of $\alpha$ w.r.t $\beta$ by

$$\mathbf{A}^{\beta\to\alpha} := \left\{\alpha_i := g_i T_> B_1^\beta \mid g_i \in \mathbf{G}^\beta\right\}, \text{ where } T_> := B_1^\alpha \left(B_1^\beta\right)^{-1}.$$

  (Each $\alpha_i$ is seen as a daughter crystal in Cayron's paper.)
- Introduce an equivalence relationship for $\alpha_i \in A^{\beta\to\alpha}$ by

  w.r.t. the same parent β

$$\alpha_i \sim \alpha_j \overset{\text{def}}{\Leftrightarrow} \alpha_i \alpha_j^{-1} = g_i g_j^{-1} \in G^{\alpha_j} \ (\Leftrightarrow g_j^{-1} g_i \in G^{\alpha_1}).$$

- Call the equivalence classes of $\alpha_i$ variants: the set of variants is given by

$$\mathbf{V}^{\beta\to\alpha} := \left\{g_i \mathbf{H}^{\alpha\beta} T_> B_1^\beta \mid g_i \in \mathbf{G}^\beta\right\}, \text{ where } \mathbf{H}^{\alpha\beta} = \mathbf{G}^{\alpha_1} \cap \mathbf{G}^\beta.$$

  We write the variants $\tilde{\alpha}_i \in \mathbf{V}^{\beta\to\alpha} \simeq \mathbf{G}^\beta / \mathbf{H}^{\alpha\beta}$.

# Summary

- We redefined the method of Cayron by using mathematics:
  - E.g. Definition of variants ($g_i \in \mathbf{G}^\beta$)

    Cayron's definition: $\alpha_i := g_i\,\mathbf{H}^\beta\ (\mathbf{H}^\beta := \mathbf{G}^\beta \cap T_>^{-1}\mathbf{G}^{\alpha_1}T_>)$

    Our definition: $\tilde{\alpha}_i := g_i\mathbf{H}^{\alpha\beta}T_>B_1^\beta\ (\mathbf{H}^{\alpha\beta} := \mathbf{G}^{\alpha_1} \cap \mathbf{G}^\beta)$
- We obtained a mathematically comprehensible representation of the method of Cayron and this lead to mathematical understanding variants that have been studied for a century in materials.





Giving it a Try in Practice: the Outcome of SGW2017

## Martenstic Transformation $\gamma \to \alpha$

森戸茂一,スマート・プロセス学会誌 第2巻, 第3号 (2013年5月)

KS orientation variants

| Variant No. | Close-packed plane parallel | Close-packed direction parallel | Rotation from Variant 1 [Axis] / Angle [deg.] |
|---|---|---|---|
| 01 | | $[101]_\gamma // [\bar{1}11]_\alpha$ | [–,–,–] / – |
| 02 | | $[101]_\gamma // [\bar{1}11]_\alpha$ | [0.577, 0.577, 0.577] / 60.0 |
| 03 | $(111)_\gamma // (011)_\alpha$ | $[01\bar{1}]_\gamma // [\bar{1}11]_\alpha$ | [0.000, 0.707, 0.707] / 60.0 |
| 04 | CP1 | $[01\bar{1}]_\gamma // [\bar{1}11]_\alpha$ | [0.000, 0.707, 0.707] / 10.5 |
| 05 | | $[1\bar{1}0]_\gamma // [\bar{1}11]_\alpha$ | [0.000, 0.707, 0.707] / 60.0 |
| 06 | | $[1\bar{1}0]_\gamma // [\bar{1}11]_\alpha$ | [0.000, 0.707, 0.707] / 49.5 |
| 07 | | $[10\bar{1}]_\gamma // [\bar{1}11]_\alpha$ | [0.577, 0.577, 0.577] / 49.5 |
| 08 | | $[10\bar{1}]_\gamma // [\bar{1}11]_\alpha$ | [0.577, 0.577, 0.577] / 10.5 |
| 09 | $(1\bar{1}1)_\gamma // (011)_\alpha$ | $[\bar{1}10]_\gamma // [\bar{1}11]_\alpha$ | [0.613, 0.186, 0.767] / 50.5 |
| 10 | CP2 | $[\bar{1}10]_\gamma // [\bar{1}11]_\alpha$ | [0.739, 0.463, 0.490] / 50.5 |
| 11 | | $[011]_\gamma // [\bar{1}11]_\alpha$ | [0.933, 0.354, 0.065] / 14.9 |
| 12 | | $[011]_\gamma // [\bar{1}11]_\alpha$ | [0.357, 0.603, 0.714] / 57.2 |
| 13 | | $[01\bar{1}]_\gamma // [\bar{1}11]_\alpha$ | [0.354, 0.933, 0.065] / 14.9 |
| 14 | | $[01\bar{1}]_\gamma // [\bar{1}11]_\alpha$ | [0.490, 0.463, 0.739] / 50.5 |
| 15 | $(\bar{1}11)_\gamma // (011)_\alpha$ | $[\bar{1}01]_\gamma // [\bar{1}11]_\alpha$ | [0.738, 0.246, 0.628] / 57.2 |
| 16 | CP3 | $[\bar{1}01]_\gamma // [\bar{1}11]_\alpha$ | [0.659, 0.659, 0.363] / 20.6 |
| 17 | | $[110]_\gamma // [\bar{1}11]_\alpha$ | [0.659, 0.363, 0.659] / 51.7 |
| 18 | | $[110]_\gamma // [\bar{1}11]_\alpha$ | [0.719, 0.302, 0.626] / 47.1 |
| 19 | | $[\bar{1}10]_\gamma // [\bar{1}11]_\alpha$ | [0.186, 0.767, 0.615] / 50.5 |
| 20 | | $[\bar{1}10]_\gamma // [\bar{1}11]_\alpha$ | [0.357, 0.714, 0.603] / 57.2 |
| 21 | $(11\bar{1})_\gamma // (011)_\alpha$ | $[01\bar{1}]_\gamma // [\bar{1}11]_\alpha$ | [0.955, 0.000, 0.296] / 20.6 |
| 22 | CP4 | $[01\bar{1}]_\gamma // [\bar{1}11]_\alpha$ | [0.302, 0.626, 0.719] / 47.1 |
| 23 | | $[101]_\gamma // [\bar{1}11]_\alpha$ | [0.246, 0.628, 0.738] / 57.2 |
| 24 | | $[101]_\gamma // [\bar{1}11]_\alpha$ | [0.912, 0.410, 0.000] / 21.1 |

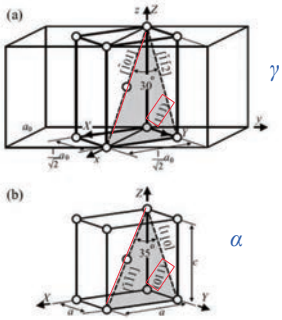


Deformation variants

(Bain's lattice correspondence)

$1/2[1\bar{1}0]_\gamma \to [100]_{\alpha'}$, $1/2[110]_\gamma \to [010]_{\alpha'}$, $[001]_\gamma \to [001]_{\alpha'}$





A condition of the closed packed plane parallel

$$(1\ \ 1\ \ 1)_\gamma // (0\ \ 1\ \ 1)_\alpha \qquad (1)$$

The corresponding above condition of the closed packed direction parallel

$$[-1\ \ 0\ \ 1]_\gamma // [-1\ \ -1\ \ 1]_\alpha \qquad (2)$$

from Eq.(1)

$$(1\ \ 1\ \ 1)_\gamma = \{(x,y,z) \mid x+y+z=0\}$$
$$(0\ \ 1\ \ 1)_\alpha = \{(X,Y,Z) \mid X+Z=0\} \qquad (3)$$

from eq.(3)

$$\begin{pmatrix} x \\ y \\ z \end{pmatrix}_\gamma = \begin{pmatrix} -1/2 \\ -1/2 \\ 1 \end{pmatrix} \Leftrightarrow \begin{pmatrix} X \\ Y \\ Z \end{pmatrix}_\alpha = \begin{pmatrix} 0 \\ -1 \\ 1 \end{pmatrix} \qquad (4)$$

from Eq.(2)

$$[-1\ \ 0\ \ 1]_\gamma = \{(x,y,z) \mid x=-z, y=0\}$$
$$[-1\ \ -1\ \ 1]_\alpha = \{(X,Y,Z) \mid X=Y=-Z\} \qquad (5)$$

from eq. (5)

$$\begin{pmatrix} x \\ y \\ z \end{pmatrix}_\gamma = \begin{pmatrix} -1 \\ 0 \\ 1 \end{pmatrix} \Leftrightarrow \begin{pmatrix} X \\ Y \\ Z \end{pmatrix}_\alpha = \begin{pmatrix} -1 \\ -1 \\ 1 \end{pmatrix} \qquad (6)$$

Since eq. (1) and eq. (2) are a rotation along the common a axis,

$$\begin{pmatrix} x \\ y \\ z \end{pmatrix}_\gamma = \begin{pmatrix} 0 \\ 0 \\ 1 \end{pmatrix} \Leftrightarrow \begin{pmatrix} X \\ Y \\ Z \end{pmatrix}_\alpha = \begin{pmatrix} 0 \\ 0 \\ 1 \end{pmatrix} \qquad (7)$$

KS orientation variants 森戸茂一

| Variant No. | Close-packed plane parallel | Close-packed direction parallel | Rotation from Variant 1 [Axis] / Angle [deg.] |
|---|---|---|---|
| 01 | | $[101]_\gamma // [\bar{1}11]_\alpha$ | [–,–,–] / – |
| 02 | | $[101]_\gamma // [\bar{1}11]_\alpha$ | [0.577, 0.577, 0.577] / 60.0 |
| 03 | $(111)_\gamma // (011)_\alpha$ | $[01\bar{1}]_\gamma // [\bar{1}11]_\alpha$ | [0.000, 0.707, 0.707] / 60.0 |
| 04 | CP1 | $[01\bar{1}]_\gamma // [\bar{1}11]_\alpha$ | [0.000, 0.707, 0.707] / 10.5 |
| 05 | | $[1\bar{1}0]_\gamma // [\bar{1}11]_\alpha$ | [0.000, 0.707, 0.707] / 60.0 |
| 06 | | $[1\bar{1}0]_\gamma // [\bar{1}11]_\alpha$ | [0.000, 0.707, 0.707] / 49.5 |

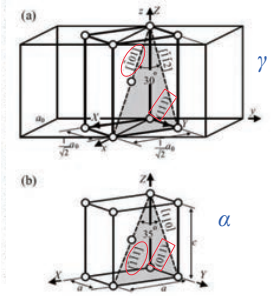

from eq.(4), eq. (6) and eq.(7)

$$\begin{pmatrix} -1 & 0 & -1/2 \\ 0 & 0 & -1/2 \\ 1 & 1 & 1 \end{pmatrix} = T_\gamma \begin{pmatrix} -1 & 0 & 0 \\ -1 & 0 & -1 \\ 1 & 1 & -1 \end{pmatrix}, \qquad T_\gamma := \begin{pmatrix} a_{11} & a_{12} & a_{13} \\ a_{21} & a_{22} & a_{23} \\ a_{31} & a_{32} & a_{33} \end{pmatrix} \tag{8}$$

The translation matrix is derived as follows.

$$T_\gamma = \begin{pmatrix} 1/2 & 1/2 & 0 \\ -1/2 & 1/2 & 0 \\ 0 & 0 & 1 \end{pmatrix} \tag{9}$$

The relationship between $(x\ y\ z)_\gamma$ and $(X\ Y\ Z)^g$ is as follows.

$$\begin{pmatrix} x \\ y \\ z \end{pmatrix} = \begin{pmatrix} 1/2 & 1/2 & 0 \\ -1/2 & 1/2 & 0 \\ 0 & 0 & 1 \end{pmatrix} \begin{pmatrix} X \\ Y \\ Z \end{pmatrix} \tag{10}$$

Variant is defined as follows.

$$V^{\gamma\to\alpha} := \left\{ g_\gamma H^{\alpha/\gamma} T_\gamma B_1^\gamma \,\middle|\, g_\gamma \in G^\gamma \cong O(3,\mathrm{Z}) \right\} \tag{11}$$

where $H^{\alpha/\gamma} = G^\gamma \cap G^\alpha$.

Since $G^\alpha \cong O(3,\mathrm{Z})$ and the rotational symmetry regarding γ and α around [0 0 1] in the previous slide's figure, $H^{\gamma/\alpha}$ should be as follows.

$$H^{\gamma\to\alpha} = \left\{ \begin{pmatrix} 1 & 0 & 0 \\ 0 & 1 & 0 \\ 0 & 0 & 1 \end{pmatrix}, \begin{pmatrix} -1 & 0 & 0 \\ 0 & -1 & 0 \\ 0 & 0 & 1 \end{pmatrix} \right\} \tag{12}$$



新日鐵住金 NIPPON STEEL & SUMITOMO METAL

The $\gamma$ lattice is described as

$$\gamma = \left\{ l\,\mathrm{e}_1^\gamma + m\mathrm{e}_2^\gamma + n\mathrm{e}_3^\gamma \,\middle|\, l,m,n \in \mathrm{Z} \right\} \tag{13}$$

The basis $B_1^\gamma$ is written by

$$B_1^\gamma = \left( e_1^\gamma, e_2^\gamma, e_3^\gamma \right) \in O(3,\mathrm{Z}) \tag{14}$$

$B_1^\gamma$ can be taken as

$$B_1^\gamma = \begin{pmatrix} 1 & 0 & 0 \\ 0 & 1 & 0 \\ 0 & 0 & 1 \end{pmatrix} \tag{15}$$



新日鐵住金 NIPPON STEEL & SUMITOMO METAL

## The 24 Variants (1/3)

$$\left\{ \begin{bmatrix} 1/2 & 1/2 & 0 \\ -1/2 & 1/2 & 0 \\ 0 & 0 & 1 \end{bmatrix}, \begin{bmatrix} -1/2 & -1/2 & 0 \\ 1/2 & -1/2 & 0 \\ 0 & 0 & 1 \end{bmatrix} \right\} \qquad \left\{ \begin{bmatrix} -1/2 & 1/2 & 0 \\ 1/2 & 1/2 & 0 \\ 0 & 0 & 1 \end{bmatrix}, \begin{bmatrix} 1/2 & -1/2 & 0 \\ -1/2 & -1/2 & 0 \\ 0 & 0 & 1 \end{bmatrix} \right\}$$

$$\left\{ \begin{bmatrix} 1/2 & 1/2 & 0 \\ -1/2 & 1/2 & 0 \\ 0 & 0 & -1 \end{bmatrix}, \begin{bmatrix} -1/2 & -1/2 & 0 \\ 1/2 & -1/2 & 0 \\ 0 & 0 & -1 \end{bmatrix} \right\} \qquad \left\{ \begin{bmatrix} -1/2 & 1/2 & 0 \\ 1/2 & 1/2 & 0 \\ 0 & 0 & -1 \end{bmatrix}, \begin{bmatrix} 1/2 & -1/2 & 0 \\ -1/2 & -1/2 & 0 \\ 0 & 0 & -1 \end{bmatrix} \right\}$$

$$\left\{ \begin{bmatrix} 1/2 & 1/2 & 0 \\ 1/2 & -1/2 & 0 \\ 0 & 0 & 1 \end{bmatrix}, \begin{bmatrix} -1/2 & -1/2 & 0 \\ -1/2 & 1/2 & 0 \\ 0 & 0 & 1 \end{bmatrix} \right\} \qquad \left\{ \begin{bmatrix} 1/2 & -1/2 & 0 \\ 1/2 & 1/2 & 0 \\ 0 & 0 & 1 \end{bmatrix}, \begin{bmatrix} -1/2 & 1/2 & 0 \\ -1/2 & -1/2 & 0 \\ 0 & 0 & 1 \end{bmatrix} \right\}$$

$$\left\{ \begin{bmatrix} 1/2 & 1/2 & 0 \\ 1/2 & -1/2 & 0 \\ 0 & 0 & -1 \end{bmatrix}, \begin{bmatrix} -1/2 & -1/2 & 0 \\ -1/2 & 1/2 & 0 \\ 0 & 0 & -1 \end{bmatrix} \right\} \qquad \left\{ \begin{bmatrix} 1/2 & -1/2 & 0 \\ 1/2 & 1/2 & 0 \\ 0 & 0 & -1 \end{bmatrix}, \begin{bmatrix} -1/2 & 1/2 & 0 \\ -1/2 & -1/2 & 0 \\ 0 & 0 & -1 \end{bmatrix} \right\}$$



新日鐵住金 NIPPON STEEL & SUMITOMO METAL

## The 24 Variants (2/3)

$$\left\{\begin{bmatrix} 1/2 & 1/2 & 0 \\ 0 & 0 & 1 \\ -1/2 & 1/2 & 0 \end{bmatrix}, \begin{bmatrix} -1/2 & -1/2 & 0 \\ 0 & 0 & 1 \\ 1/2 & -1/2 & 0 \end{bmatrix}\right\} \quad \left\{\begin{bmatrix} -1/2 & 1/2 & 0 \\ 0 & 0 & 1 \\ 1/2 & 1/2 & 0 \end{bmatrix}, \begin{bmatrix} 1/2 & -1/2 & 0 \\ 0 & 0 & 1 \\ -1/2 & -1/2 & 0 \end{bmatrix}\right\}$$

$$\left\{\begin{bmatrix} 1/2 & 1/2 & 0 \\ 0 & 0 & 1 \\ 1/2 & -1/2 & 0 \end{bmatrix}, \begin{bmatrix} -1/2 & -1/2 & 0 \\ 0 & 0 & 1 \\ -1/2 & 1/2 & 0 \end{bmatrix}\right\} \quad \left\{\begin{bmatrix} 1/2 & -1/2 & 0 \\ 0 & 0 & 1 \\ 1/2 & 1/2 & 0 \end{bmatrix}, \begin{bmatrix} -1/2 & 1/2 & 0 \\ 0 & 0 & 1 \\ -1/2 & -1/2 & 0 \end{bmatrix}\right\}$$

$$\left\{\begin{bmatrix} 1/2 & 1/2 & 0 \\ 0 & 0 & -1 \\ -1/2 & 1/2 & 0 \end{bmatrix}, \begin{bmatrix} -1/2 & -1/2 & 0 \\ 0 & 0 & -1 \\ 1/2 & -1/2 & 0 \end{bmatrix}\right\} \quad \left\{\begin{bmatrix} -1/2 & 1/2 & 0 \\ 0 & 0 & -1 \\ 1/2 & 1/2 & 0 \end{bmatrix}, \begin{bmatrix} 1/2 & -1/2 & 0 \\ 0 & 0 & -1 \\ -1/2 & -1/2 & 0 \end{bmatrix}\right\}$$

$$\left\{\begin{bmatrix} 1/2 & 1/2 & 0 \\ 0 & 0 & -1 \\ 1/2 & -1/2 & 0 \end{bmatrix}, \begin{bmatrix} -1/2 & -1/2 & 0 \\ 0 & 0 & -1 \\ -1/2 & 1/2 & 0 \end{bmatrix}\right\} \quad \left\{\begin{bmatrix} 1/2 & -1/2 & 0 \\ 0 & 0 & -1 \\ 1/2 & 1/2 & 0 \end{bmatrix}, \begin{bmatrix} -1/2 & 1/2 & 0 \\ 0 & 0 & -1 \\ -1/2 & -1/2 & 0 \end{bmatrix}\right\}$$



新日鐵住金 NIPPON STEEL & SUMITOMO METAL

## The 24 Variants (3/3)

$$\left\{\begin{bmatrix} 0 & 0 & 1 \\ 1/2 & 1/2 & 0 \\ -1/2 & 1/2 & 0 \end{bmatrix}, \begin{bmatrix} 0 & 0 & 1 \\ -1/2 & -1/2 & 0 \\ 1/2 & -1/2 & 0 \end{bmatrix}\right\} \quad \left\{\begin{bmatrix} 0 & 0 & 1 \\ -1/2 & 1/2 & 0 \\ 1/2 & 1/2 & 0 \end{bmatrix}, \begin{bmatrix} 0 & 0 & 1 \\ 1/2 & -1/2 & 0 \\ -1/2 & -1/2 & 0 \end{bmatrix}\right\}$$

$$\left\{\begin{bmatrix} 0 & 0 & 1 \\ 1/2 & 1/2 & 0 \\ 1/2 & -1/2 & 0 \end{bmatrix}, \begin{bmatrix} 0 & 0 & 1 \\ -1/2 & -1/2 & 0 \\ -1/2 & 1/2 & 0 \end{bmatrix}\right\} \quad \left\{\begin{bmatrix} 0 & 0 & 1 \\ 1/2 & -1/2 & 0 \\ 1/2 & 1/2 & 0 \end{bmatrix}, \begin{bmatrix} 0 & 0 & 1 \\ -1/2 & 1/2 & 0 \\ -1/2 & -1/2 & 0 \end{bmatrix}\right\}$$

$$\left\{\begin{bmatrix} 0 & 0 & -1 \\ 1/2 & 1/2 & 0 \\ -1/2 & 1/2 & 0 \end{bmatrix}, \begin{bmatrix} 0 & 0 & -1 \\ -1/2 & -1/2 & 0 \\ 1/2 & -1/2 & 0 \end{bmatrix}\right\} \quad \left\{\begin{bmatrix} 0 & 0 & -1 \\ -1/2 & 1/2 & 0 \\ 1/2 & 1/2 & 0 \end{bmatrix}, \begin{bmatrix} 0 & 0 & -1 \\ 1/2 & -1/2 & 0 \\ -1/2 & -1/2 & 0 \end{bmatrix}\right\}$$

$$\left\{\begin{bmatrix} 0 & 0 & -1 \\ 1/2 & 1/2 & 0 \\ 1/2 & -1/2 & 0 \end{bmatrix}, \begin{bmatrix} 0 & 0 & -1 \\ -1/2 & -1/2 & 0 \\ -1/2 & 1/2 & 0 \end{bmatrix}\right\} \quad \left\{\begin{bmatrix} 0 & 0 & -1 \\ 1/2 & -1/2 & 0 \\ 1/2 & 1/2 & 0 \end{bmatrix}, \begin{bmatrix} 0 & 0 & -1 \\ -1/2 & 1/2 & 0 \\ -1/2 & -1/2 & 0 \end{bmatrix}\right\}$$



新日鐵住金 NIPPON STEEL & SUMITOMO METAL

## A Conversion for Making Rotation Matrix

Since 24 variants in the previous slides are not the rotation matrices,
we try to make a simple conversion for making rotation matrix as follows.

$$T_> = \begin{pmatrix} 1/2 & 1/2 & 0 \\ -1/2 & 1/2 & 0 \\ 0 & 0 & 1 \end{pmatrix} \Rightarrow T_> = \begin{pmatrix} 1/\sqrt{2} & 1/\sqrt{2} & 0 \\ -1/\sqrt{2} & 1/\sqrt{2} & 0 \\ 0 & 0 & 1 \end{pmatrix}$$





新日鐵住金 NIPPON STEEL & SUMITOMO METAL

## Rotation matrix ( Rotation Axis, Angle ) and the Determinant

| Variant No. | 1 | | | |
|---|---|---|---|---|
| rotation matirix | R1 | 0.707107 | 0.707107 | 0 |
| | | -0.70711 | 0.707107 | 0 |
| | | 0 | 0 | 1 |
| rotation axis | u | 0 | | |
| | | 0 | | |
| | | 1 | | |
| angle[°] | θ | 45 | | |
| determinant | det(R1) | 1 | | |
| rotation matirix | R2 | -0.70711 | -0.70711 | 0 |
| | | 0.707107 | -0.70711 | 0 |
| | | 0 | 0 | 1 |
| rotation axis | u | 0 | | |
| | | 0 | | |
| | | 1 | | |
| angle[°] | θ | 135 | | |
| determinant | det(R2) | 1 | | |

| Variant No. | 2 | | | |
|---|---|---|---|---|
| rotation matirix | R1 | 0.707107 | 0.707107 | 0 |
| | | -0.70711 | 0.707107 | 0 |
| | | 0 | 0 | -1 |
| rotation axis | u | 0 | | |
| | | 0 | | |
| | | 1 | | |
| angle[°] | θ | 107.0313 | | |
| determinant | det(R1) | -1 | | |
| rotation matirix | R2 | -0.70711 | -0.70711 | 0 |
| | | 0.707107 | -0.70711 | 0 |
| | | 0 | 0 | -1 |
| rotation axis | u | 0 | | |
| | | 0 | | |
| | | 1 | | |
| angle[°] | θ | 180-64.651639i | | |
| determinant | det(R2) | -1 | | |

| Variant No. | 3 | | | |
|---|---|---|---|---|
| rotation matirix | R1 | 0.707107 | 0.707107 | 0 |
| | | 0.707107 | -0.70711 | 0 |
| | | 0 | 0 | 1 |
| rotation axis | u | 0 | | |
| | | 0 | | |
| | | 0 | | |
| angle[°] | θ | 0 | | |
| determinant | det(R1) | -1 | | |
| rotation matirix | R2 | -0.70711 | -0.70711 | 0 |
| | | -0.70711 | 0.707107 | 0 |
| | | 0 | 0 | 1 |
| rotation axis | u | 0 | | |
| | | 0 | | |
| | | 0 | | |
| angle[°] | θ | 0 | | |
| determinant | det(R2) | -1 | | |

| Variant No. | 4 | | | |
|---|---|---|---|---|
| rotation matirix | R1 | 0.707107 | 0.707107 | 0 |
| | | 0.707107 | -0.70711 | 0 |
| | | 0 | 0 | -1 |
| rotation axis | u | 0.92388 | | |
| | | 0.382683 | | |
| | | 0 | | |
| angle[°] | θ | 180 | | |
| determinant | det(R1) | 1 | | |
| rotation matirix | R2 | -0.70711 | -0.70711 | 0 |
| | | -0.70711 | 0.707107 | 0 |
| | | 0 | 0 | -1 |
| rotation axis | u | 0.382683 | | |
| | | -0.92388 | | |
| | | 0 | | |
| angle[°] | θ | 180 | | |
| determinant | det(R2) | 1 | | |





| Variant No. | 5 | | | |
|---|---|---|---|---|
| rotation matirix | R1 | 0.707107 | 0.707107 | 0 |
| | | 0 | 0 | 1 |
| | | -0.70711 | 0.707107 | 0 |
| rotation axis | u | -0.86286 | | |
| | | -0.35741 | | |
| | | 0.357407 | | |
| angle[°] | θ | 98.42106 | | |
| determinant | det(R1) | -1 | | |
| rotation matirix | R2 | -0.70711 | -0.70711 | 0 |
| | | 0 | 0 | 1 |
| | | 0.707107 | -0.70711 | 0 |
| rotation axis | u | 0.281085 | | |
| | | -0.6786 | | |
| | | 0.678598 | | |
| angle[°] | θ | 148.6003 | | |
| determinant | det(R2) | -1 | | |

| Variant No. | 6 | | | |
|---|---|---|---|---|
| rotation matirix | R1 | 0.707107 | 0.707107 | 0 |
| | | 0 | 0 | 1 |
| | | 0.707107 | -0.70711 | 0 |
| rotation axis | u | 0.862856 | | |
| | | 0.357407 | | |
| | | 0.357407 | | |
| angle[°] | θ | 98.42106 | | |
| determinant | det(R1) | 1 | | |
| rotation matirix | R2 | -0.70711 | -0.70711 | 0 |
| | | 0 | 0 | 1 |
| | | -0.70711 | 0.707107 | 0 |
| rotation axis | u | -0.28108 | | |
| | | 0.678598 | | |
| | | 0.678598 | | |
| angle[°] | θ | 148.6003 | | |
| determinant | det(R2) | 1 | | |

| Variant No. | 7 | | | |
|---|---|---|---|---|
| rotation matirix | R1 | 0.707107 | 0.707107 | 0 |
| | | 0 | 0 | -1 |
| | | -0.70711 | 0.707107 | 0 |
| rotation axis | u | -0.86286 | | |
| | | -0.35741 | | |
| | | 0.357407 | | |
| angle[°] | θ | 98.42106 | | |
| determinant | det(R1) | 1 | | |
| rotation matirix | R2 | -0.70711 | -0.70711 | 0 |
| | | 0 | 0 | -1 |
| | | 0.707107 | -0.70711 | 0 |
| rotation axis | u | 0.281085 | | |
| | | -0.6786 | | |
| | | 0.678598 | | |
| angle[°] | θ | 148.6003 | | |
| determinant | det(R2) | 1 | | |

| Variant No. | 8 | | | |
|---|---|---|---|---|
| rotation matirix | R1 | 0.707107 | 0.707107 | 0 |
| | | 0 | 0 | -1 |
| | | 0.707107 | -0.70711 | 0 |
| rotation axis | u | 0.862856 | | |
| | | 0.357407 | | |
| | | 0.357407 | | |
| angle[°] | θ | 98.42106 | | |
| determinant | det(R1) | -1 | | |
| rotation matirix | R2 | -0.70711 | -0.70711 | 0 |
| | | 0 | 0 | -1 |
| | | -0.70711 | 0.707107 | 0 |
| rotation axis | u | -0.28108 | | |
| | | 0.678598 | | |
| | | 0.678598 | | |
| angle[°] | θ | 148.6003 | | |
| determinant | det(R2) | -1 | | |





| Variant No. | 9 | | | |
|---|---|---|---|---|
| rotation matirix | R1 | -0.70711 | 0.707107 | 0 |
| | | 0.707107 | 0.707107 | 0 |
| | | 0 | 0 | 1 |
| rotation axis | u | 0 | | |
| | | 0 | | |
| | | 0 | | |
| angle[°] | θ | 0 | | |
| determinant | det(R1) | -1 | | |
| rotation matirix | R2 | 0.707107 | -0.70711 | 0 |
| | | -0.70711 | -0.70711 | 0 |
| | | 0 | 0 | 1 |
| rotation axis | u | 0 | | |
| | | 0 | | |
| | | 0 | | |
| angle[°] | θ | 0 | | |
| determinant | det(R2) | -1 | | |

| Variant No. | 10 | | | |
|---|---|---|---|---|
| rotation matirix | R1 | -0.70711 | 0.707107 | 0 |
| | | 0.707107 | 0.707107 | 0 |
| | | 0 | 0 | -1 |
| rotation axis | u | 0.382683 | | |
| | | 0.92388 | | |
| | | 0 | | |
| angle[°] | θ | 180 | | |
| determinant | det(R1) | 1 | | |
| rotation matirix | R2 | 0.707107 | -0.70711 | 0 |
| | | -0.70711 | -0.70711 | 0 |
| | | 0 | 0 | -1 |
| rotation axis | u | 0.92388 | | |
| | | -0.38268 | | |
| | | 0 | | |
| angle[°] | θ | 180 | | |
| determinant | det(R2) | 1 | | |

| Variant No. | 11 | | | |
|---|---|---|---|---|
| rotation matirix | R1 | -0.70711 | 0.707107 | 0 |
| | | -0.70711 | -0.70711 | 0 |
| | | 0 | 0 | 1 |
| rotation axis | u | 0 | | |
| | | 0 | | |
| | | 1 | | |
| angle[°] | θ | 135 | | |
| determinant | det(R1) | 1 | | |
| rotation matirix | R2 | 0.707107 | -0.70711 | 0 |
| | | 0.707107 | 0.707107 | 0 |
| | | 0 | 0 | 1 |
| rotation axis | u | 0 | | |
| | | 0 | | |
| | | 1 | | |
| angle[°] | θ | 45 | | |
| determinant | det(R2) | 1 | | |

| Variant No. | 12 | | | |
|---|---|---|---|---|
| rotation matirix | R1 | -0.70711 | 0.707107 | 0 |
| | | -0.70711 | -0.70711 | 0 |
| | | 0 | 0 | -1 |
| rotation axis | u | 0 | | |
| | | 0 | | |
| | | 1 | | |
| angle[°] | θ | 180-64.651639i | | |
| determinant | det(R1) | -1 | | |
| rotation matirix | R2 | 0.707107 | -0.70711 | 0 |
| | | 0.707107 | 0.707107 | 0 |
| | | 0 | 0 | -1 |
| rotation axis | u | 0 | | |
| | | 0 | | |
| | | 1 | | |
| angle[°] | θ | 107.0313 | | |
| determinant | det(R2) | -1 | | |

| Variant No. | 13 | | | |
|---|---|---|---|---|
| rotation matirix | R1 | 0 | 0 | 1 |
| | | 0.707107 | 0.707107 | 0 |
| | | -0.70711 | 0.707107 | 0 |
| rotation axis | u | 0.357407 | | |
| | | 0.862856 | | |
| | | 0.357407 | | |
| angle[°] | θ | 98.42106 | | |
| determinant | det(R1) | 1 | | |
| rotation matirix | R2 | 0 | 0 | 1 |
| | | -0.70711 | -0.70711 | 0 |
| | | 0.707107 | -0.70711 | 0 |
| rotation axis | u | 0.678598 | | |
| | | -0.28108 | | |
| | | 0.678598 | | |
| angle[°] | θ | 148.6003 | | |
| determinant | det(R2) | 1 | | |

| Variant No. | 14 | | | |
|---|---|---|---|---|
| rotation matirix | R1 | 0 | 0 | 1 |
| | | 0.707107 | 0.707107 | 0 |
| | | 0.707107 | -0.70711 | 0 |
| rotation axis | u | -0.35741 | | |
| | | -0.86286 | | |
| | | 0.357407 | | |
| angle[°] | θ | 98.42106 | | |
| determinant | det(R1) | -1 | | |
| rotation matirix | R2 | 0 | 0 | 1 |
| | | -0.70711 | -0.70711 | 0 |
| | | -0.70711 | 0.707107 | 0 |
| rotation axis | u | -0.6786 | | |
| | | 0.281085 | | |
| | | 0.678598 | | |
| angle[°] | θ | 148.6003 | | |
| determinant | det(R2) | -1 | | |

| Variant No. | 15 | | | |
|---|---|---|---|---|
| rotation matirix | R1 | 0 | 0 | -1 |
| | | 0.707107 | 0.707107 | 0 |
| | | -0.70711 | 0.707107 | 0 |
| rotation axis | u | 0.357407 | | |
| | | 0.862856 | | |
| | | 0.357407 | | |
| angle[°] | θ | 98.42106 | | |
| determinant | det(R1) | -1 | | |
| rotation matirix | R2 | 0 | 0 | -1 |
| | | -0.70711 | -0.70711 | 0 |
| | | 0.707107 | -0.70711 | 0 |
| rotation axis | u | 0.678598 | | |
| | | -0.28108 | | |
| | | 0.678598 | | |
| angle[°] | θ | 148.6003 | | |
| determinant | det(R2) | -1 | | |

| Variant No. | 16 | | | |
|---|---|---|---|---|
| rotation matirix | R1 | 0 | 0 | -1 |
| | | 0.707107 | 0.707107 | 0 |
| | | 0.707107 | -0.70711 | 0 |
| rotation axis | u | -0.35741 | | |
| | | -0.86286 | | |
| | | 0.357407 | | |
| angle[°] | θ | 98.42106 | | |
| determinant | det(R1) | 1 | | |
| rotation matirix | R2 | 0 | 0 | -1 |
| | | -0.70711 | -0.70711 | 0 |
| | | -0.70711 | 0.707107 | 0 |
| rotation axis | u | -0.6786 | | |
| | | 0.281085 | | |
| | | 0.678598 | | |
| angle[°] | θ | 148.6003 | | |
| determinant | det(R2) | 1 | | |





| Variant No. | 17 | | | |
|---|---|---|---|---|
| rotation matirix | R1 | -0.70711 | 0.707107 | 0 |
| | | 0 | 0 | 1 |
| | | 0.707107 | 0.707107 | 0 |
| rotation axis | u | 0.281085 | | |
| | | 0.678598 | | |
| | | 0.678598 | | |
| angle[°] | θ | 148.6003 | | |
| determinant | det(R1) | 1 | | |
| rotation matirix | R2 | 0.707107 | -0.70711 | 0 |
| | | 0 | 0 | 1 |
| | | -0.70711 | -0.70711 | 0 |
| rotation axis | u | -0.86286 | | |
| | | 0.357407 | | |
| | | 0.357407 | | |
| angle[°] | θ | 98.42106 | | |
| determinant | det(R2) | 1 | | |

| Variant No. | 18 | | | |
|---|---|---|---|---|
| rotation matirix | R1 | -0.70711 | 0.707107 | 0 |
| | | 0 | 0 | 1 |
| | | -0.70711 | -0.70711 | 0 |
| rotation axis | u | -0.28108 | | |
| | | -0.6786 | | |
| | | 0.678598 | | |
| angle[°] | θ | 148.6003 | | |
| determinant | det(R1) | -1 | | |
| rotation matirix | R2 | 0.707107 | -0.70711 | 0 |
| | | 0 | 0 | 1 |
| | | 0.707107 | 0.707107 | 0 |
| rotation axis | u | 0.862856 | | |
| | | -0.35741 | | |
| | | 0.357407 | | |
| angle[°] | θ | 98.42106 | | |
| determinant | det(R2) | -1 | | |

| Variant No. | 19 | | | |
|---|---|---|---|---|
| rotation matirix | R1 | -0.70711 | 0.707107 | 0 |
| | | 0 | 0 | -1 |
| | | 0.707107 | 0.707107 | 0 |
| rotation axis | u | 0.281085 | | |
| | | 0.678598 | | |
| | | 0.678598 | | |
| angle[°] | θ | 148.6003 | | |
| determinant | det(R1) | -1 | | |
| rotation matirix | R2 | 0.707107 | -0.70711 | 0 |
| | | 0 | 0 | -1 |
| | | -0.70711 | -0.70711 | 0 |
| rotation axis | u | -0.86286 | | |
| | | 0.357407 | | |
| | | 0.357407 | | |
| angle[°] | θ | 98.42106 | | |
| determinant | det(R2) | -1 | | |

| Variant No. | 20 | | | |
|---|---|---|---|---|
| rotation matirix | R1 | -0.70711 | 0.707107 | 0 |
| | | 0 | 0 | -1 |
| | | -0.70711 | -0.70711 | 0 |
| rotation axis | u | -0.28108 | | |
| | | -0.6786 | | |
| | | 0.678598 | | |
| angle[°] | θ | 148.6003 | | |
| determinant | det(R1) | 1 | | |
| rotation matirix | R2 | 0.707107 | -0.70711 | 0 |
| | | 0 | 0 | -1 |
| | | 0.707107 | 0.707107 | 0 |
| rotation axis | u | 0.862856 | | |
| | | -0.35741 | | |
| | | 0.357407 | | |
| angle[°] | θ | 98.42106 | | |
| determinant | det(R2) | 1 | | |





| Variant No. | 21 | | | |
|---|---|---|---|---|
| rotation matirix | R1 | 0 | 0 | 1 |
| | | -0.70711 | 0.707107 | 0 |
| | | 0.707107 | 0.707107 | 0 |
| rotation axis | u | -0.35741 | | |
| | | 0.862856 | | |
| | | 0.357407 | | |
| angle[°] | θ | 98.42106 | | |
| determinant | det(R1) | -1 | | |
| rotation matirix | R2 | 0 | 0 | 1 |
| | | 0.707107 | -0.70711 | 0 |
| | | -0.70711 | -0.70711 | 0 |
| rotation axis | u | -0.6786 | | |
| | | -0.28108 | | |
| | | 0.678598 | | |
| angle[°] | θ | 148.6003 | | |
| determinant | det(R2) | -1 | | |

| Variant No. | 22 | | | |
|---|---|---|---|---|
| rotation matirix | R1 | 0 | 0 | 1 |
| | | -0.70711 | 0.707107 | 0 |
| | | -0.70711 | -0.70711 | 0 |
| rotation axis | u | 0.357407 | | |
| | | -0.86286 | | |
| | | 0.357407 | | |
| angle[°] | θ | 98.42106 | | |
| determinant | det(R1) | 1 | | |
| rotation matirix | R2 | 0 | 0 | 1 |
| | | 0.707107 | -0.70711 | 0 |
| | | 0.707107 | 0.707107 | 0 |
| rotation axis | u | 0.678598 | | |
| | | 0.281085 | | |
| | | 0.678598 | | |
| angle[°] | θ | 148.6003 | | |
| determinant | det(R2) | 1 | | |

| Variant No. | 23 | | | |
|---|---|---|---|---|
| rotation matirix | R1 | 0 | 0 | -1 |
| | | -0.70711 | 0.707107 | 0 |
| | | 0.707107 | 0.707107 | 0 |
| rotation axis | u | -0.35741 | | |
| | | 0.862856 | | |
| | | 0.357407 | | |
| angle[°] | θ | 98.42106 | | |
| determinant | det(R1) | 1 | | |
| rotation matirix | R2 | 0 | 0 | -1 |
| | | 0.707107 | -0.70711 | 0 |
| | | -0.70711 | -0.70711 | 0 |
| rotation axis | u | -0.6786 | | |
| | | -0.28108 | | |
| | | 0.678598 | | |
| angle[°] | θ | 148.6003 | | |
| determinant | det(R2) | 1 | | |

| Variant No. | 24 | | | |
|---|---|---|---|---|
| rotation matirix | R1 | 0 | 0 | -1 |
| | | -0.70711 | 0.707107 | 0 |
| | | -0.70711 | -0.70711 | 0 |
| rotation axis | u | 0.357407 | | |
| | | -0.86286 | | |
| | | 0.357407 | | |
| angle[°] | θ | 98.42106 | | |
| determinant | det(R1) | -1 | | |
| rotation matirix | R2 | 0 | 0 | -1 |
| | | 0.707107 | -0.70711 | 0 |
| | | 0.707107 | 0.707107 | 0 |
| rotation axis | u | 0.678598 | | |
| | | 0.281085 | | |
| | | 0.678598 | | |
| angle[°] | θ | 148.6003 | | |
| determinant | det(R2) | -1 | | |

# Picking up Variants Making Rotation Matrix

| Variant No. | Rotation axis | Rotation angle |
|---|---|---|
| 01 : | { (0 0 1), (0 0 1)}, 11: { (0 0 1), (0 0 1)} | { 45° , 135° } |
| 04:<br>10 : | { (0.924 0.383 0), (0.383, -0.924, 0) }<br>{ (0.383 0.924 0), (0.924 -0.383 0)} | { 180° , 180° } |
| 06 :<br>07 :<br>13 :<br>16 :<br>17:<br>20:<br>22:<br>23 | { (0.863 0.357 0.357), (-0.281 0.679 0.679)}<br>{ (-0.863 -0.357 0.357), (0.281 -0.679 0.679)}<br>{ (0.357 0.823 0.357), (0.679 -0.281 0.679)}<br>{ (-0.357 -0.863 0.357), (-0.679 0.281 0.679)}<br>{ (0.281 0.679 0.679), (-0.863 0.357 0.357)}<br>{ (-0.281 -0.679 0.679), (0.863 -0.357 0.357)}<br>{ (0.357 -0.863 0.357), (0.679 0.281 0.679)}<br>{ (-0.357 0.863 0.357), (-0.679 -0.281 0.679)} | { 98.4° , 148.6° } |

01 $\begin{cases} [-1 \quad 0 \quad 1]_\gamma // [-1 \quad -1 \quad 1]_\alpha \\ (1 \quad 1 \quad 1)_\gamma // (0 \quad 1 \quad 1)_\alpha \end{cases}$





## 24 Variants in Morito's Paper and the Rotation Matricises

| Variant No. | Close-packed plane parallel | Close-packed direction parallel | Rotation from Variant 1 [Axis]/Angle(deg.) | Rotation Matrix | | |
|---|---|---|---|---|---|---|
| 1 | (1 1 1)γ//(0 1 1)α' CP1 | [-1 0 1]γ//[-1 -1 1]α' | [-, -, -]/- | - | - | - |
| | | | | - | - | - |
| | | | | - | - | - |
| 2 | | [-1 0 1]γ//[-1 1 -1]α' | [0.577, 0.577, -0.577]/60.0 | 0.6667 | 0.6667 | 0.3333 |
| | | | ↓ | -0.3333 | 0.6667 | -0.6667 |
| | | | 1/√3[1, 1, -1]/60 | -0.6667 | 0.3333 | 0.6667 |
| 3 | | [0 1 -1]γ//[-1 -1 1]α' | [0.000, 0.707, 0.707]/60.0 | 0.5 | -0.6124 | 0.6124 |
| | | | ↓ | 0.6124 | 0.75 | 0.25 |
| | | | 1/√2[0, 1, 1]/60.0 | -0.6124 | 0.25 | 0.75 |
| 4 | | [0 1 -1]γ//[-1 1 -1]α' | [0.000, -0.707, -0.707]/10.5 | 0.9833 | 0.1289 | -0.1289 |
| | | | ↓ | -0.1289 | 0.9916 | 0.0084 |
| | | | 1/√2[0, -1, -1]/10.5 | 0.1289 | 0.0084 | 0.9916 |
| 5 | | [1 -1 0]γ//[-1 -1 1]α' | [0.000, -0.707, -0.707]/60.0 | 0.5 | 0.6124 | -0.6124 |
| | | | ↓ | -0.6124 | 0.75 | 0.25 |
| | | | 1/√2[0, -1, -1]/60.0 | 0.6124 | 0.25 | 0.75 |
| 6 | | [1 -1 0]γ//[-1 1 -1]α' | [0.000, 0.707, 0.707]/49.5 | 0.6494 | -0.5377 | 0.5377 |
| | | | ↓ | 0.5377 | 0.8247 | 0.1753 |
| | | | 1/√2[0, 1, 1]/49.5 | -0.5377 | 0.1753 | 0.8247 |
| 7 | (1 -1 1)γ//(0 1 1)α' CP2 | [-1 0 1]γ//[-1 -1 1]α' | [-0.577, -0.577, 0.577]/49.5 | 0.7663 | -0.3222 | -0.5559 |
| | | | ↓ | 0.5559 | 0.7663 | 0.3222 |
| | | | 1/√3[-1, -1, 1]/49.5 | 0.3222 | -0.5559 | 0.7663 |
| 8 | | [-1 0 1]γ//[-1 1 -1]α' | [0.577, 0.577, -0.577]/10.5 | 0.9888 | 0.1108 | 0.0996 |
| | | | ↓ | -0.0996 | 0.9888 | -0.1108 |
| | | | 1/√3[1, 1, -1]/10.5 | -0.1108 | 0.0996 | 0.9888 |
| 9 | | [0 1 -1]γ//[-1 -1 1]α' | [-0.615, 0.186, -0.767]/50.5 | 0.7736 | 0.5499 | 0.3149 |
| | | | | -0.6331 | 0.6487 | 0.4224 |
| | | | | 0.028 | -0.5261 | 0.8499 |
| 10 | | [0 1 -1]γ//[-1 1 -1]α' | [-0.739, -0.463, 0.490]/50.5 | 0.8347 | -0.2535 | -0.4889 |
| | | | | 0.5024 | 0.714 | 0.4875 |
| | | | | 0.2255 | -0.6526 | 0.7234 |
| 11 | | [1 -1 0]γ//[-1 -1 1]α' | [0.933, 0.354, 0.065]/14.9 | 0.9956 | -0.0056 | 0.0931 |
| | | | | 0.0278 | 0.9706 | -0.2391 |
| | | | | -0.089 | 0.2407 | 0.9665 |
| 12 | | [1 -1 0]γ//[-1 1 -1]α' | [-0.357, 0.603, 0.714]/57.2 | 0.6001 | -0.6985 | 0.3899 |
| | | | | 0.5013 | 0.7082 | 0.4971 |
| | | | | -0.6234 | -0.1028 | 0.7751 |

$$\longrightarrow \begin{pmatrix} 2/3 & 2/3 & 1/3 \\ -1/3 & 2/3 & -2/3 \\ -2/3 & 1/3 & 2/3 \end{pmatrix}$$

$$\begin{pmatrix} (2\sqrt{6}+1)/6 & (-4+\sqrt{6})/12 & 4\sqrt{6}/12 \\ 4\sqrt{6}/12 & (7+2\sqrt{6})/12 & (5-2\sqrt{6})/12 \\ (-4+\sqrt{6})/12 & (5-2\sqrt{6})/12 & (7+2\sqrt{6})/12 \end{pmatrix}$$





## 24 Variants in Morito's Paper and the Rotation Matricises

| Variant No. | Close-packed plane parallel | Close-packed direction parallel | Rotation from Variant 1 [Axis]/Angle(deg.) | Rotation Matrix | | |
|---|---|---|---|---|---|---|
| 13 | (-1 1 1)γ//(0 1 1)α' CP3 | [-1 0 1]γ//[-1 -1 1]α' | [0.354, -0.933, -0.065]/14.9 | 0.9706 | 0.0056 | -0.2407 |
| | | | | -0.0278 | 0.9956 | -0.089 |
| | | | | 0.2391 | 0.0931 | 0.9665 |
| 14 | | [-1 0 1]γ//[-1 1 -1]α' | [-0.490, 0.463, -0.739]/50.5 | 0.7234 | 0.4875 | 0.4889 |
| | | | | -0.6526 | 0.714 | 0.2535 |
| | | | | -0.2255 | -0.5024 | 0.8347 |
| 15 | | [0 1 -1]γ//[-1 -1 1]α' | [-0.738, -0.246, 0.628]/57.2 | 0.7914 | -0.4448 | -0.4193 |
| | | | | 0.6112 | 0.5695 | 0.5496 |
| | | | | -0.0057 | -0.6913 | 0.7225 |
| 16 | | [0 1 -1]γ//[-1 1 -1]α' | [0.659, -0.659, -0.363]/20.6 | 0.9638 | 0.0999 | -0.2471 |
| | | | | -0.1555 | 0.9638 | -0.2165 |
| | | | | 0.2165 | 0.2471 | 0.9445 |
| 17 | | [1 -1 0]γ//[-1 -1 1]α' | [-0.659, 0.363, -0.659]/51.7 | 0.7848 | 0.4262 | 0.4499 |
| | | | | -0.608 | 0.6699 | 0.4262 |
| | | | | -0.1198 | -0.608 | 0.7848 |
| 18 | | [1 -1 0]γ//[-1 1 -1]α' | [-0.719, -0.302, 0.626]/47.1 | 0.8458 | -0.3892 | -0.3649 |
| | | | | 0.5279 | 0.7098 | 0.4663 |
| | | | | 0.0775 | -0.587 | 0.8058 |
| 19 | (1 1 -1)γ//(0 1 1)α' CP4 | [-1 0 1]γ//[-1 -1 1]α' | [-0.186, 0.767, 0.615]/50.5 | 0.6487 | -0.5261 | 0.5499 |
| | | | | 0.4224 | 0.8499 | 0.3149 |
| | | | | -0.6331 | 0.028 | 0.7736 |
| 20 | | [-1 0 1]γ//[-1 1 -1]α' | [0.357, 0.714, -0.603]/57.2 | 0.6001 | 0.6234 | 0.5013 |
| | | | | -0.3899 | 0.7751 | -0.4971 |
| | | | | -0.6985 | 0.1028 | 0.7082 |
| 21 | | [0 1 -1]γ//[-1 -1 1]α' | [0.955, 0.000, -0.296]/20.6 | 0.9944 | 0.1042 | -0.0181 |
| | | | | -0.1042 | 0.9361 | -0.3361 |
| | | | | -0.0181 | 0.3361 | 0.9417 |
| 22 | | [0 1 -1]γ//[-1 1 -1]α' | [-0.302, 0.626, 0.719]/47.1 | 0.7098 | -0.587 | 0.3892 |
| | | | | 0.4663 | 0.8058 | 0.3649 |
| | | | | -0.5279 | -0.0775 | 0.8458 |
| 23 | | [1 -1 0]γ//[-1 -1 1]α' | [-0.246, -0.628, -0.738]/57.2 | 0.5695 | 0.6913 | -0.4448 |
| | | | | -0.5496 | 0.7225 | 0.4193 |
| | | | | 0.6112 | 0.0057 | 0.7914 |
| 24 | | [1 -1 0]γ//[-1 1 -1]α' | [0.912, -0.410, 0.000]/21.1 | 0.9887 | -0.0251 | -0.1476 |
| | | | | -0.0251 | 0.9442 | -0.3283 |
| | | | | 0.1476 | 0.3283 | 0.933 |

A condition of the closed packed plane parallel

$$(1\ \ 1\ \ 1)_\gamma // (0\ \ 1\ \ 1)_\alpha \qquad (1)$$

The corresponding above condition of the closed packed direction parallel

$$[-1\ \ 0\ \ 1]_\gamma // [-1\ \ -1\ \ 1]_\alpha \qquad (2)$$

from Eq.(1)

$$(1\ \ 1\ \ 1)_\gamma = \{(x,y,z) \mid x+y+z=0\}$$
$$(0\ \ 1\ \ 1)_\alpha = \{(X,Y,Z) \mid X+Z=0\} \qquad (3)$$

from eq.(3)

$$\begin{pmatrix} x \\ y \\ z \end{pmatrix}_\gamma = \begin{pmatrix} -1/2 \\ -1/2 \\ 1 \end{pmatrix} \Leftrightarrow \begin{pmatrix} X \\ Y \\ Z \end{pmatrix}_\alpha = \begin{pmatrix} 0 \\ -1 \\ 1 \end{pmatrix} \qquad (4)$$

from Eq.(2)

$$[-1\ \ 0\ \ 1]_\gamma = \{(x,y,z) \mid x=-z, y=0\}$$
$$[-1\ \ -1\ \ 1]_\alpha = \{(X,Y,Z) \mid X=Y=-Z\} \qquad (5)$$

from eq. (5)

$$\begin{pmatrix} x \\ y \\ z \end{pmatrix}_\gamma = \begin{pmatrix} -1 \\ 0 \\ 1 \end{pmatrix} \Leftrightarrow \begin{pmatrix} X \\ Y \\ Z \end{pmatrix}_\alpha = \begin{pmatrix} -1 \\ -1 \\ 1 \end{pmatrix} \qquad (6)$$

Since eq. (1) and eq. (2) are a rotation along the common a axis,

$$\begin{pmatrix} x \\ y \\ z \end{pmatrix}_\gamma = \begin{pmatrix} 0 \\ 0 \\ 1 \end{pmatrix} \Leftrightarrow \begin{pmatrix} X \\ Y \\ Z \end{pmatrix}_\alpha = \begin{pmatrix} 0 \\ 0 \\ 1 \end{pmatrix} \qquad (7)$$

森戸茂一

KS orientation variants

| Variant No. | Close-packed plane parallel | Close-packed direction parallel | Rotation from Variant 1 [Axis] / Angle [deg.] |
|---|---|---|---|
| 01 | | [101]γ//[111]α | [–,–,–]/– |
| 02 | | [101]γ//[111]α | [0.577,0.577,0.577]/60.0 |
| 03 | (111)γ//(011)α CPI | [011]γ//[111]α | [0.000,0.707,0.707]/60.0 |
| 04 | | [011]γ//[111]α | [0.000,0.707,0.707]/10.5 |
| 05 | | [1$\bar{1}$0]γ//[111]α | [0.000,0.707,0.707]/60.0 |
| 06 | | [1$\bar{1}$0]γ//[111]α | [0.000,0.707,0.707]/49.5 |

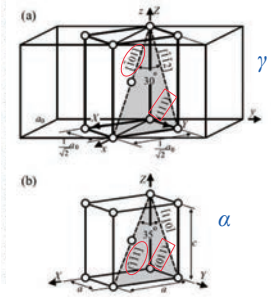


The $(x\ y\ z)_\gamma^{\mathrm{t}}$ and $(X\ Y\ Z)_\alpha^{\mathrm{t}}$ in these correspondences are not determined uniquely.

How do we determine the rotation matrix of the variant?

Thank you for your attention!

# Phase-field simulations of dendrite solidification and grain growth

**Tomohiro Takaki**

Kyoto Institute of Technology

Phase-field studies of dendrite growth and grain growth are introduces. In the dendrite growth, the competitive growth among multiple dendrites is investigated. In the grain growth, the true behaviors of ideal grain growth are investigated by the very-large simulation.

結晶の界面、転位、構造の数理　Mathematics in Interface, Dislocation and Structure of Crystals
2017年8月28日　九州大学 西新プラザ 大会議室AB

# デンドライト凝固と粒成長の フェーズフィールドシミュレーション
# Phase-field simulations of dendrite solidification and grain growth


**高木 知弘**　**Tomohiro Takaki**

機械工学系　Faculty of Mechanical Engineering
京都工芸繊維大学　Kyoto Institute of Technology


*KIT Computational Materials Design Lab.*

## Overview

1. Phase-field method
2. Necessity of large-scale simulation for solidification and grain growth
3. Parallel computation by a GPU supercomputer
4. Simulation examples
   * Dendrite competitive growth in directional solidification
   * Ideal grain growth
5. Conclusions

*KIT Computational Materials Design Lab.*

## Overview

1. Phase-field method
2. Necessity of large-scale simulation for solidification and grain growth
3. Parallel computation by a GPU supercomputer
4. Simulation examples
   * Dendrite competitive growth in directional solidification
   * Ideal grain growth
5. Conclusions

*KIT Computational Materials Design Lab.*

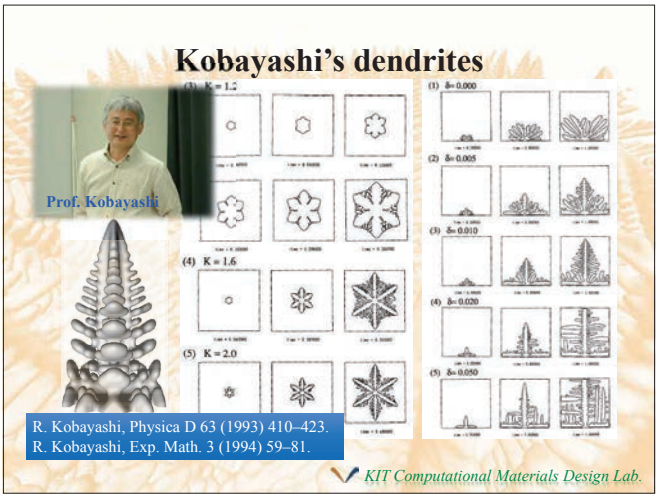
Kobayashi's dendrites
Prof. Kobayashi
(4) K = 1.6
(5) K = 2.0
(1) δ= 0.000
(2) δ= 0.005
(3) δ= 0.010
(4) δ= 0.020
(5) δ= 0.050
R. Kobayashi, Physica D 63 (1993) 410–423.
R. Kobayashi, Exp. Math. 3 (1994) 59–81.
KIT Computational Materials Design Lab.

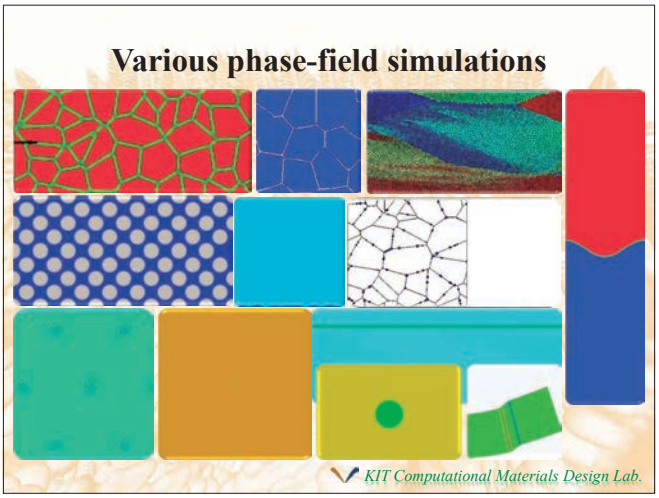
Various phase-field simulations
KIT Computational Materials Design Lab.

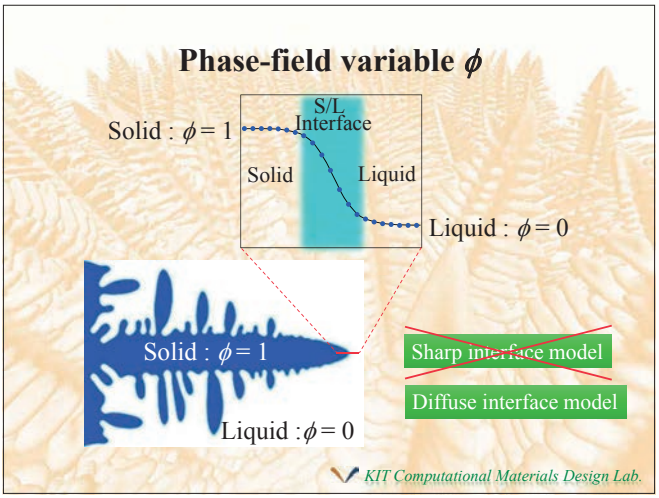
Phase-field variable $\phi$
Solid : $\phi = 1$
S/L Interface
Solid
Liquid
Liquid : $\phi = 0$
Solid : $\phi = 1$
Liquid : $\phi = 0$
Sharp interface model
Diffuse interface model
KIT Computational Materials Design Lab.

## Free energy functional

$$F = \int f dV$$

Free energy density $f = f_{chem} + f_{doub} + f_{grad}$

**Chemical free energy density**

$$f_{chem} = p(\phi) f_a + (1 - p(\phi)) f_b$$

$p(\phi)$ : energy distribution function

**Bulk energy density**

$$\begin{cases} p(\phi) = \phi^2(3 - 2\phi) \quad \text{or} \\ p(\phi) = \phi^3(10 - 15\phi + 6\phi^2) \end{cases}$$

**Double well potential**

$$f_{doub} = W q(\phi)$$

$q(\phi)$ : double well function $\quad q(\phi) = \phi^2(1-\phi)^2$

$W$ : height of energy wall

**Gradient energy density**

$$f_{grad} = \frac{a^2}{2} |\nabla \phi|^2$$

$a$ : gradient coefficient

**Interface energy density**

KIT Computational Materials Design Lab.

## Time evolution equation

Phase-field variable : $\phi$

**Non-conserved value**

**Allen-Cahn equation**

$$\frac{\partial \phi}{\partial t} = -M_\phi \frac{\delta F}{\delta \phi}$$

**Conserved value**

**Cahn-Hilliard equation**

$$\frac{\partial \phi}{\partial t} = \nabla \cdot \left[ M_\phi \left( \nabla \frac{\delta F}{\delta \phi} \right) \right]$$

Second law of thermodynamics

KIT Computational Materials Design Lab.

## Simplest AC type phase-field equation

$$\frac{\partial \phi}{\partial t} = M\gamma \left[ \nabla^2 \phi + \frac{8}{\delta^2} \phi(1-\phi) \left( \phi - \frac{1}{2} + \frac{\delta}{4\gamma} \Delta f \right) \right]$$

$M$ : Interface mobility
$\gamma$ : Interface energy
$\delta$ : Interface thickness
$\Delta f$ : free energy difference
(thermochemical driving force)

Evolution of phase-field $\phi$


Interface migration (contour line of $\phi = 0.5$)

KIT Computational Materials Design Lab.

## Advantages of phase-field method

- Smooth interface morphology can be expressed, because the phase-field method is a diffuse interface model.
- There is no need to track the interface position, because the interface migration is expressed by solving a reaction-diffusion equation numerically.
- Therefore, the complicated morphological changes can be expressed relatively easily.
- The time evolution equation can be derived based on the second low of thermodynamics. This means that the phase-field method is a thermodynamically sound method.
- The time evolution equation is reduced to the simple reaction-diffusion equation. Therefore, we can use a simple discretization method.
- The curvature effect is naturally included in the time evolution equation.

*KIT Computational Materials Design Lab.*

## Overview

1. Phase-field method
2. Necessity of large-scale simulation for solidification and grain growth
3. Parallel computation by a GPU supercomputer
4. Simulation examples
   * Dendrite competitive growth in directional solidification
   * Ideal grain growth
5. Conclusions

*KIT Computational Materials Design Lab.*

## Dendrite and solidification structure

Single dendrite | Multiple dendrites | Multiple grains | Solidification structure

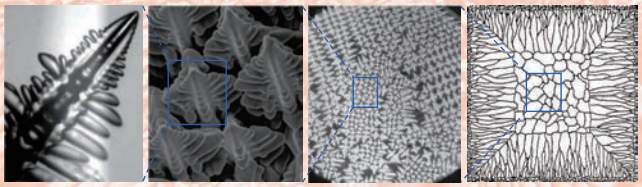

EPL, 68 (2004) 240 | Science, 257 (1992) 497 | Metall. Trans. A, 15 (1984) 1665 | Trans. AIME, 239 (1967) 1620

Competitive growth among multiple dendrites and multiple grains

*KIT Computational Materials Design Lab.*

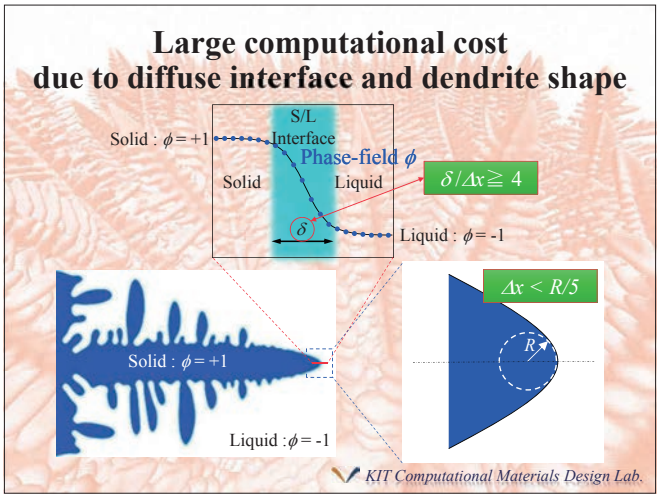
Large computational cost
due to diffuse interface and dendrite shape
S/L
Interface
Solid : $\phi = +1$
Phase-field $\phi$
Solid
Liquid
$\delta / \Delta x \geqq 4$
$\delta$
Liquid : $\phi = -1$
Solid : $\phi = +1$
Liquid : $\phi = -1$
$\Delta x < R/5$
$R$
KIT Computational Materials Design Lab.

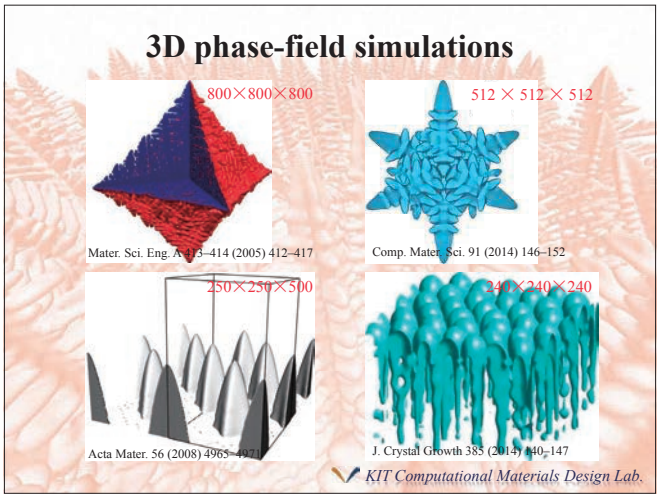
3D phase-field simulations
800×800×800
Mater. Sci. Eng. A 413–414 (2005) 412–417
512 × 512 × 512
Comp. Mater. Sci. 91 (2014) 146–152
250×250×500
Acta Mater. 56 (2008) 4965–4971
240×240×240
J. Crystal Growth 385 (2014) 140–147
KIT Computational Materials Design Lab.

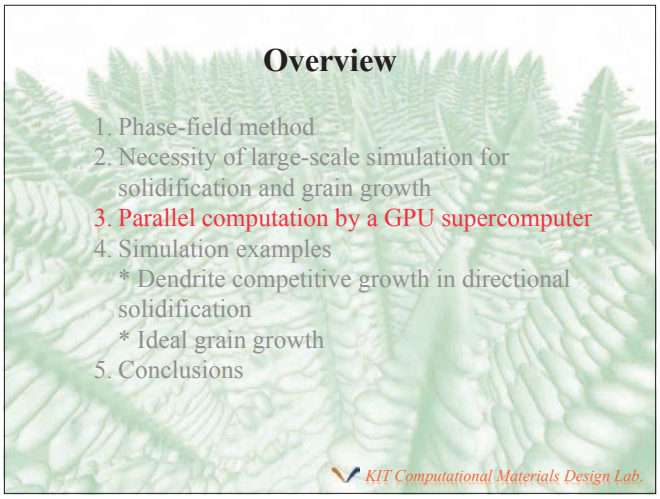
Overview
1. Phase-field method
2. Necessity of large-scale simulation for solidification and grain growth
3. Parallel computation by a GPU supercomputer
4. Simulation examples
* Dendrite competitive growth in directional solidification
* Ideal grain growth
5. Conclusions
KIT Computational Materials Design Lab.

## GPU supercomputer TSUBAME2.5

**Tokyo Institute of Technology**

1408 nodes
1 node = 3 GPU + 2 CPU
1408 × 3 = **4224 GPU**
GPU : NVIDIA Tesla K20X
CPU : Intel Xeon X5670

*KIT Computational Materials Design Lab.*

## GPU : Graphics Processing Unit

GPGPU : General-purpose computing on graphics processing units

**KEY FEATURES**

- Number of processor cores: 2,688
- Processor core clock: 732 MHz
- Package size: 45 mm × 45 mm 2397-pin ball grid array (S-FCBGA)

Board

- PCI Express Gen2 ×16 system interface
- Physical dimensions: 4.376 inches × 10.5 inches, dual-slot

Display Connectors

- None

NVIDIA
TESLA K20X


*KIT Computational Materials Design Lab.*

## Schematic illustration of parallelization

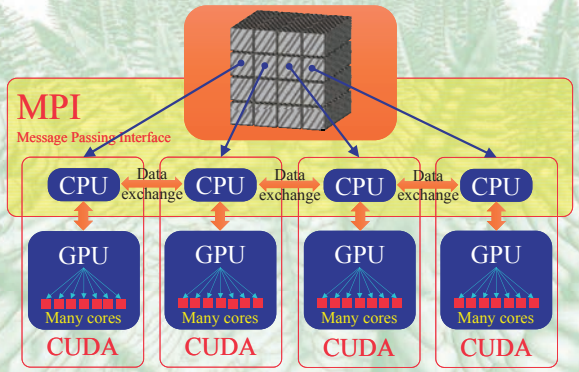


CUDA : Compute Unified Device Architecture (parallel computing platform)

*KIT Computational Materials Design Lab.*

## Overview

1. Phase-field method
2. Necessity of large-scale simulation for solidification and grain growth
3. Parallel computation by a GPU supercomputer
4. Simulation examples
   * Dendrite competitive growth in directional solidification
   * Ideal grain growth
5. Conclusions

*KIT Computational Materials Design Lab.*


## Overview

1. Phase-field method
2. Necessity of large-scale simulation for solidification and grain growth
3. Parallel computation by a GPU supercomputer
4. Simulation examples
   * Dendrite competitive growth in directional solidification
   * Ideal grain growth
5. Conclusions

*KIT Computational Materials Design Lab.*


## Primary arm array during directional solidification of a single-crystal binary alloy: Large-scale phase-field study


Contents lists available at ScienceDirect

Acta Materialia

journal homepage: www.elsevier.com/locate/actamat

ELSEVIER

Full length article


Primary arm array during directional solidification of a single-crystal binary alloy: Large-scale phase-field study


Tomohiro Takaki [a,*], Shinji Sakane [b], Munekazu Ohno [c], Yasushi Shibuta [d], Takashi Shimokawabe [e], Takayuki Aoki [e]

[a] Faculty of Mechanical Engineering, Kyoto Institute of Technology, Matsugasaki, Sakyo-ku, Kyoto 606-8585, Japan
[b] Graduate School of Science and Technology, Kyoto Institute of Technology, Matsugasaki, Sakyo-ku, Kyoto 606-8585, Japan
[c] Division of Materials Science and Engineering, Faculty of Engineering, Hokkaido University, Kita 13 Nishi 8, Kita-ku, Sapporo 060-8628, Japan
[d] Department of Materials Engineering, The University of Tokyo, 7-3-1 Hongo, Bunkyo-ku, Tokyo 113-8656, Japan
[e] Global Scientific Information and Computing Center, Tokyo Institute of Technology, 2-12-1-i7-3, Ookayama, Meguro-ku, Tokyo 152-8550, Japan



*KIT Computational Materials Design Lab.*

## Primary arm array of columnar dendrites

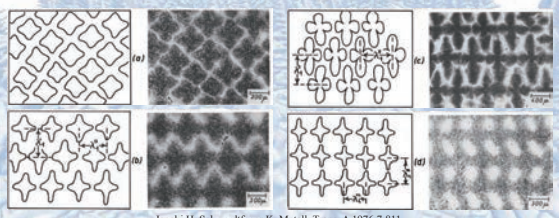

Jacobi H, Schwerdtfeger K. Metall. Trans. A 1976;7:811.

- Micro-segregation
- Permeability

*KIT Computational Materials Design Lab.*

## Quantitative phase-field model

M. Ohno, K. Matsuura
Quantitative phase-field modeling for dilute alloy solidification involving diffusion in the solid.
Phys. Rev. E, 79 031603 (2009)

*KIT Computational Materials Design Lab.*

## Variables

$\phi$

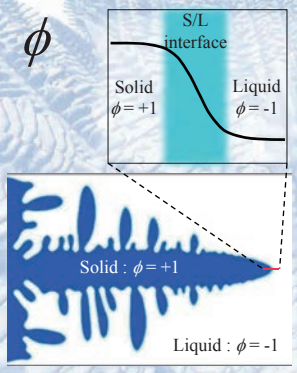


$u$

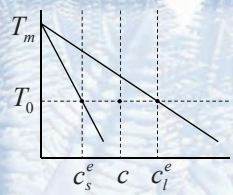


$$u = \frac{c_l - c_l^e}{c_l^e - c_s^e}$$

*KIT Computational Materials Design Lab.*

# Time evolution equations for directional solidification of binary alloy

Temperature $T(z) = T_0 + G(z - V_p t)$ Frozen temperature approximation

Phase-field [$\phi$ = +1 in solid & $\phi$ = -1 in liquid]

$$\tau(\nabla\phi)\left[1-(1-k)u'\right]\frac{\partial\phi}{\partial t} = \nabla\cdot\left[W(\nabla\phi)^2\nabla\phi\right] - \frac{df(\phi)}{d\phi} - \lambda^*\frac{dg(\phi)}{d\phi}(u+u')$$
$$+\frac{\partial}{\partial x}\left[W(\nabla\phi)\frac{\partial W(\nabla\phi)}{\partial\phi_{,x}}|\nabla\phi|^2\right] + \frac{\partial}{\partial y}\left[W(\nabla\phi)\frac{\partial W(\nabla\phi)}{\partial\phi_{,y}}|\nabla\phi|^2\right] + \frac{\partial}{\partial z}\left[W(\nabla\phi)\frac{\partial W(\nabla\phi)}{\partial\phi_{,z}}|\nabla\phi|^2\right]$$

$$u' = \frac{y - V_p t}{l_T}$$

Solute concentration [$u = (c_l - c_l^e)/(c_l^e - c_s^e)$]

$$\frac{1}{2}\left[1+k-(1-k)\phi\right]\frac{\partial u}{\partial t} = \nabla\cdot\left[D_L q(\phi)\nabla u - \mathbf{J}_{AT}\right] + \frac{1}{2}\left[1+(1-k)u\right]\frac{\partial\phi}{\partial t} - \nabla\cdot\mathbf{J}$$

KIT Computational Materials Design Lab.

# Computational conditions

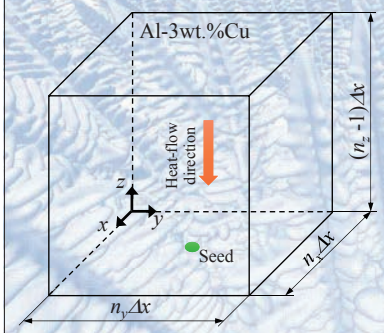


$V_p$ = 100 μm/s
$G$ = 5, 10, 20, 50, 100, 200 K/mm

For $G$ = 10, 20, 50, 100, 200 K/mm
$n_x \times n_y \times n_z$ = 1024×1024×1024
$\Delta x$ = 0.75 μm
0.77×0.77×0.77 mm³
256 GPU

For $G$ = 5 K/mm
$n_x \times n_y \times n_z$ = 1536×1536×1024
$\Delta x$ = 0.75 μm
1.15×1.15×0.77 mm³
512 GPU

Total time step = $10^7$ steps
$\Delta t = 2.6785716 \times 10^{-5}$ s
$t_{total}$ = 267.9 s (4.46 min)
$l_{total} = V_p \times t_{total}$ = 26.9 cm
Execution time ≈ one week

KIT Computational Materials Design Lab.

3 4 5 6 7 8 9

# Time changes in Voronoi decomposition

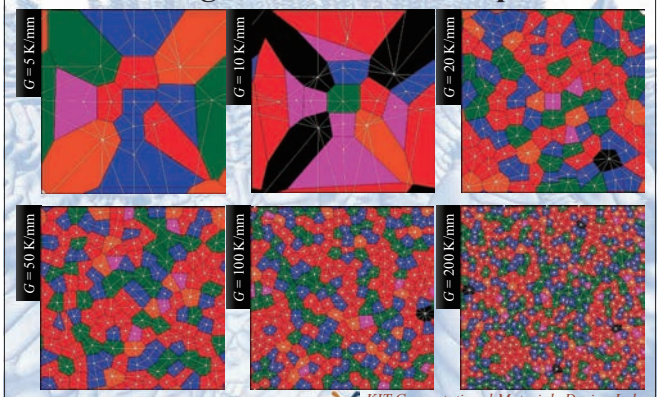


KIT Computational Materials Design Lab.

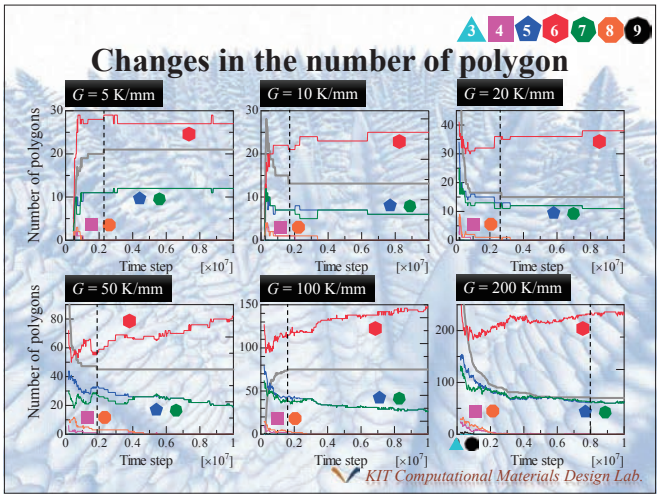


## Overview

1. Phase-field method
2. Necessity of large-scale simulation for solidification and grain growth
3. Parallel computation by a GPU supercomputer
4. Simulation examples
   * Dendrite competitive growth in directional solidification
   * Ideal grain growth
5. Conclusions

KIT Computational Materials Design Lab.

## Grain growth (GG)

Normal GG

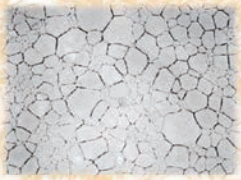

Ideal GG

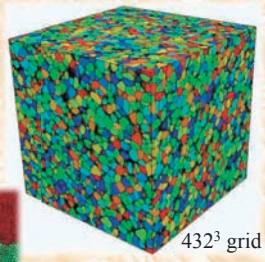

$432^3$ grid

Abnormal GG

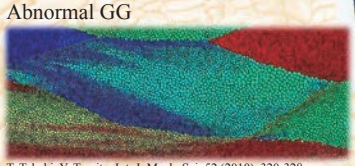

T. Takaki, Y. Tomita, Int. J. Mech. Sci. 52 (2010) 320-328.

KIT Computational Materials Design Lab.

# Very-large-scale multi-phase-field simulation for elucidating the authentic statistical behaviors of the ideal grain growth


npj | Computational Materials

www.nature.com/npjcompumats

ARTICLE OPEN

Ultra-large-scale phase-field simulation study of ideal grain growth

Eisuke Miyoshi[1], Tomohiro Takaki[2], Munekazu Ohno[3], Yasushi Shibuta[4], Shinji Sakane[1], Takashi Shimokawabe[5] and Takayuki Aoki[6]

Grain growth, a competitive growth of crystal grains accompanied by curvature-driven boundary migration, is one of the most fundamental phenomena in the context of metallurgy and other scientific disciplines. However, the true picture of grain growth is still controversial, even for the simplest (or 'ideal') case. This problem can be addressed only by large-scale numerical simulation. Here, we analyze ideal grain growth via ultra-large-scale phase-field simulations on a supercomputer for elucidating the corresponding authentic statistical behaviors. The performed simulations are more than ten times larger in time and space than the ones previously considered as the largest; this computational scale gives a strong indication of the achievement of true steady-state growth with statistically sufficient number of grains. Moreover, we provide a comprehensive theoretical description of ideal grain growth behaviors correctly quantified by the present simulations. Our findings provide conclusive knowledge on ideal grain growth, establishing a platform for studying more realistic growth processes.

*npj Computational Materials* (2017)3:25; doi:10.1038/s41524-017-0029-8

*KIT Computational Materials Design Lab.*

# Multi-phase-field (MPF) model

I. Steinbach, F. Pezzolla, Physica D, 134 (1999) 385-393

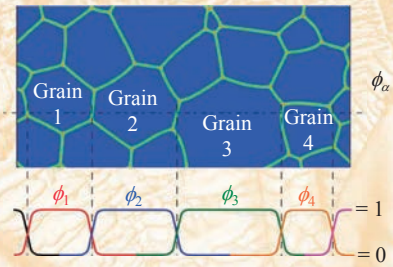


$$\phi_\alpha = \begin{cases} 1 & : \text{in } \alpha\text{th grain} \\ 0 & : \text{in other grains} \end{cases}$$

*KIT Computational Materials Design Lab.*

# MPF model (cont.)

I. Steinbach, F. Pezzolla, Physica D, 134 (1999) 385-393

**Free energy functional**

$$F = \int_V \sum_{\alpha=1}^{N} \sum_{\beta=\alpha+1}^{N} \left[ -\frac{a_{\alpha\beta}^2}{2} \nabla\phi_\alpha \cdot \nabla\phi_\beta + W_\alpha \phi_\alpha \phi_\beta \right] \mathrm{d}V$$

**Time evolution equation**

$$\frac{\partial \phi_i}{\partial t} = -\frac{2}{n} \sum_{j=1}^{n} M_{ij}^{\phi} \left( \frac{\delta F}{\delta \phi_i} - \frac{\delta F}{\delta \phi_j} \right) \Leftarrow \sum_{\alpha=1}^{N} \phi_\alpha = 1 \quad \text{(constraint condition)}$$

$$= \frac{2}{n} \sum_{j=1}^{n} M_{ij}^{\phi} \sum_{k=1}^{n} \left[ \frac{1}{2} \left( a_{jk}^2 - a_{ik}^2 \right) \nabla^2 \phi_k + \left( W_{jk} - W_{ik} \right) \phi_k \right]$$

**Phase-field parameters**

$$a_{ij} = \frac{2}{\pi} \sqrt{2\delta\gamma}, \quad W_{ij} = \frac{4\gamma}{\delta}, \quad M_{ij}^{\phi} = \frac{\pi^2}{8\delta} M$$

$\delta$: GB thickness
$\gamma$: GB energy
$M$: GB mobility

*KIT Computational Materials Design Lab.*

# Computational conditions

Dimensionless parameter

GB energy $\gamma = 1$
GB mobility $M = 1$
Time increment $\Delta t = 0.075$
Grid size $\Delta x = 1$

GB thickness $\delta = 6$
Total time step = 100000
Initial grain size :
$R_{ini} = 10.86$, $V_{ini} = 17.51^3$

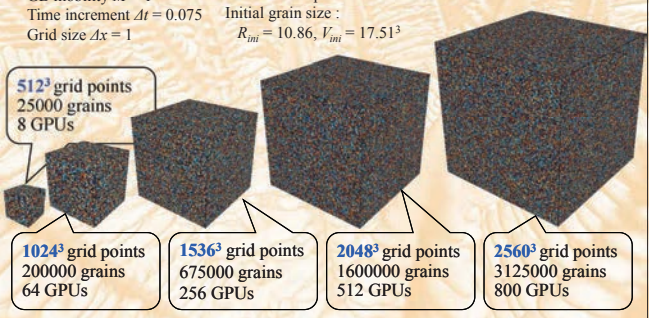


KIT Computational Materials Design Lab.

# Grain size distribution

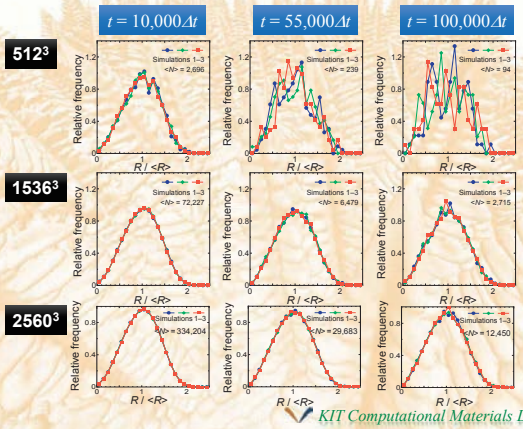


KIT Computational Materials Design Lab.

# Maximum difference in three replicated simulations

$$\delta_{\max} = \max\left\{ \left| DP(i,m) - DP(i,n) \right| \;\middle|\; i = 1, 2, 3, \cdots ;\ m, n = 1, 2, 3 \right\}$$

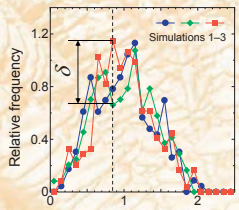


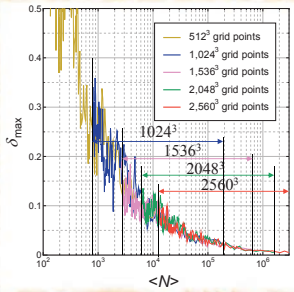


KIT Computational Materials Design Lab.

## Variations of $\delta_{max}$ and $N$

**$2560^3$**

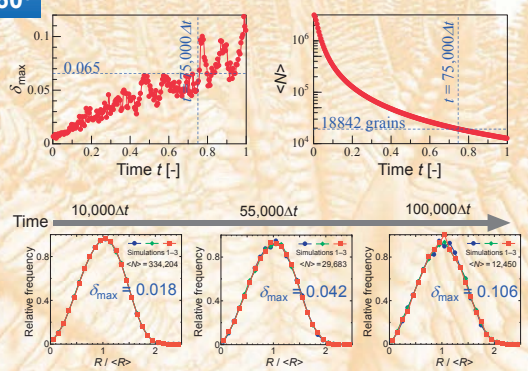


KIT Computational Materials Design Lab.

## Temporal evolution of grain size distribution

**$2560^3$**

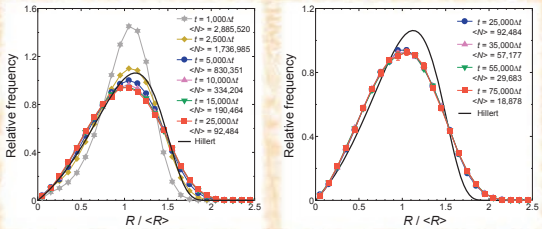


Grain size distribution is same in $t \geqq 35000\Delta t$.

KIT Computational Materials Design Lab.

## Steady state regime of ideal grain growth

$2560^3$ grid points (3125000 initial grains)

$35{,}000\Delta t \leqq t \leqq 75{,}000\Delta t$

(57,114 grains) (18,842 grains)

1.8 % 0.6 %

Steady state condition is thought to be a regime from <u>the end of initial relaxation</u> to <u>the point where the remaining grains is about 20,000</u>.

KIT Computational Materials Design Lab.

## Overview

1. Phase-field method
2. Necessity of large-scale simulation for solidification and grain growth
3. Parallel computation by a GPU supercomputer
4. Simulation examples
   * Dendrite competitive growth in directional solidification
   * Ideal grain growth
5. Conclusions

*KIT Computational Materials Design Lab.*

## Conclusions

- For a highly accurate prediction of solidification microstructure, it is essential to investigate a system with the multiple multiple dendrites and multiple grains.
- Phase-field method is the most accurate prediction method of dendrite structures. However, its high computational cost is a drawback.
- Large-scale phase-field simulation by parallel GPU computation is a powerful tool for the highly accurate prediction of solidification microstructure.

*KIT Computational Materials Design Lab.*

# Numerical analysis of moving interfaces: the level-set and phase-field approaches

**Karel Svadlenka**
Kyoto University

There are several well-established efficient numerical methods for simple interfaces evolving according to various rules, such as the curve-shortening flow or surface diffusion. Recently, the focus of researchers in this field has shifted towards numerical solution of interfacial networks with junctions, especially in the anisotropic or non-symmetric setting (for example, different surfaces tensions for each interface in the mean curvature flow).

In this talk, I will briefly review the two basic approaches to evolving interfaces that can be extended to the multiphase anisotropic/non-symmetric case including topological changes: the phase-field method and the level-set method (in particular, its simplified version proposed by Merriman, Bence and Osher). I will present an overview of the state of the art methodologies and their range of applicability, mentioning also some results of my own.

## References

[1] K. Svadlenka, E. Ginder, S. Omata: A variational method for multiphase volume-preserving interface motions, Journal of Computational and Applied Mathematics, Vol. 257, pp. 157-179, 2014.
[2] Nur Shofianah, R.Z. Mohammad, K. Svadlenka: Simulation of triple junction motion with arbitrary surface tensions, IAENG International Journal of Applied Mathematics, Vol. 45, No. 3, pp. 235-244, 2015.
[3] R.Z. Mohammad, K. Svadlenka, Multiphase volume-preserving interface motions via localized signed distance vector scheme, Discrete and Continuous Dynamical Systems - Series S, Vol. 8, No. 1, pp. 969-988, 2015.
[4] E. Ginder, K. Svadlenka, Wave-type threshold dynamics and the hyperbolic mean curvature flow, Japan J. Indust. Appl. Math. 33(2), pp. 501-523, 2016.
[5] H. Garcke: Curvature driven interface evolution, preprint.

# Numerical analysis of moving interfaces: the level-set and phase-field approaches

Karel Svadlenka, Kyoto University

**Mathematics in Interface, Dislocation and Structure of Crystals**
August 28-30, 2017
Kyushu University, Nishijin Plaza

## Outline

1) Interface evolution (in physical models)
2) Generalizations of interface evolution
   - anisotropy
   - multiphase
3) Overview of numerical approaches
4) Remarks on their extensions
   - anisotropy
   - multiphase

## Types of interface motion

1) Mean curvature flow
2) Volume-preserving mean curvature flow
3) Surface diffusion
4) Mullins-Sekerka model
5) Stefan problem
6) Hyperbolic mean curvature flow

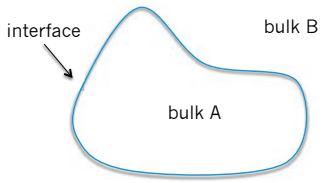

## Gradient flows

**Finite dimension ($\mathbb{R}^n$)**

- Gradient of a function $\Phi : \mathbb{R}^n \to \mathbb{R}$ is defined by

$$D\Phi_{x_0}(v) = (\nabla\Phi(x_0)) \cdot v \quad \forall v \in \mathbb{R}^n$$

directional derivative  gradient

- Gradient flow:

$$x'(t) = -\nabla\Phi(x(t))$$

- Properties:
  - $\frac{d}{dt}\Phi(x(t)) = -\|\nabla\Phi(x(t))\|^2 \leq 0$
  - among all possible directions, $-\nabla\Phi(x(0))$ decreases $\Phi$ most efficiently

**Manifold and Hilbert space**

- Gradient of a function $\Phi : M \to \mathbb{R}$ from a $n$-dim Riemannian manifold $M$ defined by

$$D_x\Phi(v) = \langle \nabla_M \Phi(x), v \rangle \quad \forall v \in T_x M$$

Gateaux derivative  gradient  tangent space at $x \in M$

$\langle \cdot, \cdot \rangle$ ... metric on $T_x M$

- Gradient flow:

$$x'(t) = -\nabla_M \Phi(x(t))$$

- Properties: the same
- Hilbert space: replace metric by inner product

## Example of gradient flow


- Area functional $E(\Gamma) = \int_\Gamma 1 \, d\mathcal{H}^{d-1} = \mathcal{H}^{d-1}(\Gamma)$

$\Gamma$ ... smooth, compact hypersurface in $\mathbb{R}^d$ without boundary

- Directional derivative

$\Gamma_t := \{x + t\zeta(x);\ x \in \Gamma\}, \quad t \in \mathbb{R}$

$\zeta : \mathbb{R}^d \to \mathbb{R}^d$ ... smooth vector field

$$\frac{d}{dt}E(\Gamma_t)\Big|_{t=0} = -\int_\Gamma \kappa V \, d\mathcal{H}^{d-1}$$

$\kappa$ ... mean curvature

$V = \zeta \cdot \nu$ ... normal velocity

- Inner product $\langle u, v \rangle_{L^2} := \int_\Gamma uv \, d\mathcal{H}^{d-1} \quad \forall u, v \in T_\Gamma \mathcal{M}$

tangent space of normal velocities

- Gradient has to satisfy

$$\langle \nabla_{\mathcal{M}} E, V \rangle_{L^2} = \frac{d}{dt}E(\Gamma_t)\Big|_{t=0} = -\int_\Gamma \kappa V \, d\mathcal{H}^{d-1}$$

- so $\nabla_{\mathcal{M}} E = -\kappa$ and the gradient flow is $V = \kappa$

## 1) Mean curvature flow

- Gradient flow of the surface energy with respect to the $L^2$-inner product

$$\boxed{V = \kappa}$$

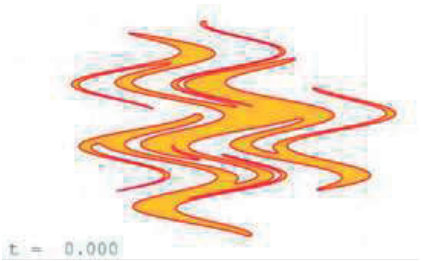


S.Angenent

## 1) Mean curvature flow: properties

- Embedded curve in the plane evolving under mean curv. flow will *become convex* in finite time [Grayson, 1987].
- A convex hypersurface in $\mathbb{R}^d$ will *shrink to a point* in finite time, asymptotically converging to a sphere [Gage & Hamilton, 1986] [Huisken, 1984].
- *Self-intersections* during the flow are not possible. Moreover, if initially one surface is contained in another, this property will be true for all later times (by maximum and comparison principles, [Ecker, 2008]).
- Nonconvex surfaces in general can develop *singularities* [Huisken, 1990, 1993].

R. Nürnberg

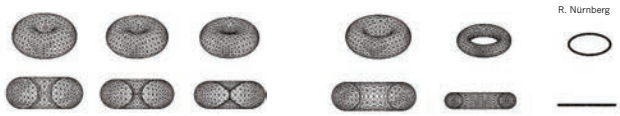

## 1) Mean curvature flow: applications

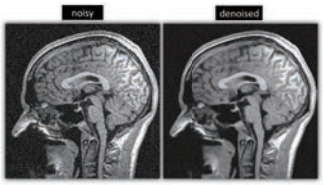


Image processing

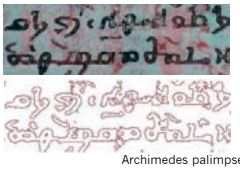

Archimedes palimpsest

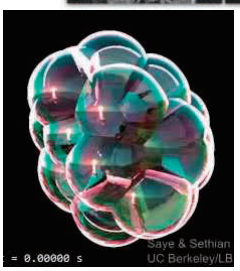


Soap films

Sethian & Saye

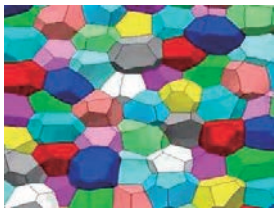

Grain boundaries

## 2) Volume-preserving curvature flow

- $\mathcal{M}_m$ ... hypersurfaces enclosing volume *m*
- Tangent space $T_\Gamma \mathcal{M}_m$ corresponds to normal velocities with zero mean because

$$\frac{d}{dt}\mathrm{vol}(\Gamma_t) = \int_{\Gamma_t} V \, d\mathcal{H}^{d-1}$$

- Gradient for $L^2$-inner product:

$$\langle \nabla_{\mathcal{M}_m} E, v \rangle = -\int_\Gamma \kappa v \, d\mathcal{H}^{d-1} \quad \forall v \in T_\Gamma \mathcal{M}_m$$

so because gradient has zero mean,

$$\nabla_{\mathcal{M}_m} E = -\kappa + \overline{\kappa}$$

$\overline{\kappa}$ ... average curvature on $\Gamma$

- Gradient flow:

$$\boxed{V = \kappa - \overline{\kappa}}$$

## 3) Surface diffusion

- Again consider $\mathcal{M}_m$ but now with $H^{-1}$-inner product on $T_\Gamma \mathcal{M}_m$ defined by

$$\langle u, v \rangle_{H^{-1}} := \int_\Gamma u(-\Delta_\Gamma)^{-1} v \, d\mathcal{H}^{d-1}$$

$\Delta_\Gamma$ ... surface Laplacian

- Gradient of area

$$\langle v, \nabla_{H^{-1}} E \rangle_{H^{-1}} = \int_\Gamma v(-\Delta_\Gamma)^{-1} \nabla_{H^{-1}} E \, d\mathcal{H}^{d-1} = -\int_\Gamma v\kappa \, d\mathcal{H}^{d-1}$$

$$\nabla_{H^{-1}} E = \Delta_\Gamma \kappa$$

- Gradient flow $\boxed{V = -\Delta_\Gamma \kappa}$

In physics this equation is derived from mass conservation laws using appropriate constitutive assumptions [Mullins, 1957].
It models phase transformation due to diffusion along the interface.

## 3) Surface diffusion: properties

- Volume preserving, area decreasing:

$$\frac{d}{dt}\mathrm{Volume}(\Gamma_t) = 0, \quad \frac{d}{dt}\mathrm{Area}(\Gamma_t) \leq 0$$

- Stability near spheres [Escher et al., 1998]
- If flow exists for all times, it converges to a sphere [Elliott & Garcke, 1997].
- Self-intersections are possible [Giga & Ito,1998].
- Does not preserve convexity [Giga & Ito, 1999].
- Singularities may appear.

R. Nürnberg

## 3) Surface diffusion: applications

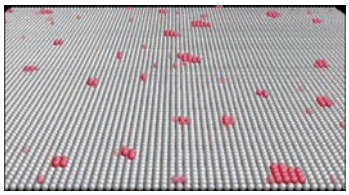

V.Kaganer & R.Shayduk

Epitaxial growth
(nanotechnology, semiconductor fabrication)

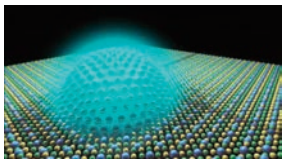

S.Kelley

Quantum dots

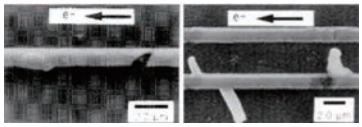

Nix, 1992

Electromigration of voids
in (micro)electrical circuits

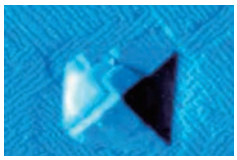

Bauer, 1999

## 4) Mullins-Sekerka problem

- Decrease of area limited by diffusion – expressed by the inner product

$$\langle v_1, v_2 \rangle_{MS} := \int_{\Omega_A \cup \Omega_B} \nabla u_1 \cdot \nabla u_2 \, dx = \int_\Gamma v_1 u_2 \, d\mathcal{H}^{d-1}$$

where $-\Delta u_i = v_i \delta_\Gamma$

- Leads to

$$\begin{aligned} -\Delta u &= 0 && \text{in } \Omega_A(t) \cup \Omega_B(t) \\ V &= -[\nabla u]_A^B \cdot \nu && \text{on } \Gamma_t \\ u &= \kappa && \text{on } \Gamma_t \end{aligned}$$

In physics, these equations are derived from conservation laws based on the principles of thermodynamics.

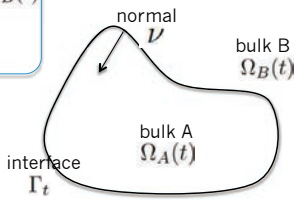


## 4) Mullins-Sekerka problem: properties

- Volume preserving, area decreasing:

$$\frac{d}{dt}\text{Volume}(\Omega_B(t)) = 0, \quad \frac{d}{dt}\text{Area}(\Gamma_t) \leq 0$$

- Oswald ripening: mean particle size grows as $t^{1/3}$, evolution laws for particle size distribution derived.

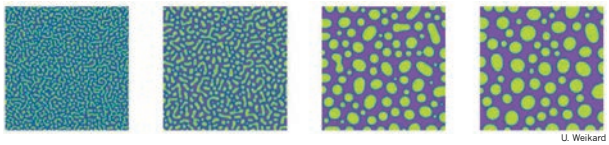

U. Weikard

- Existence of solution difficult (results in weak setting).

## 5) Stefan problem

- Describes undercooled solidification.

$$\begin{aligned} u_t &= d_i \Delta u && \text{in } \Omega_i(t) \ \text{ for } i = A, B \\ \lambda V &= -[d \nabla u]_A^B \cdot \nu && \text{on } \Gamma_t \\ \alpha u + \beta V &= \kappa && \text{on } \Gamma_t \quad \text{(Gibbs-Thomson law)} \end{aligned}$$

- Can be written as gradient flow too.

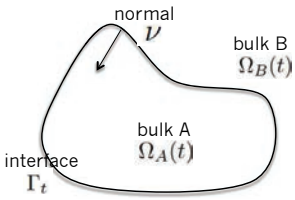

## 6) Hyperbolic mean curvature flow

**Notation**

- Family of closed curves

$$\gamma(t,\vartheta) : [0,T] \times [0,\ell] \to \mathbb{R}^2$$

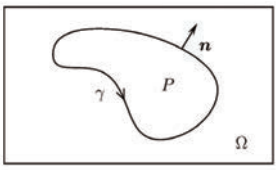


Velocity of curve

$$v\boldsymbol{n} + w\boldsymbol{t}$$

Acceleration of curve

$$a\boldsymbol{n} + b\boldsymbol{t}$$

Energy density

$$e = \frac{\rho}{2}|\gamma_t|^2 + \tau$$

$\boldsymbol{t} = \frac{\gamma'}{|\gamma'|}$ ... unit tangential vector

$\boldsymbol{n} = \frac{1}{|\gamma'|}(-\gamma_2', \gamma_1')$ ... unit normal vector

$\kappa = \frac{-\gamma_1''\gamma_2' + \gamma_2''\gamma_1'}{|\gamma'|^3}$ ... curvature

## 6) Hyperbolic mean curvature flow

- Action of internal and kinetic energy

$$\int_0^T \int_{\gamma(t)} \left(\frac{\rho}{2}|\gamma_t|^2 - 1\right) d\mathcal{H}^{d-1}\, dt$$

- Stationary points satisfy

$$\rho\gamma_{tt} + \left(\rho\frac{w'v}{|\gamma'|} + \left(\tfrac{\rho}{2}(v^2 - w^2) + 1\right)\kappa\right)\boldsymbol{n} + \frac{1}{|\gamma'|}\left(e' + \rho(w' + \kappa v|\gamma'|)w\right)\boldsymbol{t} = \boldsymbol{0}$$

- Assuming normal flow ( *w=0* )

$$\boxed{\rho\gamma_{tt} - e\kappa\boldsymbol{n} + \frac{e'}{|\gamma'|}\boldsymbol{t} = \boldsymbol{0}}$$

**Remark** *(normal flow)*

- For tangential velocity $\tilde{w} = \gamma_t \cdot \gamma'$

$$(\tilde{w}ds)_t = 0$$

➡ flow is normal for all times if the initial velocity is normal

## 6) Hyperbolic MCF: properties

- Normal flow property is preserved in time.
- Energy is preserved (globally and for normal flow also locally).
- Shocks may develop or the flow may blow up.
- Existence results for graphs or locally in time.

## 6) Hyperbolic MCF: applications

Oscillating closed spring

Melting-freezing waves
in crystals of helium [M. Gurtin et al.]

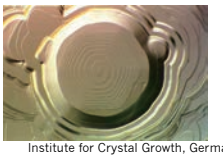

Institute for Crystal Growth, Germany

Relativistic strings
in Minkowski space [D. Kong et al.]

cronodon.com

## 6) Hyperbolic mean curvature flow

References


M. Bonafini, *A BMO-type scheme for the relativistic hyperbolic mean curvature flow*. Master thesis, Verona University, 2015.

M. E. Gurtin, P. Podio-Guidugli, *A hyperbolic theory for the evolution of plane curves*, SIAM J. Math. Anal. **22**, pp. 575–586, 1991.

C. He, D. Kong, K. Liu, *Hyperbolic mean curvature flow*, J. Differ. Equs. **246**, pp. 473–390, 2009.

M. Kang, *A level set approach for the motion of soap bubbles with curvature dependent velocity or acceleration*. Dissertation, University of California Los Angeles, 1996.

D. Kong, Z. Wang, *Formation of singularities in the motion of plane curves under hyperbolic mean curvature flow*, J. Differential Equations **247**, pp. 1694–1719, 2009.

P. G. LeFLoch, K. Smoczyk, *The hyperbolic mean curvature flow*, J. Math. Pures Appl. **90**, pp. 591–614, 2008.

H. G. Rotstein, S. Brandon, A. Novick-Cohen, *Hyperbolic flow by mean curvature*, Journal of Crystal Growth **198/199**, pp. 1256–1261, 1999.


**Next topic:**

Generalizations of interface evolution

## Two generalizations

- **Anisotropy** of surface energy
  - the surface energy depends on the orientation of the surface normal

$$E_\gamma(\Gamma) = \int_\Gamma \gamma(\nu)\, d\mathcal{H}^{d-1} \quad \text{where } \gamma : \mathbb{R}^d \to [0,\infty)$$

- **Multiphase** setting
  - there are more than two phases and thus several interfaces meet at junctions

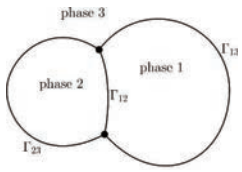


## Anisotropy

- Surface energy $E_\gamma(\Gamma) = \int_\Gamma \gamma(\nu)\, d\mathcal{H}^{d-1}$

  where $\gamma : \mathbb{R}^d \to [0,\infty)$ is one-homogeneous, i.e.,

$$\gamma(\lambda x) = \lambda \gamma(x) \quad \forall \lambda > 0,\ x \in \mathbb{R}^d$$

  - if $\gamma(x) = |x|$, we get the isotropic case
  - if $\gamma$ non-constant on unit vectors, some directions are energetically more favorable
- Wulff shape solves the isoperimetric problem:

  *"minimize $E_\gamma(\Gamma)$ under given enclosed volume"*

(1) cubic

(2) hexagonal

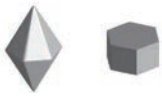

Frank diagram and Wulff shape

$$\mathcal{F}_\gamma := \{x \in \mathbb{R}^d;\ \gamma(x) \le 1\}$$
$$\mathcal{W}_\gamma := \{x \in \mathbb{R}^d;\ x \cdot y \le \gamma(y)\ \forall y \in \mathbb{R}^d,\ |y| = 1\}$$

## Anisotropic gradient

- Variation

$$\frac{d}{dt}\int_{\Gamma_t} \gamma(\nu)\, d\mathcal{H}^{d-1} = \int_{\Gamma_t} \nabla_\Gamma \cdot (D\gamma(\nu))\, V\, d\mathcal{H}^{d-1}$$

  so the $L^2$-gradient is

$$\begin{aligned} -\nabla_{L^2} E_\gamma &= -\nabla_\Gamma \cdot (D\gamma(\nu)) =: \kappa_\gamma \\ &= -(\hat{\gamma}(\theta) + \hat{\gamma}''(\theta))\kappa \end{aligned}$$

Here,
$\nu(\theta) = (\cos\theta, \sin\theta)$
$\hat{\gamma}(\theta) = \gamma(\nu(\theta))$

Here the surface divergence $\nabla_\Gamma \cdot F = \sum_{i=1}^{d-1} (\partial_{\tau_i} F) \cdot \tau_i$

where $\{\tau_1, \ldots, \tau_{d-1}\}$ is an orthonormal basis of tangent space

## Anisotropic interface evolution

- Mean curvature flow

  $V = \kappa_\gamma$ or more generally $\beta(\nu)V = \kappa_\gamma$

- Surface diffusion

  $V = -\Delta_\Gamma \kappa_\gamma$ (preserves volume)

decrease anisotropic surface energy and converge to the Wulff shape

- Stefan problem

$$
\begin{aligned}
\vartheta u_t &= d_i \Delta u && \text{in } \Omega_i(t) \text{ for } i = A, B \\
\lambda V &= -[d\nabla u]_A^B \cdot \nu && \text{on } \Gamma_t \\
\beta(\nu)V &= \kappa_\gamma - \alpha u && \text{on } \Gamma_t
\end{aligned}
$$

## Anisotropy: applications

Crystal growth

G.Demange, 2017

## Multiphase problem

- Surface energy

  $E(\Gamma) = E(\Gamma_{12}) + E(\Gamma_{13}) + E(\Gamma_{23})$

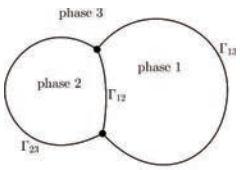


- Variation (gradient) away from junctions gives the same motion laws as before.

- From perturbation of junctions arises a boundary condition to hold at the junction (balance of forces).

## Multiphase problem

**Mean curvature flow**

- Each interface moves by

$$V = \gamma_{ij}\kappa \qquad \gamma_{ij}$$ ... surface tension of interface separating phases *i* and *j*

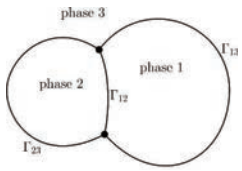


- At junctions forces are balanced: $\sum_{i,j} \gamma_{ij}\boldsymbol{\tau}_{ij} = \mathbf{0}$

*Example*: at triple junction

$$\gamma_1\boldsymbol{\tau}_1 + \gamma_2\boldsymbol{\tau}_2 + \gamma_3\boldsymbol{\tau}_3 = \mathbf{0}$$

or $\frac{\sin\theta_1}{\gamma_1} = \frac{\sin\theta_2}{\gamma_2} = \frac{\sin\theta_3}{\gamma_3}$

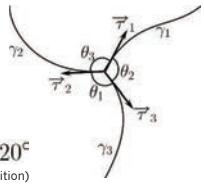


If $\gamma_1 = \gamma_2 = \gamma_3$ ➡ $\theta_1 = \theta_2 = \theta_3 = 120^\circ$

(Herring condition)

## Multiphase problem

**Anisotropic case**

- Condition at junctions becomes

$$\sum_{i,j} D\gamma_{ij}(\nu_{ij})^{\perp} = \mathbf{0}$$

Here,

$$D\gamma(\nu)^{\perp} = \gamma(\nu)\boldsymbol{\tau} - (D\gamma(\nu)\cdot\boldsymbol{\tau})\boldsymbol{\nu}$$

surface tension (tangential direction)

Herring torque (normal direction)

## Multiphase problem: applications

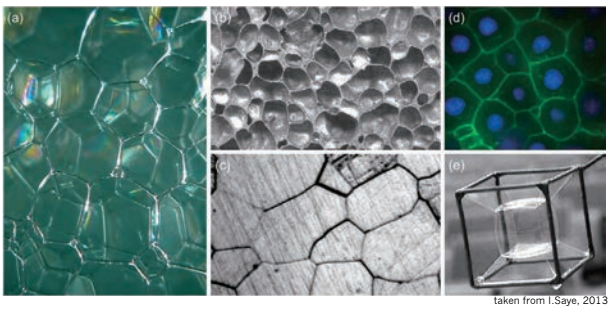


taken from I.Saye, 2013

(a) Soap bubble foam made with common washing detergent
(b) Metallic foam made out of aluminium
(c) Grains in a polycrystalline metal
(d) Cells in a zebrafish (stained)
(e) Minimal surfaces formed by steady-state soap films

**Next topic:**

Overview of basic numerical approaches

## Main numerical approaches

I will explain the methods using the example of mean curvature flow of a closed curve in a plane.

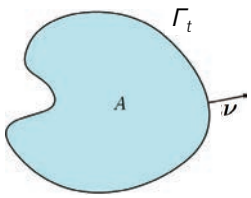


$$\boldsymbol{v} = -\kappa \boldsymbol{\nu}$$

## Main numerical approaches

① Parametric method
② Level-set method
③ Phase-field method
④ MBO algorithm
⑤ Voronoi implicit interface method
...

## Aspects to focus on

- Topological changes and other singularities
- Accurate tracking of junctions
- Anisotropy
- Coupling to physics

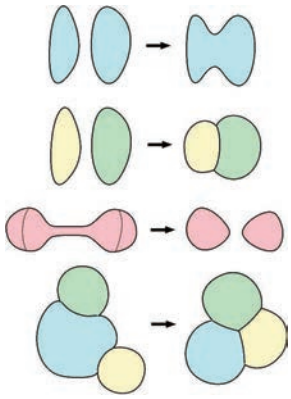

## Parametric method

**Simple algorithm:**

1. Discretize curve into points.
2. Compute curvature $\kappa$ and normal $\boldsymbol{\nu}$ at each point.
3. Advance each point by $-(\Delta t)\kappa\boldsymbol{\nu}$.
4. Repeat the above until desired time.

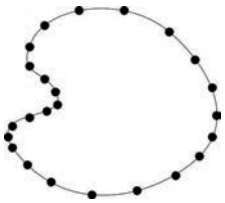

## Parametric method

- Assumption: surface is given by parametrization over a fixed manifold.
- Surface is *triangulated* and triangles moved in time.
- Mesh often *degenerates* but tangential degrees of freedom can be used to keep good mesh properties.
- *Anisotropy* handled by suitable discretization of the anisotropic mean curvature.

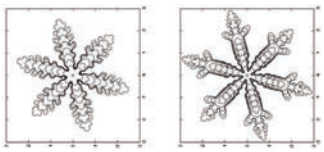

R. Nürnberg

- *Surface evolver* (non-physical, stationary)
- *Immersed boundary method* (fluid-structure interaction)
- Work by [Garcke – Barrett – Nürnberg], [Dziuk] (FEM).

## Parametric method

**Advantages**

- Simple, efficient and straightforward.

**Disadvantages**

- How to deal with *topological changes* and *singularities*?

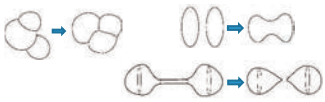

- Requires computing curvature.
- Does not "see" outside and inside of the interface.

## Level-set method

1. Express the curve $\Gamma_t$ as level set of a function *u(t,x)*:

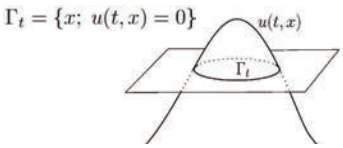


View from above:


2. Find an evolution equation for *u(t,x)* such that the level sets move according to the given law ($v = -\kappa\nu$).
3. Solve the equation for *u(t,x)* and detect level sets of the solution.

Can be done for any type of evolution (hyperbolic too).

## Level-set method

**Advantages**

- Handles naturally topological changes.

Deckelnick et al.

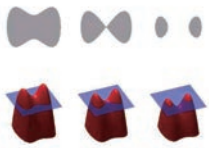

Wikipedia

**Disadvantages**

- The governing equation is nonlinear and degenerate. For example, for the mean curvature flow

$$\frac{\partial u}{\partial t} - |\nabla u| \operatorname{div}\left(\frac{\nabla u}{|\nabla u|}\right) = 0$$

- Dimension of the problem increases by 1.

## Level-set method

- Work by Osher, Sethian, Fedkiw, etc.: based on methods for Hamilton-Jacobi PDEs
  - stationary approach (arrival time) → fast marching method
  - evolution approach (level sets) → narrow band method

  Developed efficient upwind schemes.

- Regularization approach

$$u_t - \sum_{i,j}\left(\delta_{ij} - \frac{u_{x_i}u_{x_j}}{|\nabla u|^2}\right)u_{x_ix_j} = 0 \Rightarrow u_t^\varepsilon - \sum_{i,j}\left(\delta_{ij} - \frac{u^\varepsilon_{x_i}u^\varepsilon_{x_j}}{\varepsilon^2 + |\nabla u^\varepsilon|^2}\right)u^\varepsilon_{x_ix_j} = 0$$

Then $\sup_t \|u - u^\varepsilon\|_{L^\infty} \le C\varepsilon^\alpha, \quad \alpha < \frac{1}{2}$ (Deckelnick et al.)

## Phase-field method: idea

- Ginzburg-Landau energy

$$E_\varepsilon(\varphi) := \int_\Omega \left(\frac{\varepsilon}{2}|\nabla\varphi|^2 + \frac{1}{\varepsilon}W(\varphi)\right)dx$$

penalizes rapid changes of $\phi$ in space — penalizes values of $\phi$ differing from ±1

as ε→0 Γ-converges to area functional

$$E(\varphi) = c_W \int_\Omega |\nabla\chi_{\{\varphi=1\}}|\,dx = c_W \times \text{area of interface}$$

$$c_W = \int_{-1}^{1}\sqrt{2W(z)}\,dz$$

(which means that minima of $E_\varepsilon$ are close to minima of $E$)

⇒ Gradient flow of $E_\varepsilon$ should approximate gradient flow of $E$

(which is mean curvature flow).

Double-well potential $W$

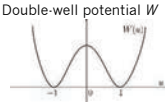

For moderate values of $E_\varepsilon$, $\phi$ looks like

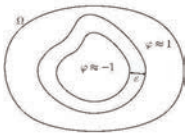


Profile of $\phi$

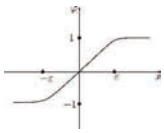


## Γ-convergence

**Definition.** Let $(X, d)$ be a metric space and $(F_\varepsilon)_{\varepsilon>0}$ a family of functionals $F_\varepsilon : X \to [-\infty, \infty]$.
We say that $(F_\varepsilon)$ Γ-converges to a functional $F : X \to [-\infty, \infty]$ if the following properties hold:

(i) For every $u \in X$ and $u_\varepsilon \in X$, $\varepsilon > 0$, such that $u_\varepsilon \to u$ as $\varepsilon \to 0$ it holds

$$F(u) \le \liminf_{\varepsilon\to 0} F_\varepsilon(u_\varepsilon).$$

(ii) For every $u \in X$ there exist $u_\varepsilon \in X$, $\varepsilon > 0$, such that $u_\varepsilon \to u$ as $\varepsilon \to 0$ and

$$\limsup_{\varepsilon\to 0} F_\varepsilon(u_\varepsilon) \le F(u).$$

## Phase-field method: example 1

- Gradient flow of Ginzburg-Landau energy w.r.t. $L^2$-inner product yields **Allen-Cahn equation**

$$\begin{aligned} \frac{\partial \varphi_\varepsilon}{\partial t} &= \varepsilon \Delta \varphi_\varepsilon - \frac{1}{\varepsilon} W'(\varphi_\varepsilon) && \text{in } \Omega \\ \frac{\partial \varphi_\varepsilon}{\partial t} &= 0 && \text{on } \partial\Omega \end{aligned}$$

- **Sharp-interface limit**: in the limit as ε→0, the sharp interface separating the sets $\{\varphi_0 = 1\}$ and $\{\varphi_0 = -1\}$ evolves by **mean curvature flow**.
- Similarly, for gradient flow preserving the volume one obtains in the limit the volume-preserving mean curvature flow.

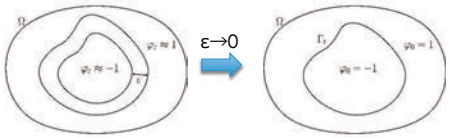


## Phase-field method: example 2

- Gradient flow of Ginzburg-Landau energy preserving volume w.r.t. $H^{-1}$-inner product yields **Cahn-Hilliard equation**

$$\begin{aligned} \frac{\partial \varphi_\varepsilon}{\partial t} &= \Delta \left( -\varepsilon \Delta \varphi_\varepsilon + \frac{1}{\varepsilon} W'(\varphi_\varepsilon) \right) && \text{in } \Omega \\ \frac{\partial \varphi_\varepsilon}{\partial n} &= 0, \quad \frac{\partial \Delta \varphi_\varepsilon}{\partial n} = 0 && \text{on } \partial\Omega \end{aligned}$$

Rewrite as system:

$$\begin{aligned} \frac{\partial \varphi_\varepsilon}{\partial t} &= \Delta u_\varepsilon \\ u_\varepsilon &= -\varepsilon \Delta \varphi_\varepsilon + \frac{1}{\varepsilon} W'(\varphi_\varepsilon) \end{aligned}$$

- **Sharp-interface limit**: in the limit as ε→0, the sharp interface separating the sets $\{\varphi_0 = 1\}$ and $\{\varphi_0 = -1\}$ evolves by **Mullins-Sekerka model**:

$$\begin{aligned} 0 &= \Delta u && \text{in } \Omega_i(t) \text{ for } i = A, B \\ 2V &= -[\nabla u]_A^B \cdot \nu && \text{on } \Gamma_t \\ 2u &= c_W \kappa && \text{on } \Gamma_t \end{aligned}$$

## Phase-field method: example 3

- Gradient flow of Ginzburg-Landau energy with degenerate mobility w.r.t. $H^{-1}$-inner product yields equation of **Cahn-Hilliard** type

$$\begin{aligned} \frac{\partial \varphi_\varepsilon}{\partial t} &= \nabla \cdot \left( \underline{(1 - \varphi_\varepsilon^2)_+} \nabla u_\varepsilon \right) \\ u_\varepsilon &= -\varepsilon \Delta \varphi_\varepsilon + \frac{1}{\varepsilon} W'(\varphi_\varepsilon) \end{aligned}$$

- **Sharp-interface limit**: in the limit as ε→0, the sharp interface evolves by **surface diffusion**:

$$V = -\Delta_\Gamma \kappa$$

## Phase-field method: example 4

- Gradient flow of $E_\varepsilon(e,\varphi) := \int_\Omega \left( s(e,\varphi) + \frac{\varepsilon}{2}|\nabla\varphi|^2 + \frac{1}{\varepsilon}W(\varphi) \right) dx$

  w.r.t. inner product $\langle e_1, e_2\rangle_{H^{-1}} + \langle \varphi_1, \varphi_2\rangle_{L^2}$ with $s(e,\varphi) := \frac{1}{2}(e-\varphi)^2$

  and $u := e - \varphi$ yields the **phase-field system**

$$\begin{aligned} \frac{\partial(u_\varepsilon + \varphi_\varepsilon)}{\partial t} &= \Delta u_\varepsilon \\ \frac{\partial \varphi_\varepsilon}{\partial t} &= \varepsilon \Delta \varphi_\varepsilon - \frac{1}{\varepsilon} W'(\varphi_\varepsilon) + u_\varepsilon \end{aligned}$$

- **Sharp-interface limit**: in the limit as ε→0, the sharp interface evolves by **Stefan problem**:

$$\begin{aligned} u_t &= \Delta u && \text{in } \Omega_i(t) \text{ for } i = A, B \\ 2V &= -[\nabla u]_A^B \cdot \nu && \text{on } \Gamma_t \\ \tfrac{2}{c_W} u + V &= \kappa && \text{on } \Gamma_t \end{aligned}$$

## Thermodynamically consistent PF

**Isothermal case:** Helmholtz free energy

$$\mathcal{F}(\varphi) = \int_\Omega \left( \underbrace{f(T,\varphi)}_{\text{free-energy density}} + \frac{\xi_0^2}{2}|\nabla\varphi|^2 \right) dx$$

- Requirement of fastest decrease leads to phase-field equation (Allen-Cahn).

**Non-isothermal case:** Entropy functional

$$\mathcal{S}(e,\varphi) = \int_\Omega \left( \underbrace{\tilde{s}}_{\text{entropy density}}(\underbrace{e}_{\text{internal energy density}},\varphi) - \frac{\xi^2}{2}|\nabla\varphi|^2 \right) dx$$

- Requirement of positive entropy production (for non-conserved $\varphi$) and conservation law for $e$ lead to phase-field system.

## Phase field method

**Advantages**

- Handles naturally topological changes.
- Can be linked to physics via thermodynamically consistent derivation.
- Equations are relatively simple (semilinear parabolic).

**Disadvantages**

- Requires fine meshes to resolve the interfacial layer (= computational stiffness).

## Phase-field method

- In **numerical solution**, either one discretizes the Allen-Cahn equation etc. as it is, or
- Uses a different form of $W$ (double obstacle):

$$W(r) = (1-r^2)^2 \quad \Rightarrow \quad W(r) = \begin{cases} 1-r^2, & r \in [-1,1] \\ \infty, & |r| > 1 \end{cases}$$

⇒ leads to variational inequality but in practice, it can be solved by a simple explicit scheme or implicit quadratic minimization problem with constraint.

**Advantage**: the phase field differs from ±1 only in a band of width $c(t)\varepsilon$, which saves computational costs.

## MBO algorithm: idea (MCF)

- <u>From level sets:</u> $\frac{\partial u}{\partial t} - |\nabla u| \operatorname{div}\left(\frac{\nabla u}{|\nabla u|}\right) = 0$

  If we start from signed distance function to interface ($|\nabla u| = 1$) then for a short time $|\nabla u| \operatorname{div}\left(\frac{\nabla u}{|\nabla u|}\right) \approx \operatorname{div}(\nabla u) = \Delta u$

  ⇒ Solve **heat equation** and **re-distance** every now and then.

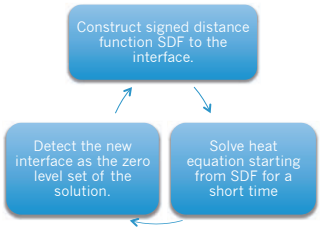


**= MBO algorithm**
(works for piecewise constant initial conditions too: u=±1)

B. Merriman, J.K. Bence, S.J. Osher, *Motion of multiple junctions: a level set approach*, J. Comp. Phys. 112 (1994).

## MBO algorithm: idea (MCF)

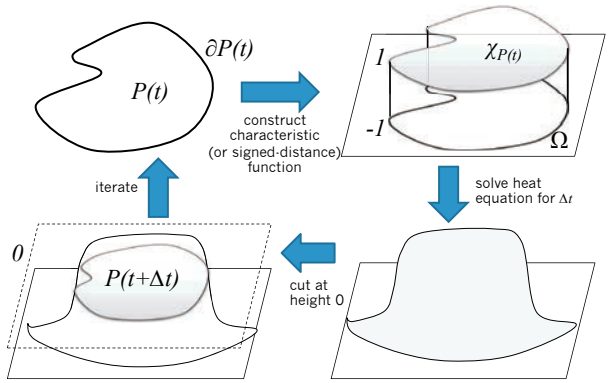

## MBO algorithm: idea (MCF)

- <u>From phase field:</u>
  splitting scheme

Allen-Cahn equation

$$\varepsilon\frac{\partial u}{\partial t} = \varepsilon\Delta u - \frac{1}{\varepsilon}W'(u)$$

$$\frac{\partial u}{\partial t} = \Delta u$$

**Heat equation**!

$$\frac{\partial u}{\partial t} = -\frac{1}{\varepsilon^2}W'(u)$$

Splits domain into two:
with value -1 and value 1
= **thresholding**.

## MBO algorithm: idea (MCF)

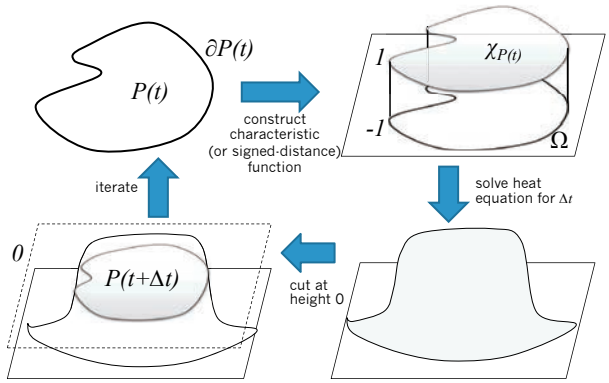


## MBO algorithm: convergence

Proofs of convergence

- semigroup theory

  L.C. Evans, *Convergence of an Algorithm for Mean Curvature Motion*, Indiana U. Math. J., 1993

- viscosity solutions

  G. Barles, C. Georgelin, *A Simple Proof of Convergence for an Approximation Scheme for Computing Motions by Mean Curvature*, SIAM J. Num. Anal., 1995

- distance function

  Y. Goto, K. Ishii, T. Ogawa, *Method of the Distance Function to the BMO Algorithm for Motion by Mean Curvature*, Comm. Pure Appl. Anal., 2005

## MBO algorithm

**Advantages**

- Handles naturally topological changes.
- Only heat equation has to be solved.
- Scheme can be made unconditionally stable → suitable for long time simulations (foams, etc.).

**Disadvantages**

- No direct relation to physics.

**Remark**. *It was said that MBO is limited to mean curvature flow but it was recently extended to other evolutions (Esedoglu, Elsey, ...), even to hyperbolic MCF (Ginder & Svadlenka).*

## MBO algorithm

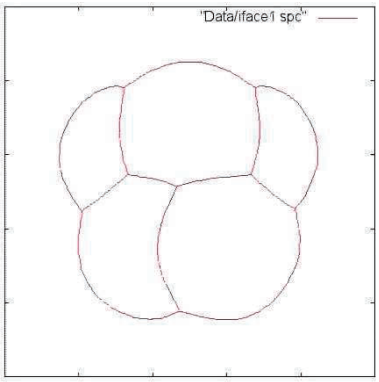


Multiphase hyperbolic mean curvature flow computed by the MBO algorithm

## Voronoi implicit interface method

by J.Sethian & R.Saye

**Idea** based on level-set method: the motion of $\varepsilon$-level sets regularizes motion of the interface (0-level set), even when there are junctions

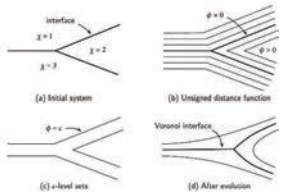


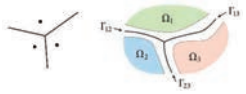


(Taken from the dissertation of R.Saye)

**Algorithm 1** The Voronoi Implicit Interface Method

Given a multiphase system, calculate the initial unsigned distance function $\phi$ and indicator function $\chi$.
**for** time step $n = 0, 1, 2, \ldots$ **do**
  Define a speed function $F$, which may depend on interface geometry, physics, etc.
  Evolve the $\epsilon$-level sets of $\phi$ by solving $\phi_t + F|\nabla\phi| = 0$ for one time step $\Delta t$.
  Reconstruct $\phi$ and $\chi$ by using the Voronoi interface of the updated $\epsilon$-level sets.

## Voronoi implicit interface method

**Advantages**

- Handles naturally topological changes.
- Accurate, efficient and robust.
- Ability to couple to physics.

**Disadvantages**

- Not yet fully analyzed.
- How to deal with anisotropy?


J.Sethian & R.Saye

## Next topic:

Handling of anisotropy and multiphase

## Anisotropy

- Consider only smooth anisotropies (for non-smooth anisotropies we either use smoothing or the crystalline approach).

Frank diagram and Wulff shape
for the smoothed cubic anisotropy

$$\gamma(p) = |p_1| + |p_2| + |p_3| \Rightarrow \gamma_\varepsilon(p) = \sum_{i=1} \sqrt{\varepsilon^2 |p|^2 + p_i^2}$$

- **Parametric method**: discretize in the same way
- **Level set method**: regularize

Barrett et al. 2013

$$\beta\left(\frac{\nabla u}{|\nabla u|}\right) u_t - |\nabla u| \sum_{j,k=1}^{n} \gamma_{p_j p_k}(\nabla u) u_{x_j x_k} = 0$$

$$\Rightarrow \quad \beta\left(\frac{\nabla u_\epsilon}{\sqrt{\epsilon^2 + |\nabla u_\epsilon|^2}}\right) u_{\epsilon t} - \sqrt{\epsilon^2 + |\nabla u_\epsilon|^2} \sum_{j,k=1}^{n+1} \gamma_{p_j p_k}(\nabla u_\epsilon, -\epsilon) u_{\epsilon x_j x_k} = 0$$

## Anisotropy

- **Phase field method**

$$E_\varepsilon^\gamma(\varphi) = \int_\Omega \left( \frac{\varepsilon}{2} |\gamma(\nabla\varphi)|^2 + \frac{1}{\varepsilon} W(\varphi) \right) dx$$

Corresponding Allen-Cahn equation

$$\epsilon\varphi_t - \epsilon\nabla \cdot DA(\nabla\varphi) + \frac{1}{\epsilon} W'(\varphi) = 0 \qquad \text{where } A(p) = \frac{1}{2}\gamma(p)^2$$

Sharp interface limit $\frac{1}{\gamma(\nu)} V = \kappa_\gamma$

- **MBO algorithm**: we solve anisotropic heat equation

$$u_t = \nabla \cdot (\gamma(\nabla u) D\gamma(\nabla u))$$

## Multiphase

- **Parametric method**: not suitable ("surgery" needed).
- **Level set method**: use multiple level set functions. To avoid creation of voids and overlaps a "repair" procedure (usually projection or penalty) is required at the end of each time step but it is not clear how this affects the motion (→used in image processing).
- **Voronoi IIM**: works nicely.

## Multiphase

- **Phase field**: junction behavior sensitive to the choice of potential functions.
- Work of Garcke, Nestler et al.:
  - Phase field function for each phase

$$u = (u_1, \ldots, u_n) \text{ such that } \sum_{i=1}^N u_i = 1$$

  - Ginzburg-Landau energy

$$E(u) = \int_\Omega \left( \varepsilon f(u, \nabla u) + \tfrac{1}{\varepsilon} W(u) \right) dx \quad \text{with } f(u, \nabla u) = \sum_{i,j} A_{ij}(u_i \nabla u_j - u_j \nabla u_i)$$

(includes anisotropy)
and suitable multi-well function *W*

  - Yields correct sharp interface motion laws but it is hard to relate the potential to given physical parameters, e.g.,

surface tension $\sigma_{ij}(\nu) = 2 \inf_{\mathbf{p}} \int_{-1}^{1} \sqrt{W(\mathbf{p}) f(\mathbf{p}, \mathbf{p}' \times \nu)}\, dy$

where **p** ranges over Lipschitz paths connecting two minima of *W*

## Multiphase MBO algorithm (equal surface tensions)

**Multiphase case**

1. Assign reference vector to each phase

reference vectors

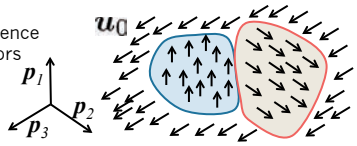


2. Solve vector-valued heat equation

$$\boldsymbol{u}_t = \Delta \boldsymbol{u}$$

$$\boldsymbol{u}(t=0,x) = \boldsymbol{u}_0(x)$$

3. Detect interface (closest ref. vector)

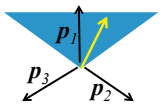


**Two-phase case**

1. Assign value 1 inside, -1 outside.

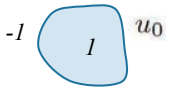


2. Solve heat eq.

$$u_t = \Delta u$$

$$u(t=0,x) = u_0(x)$$

3. Detect interface

0-level set: check if closer to 1 or to -1

## Multiphase MBO (example)

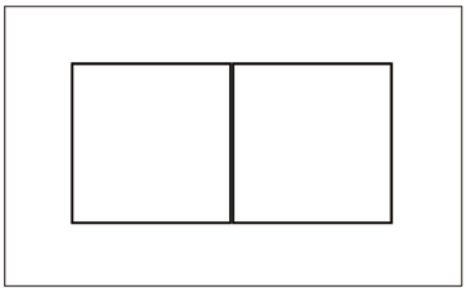

*initial interface*

## Multiphase MBO (example)

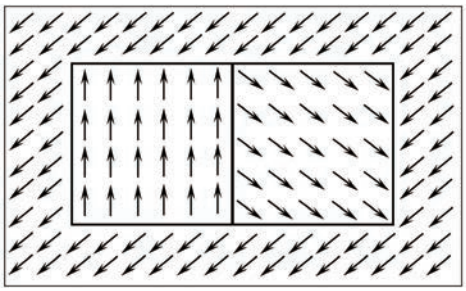

*reference vectors*

## Multiphase MBO (example)

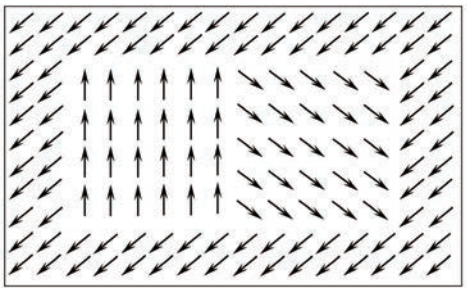

*initial condition for the heat equation ($\boldsymbol{u}_0$)*

## Multiphase MBO (example)

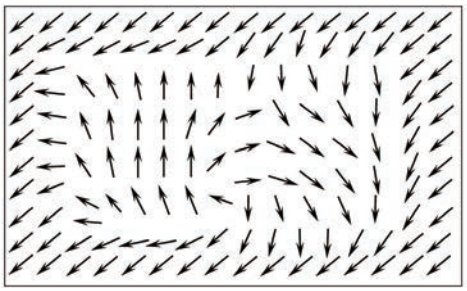

*after diffusing for short time ($\boldsymbol{u}(\Delta t,x)$)*

## Multiphase MBO (example)

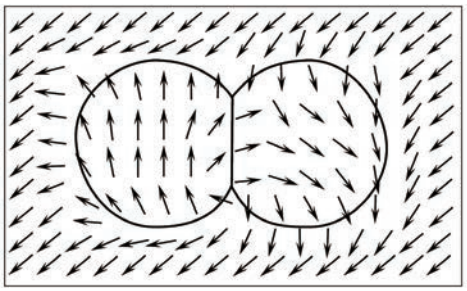

*interface detection: interface between $P_i$ and $P_j$ is at points $x$ which satisfy*

$$\boldsymbol{p}_i \cdot \boldsymbol{u}(\Delta t, x) = \boldsymbol{p}_j \cdot \boldsymbol{u}(\Delta t, x) \quad \Leftrightarrow \quad \boxed{\boldsymbol{u}(\Delta t, x) \cdot (\boldsymbol{p}_i - \boldsymbol{p}_j) = 0}$$

## Multiphase MBO (example)

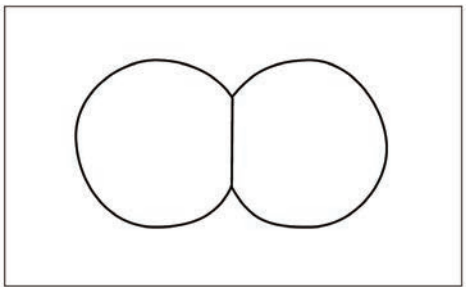

*new interface*

## MBO: troubles on uniform mesh

- Piecewise constant identification of the interface has too little degrees of freedom:

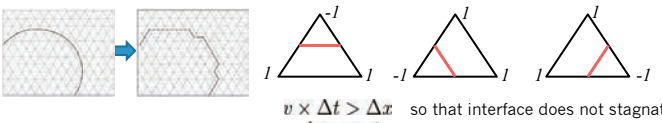


$v \times \Delta t > \Delta x$ so that interface does not stagnate

$\Delta t << 1$ not to pollute evolution

- Can be improved by using signed distance function:

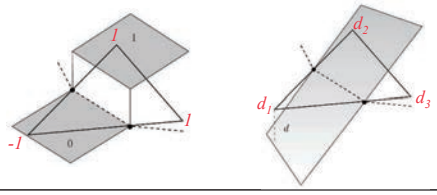


Can we construct a vector-valued analogy?

## MBO: Vector-valued signed distance

R.Z. Mohammad, K. Svadlenka: *Multiphase volume-preserving interface motions via localized signed distance vector scheme*, Discrete and Continuous Dynamical Systems - Series S, 2014.

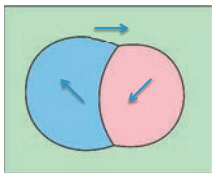

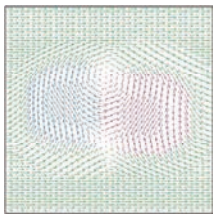

Consider a suitable combination of reference vectors with coefficients depending on distances to phases:

$$\mathbf{d}(x) = \sum_{i=1}^{k} \left(1 - \min\left\{\frac{d_i(x)}{\varepsilon}, 1\right\}\right) \mathbf{p}_i$$

$d_i(x)$ ... distance of $x$ from phase $P$

$\varepsilon$ ... band width

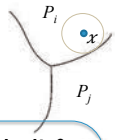


**Analysis**

- **Does it give correct interface velocity?**

$$v = \tau\kappa + O(\Delta t)$$

- **Is the condition at junction satisfied?**

Angles $\theta_i^n$ at $n$-th step of the scheme with time step $\Delta t$ satisfy

$$\left|\theta_i^n - \frac{2\pi}{3}\right| \le C\left((\Delta t)^{1/2} + \sigma^n\right), \quad \sigma \approx 0.25$$

## MBO algorithm

## Thank you for your attention!

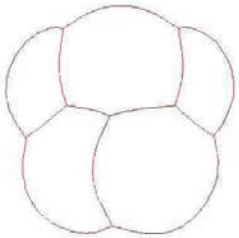

# Exact solution of nonlinear boundary value problems for surface diffusion

**Philip Broadbridge**
La Trobe University / IMI, Kyushu University

Curvature-driven surface diffusion on crystalline surfaces is modelled by a fourth order nonlinear diffusion equation. There is a class of nonlinear weakly anisotropic models that is fully integrable. Exact solutions are constructed for development of a grain boundary groove and for smoothing of an initial ramp dislocation.

Even for linear fourth order "diffusion", there are strange overshoot phenomena that are no longer proscribed by maximum principles of second order diffusion.

There are additional phenomena due entirely to the nonlinearity. For example, in a solvable quasilinear model, the depth of a grain boundary groove remains bounded as the dihedral angle approaches vertical.

At a dislocation point of infinite curvature, the quasilinear Mullins model should be extended to a fully nonlinear degenerate model to account for Gibbs-Thompson evaporation-condensation. An exactly solvable fully nonlinear degenerate diffusion model shows that unlike in the quasilinear model, deposition rate at the dislocation point is bounded, and the slope remains discontinuous for a finite delay time.

My group is currently working on classical and non-classical symmetry reductions of the fourth-order evolution of crystal surfaces near cores with cylindrical phase boundaries.

## Exact Solution of Nonlinear Boundary Value Problems with Surface Diffusion.

P. Broadbridge[1,2], D. Gallage[1], D. Triadis[2], P. Cesana[2], J. Goard[3] and P. Tritscher[3].

1. Dept. of Mathematics and Statistics, La Trobe University, Bundoora VIC 3086, Australia.

2. Institute of Mathematics for Industry, Kyushu University, 744 Motooka, Nishi-ku, Fukuoka, Japan

3. School of Mathematics and Applied Statistics, University of Wollongong NSW 2522, Australia.

Acknowledgements to M. Lee, D. Arrigo, W. Miller Jr., P. Vassiliou for useful discussions. D. Gallage is grateful for the support of a La Trobe University Postgraduate Scholarship.

## Introduction

Partial differential equations for the evolution of curves and surfaces, under isotropic and homogeneous processes, should be invariant under the Euclidean group. A comparatively simple example is evolution by mean curvature. Consider a hypersurface of dimension n-1 embedded in $R^n$:

$$\underline{\theta} \longmapsto \Re^n$$

$\hat{\mathbf{n}}$ = 'inward' unit normal vector.

$$\hat{\mathbf{n}} \cdot \frac{\partial \mathbf{r}(\underline{\theta}, t)}{\partial t} = B\bar{\kappa}$$

, proportional to mean curvature. This models the surface of volatile metals such as Mg. Surfaces of stable metals such as Au, evolve by 4th order surface diffusion [ Mullins 1957, Cahn & Taylor 1994]. In 2D,

$$\frac{\partial N}{\partial t} = -\frac{B}{2}\frac{\partial^2 \kappa}{\partial s^2}$$

The 2D surface diffusion equation in Cartesian coordinates is

$$y_t \;=\; -B\,\partial_x \left\{ \left(1+y_x^2\right)^{-1/2} \partial_x \frac{y_{xx}}{\left(1+y_x^2\right)^{3/2}} \right\}$$

This equation is invariant under rotations in the XY plane. The 3D surface diffusion equation, to be revisited later, is invariant under SO(3). This compares with the linear diffusion equation, $z_t = z_{xx} + z_{yy}$, which does not have SO(3) invariance.

We will be considering the evolution of grain boundary grooves at the surface of a polycrystalline surface. These can be clearly discerned on a surface at the nanoscale, by high-resolution transverse electron microscopy [e.g. Zhang et al, 2007] or by atomic force microscopy [e.g. Sachenko et al., 2002].

**Schematic diagram of a symmetric surface groove where two crystals meet.**

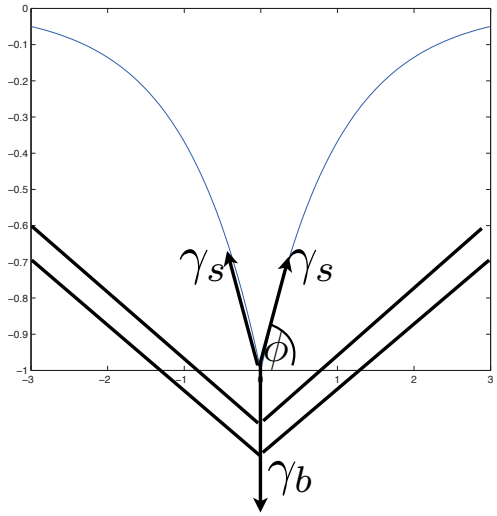


Balance of surface tension and grain boundary tension gives

$$m = tan(\phi) \; ; \; \gamma_b(T) = 2\gamma_s(T)sin(\phi)$$

The nonlinear boundary value problem for the shape of a symmetric grain boundary groove, was solved by Tritscher & Broadbridge, 1995.

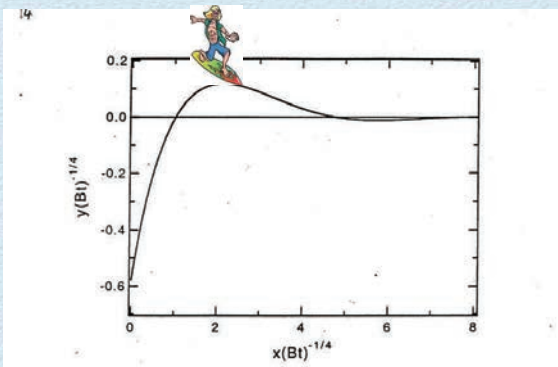


analytic solution with groove slope $y_x = 1$ at $x = 0$

**The physically based model of Mullins, 1957.**

Volume flux on surface $J = \nu \Omega v$

$\nu$ = particle density

$\Omega$ = mean volume per particle

$v$ = mean drift velocity

Nernst-Einstein Relation $v = \dfrac{-D_s}{kT}\dfrac{\partial \Phi}{\partial s}$

$\Phi$ = chemical potential per particle;

T = absolute temperature; k = Boltzmann constant; $D_s$ = surface diffusion constant.

For isotropic material with spherical surface, surface energy is

$$\mathcal{E} = \gamma A = 4\pi\gamma R^2;$$
$$V = \frac{4}{3}\pi R^3;$$
$$\frac{d\mathcal{E}}{dV} = \frac{d\mathcal{E}}{dR}\Big/\frac{dV}{dR} = \frac{2\gamma}{R} = 2\gamma\bar{\kappa}$$

so specific energy (per particle) is $\Phi = 2\Omega\gamma\bar{\kappa}$ .

This Laplace formula applies to a general surface (e.g. Defay and Prigogine, 1966).

Laplace-Herring Equation 1814 - 1950

$$\Phi = \Omega\left[\gamma_s(\phi) + \gamma_s''(\phi)\right]\kappa.$$

$\gamma_s$ = surface tension

$$\phi = \arctan y_x$$

In Cartesian coordinates, the two-dimensional curvature is

$$\kappa = \frac{-y_{xx}}{(1+y_x^2)^{3/2}}$$

Substituting the Mullins flux model into the equation of continuity for local conservation of mass,

$$\frac{\partial N}{\partial t} + \frac{\partial J}{\partial s} = 0$$

$$\frac{\partial N}{\partial t} = B\frac{\partial^2 \kappa}{\partial s^2} \qquad \text{(B constant)}$$

That is,

$$cos(\phi)\frac{\partial y}{\partial t} = B\frac{\partial^2 \kappa}{\partial s^2}$$

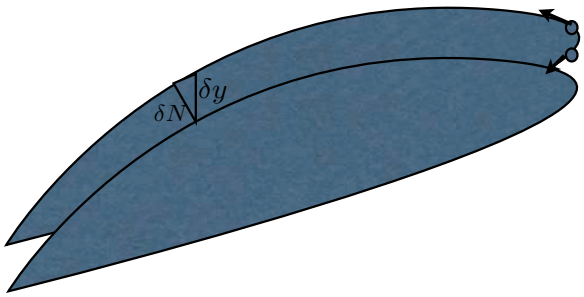


$$\text{Now use} \quad \kappa = \left|\frac{d^2\mathbf{r}}{ds^2}\right|$$

$$= \sqrt{\left[\frac{dx}{ds}\frac{d}{dx}\frac{1}{\sqrt{1+y_x^2}}\right]^2 + \left[\frac{dx}{ds}\frac{d}{dx}\left(\frac{1}{\sqrt{1+y_x^2}}y_x\right)\right]^2}$$

$$= f(\theta)\,\theta_x\sqrt{[f'(\theta)]^2 + [\theta f'(\theta) + f(\theta)]^2}$$

where $\theta = y_x$ , $f(\theta) = \dfrac{1}{\sqrt{1+\theta^2}} = \cos\phi$

. Hence,

$$y_t = -B\,\partial_x\left\{\left(1+y_x^2\right)^{-1/2}\partial_x\frac{y_{xx}}{\left(1+y_x^2\right)^{3/2}}\right\}$$

and after differentiating each side with respect to x, we arrive at the boundary value problem

$$\theta_t = -B\,\partial_x^2\left\{f(\theta)\,\partial_x\left[\theta_x f(\theta)\sqrt{[f'(\theta)]^2 + [\theta f'(\theta) + f(\theta)]^2}\right]\right\}$$

$$\mathrm{y_x} = \theta = m \quad , x = 0, \quad t > 0$$

$$\theta = 0 \quad , t = 0 \quad x \geq 0\ ;$$

$$\partial_x\left[\theta_x f(\theta)\sqrt{[f'(\theta)]^2 + [\theta f'(\theta) + f(\theta)]^2}\right] = 0 \quad , \quad x = 0$$

$$\theta \to 0 \quad , \theta_x \to 0, \quad x \to \infty.$$

For surface diffusion on an anisotropic material, both mobility and energy depend on orientation. In terms of rescaled dimensionless variables,

$$y_\tau = -\partial_x \left[ D(y_x) \partial_x \left[ E(y_x) y_{xx} \right] \right]$$

$$\tau = 0; \; y = 0$$

$$x \to \infty; \; y \to 0 \; , \; y_x \to 0$$

$$x = 0; \; J = 0 \iff \partial_x \left[ E(y_x) y_{xx} \right] = 0$$

$$x = 0 \; ; \; y_x = m(\tau).$$

$$m = tan(\phi) \; ; \quad \gamma_b(T) = 2\gamma_s(T) sin(\phi)$$

In the above, surface tension and grain boundary tension may depend on temperature T which may vary in time. Therefore the equilibrium groove slope m may depend on a time coordinate tau.

**The Integrable Model**

Progress has been made on this problem because of an integrable nonlinear anisotropic model

$$D(\theta) = \frac{\beta}{\beta + \theta}, \quad E(\theta) = \frac{1}{(1+\theta^2)^{3/2}}$$

This is closest to the isotropic model in $L_\infty$ when $\beta = 2.026$

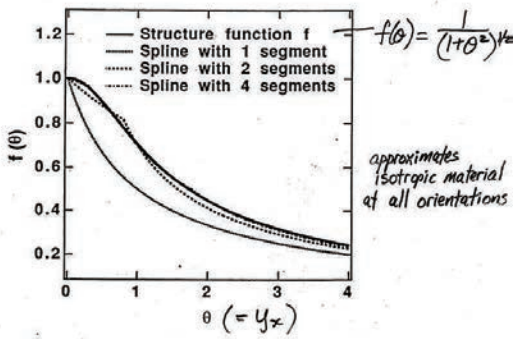


We can construct an explicit solution to Prob. II when f is piecewise inverse linear

spline $f_s$ : $f_s(\theta) = \frac{\alpha_j}{\beta_j + \theta}$ $\quad m_{j-1} \le \theta \le m_j$

cont. at $\theta = m_j$ , symmetric $f_s(-\theta) = f_s(\theta)$

constraints $f_s(0) = 1$ , $f_s(\theta) \sim \theta^{-1}$ $(\theta \to \infty)$

minimising Chebyschev norm $\| f_s - f \|$

Polar plot of surface tension vs angle for integrable model

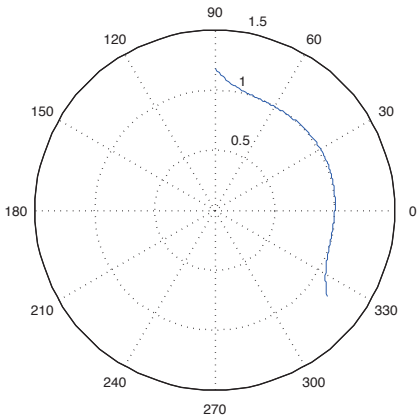


With a single reciprocal linear function for $f(y_x)$, the anisotropic surface tension is close to constant for approximately quarter of the circle. With four segments of a reciprocal linear spline, the surface tension is approximately constant over all orientations.

The linear model has groove depth proportional to groove slope m. However, the nonlinear model predicts a bounded groove depth, and has an explicit solution with vertical groove root. This occurs just before the surface tension is not strong enough to support the groove, which will be swallowed by an overarching crystal, as has been observed.

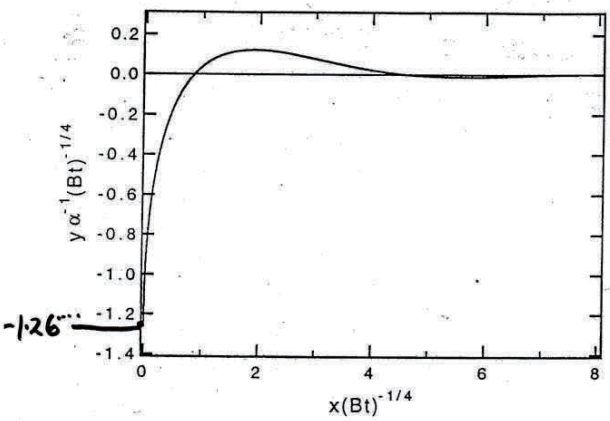


Thermal groove with infinite slope at $x=0$

When mobility and surface tension depend explicitly on time, due to temperature change,

$$D = D_1(t)D_2(y_x); \quad E = E_1(t)E_2(y_x)$$

, which prompts us define a new separable new time coordinate

$$\tau = \int_0^t D_1(\bar{t})E_1(\bar{t})d\bar{t}$$

A change of variables $\mu = \dfrac{\beta}{\beta+\theta}$ ; $z = \displaystyle\int_0^x \frac{\beta+\theta}{\beta}\, dx$

results in the governing equation transforming to a linear PDE

$$\mu_\tau = -\mu_{zzzz} - \frac{1}{\beta}R(\tau)\mu_z \ , \quad \text{where } R(\tau) = -y_\tau(0,\tau).$$

$$\Longrightarrow \ z = 0, \quad \mu_{zzz} = \frac{-R(\tau)}{\beta + m(\tau)}.$$

After a change of accelerating reference frame, this results in an equation with constant coefficients:

$$Z = z + \frac{1}{\beta}y(0,\tau) \qquad , \mu_\tau = -\mu_{ZZZZ}$$

which has scaling symmetry $\bar{Z} = e^{\varepsilon}Z, \quad \bar{\tau} = e^{4\varepsilon}\tau, \quad \bar{\mu} = \mu.$

In terms of canonical coords, $Y = Z\tau^{-1/4}, \quad S = log(\tau^{1/4}),$

the scaling transformation is simply a translation in S,

$$\bar{Y} = Y, \quad \bar{S} = S + \varepsilon, \quad \bar{\mu} = \mu.$$

For any linear equation with a one-parameter Lie group of symmetries, separation of variables is possible (Miller 1976). Separation of variables allows more general solutions than the similarity solutions in which S-dependence is neglected:

$$\mu = F(S)G(Y).$$

In fact, F(S) may be any power $S^k$ . By linear superposition we can construct a power series in time, for which the similarity solution is the leading term at zero degree.

In the following, the similarity solution (j=0) has been separated from the terms of higher degree, which begin at j=1.

$$\mu_0(Y) + \sum_{j=1}^{\infty} \tau^{j/4} \quad K_{1j}\ {}_1F_3\left(\left[\frac{-j}{4}\right], \left[\frac{1}{4}, \frac{1}{2}, \frac{3}{4}\right], \frac{Y^4}{256}\right)$$

$$+K_{2j}Y\ {}_1F_3\left(\left[\frac{1}{4} - \frac{j}{4}\right], \left[\frac{1}{2}, \frac{3}{4}, \frac{5}{4}\right], \frac{Y^4}{256}\right)$$

$$+K_{3j}Y^2{}_1F_3\left(\left[\frac{1}{2} - \frac{j}{4}\right], \left[\frac{3}{4}, \frac{5}{4}, \frac{3}{2}\right], \frac{Y^4}{256}\right)$$

$$+K_{4j}Y^3{}_1F_3\left(\left[\frac{3}{4} - \frac{j}{4}\right], \left[\frac{5}{4}, \frac{3}{2}, \frac{7}{4}\right], \frac{Y^4}{256}\right).$$

The Y-dependence is expressed exactly in terms of generalized hypergeometric functions that are evaluated easily:

$$\left[\ {}_1F_3([a],[b1,b2,b3],z) = \sum_{k=0}^{\infty} \frac{(a)_k}{(b1)_k(b2)_k(b3)_k}\frac{z^k}{k!}\ \right]$$

$$(a)_k = a(a+1)(a+2)\ldots(a+k-1)$$

It must be stressed that when the above series is truncated, it still gives an exact solution to the nonlinear surface diffusion equation with some time dependent slope at the groove root. For constant groove slope m, we have a similarity solution of form

$$y\tau^{-1/4} = H(x\tau^{-1/4})$$

For m varying with time, assume the simplest possible power-series extension

$$y(0,\tau) = \beta\tau^{1/4}\sum_{i=0}^{\infty} b_i\tau^{i/4}$$

The boundary conditions then imply a system of recurrence relations for the unknown coefficients (Broadbridge and Goard, 2010). An example of the solution is given below. Fourth-order diffusion typically generates numerous extrema. Unlike second-order diffusion, there is no maximum principle. The solution has an infinite number of extrema but these have rapidly diminishing displacement. In practice, only the secondary minimum has been observed at the nano-scale (e.g. Sachenko et al, 2002).

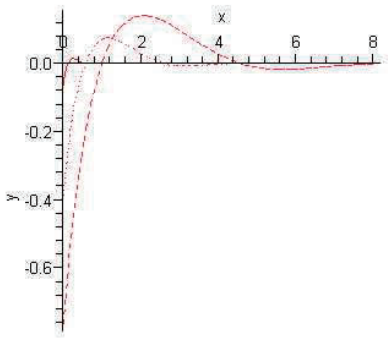


_____ t=0.0002
……t=0.1
----------t=1

Exact solution of surface diffusion around a groove with time-dependent slope at the root. $m(\tau) = {}^1/_2 + {}^1/_2\ \tau^{1/4}$

**Grooving by evaporation-condensation.**

In the Mullins 1957 theory of evaporation-condensation, lateral mixing of vapour keeps pressure p close to the equilibrium value above a flat surface, which is below the equilibrium value $p_{eq}$ above a bulging surface and above $p_{eq}$ for an indented surface. The Nernst-Einstein theory of non-equilibrium evaporation gives

$$-\frac{\partial N}{\partial t} = \frac{\Omega\chi(p_{eq}-p)}{\sqrt{2\pi m_0 kT}},$$

where $m_0$ is the particle mass and $\chi$ is the evaporation coefficient.

Equilibrium vapour pressure will be proportional to the probability of a particle escaping the potential well at the solid surface. From the Gibbs canonical distribution,

$$p_{eq} - p = p(e^{E/kT} - 1) \approx 2p\Omega\gamma\bar{\kappa}/kT$$

which is commonly referred to as the Gibbs-Thompson formula. It follows that in 2D Cartesian coordinates, the evolution equation on the surface of a volatile crystal takes the general form of the curve-shortening equation

$$y_t = \nu \frac{y_{xx}}{1 + y_x^2}.$$

The exact solution for grain boundary grooving by this nonlinear model of evaporation-condensation on an isotropic material, was given by Broadbridge, 1989.

Note that the usual Gibbs-Thompson formula embodies an approximation E/kT<<1. This need not be true over typically short periods of time and small regions wherein the curvature is very large. For situations in which slopes are small but curvatures may be large, it is instructive to consider a fully nonlinear model

$$y_t = -\nu\left[\exp(-\gamma y_{xx}/kT) - 1\right]$$

After choosing length and time scales $\ell_s = \gamma/kT, \quad t_s = \ell_s/\nu,$

$$y_t = 1 - \exp(-y_{xx}) \quad (y_{xx} >> 1).$$

A degenerate model of this type was solved by Broadbridge and Goard, 2004.

$$y_t = 1 + e^{-2y_{xx}} - 2e^{-y_{xx}} = 1 - 2\exp(-y_{xx}) \quad (y_{xx} >> 1).$$

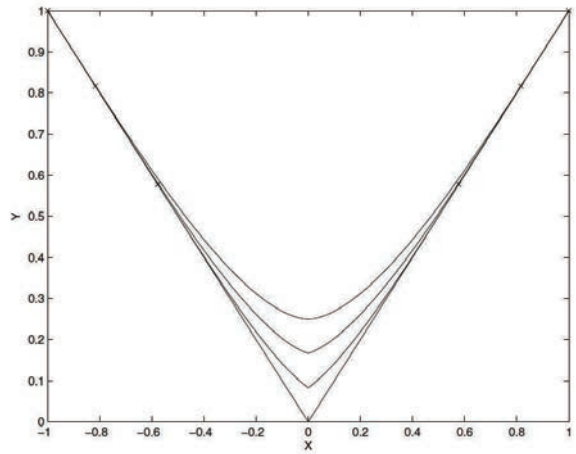


Figure 1. Profiles $Y(X,T)$ progressing upward at times $T = 0, \frac{1}{3}, \frac{2}{3}, 1$ (smoothing time), with m=1. Crosses show finite extent of the disturbance.

"The solution is depicted in Figure 1. Note that $y_t$ is bounded at all times, since $y_t = F(y_{xx})$ with $F$ bounded. In particular, $y_t(0,0) = F_\infty = \frac{a^2}{4\beta}$. This contrasts with the linear model $y_t = \beta y_{xx}$, which has $y_t(0,0)$ infinite. Similarly, for these intial conditions, the quasilinear Mullins equation (1.2) has an unbounded ...."

The solution shows that a sharp surface dislocation does indeed retain infinite curvature until a finite time delay before the surface is smooth.

## Concomitant surface diffusion and evaporation-condensation at a ramp.

The flux from a grain boundary due to surface diffusion alone, is proportional to $t^{-3/4}$. Up to some time scale, this will dominate a flux due to evaporation-condensation, which is proportional to $t^{-1/4}$. For a stable metal such as Au, surface diffusion will dominate for more than 10,000 years. For an unstable metal such as Mg, evaporation-condensation will dominate less than an hour after formation of the grain boundary. When both mechanisms are combined additively in the transport equation, there is no longer a similarity solution. However if we add an extra second-order diffusion term to model transport by evaporation-condensation, the following equation remains integrable by the same sequence of transformations that was used above:

$$y_t = \nu f(y_x)^2 y_{xx} - \partial_x \left( f(y_x) \partial_x \left[ f(y_x)^3 y_{xx} \right] \right),$$

$$f(\theta) = \frac{\alpha}{(\alpha+\theta)^2}.$$

For illustrative purposes, the solutions of Tritscher 1996 for smoothing of a ramp dislocation, assumed

$$\nu = \frac{(\alpha m)^2}{(\alpha+m)^2} \frac{(1+\alpha^2)^{1/2}}{\alpha}.$$

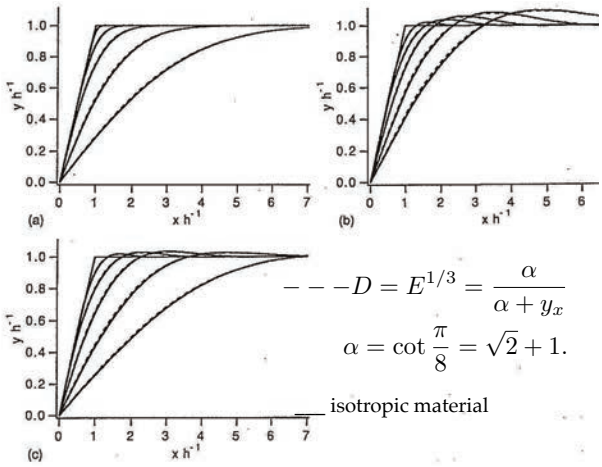


$$- - - D = E^{1/3} = \frac{\alpha}{\alpha + y_x}$$

$$\alpha = \cot\frac{\pi}{8} = \sqrt{2} + 1.$$

___ isotropic material

P. Tritscher 1996

Figure 3.5: Surface profiles for: (a) evaporation-condensation only, (b) surface diffusion only and (c) concomitant evaporation-condensation and surface diffusi with $\nu = 1$. The ramp is initially inclined at $\pi/4$ rad:
———— isotropic material; – – – – – theoretical anisotropic materi
Dimensionless times from left to right: $t^\dagger = 0$, 0.005, 0.061, 0.242, 0.970, 3.88 $t^\dagger = h^{-2}At$ for evaporation-condensation, or $t^\dagger = h^{-4}Bt$ for surface diffusion concomitant evaporation-condensation and surface diffusion.

## Axi-symmetric surface evolution.

Evaporation-condensation at an axi-symmetric surface, leads to flow by mean curvature:

$$z_t = 2(1+z_r^2)^{1/2} B\bar{\kappa} = B\left[\frac{z_{rr}}{1+z_r^2} + \frac{1}{r} z_r\right]$$

(in anisotropic case) $\quad = BD(\theta)[\theta_r + \frac{1}{r}\theta(1+\theta^2)]$

$$z_r = m, \quad r = at^{1/2}\ ; \quad z = 0,\ t = 0\ ; \quad z \to 0,\ r \to \infty$$

$$\theta = z_r; \quad \rho = rt^{-1/2}; \quad \theta = f(\rho)$$

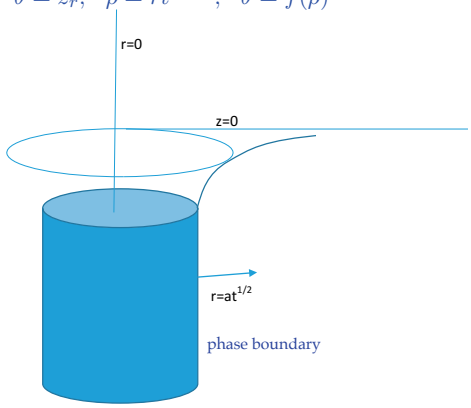


For the axi-symmetric flow, Gallage, Broadbridge, Triadis and Cesana are using the inverse method previously applied to 1D nonlinear diffusion by J. R. Philip, 1960.

$$D(\theta) = \frac{-0.5B^{-1}\frac{d\rho}{d\theta}\int_0^\theta \rho d\theta}{1+\theta(1+\theta^2)d\ln(\rho)/d\theta}$$

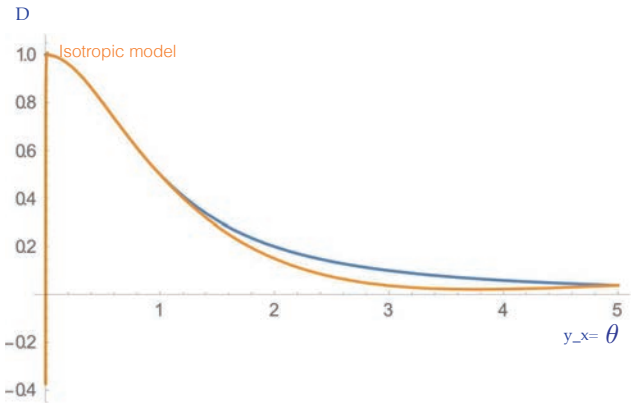


For axisymmetric surface diffusion on surface z=f(r,t),

$$z_t = -\frac{\partial J}{\partial r} - \frac{1}{r}J; \quad J = -D(z_r)\frac{\partial}{\partial r}(E(z_r)\bar{\kappa}).$$

$$\bar{\kappa} = \frac{1}{2}\frac{-z_{rr}}{[1+z_r^2]^{3/2}} - \frac{1}{2}\frac{1}{r}\frac{z_r}{[1+z_r^2]^{1/2}}$$

, scaling invariance allows reduction to a nonlinear ODE for g, with

$$z_r = g(\rho);\ zt^{-1/4} = G(\rho);$$
$$G' = g;\ \rho = rt^{-1/4}$$

Inverse method: choose solution form G, deduce explicit relationship between functions D and E. We are progressing on the problem of posing a physically reasonable solution g, from which we can construct physically reasonable functions D and E.

$$D(z_r)[1 + z_r^2]^{1/2} \ > 0 \text{ bounded,}$$
$$E(z_r)[1 + z_r^2]^{3/2} \ > 0 \text{ bounded.}$$

$$D(g) = \frac{\int_\infty^\rho \rho^2 g(\bar{\rho})d\bar{\rho} - \rho^2 \int_\infty^\rho g(\bar{\rho})d\bar{\rho}}{4\rho[E(g)\{g' + \frac{g}{\rho}(1+g^2)\}]'}$$

The assumption D=E=1 and the small-slope approximation $1 + g^2 \approx 1$ gives the linear radial model, for which we have constructed the solution g as sum of generalized hypergeometric functions ${}_1F_3$ and Meijer G functions.

The radial solution has either zero slope or infinite slope at r=0. We can substitute the solution of the linear problem, plus an assumed energy function into the nonlinear inverse problem for D(g), wherein the small-slope approximation is no longer assumed. Several speakers at this workshop have shown that mobility within a crystal may be strongly anisotropic.

For example, the solution depicted below, has an axisymmetric indentation with very small maximum slope, an isotropic surface energy E=1 and a weakly anisotropic mobility function D (notation M below).

Axisymmetric surface slope profile.

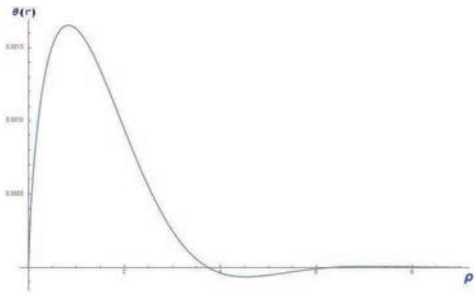


Dependence of mobility on radial surface slope.

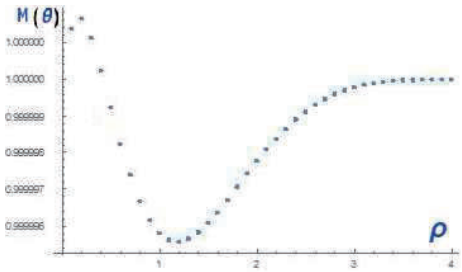

**References**

D. J. Arrigo, P. Broadbridge, P. Tritscher & Y. Karciga, "The Depth of a Steep Evaporating Grain Boundary Groove: Application of Comparison Theorems", Math. Comp. Modelling, 25 (10), 1-8 (1997).

P. Broadbridge, "Exact Solvability of the Mullins Nonlinear Diffusion Model of Groove Development", J. Math. Phys. 30, 1648-51 (1989).

P. Broadbridge & J. M. Goard, "Temperature-dependent surface diffusion near a grain boundary", J. Eng. Math., 66(1-3), 87-102 (2010).

P. Broadbridge & J. M. Goard, "When central finite differencing gives complex values for a real solution !", Complex Variables and Elliptic Equations, 57 (2-4), 455-467 (2012).

P. Broadbridge & P. Tritscher, " An integrable fourth order nonlinear evolution equation applied to thermal grooving of metal surfaces", I.M.A. J. App Math., 53,249-265(1994).

P. Broadbridge & P. J. Vassiliou, "The Role of Symmetry and Separation in Surface Evolution and Curve Shortening",
Symmetry, Integrability & Geom: Methods & Applics (SIGMA), 7, 052, 19 pages (2011).

J. W. Cahn & J. E. Taylor, "Surface Motion by Surface Diffusion", Acta Metall. Mater. 42, 1045-1063 (1994).

R. Defay and I. Prigogine, Surface tension and adsorption, Wiley, New York, 1966.

J. M. Goard & P. Broadbridge, "Exact solution of a degenerate fully nonlinear diffusion equation", Journal of Appl. Math. and Physics (Z.A.M.P.) 55(3), 534-538 (2004).

W. W. Mullins, "Theory of Thermal Grooving", J. Appl. Phys. 28, 333-339 (1957).

J. R. Philip, "General method of exact solution of the concentration dependent diffusion equation", Austral. J. Phys., 13, 1–12.

P. Sachenko, J. H. Schneibel and W. Zhang, "Effect of faceting on the thermal grain-boundary grooving of tungsten", Phil. Mag. A 82(4), 815-829 (2002).

P. Tritscher, *Integrable nonlinear evolution equations applied to solidification and surface redistribution*, PhD thesis, University of Wollongong, 1996.

P. Tritscher & P. Broadbridge, "Grain Boundary Grooving by Surface Diffusion : an Analytic Nonlinear Model for a Symmetric Groove", Proc. Roy. Soc. A, 450, 569-587 (1995).

# On observation of dislocations in crystals

**Kenji Higashida**
National Institute of Technology, Sasebo College

In this talk, several observation results of dislocations in crystals are reported. Some experimental results exhibit that the properties of dislocations should play more important roles in materials for the next generations.

結晶転位の観察から：現状と課題

# On observation of dislocations in crystals

K. Higashida
National Institute of technology, Sasebo College,
Sasebo, Japan
(Department of Materials Science & Engineering, Kyushu University)

**Coworkers: M. Tanaka, S. Sadamats, S. Matsumura, Y. Tomokiyo (Kyushu Univ.)**
**N.Narita (Kyoto Univ.)**

**IMI Workshop on "Mathematics in Interface, Dislocation and Structure of Crystals"**
**at Nishijin Plaza, Fukuoka, Japan, August 29, 2017**

## Outline

**Dislocations and Plastic deformation**

**Interaction between dislocations and a crack**
**Fracture toughness increased by plastic deformation**

**Dislocation configuration observed**
**by high voltage electron microscope (HVEM)**

## Lattice image of a silicon crystal irradiated by electron beam

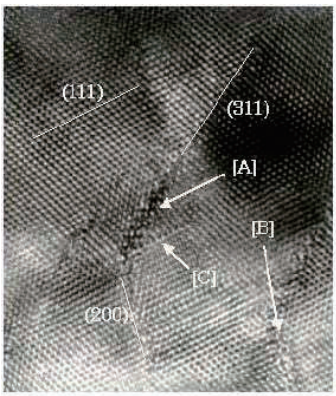


**lattice defects**

http://www.ion-eng.co.jp

## Crystal lattice defects (結晶格子欠陥)

**Point defect**: vacancy, interstitial atom
点欠陥: 原子空孔, 格子間原子

**Line defect**: Dislocation
線欠陥: 転 位

**Plane defect**: Stacking fault, free surface
面欠陥: 積層欠陥 自由表面

---

### Volterra distortions in an elastic cylinder

Linear defects in structure-less continuum. There are no low bound restrictions on the strength of disclinations and dislocations in the continuum.

Dislocation Volterra (1907)

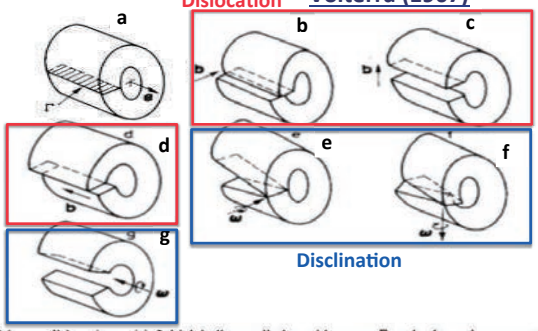


Volterra dislocations. (a) Initial hollow cylinder with a cut Γ, **e** is the unit vector along cylinder axis. (b, c) Edge dislocations of Burgers vector ***b***. (d) A screw dislocation. (e, f) Twist disclinations of Frank vector ***ω***. (g) A wedge disclination.

---

### Why were dislocations recognized in crystalline materials?

Crystal growth

X-ray diffraction spot

Mechanical properties

**Mechanism of plastic deformation**

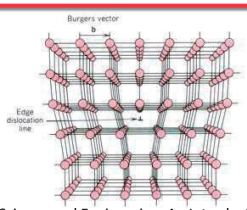


W.D. Callister, Materials Science and Engineering, An Introduction

## Mechanism of plastic deformation in a crystal

**Slip deformation**

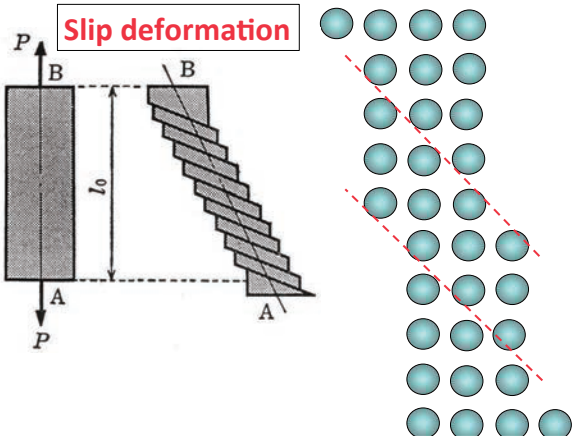


## Slip bands
すべり帯

Zinc single crystal

Tensile stress

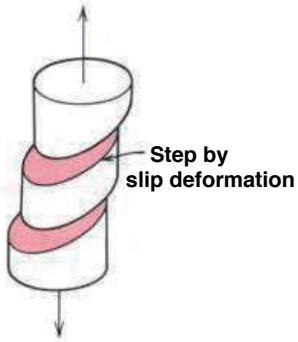


(From C. F. Elam, *The Distortion of Metal Crystals*, Oxford University Press, London, 1935.)

## Slip deformation in crystals

**Slip system** : **slip direction**
すべり系 **slip plane**

depends on crystal structure

Face-centered cubic crystal
{111}plane, <110>direction

Body-centered cubic crystal
{110}plane, <111>direction

Closed-packed hexagonal lattice
(0001)plane, <11$\bar{2}$0> direction

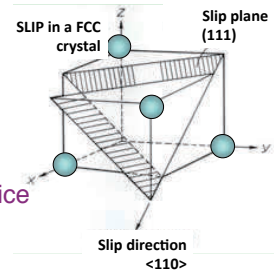

Proceedings of the Royal Society of London Series A(1934)

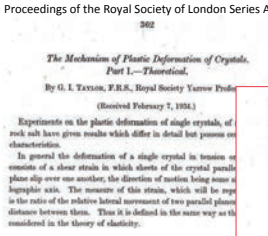
362

*The Mechanism of Plastic Deformation of Crystals.*
*Part I.—Theoretical.*

By G. I. Taylor, F.R.S., Royal Society Yarrow Profe

(Received February 7, 1934.)

Experiments on the plastic deformation of single crystals, of rock salt have given results which differ in detail but possess co characteristics.

In general the deformation of a single crystal in tension or consists of a shear strain in which sheets of the crystal parall plane slip over one another, the direction of motion being some a lographic axis. The measure of this strain, which will be repr is the ratio of the relative lateral movement of two parallel planes distance between them. Thus it is defined in the same way as th considered in the theory of elasticity.

G.I. Taylor (1934)

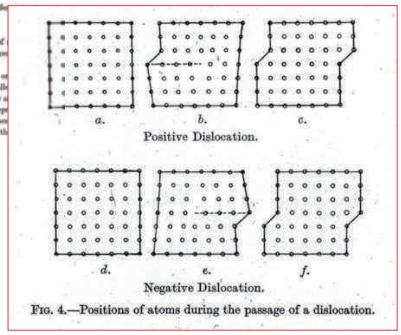

Fig. 4.—Positions of atoms during the passage of a dislocation.

1886-1975

British physicist and mathematician,
and a major figure in fluid dynamics and wave theory.

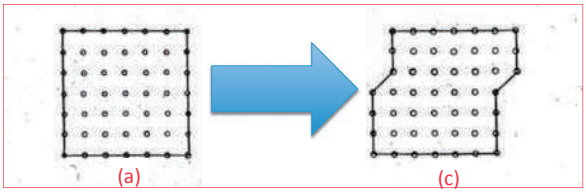


The mechanism of slipping may be like the simple shift from fig.(a) to (c), in which the whole of the material on one side of a definite plane shifts through the length of one lattice cell.

The mechanism of this simple shift differs from what is observed in real materials.

## Differences from real materials:

**(1) This ideal slipping would leave the material in the form of a perfect crystal and the strength would be unaltered by the distortion.**

**(2) To shift the whole of the upper row of atoms simultaneously over the lower row would necessitate the application of a stress comparable with the elastic moduli of the material ( 1000 times larger than the real strength)**

**(3) No room for explanation of the large observed effect of temperature on plastic distortion.**

## Illustration of stress – strain curves in fcc, bcc and hcp crystals

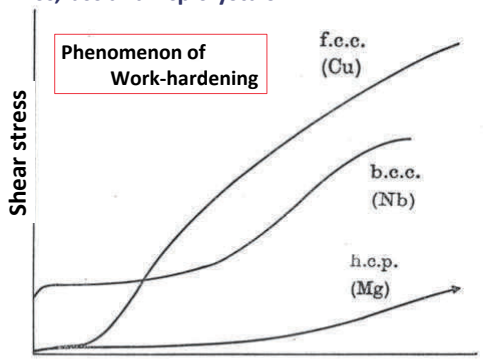


## Ideal strength for slip deformation

Simple shear along
the whole of the slip plane

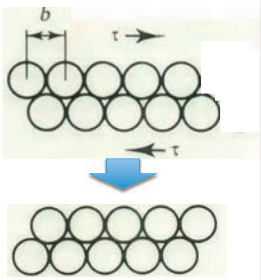


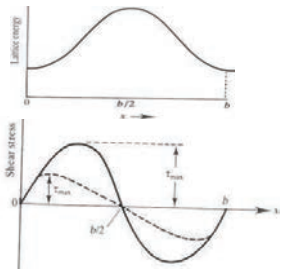


$$\tau_{ideal} \doteqdot G$$

*Shear modulus*

1000 times larger
than the real strength

## Temperature dependence of s-s relations

### Nb crystals

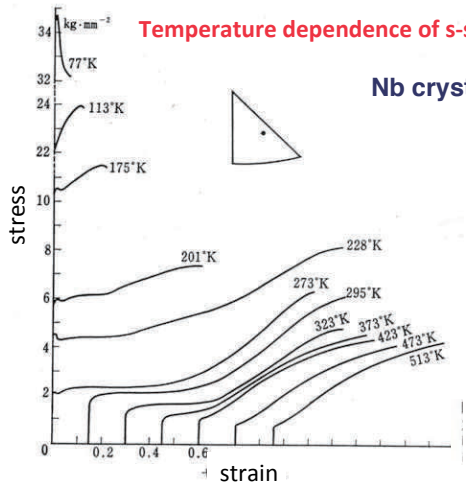


P.B.Hirsch *et.al*

## Slip by dislocatios

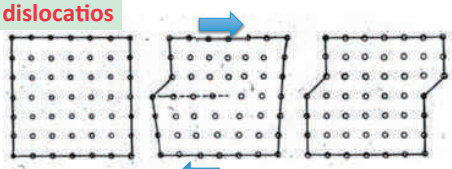


The slipping is considered to occur not simultaneously over all atoms in the slip plane but over a limited region which is propagated from side to side of the crystal.

(a) The atoms in the lattice of a crystal block,
(b) A slip of one atomic spacing has been propagated from left to right into the middle.
(c) The block after the unit slip (dislocation) has passed through from left to right.

## A looper

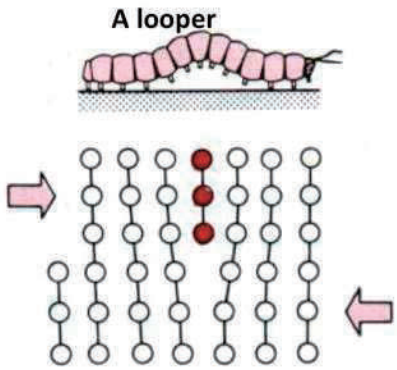

## High voltage Transmission Electron Microscope at Kyushu University

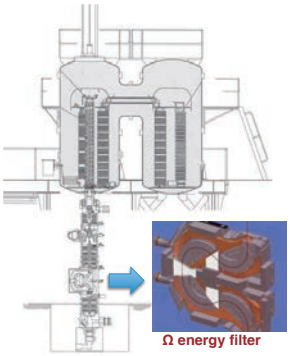


Accelerating voltage
1250kV

JEM-1300NEF with Ω energy filter

## In-situ observation in silicon crystals

deformed at 700°C


0.3μm

## Characters of dislocations in crystals

defined by two vectors

1. Burgers vector ***b***
2. Dislocation line vector ***t***

**Edge dislocation:** $b \perp t$

**Screw dislocation:** $b \parallel t$

**Mixed dislocation: combination of two components of edge and screw dislocs.**

## Edge Dislocation

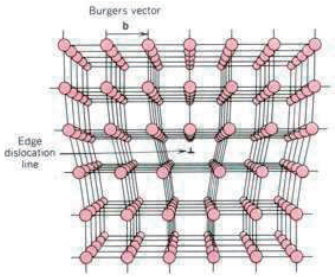


W.D. Callister, Materials Science and Engineering, An Introduction

## Edge dislocation

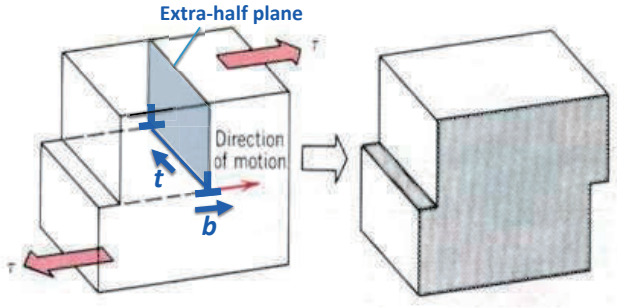


## Signs of edge dislocations

**determined by the direction of extra-half plane**

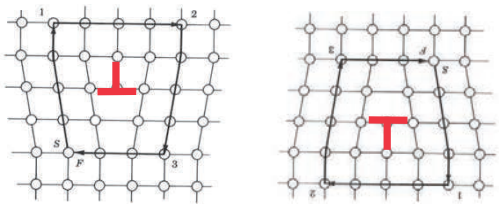

**positive** **negative**

## Screw Dislocation

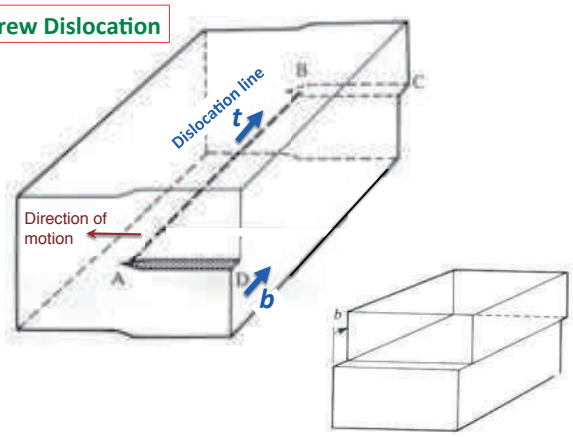

## Screw Dislocation

Top view from the direction perpendicular to the plane on which dislocation line is lying

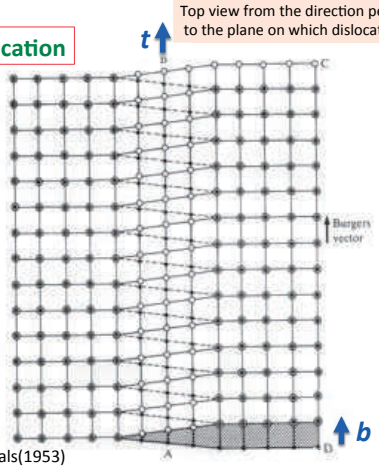


W.T.Read:
Dislocations in crystals(1953)

## Signs of screw dislocations

**determined by the direction of spiral configuration of atoms**

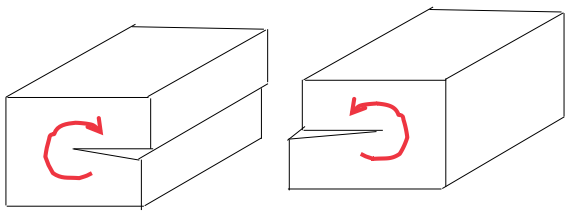

**Right-handed (R-H) Screw dislocation**

**Left-handed (L-H) Screw dislocation**

## Mixed Dislocation

**Burgers vector is conservative on one dislocation line**

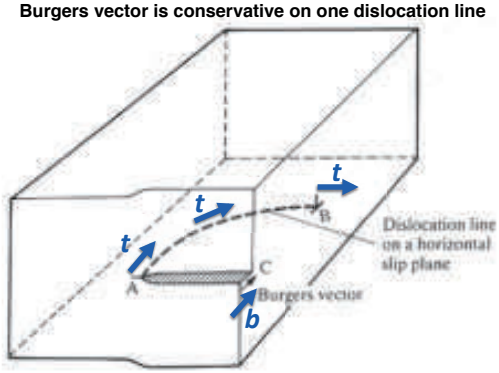

## Mixed Dislocation

Top view from the direction perpendicular to the plane on which dislocation line is lying

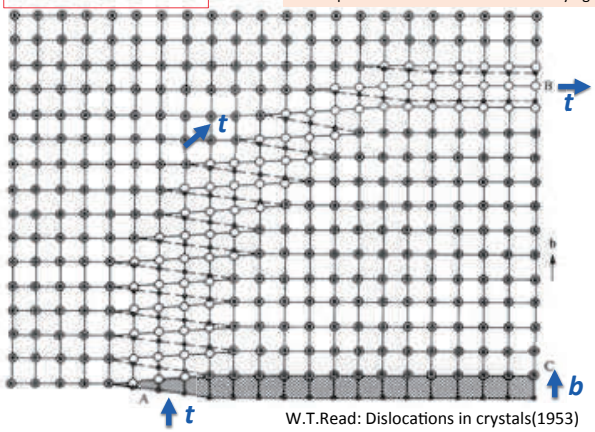


W.T.Read: Dislocations in crystals(1953)

## Dislocation loop

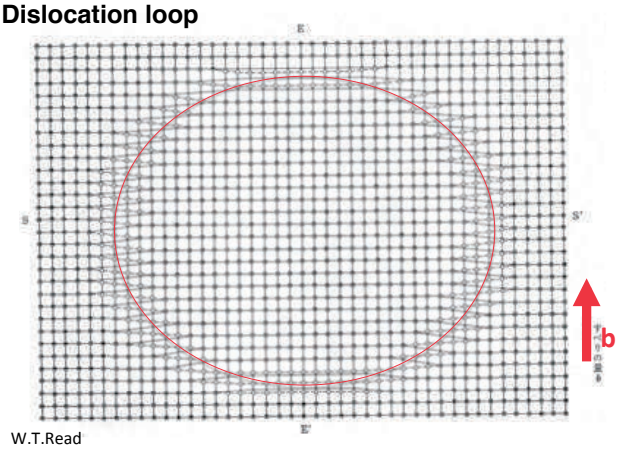


W.T.Read

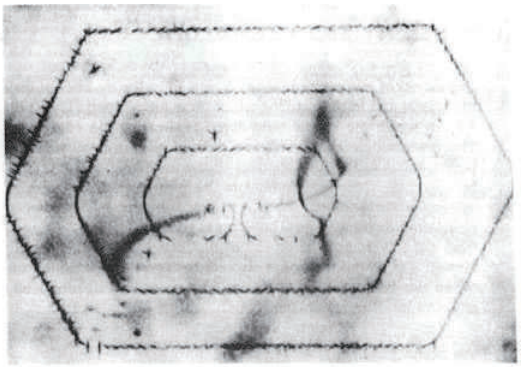

An example of a Frank–Read source in silicon. The dislocation loops have been delineated by chemical etching. In silicon, the loops are not circular; the anisotropic bonding of Si creates "loops" composed of approximately straight segments. (*From W. G. Dash, Dislocations and Mechanical Properties of Crystals. ed. J. C. Fisher, Wiley, New York, 1957.*)

## Frank-Read Source

Dislocation source in a crystal

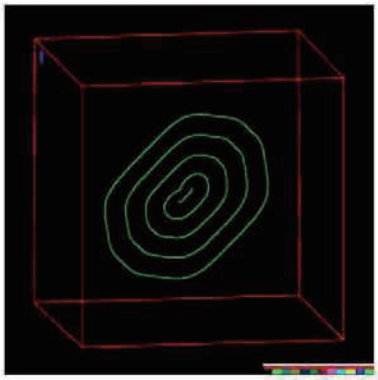

http://zig.onera.fr/DisGallery/

## Role of dislocations on mechanical properties

**Not only the mechanism of plastic deformation but also strengthening**

**Work-hardening:** To increase flow stress with increasing dislocation density
加工硬化

**Toughening:** To suppress crack extension by dislocation emission from the crack-tip
強靭化

## Temperature dependence of fracture toughness and yield strength in Steel

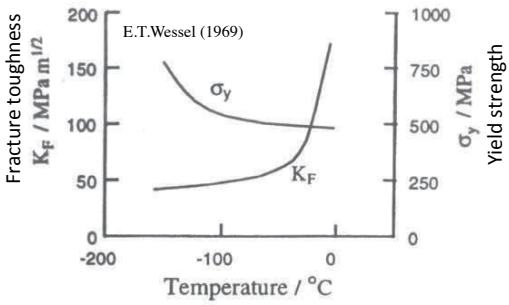


**Brittle-to-Ductile Transition (BDT)**

P.B. Hirsch and S.G.Roberts (1997)

## BDT in ionic crystals and semiconductor

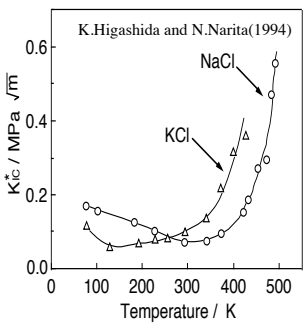


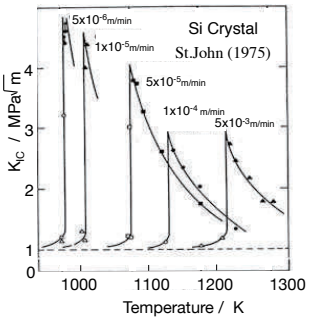


BDT: general phenomenon in crystalline materials
Increase in fracture toughness ⟺ plastic deformation around a crack-tip

## Stress Relaxation Mechanism ?

Crack-tip blunting, Plastic work ⇨ well known, but not enough to understand what toughness is

**Crack tip shielding by dislocations**

proposed independently by R.Thomson and J. Weertman in 1978

***Questions***

Are there any actual evidences on crack-tip shielding?

Is the nature of crack-tip dislocations shielding type ?

⇩

*Direct observation of Crack-tip fields and dislocations*

## Stress field around a crack tip

(I) Stress from the external applied load

$$\sigma_{ij} = \frac{K_I}{\sqrt{r}} f_{ij}(\theta)$$

**Stress intensity factor**

$$K_I = \sigma_0 \sqrt{\pi a} F$$

$\sigma_0$ : Applied external stress
$a$ : Crack length
$F$ : Specimen shape factor

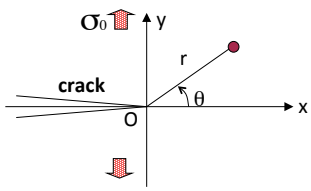


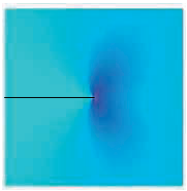

## Local Stress around a Crack Tip

(I) Stress from the applied external stress

$$\sigma_{ij} = \frac{K_I}{\sqrt{r}} f_{ij}(\theta)$$

(II) Stress from the internal source

$$\sigma_{ij}^{D} = \frac{k_D}{\sqrt{r}} f_{ij}(\theta)$$

(I)+(II) Total stress from the external stress and internal stress

$$\sigma_{ij}^{T} = \sigma_{ij} + \sigma_{ij}^{D} = \frac{k_I}{\sqrt{r}} f_{ij}(\theta)$$

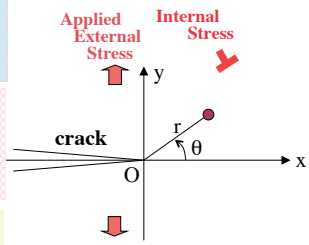


**Local stress intensity factor**

$$k_I = K_I + k_D$$

*Applied stress intensity factor* — *Local k by dislocations*

## Critical condition for crack extension


surface tension — crack extension force

$$F_I = \boxed{\frac{(1-\nu)}{2\mu} k_I^2 = 2\gamma}$$

*where* $k_I = K_I + k_D$

*Local stress intensity factor* — *Applied stress intensity factor* — *Local k due to dislocations*

$\mu$: shear modulus, $\nu$: Poisson's ratio

## Critical condition for crack extension

$$\frac{(1-\nu)}{2\mu}(K_{IC} + k_D)^2 = 2\gamma$$

*Fracture Toughness*

$$K_{IC} = \sqrt{\frac{4\mu\gamma}{1-\nu}} - k_D$$

*Interatomic bonding* — *Dislocation shielding*

$k_D < 0$ : Shielding ➡ $K_{IC}$ ↗ increase

## Local stress intensity factor *k* due to dislocations

$$\bar{k}_D = \frac{\mu}{2i(1-\nu)} \sum_j \left\{ \frac{b_j}{\sqrt{2\pi\zeta_j}} + \frac{b_j}{\sqrt{2\pi\bar{\zeta}_j}} + \frac{\pi \bar{b}_j (\zeta_j - \bar{\zeta}_j)}{(2\pi\bar{\zeta}_j)^{3/2}} \right\}$$

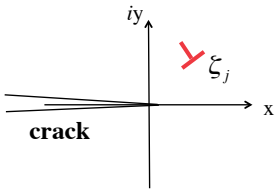


$B_j$ : Burgers vector
μ : Shear modulus
ν : Poisson's ratio

## Critical condition for crack extension

$$\frac{(1-\nu)}{2\mu}\left(K_{IC} + k_D\right)^2 = 2\gamma$$

*Fracture Toughness*

$$K_{IC} = \sqrt{\frac{4\mu\gamma}{1-\nu}} - k_D$$

*Interatomic bonding* *Dislocation shielding*

$k_D < 0$ : Shielding ➡ $K_{IC}$ ↗ increase

## Crack-tip shielding by dislocations

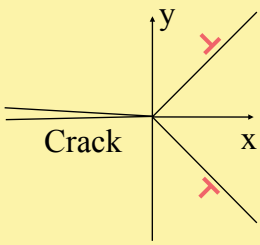


No external stress

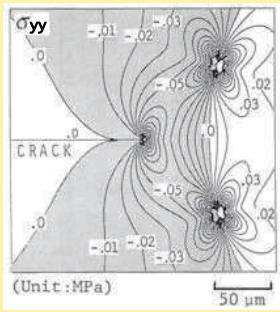


Tension
Compression

## Crack-tip shielding due to dislocations

Under the same tensile loading

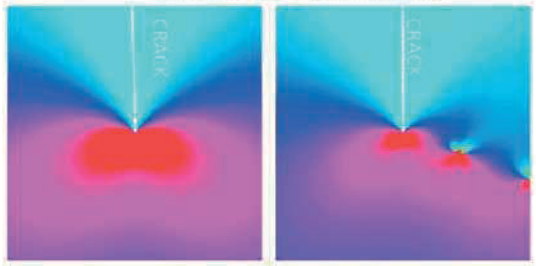


Without disloc. emission

With disloc. emission

## High voltage Transmission Electron Microscope at Kyushu University

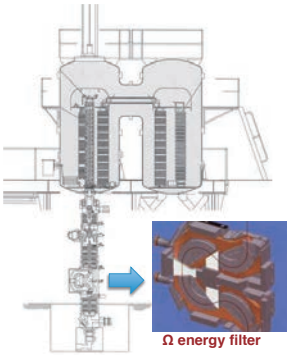

Ω energy filter

Accelerating voltage 1250kV

JEM-1300NEF with Ω energy filter

## Dislocation configuration in front of a crack-tip in a MgO crystal

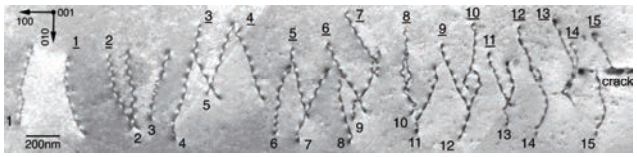


{001} incidence, g=020

Simulated image of screw disloc.

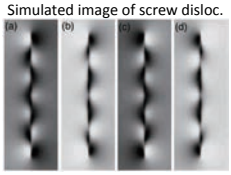


RH screw LH screw

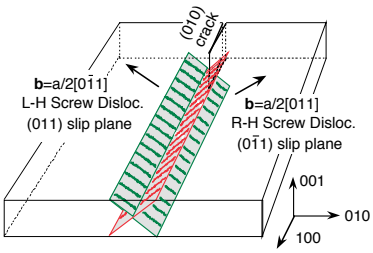

**Simulated image of screw dislocations Inclining to the foil surface**

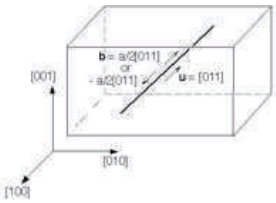


Under just Bragg condition

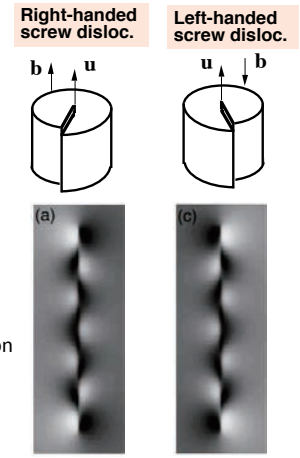


Local Stress Intensity Factor due to a Disloc. $k_D$ (3-Dimensional Problem)

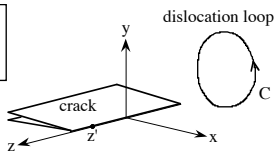


$$k_{ID}(z') = -2\mu \int_C [\{b_y G_z - y(b_y G_{yz} - b_z G_{yy})\}dx + \{(1-2\upsilon)(b_x G_z - b_z G_x) + y(b_x G_{yz} - b_z G_{yx})\}dy - \{b_y G_x + y(b_x G_{yy} - b_y G_{yx})\}dz]$$

Bueckner potential

$$G = -\frac{1}{4(1-\upsilon)\pi^{3/2}\zeta}\log\left(\frac{q+\zeta}{q-\zeta}\right), \quad \zeta = \sqrt{x + i(z - z')}, \quad q = \mathrm{Re}[\sqrt{2(x+iy)}]$$

H.Gao(1991)

**Local Stress Intensity Factor $k_D$ due to a Screw Dislocation**

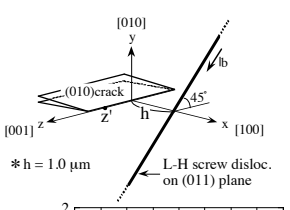


∗h = 1.0 μm

L-H screw disloc. on (011) plane

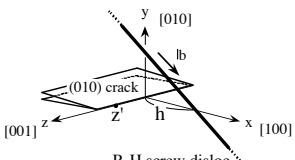


∗h = 1.0 μm

R-H screw disloc. on (0$\bar{1}$1) plane

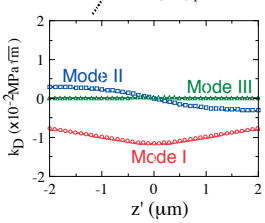


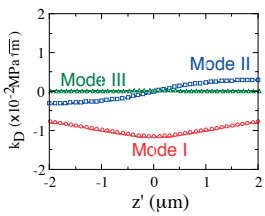

Crack and dislocations in Si crystal

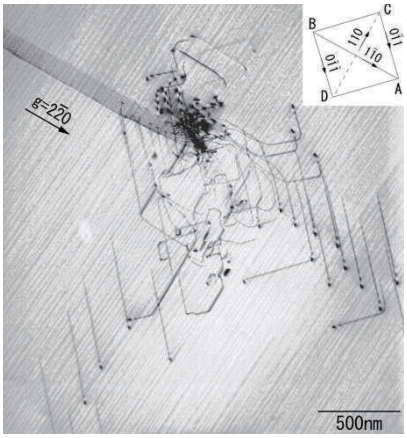


Dislocations in a Si crystal

TEM image

Thickness : 9.89μm

80eV slit
centered on 1300eV

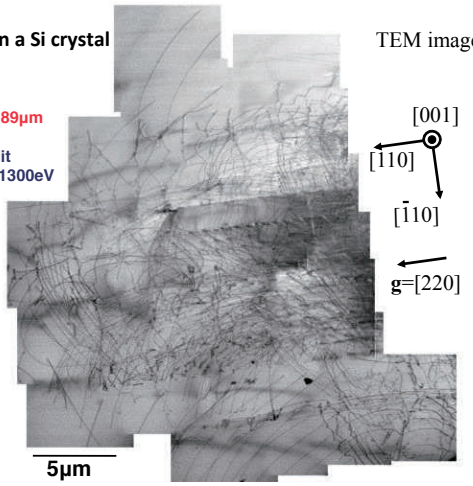


## Further research necessary in dislocation-related problems

**Core structure of screw dislocations in bcc crystals**
**High Peierls Potential, low-temperature embrittlement**

**Interaction between dislocations and other defects**
**Work-hardening, Solution hardening,**
**fine-grain strengthening**

**Fracture toughness and hydrogen embrittlement**

**Dislocation Engineering**

# Analysis of stress field of kink boundary based on lattice defect theory

**Akihiro Nakatani**
Osaka University
(joint work with Xiao-Wen Lei (Fukui University))

An expression of the displacement field of the continuum limit of uniformly distributed dislocations on afinite straight segment in an infinite elastic body is formulated as a closed-form. The exact solution based on the linear elasticity is applied to describe the elastic field near a kink boundary in magnesium alloy with long-period stacking ordered structure. Stress singularity of line of intersection between two kink boundaries will be discussed in detail by an asymptotic analysis as well as computational analysis.

# Structure of tilt grain boundaries from mathematical perspective

**Kazutoshi Inoue**

AIMR, Tohoku University

(joint work with Motoko Kotani[1] and Yuichi Ikuhara[1,2])

Functional materials are often used by a polycrystalline form, and their electrical and physical properties are strongly affected by crystalline defects such as dislocations and grain boundaries (GBs). Structures and properties of GBs have been intensively studied both experimentally and numerically for decades. Simplified system of bicrystals has been often investigated in order to determine individual contributions from various components to the macroscopic properties. Many studies have mainly focused on special commensurate GBs with a short periodicity. However, any GB deviated from a typical commensurate orientations can have a rather long periodicity which are well described by the structural-unit model. It has been shown that the structures of symmetrical tilt GBs can be described by a part of quasi-periodical arrangements of structural units as a realization of the lowest energy structure under an assumption that the structure may change as continuously as possible as a function of misorientations. Consequently, two types of structural units are arranged in a way that GB dislocations are maximally separated. Because of this property, the periodicity and the arrangement of structural units in symmetrical tilt GBs can be closely related to the distribution of rational numbers that is well represented by the Farey sequence. We have systematically predicted the arrangement of structural units in various types of GBs in ceramic materials by utilizing the Farey sequence. The atomic configurations in GBs were characterized by the aberration-corrected scanning transmission electron microscopy, showing a nice agreement with the prediction [1-3].

## References

[1] K. Inoue, M. Saito, Z. Wang, M. Kotani and Y. Ikuhara: On the periodicity of ⟨001⟩ symmetrical tilt grain boundaries, Mater. Trans. (2015) 56(3), 281-287.

[2] K. Inoue, M. Saito, Z. Wang, M. Kotani and Y. Ikuhara: On the decomposition formula of ⟨001⟩ symmetrical tilt grain boundaries, Mater. Trans. (2015) 56(12), 1945-1952.

[3] K. Inoue, M. Saito, C. Chen, M. Kotani and Y. Ikuhara: Mathematical analysis and STEM observations of arrangement of structural units in ⟨001⟩ symmetrical tilt grain boundaries, Microscopy. (2016) 65(6), 479-487.

[1]WPI Research Center, Advanced Institute for Materials Research, Tohoku University, Katahira 2-1-1, Aoba-ku, Sendai; 980-8577

[2]Institute of Engineering Innovation, School of Engineering, The University of Tokyo, 2-11-16, Yayoi, Bunkyo-ku, Tokyo; 113-8656

## 1. Introduction

Materials are often used by a polycrystalline form, and their macroscopic properties are strongly affected by crystalline defects such as dislocations and grain boundaries (GBs). Grain boundary (GB) is an interface formed by two adjacent crystal grains. Atomic structures and functional properties of GB have been intensively studied experimentally and numerically. Most of the studies have mainly focused on special commensurate GBs such as coincidence-site lattice (CSL) GBs with short periodicity [1–4]. Commensurate GBs have been classified by the coincidence index $\Sigma$, and the CSL theory of high dimensional lattices has been developed after the discovery of quasicrystals [5, 6]. Especially, simplified system of symmetrical tilt GBs have been often investigated in order to determine individual contributions of various components to their properties. A GB deviated from a commensurate orientation with short periodicity may show a long periodicity which can be well described by the structural-unit model [7–9]. High index CSL GBs can be described by a relatively long periodicity of structural units which form a part of a quasi-periodicity instead of *random* structures. It has been found that the arrangement of structural units in a GB can strongly affect the GB energy which should be important in mechanical behavior, ductility, segregation and so forth [10–20]. Since there exist only a few CSL orientations with short periodicity, the O-lattice theory has been proposed in 1960's in order to interpolate short-periodicity structures [21–23]. A general theoretical framework in regard to the symmetry of crystallographic groups on the dichromatic complex of two adjacent lattices was developed [24, 25]. Then, a general principle to obtain the arrangement of structural units has been proposed, assuming that the GB structure can be described by a combination of two reference structures, and change as continuously as possible according to the misorientation [26–28]. Relatively recently, irrational interfaces resulting in quasi-periodic structures have been studied and a method to approximate the structure has been demonstrated [29, 30]. According to the rapid development of experimental techniques, direct observation of GB structures due to aberration-corrected scanning transmission electron microscopy (STEM) combined with the first-principles calculations has been making important progress in materials science [31, 32].

However, a general mathematical principle is also necessary to be developed for predicting the stable structure of GBs and their relation to properties in various materials. We found that the periodicity and the arrangement of structural units in symmetrical tilt GBs can be closely related to the distribution of rational numbers that was well represented by the Farey sequence. The arrangement of structural units in various types of GBs in ceramic materials were systematically predicted by utilizing the Farey sequence which nicely agreed with STEM observations in atomic-resolution. This article is mainly based on [33, 34].

## 2. Preliminaries

2.1. **The CSL theory.** Let L be an $n$-dimensional lattice in $\mathbb{R}^n$, which is isomorphic to a finitely generated Abelian subgroup of full rank with the co-compact property, and $O(n)$ be the group of orthogonal transformations in $\mathbb{R}^n$. One of the lattice points in L is chosen to be the origin, and $R\mathrm{L}$ stands for the transformation of L by $R \in O(n)$. Then, the sublattice $\mathrm{L} \cap R\mathrm{L}$ is called the coincident-site lattice (CSL) and $R \in O(n)$ is a coincidence isometry if the intersection $\mathrm{L} \cap R\mathrm{L}$ forms a sublattice of full rank with a finite index. The index is defined as the group index $\Sigma := \Sigma_R(\mathrm{L}) = [\mathrm{L} : \mathrm{L} \cap R\mathrm{L}]$,

which is equivalent to the ratio $|\mathrm{L} \cap R\mathrm{L}|/|\mathrm{L}|$ where $|\mathrm{L} \cap R\mathrm{L}|$ and $|\mathrm{L}|$ denote the volume of the fundamental domains of $\mathrm{L} \cap R\mathrm{L}$ and L as well as to the reciprocal density of CSL points. Let $\mathrm{Isom}_{\mathrm{C}}(n)$ denote the group of coincidence isometries in $\mathbb{R}^n$. Then, $R \in SO(n) \cap \mathrm{Isom}_{\mathrm{C}}(n)$ is called a coincidence rotation. The CSL is considered as the maximal sublattice that is contained in both of L and $R$L. The union $\mathrm{L} \cup R\mathrm{L}$ may form so-called a dichromatic pattern [24]. The CSL dichromatic patterns of $\Sigma 17$ and $\Sigma 5$ are shown in Fig.1. For $R \in \mathrm{Isom}_{\mathrm{C}}(n)$, the group

$$\mathrm{L} + R\mathrm{L} = \{v_1 + v_2; v_1 \in \mathrm{L},\ v_2 \in R\mathrm{L}\} \tag{1}$$

may form a super-lattice of L (and $R$L) which is called the displacement-shift complete (DSC) lattice [35]. The DSC lattice is the minimal super-lattice that contains both L and $R$L, generated by the minimal translations which preserve the CSL dichromatic pattern. Later, we may see that a GB dislocation can be introduced according to the DSC lattice in order to minimize the GB energy by the minimal displacement of lattices. Therefore, a GB dislocation especially in a high-angle GB is called a DSC dislocation.

2.2. **The O-lattice theory.** The O-lattice theory was introduced to generalize the CSL theory [21–23]. For a lattice L in $\mathbb{R}^n$ and $R \in O(n)$, the O-lattice is defined by

$$\mathcal{O}_R(\mathrm{L}) := \{\boldsymbol{a} \in \mathbb{R}^n\ ;\ (I - R^{-1})\boldsymbol{a} \in \mathrm{L}\}, \tag{2}$$

where $I$ is the identity transformation. The lattice structure of $\mathcal{O}_R(\mathrm{L})$ is induced from L unless $I - R^{-1}$ degenerates. An element in $\mathcal{O}_R(\mathrm{L})$ is called an O-lattice point. From Eq.(2), $\boldsymbol{a} \in \mathcal{O}_R(\mathrm{L})$ is recognized as the origin of $R \in O(n)$ in the dichromatic pattern of L and $R$L. When $\det(I - R^{-1}) = 0$, a family of hyperplanes may appear. It should be noted that a smooth variation of $R \in O(n)$ induces the smooth variation of O-lattice while CSL configurations with low $\Sigma$ only exist discretely.

The idea of O-lattice was introduced in order to analyze the *best matching points* of two lattices where misfit is maximized on the boundary of Voronoi cells of O-lattice points. We expect that dislocations can be introduced if a GB plane intersects the boundary of the Voronoi cells of O-lattice points. Therefore, the low density of O-lattice points results in the low dislocation density. The O-lattice is a way to generalize the CSL since any CSL points can be the origin of a coincidence rotation. Conversely, given an O-lattice point and the transformation $R$, the lattice configuration around it can be recovered. From Eq.(2), one may see that $|\mathrm{L}|/|\det(I - R^{-1})|$ gives the volume of the fundamental domain of the O-lattice, and therefore that $|\det(I - R^{-1})|$ is the density of O-lattice points as with $\Sigma$ in the CSL theory. Generally, $\mathcal{O}_R(\mathrm{L})$ is a super-lattice of the CSL if $R$ is a coincidence rotation.

O-lattice points can be classified in terms of the internal coordinates which is given by a projection of $\mathcal{O}_R(\mathrm{L})$ to the quotient $\mathbb{R}^n/\sim$ with respect to the translation symmetry of L. The set of projected O-lattice points is denoted by $\tilde{\mathcal{O}}_R(\mathrm{L})$ which is conventionally called the reduced O-lattice. Let $\#\tilde{\mathcal{O}}_R(\mathrm{L})$ denote the number of elements in $\tilde{\mathcal{O}}_R(\mathrm{L})$. Then, $\#\tilde{\mathcal{O}}_R(\mathrm{L})$ is finite if $R$ is a coincidence isometry. For $R \in \mathrm{Isom}_C(n)$, we have $\#\tilde{\mathcal{O}}_R(\mathrm{L})/|\det(I - R^{-1})| = \Sigma_R(\mathrm{L})$ unless $\det(I - R^{-1}) = 0$. The translations which preserve the total CSL pattern can be classified by the translations in $\tilde{\mathcal{O}}_R(\mathrm{L})$ [23]. Examples of reduced O-lattice points are shown in table 1 for a 2-dimensional square lattice L and the coincidence rotation $R$ with the rotation angle $2\theta$ around the [001]-axis.

TABLE 1. A classification of reduced O-lattice points for the $(m\ 1\ 0)$-GBs with the rotation angle $2\theta$ around the [001]-axis for a positive integer $k$.

| $\cot\theta$ | GB plane | $\Sigma$ | reduced O-lattice points |
|---|---|---|---|
| $2k$ | $(2k\,1\,0)$ | $4k^2+1$ | $(0,0),\ (1/2,1/2),\ (0,1/2),\ (1/2,0)$ |
| $2k+1$ | $(2k+1\,1\,0)$ | $2k^2+2k+1$ | $(0,0),\ (1/2,1/2)$ |

2.3. **Structural-unit Model.** The periodicity of GBs can be described by the structural-unit model. A structural unit is a polyhedron of atomic sites which typically appear around the GB. The cubic crystal viewed along the [001]-direction can form a square lattice, and the Miller index for the [001]-symmetrical tilt GB with a tilt angle $2\theta$ is given by $(q\ p\ 0)$ satisfying $\cot\theta = q/p$ where $q$ and $p$ are coprime positive integers with $q > p$ (except the case $q = 1$ and $p = 0$). It might be useful to consider a polygon of atomic sites if the problem can be deduced to 2-dimension. As highlighted in Fig.1, a structural unit of the $(q\ p\ 0)$-structure of the [001]-symmetrical tilt CSL GB is defined to be a kite-shaped tetragon which is made by gluing a pair of right triangles of atomic sites at their hypotenuses whose sides in the right angles are $q$ and $p$ in the unit of the lattice constant. It can be useful to utilize the O-lattice as an indicator of the periodicity of the structural units. In Fig.1, the CSL GBs are defined by the line passing through the CSL points below which there are points of L and above which there are points of $R$L. GBs in Fig.1 can be described by an array of single type structural units. Let $\mathcal{O}_R(\mathrm{L})|_{\mathrm{GB}}$ and $\tilde{\mathcal{O}}_R(\mathrm{L})|_{\mathrm{GB}}$ denote the subset of $\mathcal{O}_R(\mathrm{L})$ and $\tilde{\mathcal{O}}_R(\mathrm{L})$ restricted on the GB. We notice $(0,0),\ (0,1/2) \in \tilde{\mathcal{O}}_R(\mathrm{L})|_{\mathrm{GB}}$ for the $\Sigma 17$ dichromatic pattern in Fig.1(a), and $(0,0),\ (1/2,1/2) \in \tilde{\mathcal{O}}_R(\mathrm{L})|_{\mathrm{GB}}$ for the $\Sigma 5$ dichromatic pattern in Fig.1(b). Two types of points in $\tilde{\mathcal{O}}_R(\mathrm{L})|_{\mathrm{GB}}$ exist periodically on the GBs and structural units are superposed passing through the CSL points $(0,0) \in \tilde{\mathcal{O}}_R(\mathrm{L})|_{\mathrm{GB}}$.

2.4. **Diophantine problem.** For any irrational number $x$ and an integer $t > 0$, there are positive coprime integers $p$ and $q$ such that $|x - p/q| < 1/tq$ [36]. One of the efficient ways to approximate an irrational number by a rational number can be demonstrated by the continued-fraction expansion. The principal continued-fraction expansion of a positive real number $x$ is given by

$$x = a_0 + \cfrac{1}{a_1 + \cfrac{1}{a_2 + \cfrac{1}{a_3 + \cfrac{1}{\ddots}}}}, \tag{3}$$

with a non-negative integer $a_0$ and positive integers $a_i$'s $(i \geqq 1)$, which can be denoted by $x = [a_0; a_1, a_2, a_3, \cdots]$. Let $\{P_n\}$ and $\{Q_n\}$ $(n \geqq 0)$ be sequences defined by $P_0 = 1,\ P_1 = a_0,\ Q_0 = 0,\ Q_1 = 1,\ P_{n+1} = P_{n-1} + a_n P_n$ and $Q_{n+1} = Q_{n-1} + a_n Q_n$. Then $P_n$ and $Q_n$ are coprime and satisfy $|x - P_n/Q_n| < 1/Q_n Q_{n+1}$. Thus, an approximating sequence $\{P_n/Q_n\}$ of $x$ can be obtained, and the $\{(Q_n\ P_n\ 0)\}$-structures may form a sequence of the *Rational Approximant Structure*(RAS)s [30] which may converge to the $(x\ 1\ 0)$-structure, realizing a part of a quasi-periodic arrangement of structural units.

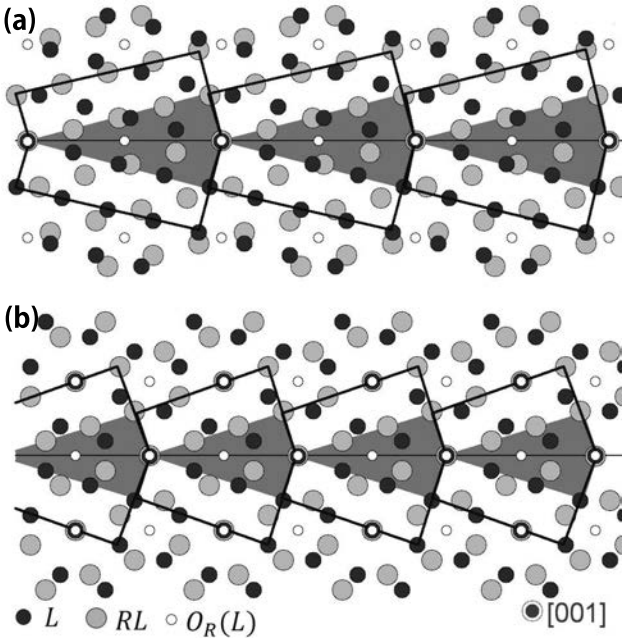


FIGURE 1. Dichromatic patterns of lattices of (a) $\Sigma 17$, (410)-structure with $2\theta_1 \simeq 28.07^\circ$ ($\cot\theta_1 = 4$) and (b) $\Sigma 5$, (310)-structure with $2\theta_2 \simeq 36.87^\circ$ ($\cot\theta_2 = 3$). The O-lattice $\mathcal{O}_R$(L) corresponding to each coincidence rotation $R$, and structural units are superposed [33].

Note that we have

$$[a_0; a_1, \cdots, a_n] = [a_0; a_1, \cdots, a_{n-1}] \boxplus [a_0; a_1, \cdots, a_{n-1}, a_n - 1], \tag{4}$$

indicating that the rational number $[a_0; a_1, \cdots, a_n]$ is uniquely produced by the *parent* rational numbers $[a_0; a_1, \cdots, a_{n-1}]$ and $[a_0; a_1, \cdots, a_{n-1}, a_n - 1]$.

## 3. Application to the GB structure

3.1. **Application of the O-lattice theory.** We demonstrate an application of the O-lattice theory by focusing on the symmetrical tilt CSL GBs. The rotation axis is set to be the [001]-axis. Since the $(q\ p\ 0)$-plane is spanned by the [001] and the $[p\bar{q}0]$-axes, the problem deduces to a 2-dimensional one. By taking the standard coordinates for a square lattice L, and letting $R = R(2\theta)$ be the rotation of $2\theta$ around the [001]-axis, we have

$$(I - R(2\theta)^{-1})^{-1} = \frac{1}{2}\begin{pmatrix} 1 & \cot\theta & 0 \\ -\cot\theta & 1 & 0 \\ 0 & 0 & 1 \end{pmatrix}, \tag{5}$$

restricted on the plane perpendicular to the [001]-axis. By applying Eq.(5) with $\cot\theta = q/p$ to a translational vector ${}^t(0,l,0) \in \mathrm{L} \simeq \mathbb{Z}^3$ to obtain the O-lattice on the $(q\ p\ 0)$-plane, one may see

$$(I - R(2\theta)^{-1})^{-1} \begin{pmatrix} 0 \\ l \\ 0 \end{pmatrix} = \frac{l}{2} \begin{pmatrix} q/p \\ 1 \\ 0 \end{pmatrix}, \tag{6}$$

which is on the $(q\ p\ 0)$-plane. The CSL points are obtained by Eq.(6) if $l$ is divisible by $2p$. If $l$ is odd, the first component of Eq.(6) varies while the second component is maintained at 1/2 in $\tilde{\mathcal{O}}_R(\mathrm{L})$. Therefore, the periodicity of Eq.(6) in $\tilde{\mathcal{O}}_R(L)$ can be given by $2p$. Recalling the case of CSL GBs with short periodicity in Fig.1, it can be shown that the periodicity of the structural units is given by $p$ by drawing structural units as in Fig.3(b) starting with a CSL point and passing through O-lattice points alternately. Now, we consider the GB with the misorientation angle $2\theta \simeq 35.30^\circ$ $(\cot\theta = 22/7)$ corresponding to the (22 7 0)-structure which is a near $\Sigma 5$, (310)-structure with $2\theta_2 \simeq 36.87^\circ$ $(\cot\theta_2 = 1/3)$. In Fig.3(b), the dichromatic pattern of the (22 7 0)-structure with the fundamental domains of L is presented. As in Fig.1, the CSL GBs are defined by the line passing through the CSL points at the edge of the figure below which there are points of L and above which there are points of $R$L. It can be seen that O-lattice points in the structural unit shifts periodically in $\tilde{\mathcal{O}}_R(\mathrm{L})$. In the fourth structural unit from the left, an O-lattice point reaches at the edge of the fundamental domain of L whose internal coordinates are $(0, 1/2, 0) \in \tilde{\mathcal{O}}_R(\mathrm{L})$ with respect to the coordinate system of L. Since the theoretical GB is on the (22 7 0)-plane, the above argument suggests that the periodicity of the structural units is 7. The angle $2\theta \simeq 35.30^\circ$ $(\cot\theta = 22/7)$ corresponds to the CSL configuration of $\Sigma 533$ which is in between $\Sigma 17$, (410) $(2\theta_1 \simeq 28.07^\circ, \cot\theta_1 = 4)$ and the $\Sigma 5$, (310) $(2\theta_2 \simeq 36.87^\circ, \cot\theta_2 = 3)$, and the structure may be composed of the (410) and the (310)-structural units. Eq.(6) becomes $(0, 1/2)$ for $l \equiv 7 (\mathrm{mod}\ 14)$ which appears typically in the $\Sigma 17$, (410) structure (Table 1). Namely, we have (22 7 0) = (4 1 0)+6(3 1 0), which is viewed as a decomposition of a reciprocal vector. As we see, a GB is called the *reference structure* if it is described by an array of a single type structural units which can interpolate intermediate GBs in between them. Once two reference structures are determined appropriately, one can obtain the integral coefficients uniquely for each GB.

3.2. **Farey sequence and GB structure.** The periodicity of the structural units of the $(q\ p\ 0)$-structure can be $p$ corresponding to the periodicity of the O-lattice points. A mirror-symmetrical sequence $\{p_l\}_{l=1}^{29}$:

$$1, \underline{\mathbf{9}}, 8, 7, 6, 5, \underline{\mathbf{9}}, 4, \underline{\mathbf{7}}, 3, \underline{\mathbf{8}}, 5, 7, \underline{\mathbf{9}}, 2, \underline{\mathbf{9}}, 7, 5, \underline{\mathbf{8}}, 3, \underline{\mathbf{7}}, 4, \underline{\mathbf{9}}, 5, 6, 7, 8, \underline{\mathbf{9}}, 1 \tag{7}$$

may appear repeatedly for $p < 10$, corresponding to $0^\circ \leqq 2\theta \leqq 90^\circ$. The sequence is recognized as the numerators of irreducible rational numbers in between $1/m$ and $1/(m-1)$. For instance, irreducible rational numbers in between 1/4 and 1/3 whose numerators are less than 10 can be given by 1/4, 9/35, 8/31, 7/27, 6/23, 5/19, 9/34, 4/15, 7/26, 3/11, 8/29, 5/18, 7/25, 9/32, 2/7, 9/31, 7/24, 5/17, 8/27, 3/10, 7/23, 4/13, 9/29, 5/16, 6/19, 7/22, 8/25, 9/28, 1/3. Therefore, if $p_1 = 1$ and $p_{29} = 1$ correspond to the $\Sigma 17$, (410)-structure with $2\theta_1 \simeq 28.07^\circ (\cot\theta_1 = 4)$ and the $\Sigma 5$, (310)-structure with $2\theta_2 \simeq 36.87^\circ$ $(\cot\theta_2 = 3)$, respectively, $p_{26} = 7$ corresponds to the (22 7 0)-structure with $2\theta \simeq 35.30^\circ$ $(\cot\theta = 22/7)$. It is observed that $p_l = p_{l-1} + p_{l+1}$ holds for underlined

terms in the sequence (7), corresponding to the decomposition of a periodicity $p_l$ to $p_{l-1}$ and $p_{l+1}$.

The hierarchical structure in the distribution of rational numbers can be typically shown in the Farey sequence [37–39]. The Farey sequence of the order $N$ denoted by $F_N$ is defined to be an increasing sequence of irreducible rational numbers whose denominator is not bigger than $N$. It is closely related to physical phenomena [40–45]. As we see, the sequence (7) appears in the numerators in between $1/m$ and $1/(m-1)$ ($m \geqq 2$) as well as in the denominators of the Farey sequence of the order 9. By introducing the operation $\boxplus$ (the Farey summation) defined by

$$\frac{a}{b} \boxplus \frac{c}{d} = \frac{a+c}{b+d}, \tag{8}$$

$F_{N+1}$ can be produced by applying the operation to adjacent rational numbers in $F_N$. By setting $F_1$ to be $\{0/1, 1/1\}$, the Farey diagram can be inductively obtained as in Fig.2. The diagonal line segments in Fig.2 indicate the Farey summation defined in Eq.(8). Each rational number $p/q$ in Fig.2 may correspond to $\cot\theta = q/p$ of a CSL configuration and thus, it can represent the $(q\ p\ 0)$-structure. Note that rational numbers in the early order of the Farey sequence correspond to the low index GBs. Here, we assume the summation in Eq.(8) is assumed to be non-commutative, but cyclic permutations are allowed in order to describe the unique periodical arrangement of structural units.

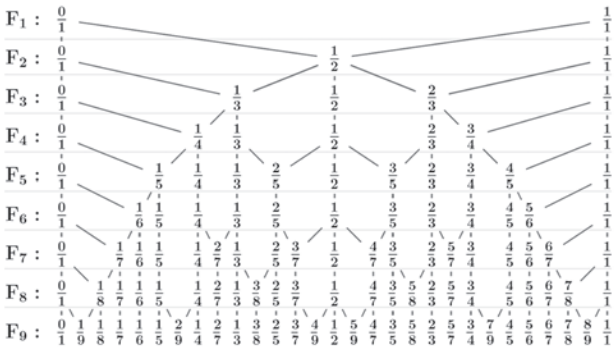


FIGURE 2. The Farey diagram up to the order 9 [34].

Many of the previous investigations have shown that the $(q\ p\ 0)$-structure of a symmetrical tilt GB can be composed of an integral linear combination of two types of reference structures [10–20, 46–49]. Let $p_i$ and $q_i$ be coprime, positive integers (except the case $q_i = 1$ and $p_i = 0$), respectively for $i = 1, 2$. The $(q\ p\ 0)$-structure can be in between the $(q_1\ p_1\ 0)$ and the $(q_2\ p_2\ 0)$-structures if $p_1/q_1 < p/q < p_2/q_2$ is satisfied. Moreover, we assume

$$\det \begin{pmatrix} p_1 & p_2 \\ q_1 & q_2 \end{pmatrix} = -1. \tag{9}$$

Then the general decomposition formula for the $(q\ p\ 0)$-structure of a [001] symmetrical tilt GBs which is in between the $(q_1\ p_1\ 0)$ and the $(q_2\ p_2\ 0)$-structures can be given by

$$(q\ p\ 0) = n_1(q_1\ p_1\ 0) + n_2(q_2\ p_2\ 0), \tag{10}$$

corresponding to a decomposition of a reciprocal vector. If $p_1/q_1$ and $p_2/q_2$ are adjacent rational numbers in the Farey sequence, Eq.(9) can be always satisfied. Therefore, the value of $\tan\theta$ corresponding to the reference structures can be chosen from an adjacent pair of rational numbers in the certain order of the Farey sequence. Once two reference structures satisfying Eq.(9) are determined, the positive integral coefficients $n_1$ and $n_2$ are uniquely obtained for each GB. While $n_1 + n_2 = p$ gives the periodicity of the structural units, the ratio of the number of the structural units can be given by

$$\frac{n_2}{n_1} = -\frac{p_1}{p_2} + \frac{1}{p_2(p_2\cot\theta - q_2)}, \tag{11}$$

which is continuous as a function of the misorientation angle. The $(q\ p\ 0)$-structure is said to be *closer* to the $(q_1\ p_1\ 0)$-structure than the $(q_2\ p_2\ 0)$-structure if $n_1 > n_2$ is satisfied which is equivalent to $p_1/q_1 < p/q < (p_1 + p_2)/(q_1 + q_2)$. Eq.(11) is closely related to the average spacing of DSC dislocations [11, 19, 20, 34]. It is characterized by the DSC Burgers vector defined by the closure failure of a closed circuit of atomic sites in the reference structure of the minority structural unit expanded in the reference structure of the majority structural unit. Its magnitude and orientation is determined by the DSC lattice. The DSC Burgers vector of the $(q_2\ p_2\ 0)$-structure defined in the $(q_1\ p_1\ 0)$-structure by the Left-Handed-First-to-Start manner can be provided by

$$\boldsymbol{b}_{\mathrm{DSC}} = \frac{-2a_0}{q_1^2 + p_1^2}[q_1\ p_1\ 0] \tag{12}$$

for the reference structures satisfying Eq.(9) where $a_0$ is the lattice parameter. If the $(q\ p\ 0)$-structure satisfies Eq.(10) with $n_1 > n_2$, the DSC Burgers vector can be $n_2$ times larger than the one in Eq.(12), resulting in the introduction of $n_2$-dislocations at each of the minority $(q_2\ p_2\ 0)$-structure which may be maximally separated.

It has been assumed that the arrangement of structural units should vary as continuously as possible with respect to the misorientation angle [29]. Thus, for each angle, the arrangement can be determined uniquely among a number of possibilities. Suppose that a GB structure may be described by $s$ copies of A units and $t$ copies of B units $(s > r > 1)$ where $s$ and $r$ are coprime, positive integers (i.e. the CSL configuration is assumed). Let $\lfloor x \rfloor$ denote the maximal integer which does not exceed $x$. The algorithm is to arrange the structural units as evenly as possible by applying the Euclidean division to $r_{-1} = s$ and $r_0 = t$. Namely,

(13)

$$\begin{aligned}
&r_{-1}\mathrm{A} + r_0\mathrm{B}\ (r_{-1} > r_0 > 1)\\
&= r_0\mathrm{A}_1 + r_1\mathrm{A}_0\ (\mathrm{A}_0 = \mathrm{A}, \mathrm{A}_1 = s_0\mathrm{A}_0 + \mathrm{B},\ s_0 = \lfloor r_{-1}/r_0 \rfloor,\ r_0 > r_1 = r_{-1} - r_0 s_0 > 1)\\
&= \cdots = r_k\mathrm{A}_{k+1} + r_{k+1}\mathrm{A}_k\\
&\qquad (\mathrm{A}_{k+1} = s_k\mathrm{A}_k + \mathrm{A}_{k-1},\ s_k = \lfloor r_{k-1}/r_k \rfloor,\ r_k > r_{k+1} = r_{k-1} - s_k r_k > 1)
\end{aligned}$$

which can be iterated until $r_k$ becomes 1 for some $k > 0$.

## 4. Experimental Verification

A crystal of high purity MgO (99.9%) (Shinkosha,Ltd., Tokyo) was purchased to obtain bicrystals. Symmetrical tilt GBs were fabricated based on the bicrystallographic relationships of $2\theta = 35.3°$ (a near the $\Sigma 5$ structure of $2\theta_2 \simeq 36.87°$ ($\cot\theta_2 = 3$)) by high-temperature diffusion bonding of the two single crystals at 1500°C for 10 hours in air. The obtained bicrystals were thinned for STEM observations. The STEM images were taken with the high-angle annular dark field mode (the semi-angle of 60-180 mrad) which provided the intensity proportional to the atomic number [50].

As we see, the misorientation angle $2\theta \simeq 35.3°$ may correspond to the (22 7 0) structure with $\cot\theta = 22/7$. We have $\frac{22}{7} = [3;7] = 6 \circ \frac{3}{1} \boxplus \frac{4}{1}$, supporting the decomposition (22 7 0) = 6(3 1 0)+1(4 1 0). It is assumed that DSC dislocations are introduced in the minority $\Sigma 17$, (410) structural units. In Fig.3(a), a STEM image of the symmetrical tilt GB in MgO with the misorientation angle of 35.3° is presented and a corresponding schematic structural units are superposed. It shows that the periodicity of the structural units can be verified as 7. Although it is a simple example, the way to obtain RAS's is identical to other GBs [51, 52].

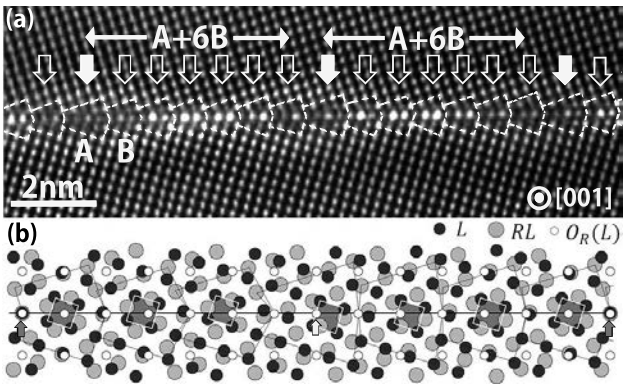


Figure 3. (a) A STEM image of a symmetrical tilt GB in MgO. The tilt angle is approximately 35.3° which is a near $\Sigma 5$ GB of $2\theta_2 \simeq 36.87°$ ($\cot\theta_2 = 3$). The GB is composed of a $\Sigma 17$ structural unit A and 6 copies of $\Sigma 5$ structural unit B in a periodical unit. (b) The dichromatic pattern of lattices L and $R$L for the misorientation of 35.3°. CSL points exist at the edge of the figure. The O-lattice and structural units are superposed so that they pass O-lattice points alternately. The O-lattice point in the middle of the figure reaches at the edge of the fundamental domain with $(0, 1/2) \in \tilde{\mathcal{O}}_R(\mathrm{L})$. The internal coordinate of O-lattice points inside the structural units shift gradually, indicating the periodicity of the GB is 7.

## 5. Summary

Atomic structure of symmetrical tilt GBs are analyzed from mathematical perspective. Under the assumption that GB structure may change as continuously as possible

as a function of misorientation, two types of structural units are arranged so that minority units where DSC dislocations are introduced are maximally separated. Because of this property, the structures of symmetrical tilt GBs can be described by a part of quasi-periodical arrangements of structural units as a realization of the lowest energy structure. Then, reference structures can linearly interpolate intermediate GBs. The major structures were well predicted by a simple decomposition formula of symmetrical tilt GBs with an algorithm due to the Farey sequence. The arrangement of structural units can be derived so as to maximize the separation of minority units which can be applicable to other GBs.

Although direct STEM observations in atomic scale can show the combination of structural units at GBs, the origin and the mechanism of GB phenomena have not been fully understood yet. For instance, the general criterion for reference structures of GBs which cannot be easily determined by their GB energy. The mathematical formulation for the structures of asymmetrical tilt, twist, and their combination are yet unknown. It should also be important to discuss configurational entropy in the structural unit model as well as the dependence on geometrical restrictions.

## 6. Acknowledgements

This work is supported in part by the Elements Strategy Initiative for Structural Materials by the MEXT of Japan and the JSPS Grant-in-Aid for Scientific Research (grant no.15K06420). The STEM image in Fig.3(a) is provided by Dr. Mitsuhiro Saito (the University of Tokyo).

## References

[1] Friedel G (1911) Leçons de cristallographie. (Blanchard, Paris).
[2] Krönberg M L and Wilson F H (1949) Secondary recrystallization in copper. *Trans. AIME.* **185**, 501–514.
[3] Ranganathan S (1966) On the geometry of coincidence-site lattices. *Acta Cryst.* **21**, 197–199.
[4] Brandon D G (1966) The structure of high-angle grain boundaries. *Acta Metall.* **14**, 1479–1484.
[5] Baake M (1997) Solution of the coincidence problem in dimensions $d \leqq 4$. (Kluwer, Dordrecht) In: *The Mathematics of Long-Range Aperiodic Order*, ed. Moody R V, pp. 9-44.
[6] Baake M and Zeiner P (2007) Multiple coincidences in dimensions $d \leq 3$. *Philos. Mag.* **87**(18-21), 2869–2876.
[7] Bishop G H and Chalmers B (1968) A coincidence ledge - dislocation description of grain boundaries. *Scripta Metall.* **2**, 133–140.
[8] Pond R C, Smith D A and Vitek V (1979) Computer simulation of $\langle 110 \rangle$ tilt boundaries: structure and symmetry. *Acta Metall.* **27**, 235–241.
[9] Sutton A P and Vitek V (1980) On the coincidence site lattice and DSC dislocation network model of high angle grain boundary structure. *Scripta Metall.* **14**, 129–132.
[10] Wang G-J, Sutton A P and Vitek V (1984) A computer simulation study of $\langle 001 \rangle$ and $\langle 111 \rangle$ tilt boundaries: the multiplicity of structures. *Acta Metall.* **32**(7), 1093–1104.
[11] Wang G-J and Vitek V (1986) Relationships between grain boundary structure and energy. *Acta Metall.* **34**(5), 951–960.
[12] Morita K and Nakashima H (1997) Atomic periodicity of $\langle 001 \rangle$ symmetric tilt boundary in molybdenum. *Mat. Sci. Eng. A.* **234-236**, 1053–1056.
[13] Tsurekawa S, Tanaka T and Yoshinaga H (1994) Grain boundary structure, energy and strength in molybdenum. *Mat. Sci. Eng. A.* **176**, 341–348.
[14] Nakashima H and Takeuchi M (2000) Grain boundary energy and structure of $\alpha$-Fe $\langle 110 \rangle$ symmetric tilt boundary. *Tetsu-to-Hagane.* **86**(5), 357–362.
[15] Takata N, Mizuguchi T, Ikeda K and Nakashima H (2004) Atomic and electronic structure of $\langle 110 \rangle$ symmetric tilt boundaries in palladium. *Mater. Trans.* **45**(7), 2099–2105.

[16] Tschopp M A and Mcdowell D L (2007) Structures and energies of Σ3 asymmetric tilt grain boundaries in copper and aluminium. *Philos. Mag.* **87**(22), 3147–3173.
[17] Tschopp M A and Mcdowell D L (2007) Asymmetric tilt grain boundary structure and energy in copper and alminium. *Philos. Mag.* **87**(25), 3871–3892.
[18] Rhodes N R, Tschopp M A and Solanki K N (2013) Quantifying the energetics and length scales of carbon segregation to $\alpha$-Fe symmetric tilt grain boundaries using atomistic simulations. *Modelling Simul. Mater. Sci. Eng.* **21**, 035009.
[19] Saito M, Wang Z-C, Tsukimoto S and Ikuhara Y (2013) Local atomic structure of a near-sigma 5 tilt grain boundary in MgO. *J. Mater. Sci.* **48**, 5470–5474.
[20] Saito M, Wang Z-C and Ikuhara Y (2014) Selective impurity segregation at a near-Σ5 grain boundary in MgO. *J. Mater. Sci.* **49**, 3956–3961.
[21] Bollmann W (1967) On the geometry of grain and phase boundaries: I. General theory. *Philos. Mag.* **16**(140), 363–381.
[22] Bollmann W (1967) On the geometry of grain and phase boundaries: II. Applications of general theory. *Philos. Mag.*. **16**(140), 383–399.
[23] Bollmann W (1970) Crystal Defects and Crystalline Interfaces. Springer-Verlag, Berlin.
[24] Pond R C and Bollmann W (1979) The symmetry and interfacial structure of bicrystals. *Phil. Trans. R. Soc. Lond. A.* **292**(1395), 449–472.
[25] Pond R C and Vlachavas D S (1983) Bicrystallography. *Proc. R. Soc. A.* **386**(1790), 95–143.
[26] Sutton A P and Vitek V (1983) On the structure of tilt boundaries in cubic metals I. Symmetrical tilt boundaries. *Phil. Trans. R. Soc. Lond. A.* **309**, 1–36.
[27] Sutton A P and Vitek V (1983) On the structure of tilt boundaries in cubic metals II. Asymmetrical tilt boundaries. *Phil. Trans. R. Soc. Lond. A.* **309**, 37–54.
[28] Sutton A P and Vitek V (1983) On the structure of tilt boundaries in cubic metals III. Generalizations of the structural study and implications for the properties of grain boundaries. *Phil. Trans. R. Soc. Lond. A.* **309**, 55–68.
[29] Sutton A P (1992) Irrational interfaces. *Prog. Mat. Sci.* **36**, 167–202.
[30] Ranganathan S, Srivastava A K and Lord E A (2006) Coincidence-site lattices as rational approximants to irrational twins. *J. Mater. Sci.* **41**, 7696–7703.
[31] Ikuhara Y (2011) Grain boundary atomic structures and light-element visualization in ceramics: combination of Cs-corrected scanning transmission electron microscopy and first-principles calculations. *J. Elect. Microscopy.* **60**(S1), S173–S188.
[32] Pennycook S J and Nellist P D, ed. (2011) Scanning Transmission Electron Microscopy. Springer-Verlag, New York.
[33] Inoue K, Saito M, Wang Z-C, Kotani M and Ikuhara Y (2015) On the periodicity of $\langle 001 \rangle$ symmetrical tilt grain boundaries. *Mater. Trans.* **56**(3), 281–287.
[34] Inoue K, Saito M, Wang Z-C, Kotani M and Ikuhara Y (2015) On the decomposition formula of $\langle 001 \rangle$ symmetrical tilt grain boundaries. *Mater. Trans.* **56**(12), 1945–1952.
[35] Grimmer H, Bollmann W, Warrington D H (1974) Coincidence-site lattices and complete pattern shift lattices in cubic crystals. *Acta Cryst.*
[36] Dirichlet P G L (1899) Verallgemeinerung eines satzes aus der lehre von den kettenbrüchen nebst einigen anwendungen auf die theorie der zahlen. In: *G. Lejune Dirichlet's werke*, ed. Kronecker L, pp. 633-638, (G. Reimer, Berlin); originally appeared in Akad. Wiss. Königl Preuss (1842) 93-95.
[37] Haros C (1802) Tables pour évaluer une fraction ordinaire avec autant de decimals qu'on voudra; et pour trouver la fraction ordinaire la plus simple, et qui approche sensiblement d'une fraction décimale. *J. Ecole Polytechn.* **4**, 364–368.
[38] Farey J (1816) On a curious property of vulger fractions. *Philos. Mag.* **47**(217), 385–386.
[39] Cauchy A (1816) Démonstration d'un théorème curieux sur les nombres. *Bull. Sci. Soc. Philomatique (Paris).* **1816**, 133–135.
[40] Ford L R (1938) Fractions. *Amm. Math. Monthly.* **45**(9), 586–601.
[41] Gourdon O, Izaola Z, Elecoro L, Petricek V and Miller G J (2006) $\mathrm{Zn}_{1-x}\mathrm{Pd}_x (x = 0.14 - 0.24)$: a missing link between intergrowth compounds and quasicrystal approximants. *Philos. Mag.* **86**(3-5), 419–425.
[42] Tomás R (2014) From Farey sequences to resonance diagrams. *Phys. Rev. ST Accel. Beams.* **17**, 014001.

[43] Devaney R L (1999) The Mandelbrot Set, the Farey tree, and the Fibonacci sequence. *Amm. Math. Monthly.* **106**(4), 289–302.
[44] Li A Z, Harter W G (2015) Quantum revivals of Morse oscillators and Farey-Ford geometry. *Chem. Phys. Lett.* 633, 208–213.
[45] Haldane F D M (1983) Fractional quantization of the Hall effect: A hierarchy of incompressible quantum fluid states. *Phys. Rev. Lett.* **51**(7), 605–608.
[46] Nazarov A A and Romanov A E (1987) On the average misorientation angle of general tilt boundaries. *Philos. Mag. Lett.* **60**(5), 187–193.
[47] Chen S P, Srolovitz D J and Voter A F (1989) Computer simulation on surfaces and [001] symmetric tilt grain boundaries in Ni, Al, and $Ni_3Al$. *J. Mat. Res.* **4**, 62–77.
[48] Browning N D, Pennycook S J, Chisholm M F, McGibbon M M and McGibbon A J (1995) Observation of structural units at symmetric [001] tilt boundaries in $SrTiO_3$. *Interface Sci.* **2**, 397–423.
[49] Ohno T, Ii S, Shibata N, Matsunaga K, Ikuhara Y, and Yamamoto T (2004) High Resolution Microscopy Study for [001] Symmetric Tilt Boundary with a Tilt Angle of 66 DEG. in Rutile-type TiO2 Bicrystal. *Mater. Trans.* **45**(7), 2117–2121.
[50] Pennycook S J and Jesson D E (1991) High-resolution Z-contrast imaging of crystals. *Ultramicroscopy.* **37**(1-4), 14–38.
[51] Inoue K, Saito M, Chen C, Kotani M and Ikuhara Y (2016) Mathematical analysis and STEM observations of arrangement of structural units in $\langle 001 \rangle$ symmetrical tilt grain boundaries. *Microscopy.* **65**(6), 479–487.
[52] Inoue K, Feng B, Shibata N, Kotani M and Ikuhara Y (2016) Structure of $\langle 110 \rangle$ tilt boundaries in cubic zirconia. *J. Mat. Sci.* **52**, 4278–4287.

# Lattice defects from monodromy

**FMSP Mathematical Research on Real World Problems, Group G, The University of Tokyo**

Hokuto Konno (The Univ. of Tokyo),
Tsukasa Ishibashi (The Univ. of Tokyo),
Sho Ejiri (The Univ. of Tokyo),
Junichi Nakagawa (Nippon Steel & Sumitomo Metal Co.),
Yasuhiro Wakabayashi (The Univ. of Tokyo)

We study some lattice defects in terms of monodromy in the sense of William Thurston. This description of lattice defects enables us to encode some special structure of it which arises from original lattice structure.

# Lattice defects from monodromy

Hokuto Konno, Tsukasa Ishibashi, Sho Ejiri, Junichi Nakawaga, Yasuhiro Wakabayashi

The University of Tokyo

August 29, 2017
Mathematics in Interface, Dislocation and Structure of Crystals
at Nishijin Plaza, Kyushu University



## Outlines





## Outlines

## Aim of this talk

Describe "lattice defect" in terms of monodromy.

"Lattice defect" · · · Most parts look like usual "lattice", but the lattice structure is broken somewhere.

Typical examples of lattice defects · · · Dislocations

- edge dislocation

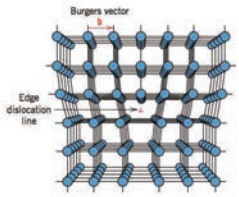


1

[1] Adapted from A. G. Guy, Essentials of Materials Science, McGraw-Hill Book Company, 1976, p. 153.



- screw dislocation

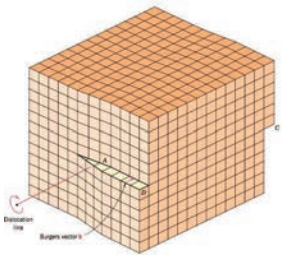

2

[2] Adapted from W. D. Callister, Jr., Materials science and engineering : an introduction, John Wiley & Sons, Inc., 1940, p. 90.



Screw dislocation (from another angle):

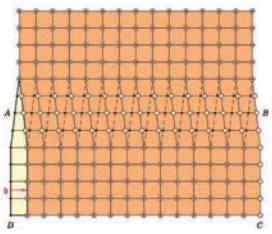


3

[3] Adapted from W. T. Read, Jr., Dislocations in Crystals, McGraw- Hill Book Company, New York, 1953

- Some screw dislocations are described in terms of monodromy by Hamada–Matsutani–Nakagawa–Saeki–Uesaka '16.
- We shall consider a kind of generalization of their description using monodromy in the sense of William Thurston. It can be applied also to edge dislocations (and also to further general lattice defects).



## Outlines





To describe monodromy in the sense of Thurston, we need the notion of $(G, X)$-*manifold*. The content of this section is based on W. Thurston's book entitled *"The geometry and topology of three-manifolds"* (unpublished notes).

**Basic Setting**

$X$ : a topological space
$G$ : a group
Assume that $G$ continuously acts on $X$: we have a group homomorphism $\rho : G \to \mathrm{Homeo}(X)$, where
$\mathrm{Homeo}(X) := \{ f : X \to X \mid f \text{ is a homeomorphism} \}$.

Actually we will only use the case that

- $X$ is a $C^\omega$-manifold, and
- $G \subset \mathrm{Diff}^\omega(X) := \{ f : X \to X \mid f \text{ is a } C^\omega\text{-diffeomorphism} \}$

for our main purpose.

**Definition ((G, X)-manifold)**

$M$ : a topological space
(1) $\{(U_\alpha, \phi_\alpha)\}_\alpha$ is a $(G, X)$-*atlas* on $M$ if

- $\{U_\alpha\}_\alpha$ is an open covering of $M$,
- each $\phi_\alpha : U_\alpha \to X$ is a homeomorphism onto its image, and
- $\phi_\alpha \circ \phi_\beta^{-1}|_{\phi_\beta(U_\alpha \cap U_\beta)} : \phi_\beta(U_\alpha \cap U_\beta) \to \phi_\alpha(U_\alpha \cap U_\beta)$ is the restriction of an element of $\rho(G)$.

(2) $M$ equipped with a $(G, X)$-atlas is called a $(G, X)$-*manifold*.

Each $(U_\alpha, \phi_\alpha)$ is called a $(G, X)$-*chart*.



**Example**

1. $X = \mathbb{R}^n$, $G = \mathrm{Homeo}(\mathbb{R}^n)$
   $\Rightarrow$ $(G, X)$-manifold $=$ topological manifold
2. $X = \mathbb{R}^n$, $G = \mathrm{Diff}(\mathbb{R}^n)$
   $\Rightarrow$ $(G, X)$-manifold $=$ smooth manifold
3. $X = \mathbb{C}^n$, $G = \mathrm{Hol}(\mathbb{C}^n)$
   $\Rightarrow$ $(G, X)$-manifold $=$ complex manifold
4. $X = \mathbb{H}^n$ (hyperbolic space), $G = \mathrm{Isom}(\mathbb{H}^n)$
   $\Rightarrow$ $(G, X)$-manifold $=$ hyperbolic manifold



Henceforth assume that

- $X$ is a $C^\omega$-manifold, and
- $G \subset \mathrm{Diff}^\omega(X) := \{ f : X \to X \mid f \text{ is a } C^\omega\text{-diffeomorphism} \}$.

For each $(G, X)$-manifold $M$, we can define a group homomorphism which is called the *monodromoy*

$$\mathrm{Mon} : \pi_1(M, p_0) \to G$$

if we fix a point $p_0 \in M$ and a $(G, X)$-chart $(U_0, \phi_0)$ near $p_0$. (If we change the initial data $p_0$ and $(U_0, \phi_0)$, the map is changed by conjugation. )
We now sketch the construction of the monodromy map.

Idea of the construction:

1. Take a loop $\gamma : [0,1] \to M$ with base point $p_0$.
2. Take $(G, X)$-charts $(U_1, \phi_1), \ldots, (U_n, \phi_n)$ which cover the image of $\gamma$. (Note that the neighborhood of the base point is already covered by $U_0$.) Take the covers so that $U_i \cap U_{i+1}$ is non-empty and connected $(0 \leqslant \forall i \leqslant n-1)$.
3. $\exists! g_i \in G$ s.t. $g_i$ gives the coordinate change of $(U_i, \phi_i)$ and $(U_{i+1}, \phi_{i+1})$. (Here, for the uniqueness, we need to assume $C^\omega$.)
4. One can show that $\mathrm{Mon}([\gamma]) := g_0 \cdots g_{n-1} \in G$ depends only on the homotopy class of $\gamma$ (for the fixed chart $(U_0, \phi_0)$).

If we take another base point $p_0'$ and a chart $(U_0', \phi_0')$ near $p_0'$, the monodoromy map is changed by conjugation. In particular, if $G$ is abelian, we have a homomorphism $\mathrm{Mon} : \pi_1(M) \to G$ which is independent of the choice of base points and charts near that.



## Outlines





Recall:
"Lattice defect" $\cdots$ Most parts look like usual "lattice", but the lattice structure is broken somewhere.

LOCALLY, it looks like the standard $\mathbb{Z}^3$ in $\mathbb{R}^3$.
$\rightsquigarrow$ One can hope to give a $(\mathbb{Z}^3, \mathbb{R}^3)$-manifold structure corresponding to the graph of the given lattice defect.
$\rightsquigarrow$ One can obtain the monodromy (like as "invariant" of lattice defects).

Given a picture of a lattice defect,

- assume that we have the notion of "vertices" ($\leftrightarrow$ lattice point), and
- assume that we have the notion of "edges" ($\leftrightarrow$ nearest lattice points).

e.g. edge dislocation

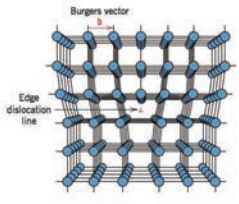


[4]

[4] Adapted from A. G. Guy, Essentials of Materials Science, McGraw-Hill Book Company, 1976, p. 153.



Define $M$ as the "fat graph":

$$M := \bigcup_{E:edge,\ p\in E} B_p(\epsilon),$$

where $\epsilon > 0$ is a sufficiently small number, and $B_p(\epsilon)$ is the open ball centered at $p$ with radius $\epsilon$. $M$ is an open submanifold of $\mathbb{R}^3$.

In some good situation, we can give a $(\mathbb{Z}^3, \mathbb{R}^3)$-manifold structure on $M$. We now explain the $(\mathbb{Z}^3, \mathbb{R}^3)$-manifold structure for edge/screw dislocation.

We first consider a 2-dimensional model of edge dislocation.



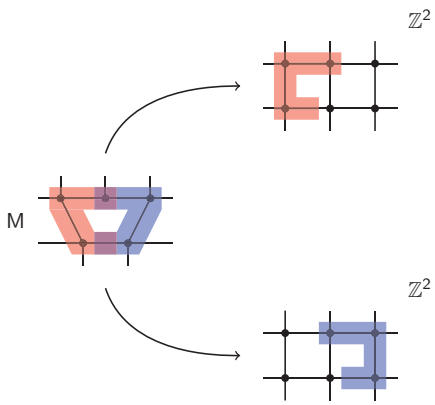


Figure: $(\mathbb{Z}^2, \mathbb{R}^2)$-charts on the edge dislocation

Strictly speaking, to calculate the monodromy following the definition, we have to decompose these two charts to be "$U_i \cap U_{i+1}$ is connected for each $i$". The coordinate change between new two charts arising from the previous one chart is just $\mathrm{id}$.

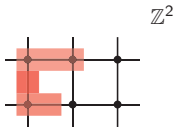


Figure: Example of decomposition



Calculation of monodromy:

- (coordinate change between (1) and (1)') $= (0,0) \in \mathbb{Z}^2$.
- (coordinate change between (2) and (2)') $= (1,0) \in \mathbb{Z}^2$.

$\rightsquigarrow$ monodromy along this loop $= (0,0) + (1,0) = (1,0) \in \mathbb{Z}^2$.
(Since $G = \mathbb{Z}^2$ is abelian, we don't care about base points.)

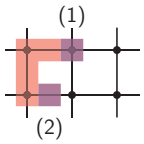


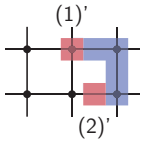




Except for near this loop, one can trivially give $(\mathbb{Z}^2, \mathbb{R}^2)$-charts on $M$.
Since $M \sim \bigvee_{\mathbb{Z}} S^1$ (homotopy equivalent), we have $\pi_1(M) \cong *_{\mathbb{Z}}\mathbb{Z}$.
The monodromy map

$$\mathrm{Mon} : \pi_1(M) \cong *_{\mathbb{Z}}\mathbb{Z} \to \mathbb{Z}^2$$

is non-trivial: (the above loop) $\mapsto (1,0)$.

Of course one can consider 3-dimensional model of edge dislocation, and similarly obtain

$$\mathrm{Mon} : \pi_1(M) \cong *_{\mathbb{Z}}\mathbb{Z} \to \mathbb{Z}^3.$$

We have similarly have a distinguished loop, and
(the distinguished loop) $\mapsto (1,0,0)$.

**Remark**

The non-trivial direction $(1, 0, 0)$ for monodromy is perpendicular to the dislocation line $\mathbb{R} \cdot (0, 0, 1)$.

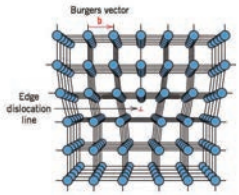


[5]

[5] Adapted from A. G. Guy, Essentials of Materials Science, McGraw-Hill Book Company, 1976, p. 153.



For screw dislocation, we have to get rid of the "zigzag" part to give a $(\mathbb{Z}^3, \mathbb{R}^3)$-manifold structure on M, obtained from the following graph:

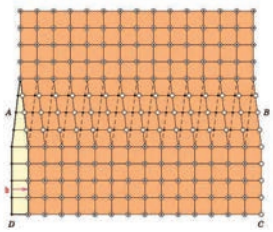


[6]

One reason why we have to do is, for example, the existence of a vertex with three edges. This part cannot be a subgraph of $\mathbb{Z}^3$.

[6] Adapted from W. T. Read, Jr., Dislocations in Crystals, McGraw- Hill Book Company, New York, 1953



However, if we get rid of this zigzag part, we can give a $(\mathbb{Z}^3, \mathbb{R}^3)$-manifold structure on $M$, and calculate the monodromy.

This monodromy corresponds to Hamada–Matsutani–Nakagawa–Saeki–Uesaka 's description.

**Remark**

The non-trivial direction for monodromy is parallel to the dislocation line.

This suggests that the monodromy detects the difference between edge and screw dislocations.

## Question

- Give a mathematical definition of "lattice defect" so that one can give a $(\mathbb{Z}^3, \mathbb{R}^3)$-manifold structure on it.
- More precisely, construct $(\mathbb{Z}^3, \mathbb{R}^3)$-manifold structure on a given lattice defect *canonically*. (Then the monodromy turns out to be an invariant of lattice defects.)
- If one need, consider another group $G \subset \mathrm{Diff}^{\omega}(\mathbb{R}^3)$ rather than $\mathbb{Z}^3$ to describe more complicated lattice defect.

# Geometry of closed kinematic chain

**Shizuo Kaji**

Yamaguchi University

(joint work with Eliot Fried, Michael Grunwald, and Johannes Schoenke at OIST)

Consider a system consisting of rigid bodies connected to each other. Such a system can be modelled by a graph with edges labelled by elements of the Euclidean group SE(3), where each cycle satisfies a certain closedness condition. We are particularly interested in a system consisting of hinges. To each vertex is assigned one degree-of-freedom, namely the rotation angle, and the configuration space of the system is described by the real solution to a system of polynomial equations. We found an interesting family of systems on cycle graphs, whose configuration spaces form positive dimensional real algebraic varieties. They are a type of so called Kaleidocycle (e.g., [1, 2]), but exhibit intriguing properties such as anti-symmetry and constant bending energy.

## References

[1] Safsten, Clarke A., Fillmore, Travis B., Logan, Andrew E., Halverson, Denise M., and Howell, Larry L, *Analyzing the Stability Properties of Kaleidocycles*, ASME. J. Appl. Mech.2016;83(5):051001-051001-13. doi:10.1115/1.4032572.

[2] D. Schattschneider, D. and W. M. Walker, *M. C. Escher Kaleidocycles*, Pomegranate Communications: Rohnert Park, CA, 1987.

# Discrete-to-continuum limits of moving straight edge dislocations in 2D

**Patrick van Meurs**
Kanazawa University
(joint work with Adriana Garroni, Mark Peletier, Lucia Scardia)

In the celebrated paper by Groma and Balogh [3] the evolution for the edge dislocation density given by $(P_n)$ is based on performing statistical mechanics on the discrete edge dislocation dynamics given by $(P)$ for a large number of dislocations. Here, we present the first rigorous result of — and *counterexample* to — the evolutionary convergence of $(P_n)$ to $(P)$.

We consider $n$ edge dislocations with positions $(x_1, \dots, x_n) \in (\mathbb{T}^2)^n$ ($\mathbb{T}^2$ is the flat two-dimensional torus) and Burgers vectors $b_i e_1$ with $b_i \in \{-1, +1\}$. The evolution equation is given by

$$(P_n) \qquad \frac{dx_i}{dt} = -\left[\partial_1 U(x_i) + \frac{1}{n}\sum_{j=1}^{n} b_j \partial_1 V(x_i - x_j)\right] b_i e_1, \quad t \in (0,T),\ i = 1, \dots, n,$$

where $\partial_1 := e_1 \cdot \nabla$, $U : T^2 \to \mathbb{R}$ is an external potential, and $V$ is the interaction potential for edge dislocation in $\mathbb{T}^2$ with the same Burgers vector (in particular, $V(x) = (e_1 \cdot x/|x|)^2 - \log|x| + o(1)$ for $|x| \ll 1$). The evolution for the dislocation densities $\rho^+$ and $\rho^-$ of the positive ($b_i = 1$) and negative ($b_i = -1$) dislocations are given by

$$(P) \qquad \begin{cases} \partial_t \rho^+ = \partial_1\big(\rho^+(\partial_1 V * (\rho^+ - \rho^-) + \partial_1 U)\big) & \text{in } \mathcal{D}'(\mathbb{T}^2 \times (0,T)), \\ \partial_t \rho^- = \partial_1\big(\rho^-(\partial_1 V * (\rho^- - \rho^+) - \partial_1 U)\big) & \text{in } \mathcal{D}'(\mathbb{T}^2 \times (0,T)). \end{cases}$$

The counterexample is constructed for $U \not\equiv 0$ and the initial data $\rho^+_\circ = \rho^-_\circ \equiv \frac{1}{2}$, which is not a stationary solution of $(P)$. However, the discrete approximating sequence of $\rho^\pm_\circ$ given by well-separated dipoles (i.e., $|x^+_{\circ,i} - x^-_{\circ,i}| \ll \frac{1}{n}$ and $|x^+_{\circ,i} - x^+_{\circ,j}| > \frac{c}{n}$ for all $i, j, n$) results in an approximately stationary solution to $(P_n)$. Hence, $(P)$ may not be a good approximation for $(P_n)$ for any $n$ large enough.

Our second result is a theorem which specifies evolutionary convergence of a *regularised* version, called $(P_n^{\delta_n})$, of $(P_n)$ to $(P)$. $(P_n^{\delta_n})$ is obtained from $(P_n)$ by replacing $V$ by $V_{\delta_n}$, where $\delta_n \to 0$ as $n \to \infty$ is the length scale at which the logarithmic singularity of $V$ is regularized (e.g., by convolution with the usual mollifier). The proof of evolutionary convergence is divided into two steps. In the first step, the limit passage $n \to \infty$ is performed for $\delta_n = \delta > 0$ fixed by employing the theory of $\lambda$-convex Wasserstein gradient flows in [1], which yields an explicit convergence rate of the solutions to $(P_n^\delta)$ to those of $(P^\delta)$, where $(P^\delta)$ is obtained from $(P)$ by replacing $V$ by $V_\delta$. The second step establishes evolutionary convergence of $(P^\delta)$ to $(P)$ as $\delta \to 0$ by modifying the well-posedness proof of $(P)$ developed in [2].

## References

[1] L. Ambrosio, N. Gigli, and G. Savaré. *Gradient Flows: In Metric Spaces and in the Space of Probability Measures.* Birkhäuser Verlag, New York, 2008.

[2] M. Cannone, A. El Hajj, R. Monneau, and F. Ribaud. Global existence for a system of non-linear and non-local transport equations describing the dynamics of dislocation densities. *Archive for Rational Mechanics and Analysis*, 196(1):71–96, 2010.

[3] I. Groma and P. Balogh. Investigation of dislocation pattern formation in a two-dimensional self-consistent field approximation. *Acta Materialia*, 47(13):3647–3654, 1999.

# Discrete-to-continuum limits of moving straight edge dislocations in 2D

Patrick van Meurs

Post Doc. under guidance of **Prof. M. Kimura** at **Kanazawa University**

Funding: **JSPS** (as International Research Fellow)

Presented work is done in collaboration with:
**A. Garroni** (La Sapienza, Rome, Italy)
**M. A. Peletier** (TU Eindhoven, Netherlands)
**L. Scardia** (University of Bath, United Kingdom)

30 August, 2017



## Setting

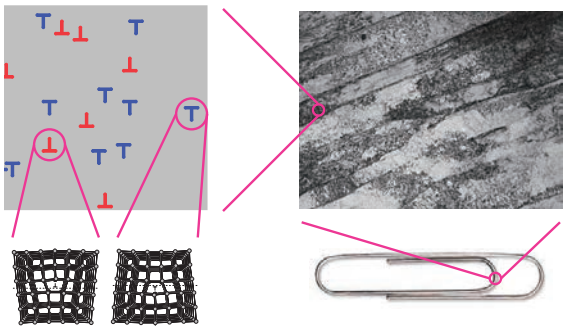

The density picture is by courtesy of © Fraunhofer IWS Dresden, Germany



## Dislocation dynamics as a system of ODEs

- $n$: number of dislocations
- $x = (x_1, \dots, x_n) \in (\mathbb{R}^2)^n$: dislocation positions [unknowns]
- $b_i \in \{+1, -1\}$: sign of the dislocations [given]
- $V$: interaction potential
$$V(r,\theta) = -\log r + \cos^2\theta$$
$$-\partial_1 V(r,\theta) = \tfrac{1}{r}\cos(\theta)\cos(2\theta)$$
$$\partial_1 V(0) := 0, \quad \partial_1 := e_1 \cdot \nabla$$
- $F \in \mathbb{R}$: external horizontal force
- Evolution driven by **interactions**:

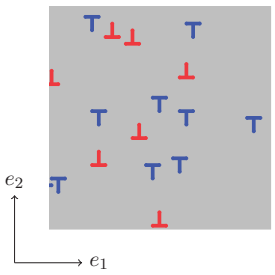


$$(P_n) \quad \frac{d}{dt}x_i(t) = \left[F + \frac{1}{n}\sum_{j=1}^{n} b_j[-\partial_1 V](x_i(t) - x_j(t))\right] b_i e_1, \quad i = 1, \dots, n.$$

## Main question

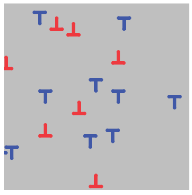

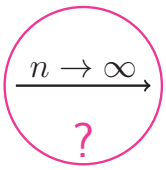


$(P_n)$ $\qquad\qquad$ $(P)$

$$\frac{dx_i}{dt} = \left[F + \frac{1}{n}\sum_{j=1}^{n} b_j[-\partial_1 V](x_i - x_j)\right] b_i e_1 \qquad \begin{aligned} \partial_t \rho^+ &= \partial_1\big(\rho^+[\partial_1 V * (\rho^+ - \rho^-) - F]\big) \\ \partial_t \rho^- &= \partial_1\big(\rho^-[\partial_1 V * (\rho^- - \rho^+) + F]\big) \end{aligned}$$

- Continuum PDE proposed by [Groma, Balogh; 1999]
- No **rigorous** connection is known
- General theme: micro–macro connection



## Lit overview: courtesy of M.A.Peletier

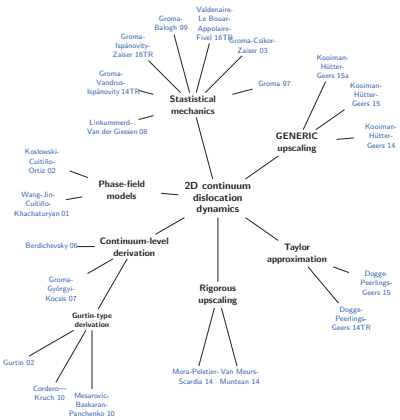




## Simulation with $F > 0$: initial condition

$(P_n)$ $\qquad\qquad$ $(P)$

$$\frac{dx_i}{dt} = \left[F + \frac{1}{n}\sum_{j=1}^{n} b_j[-\partial_1 V](x_i - x_j)\right] b_i e_1 \qquad \begin{aligned} \partial_t \rho^+ &= \partial_1\big(\rho^+[\partial_1 V * (\rho^+ - \rho^-) - F]\big) \\ \partial_t \rho^- &= \partial_1\big(\rho^-[\partial_1 V * (\rho^- - \rho^+) + F]\big) \end{aligned}$$

$(P_n)$

$(P)$

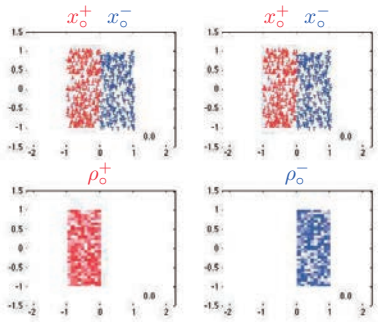

## Simulation with $F > 0$ at $t = t_1$

$(P_n)$

$$\frac{dx_i}{dt} = \left[F + \frac{1}{n}\sum_{j=1}^{n} b_j[-\partial_1 V](x_i - x_j)\right] b_i e_1$$

$(P)$

$$\begin{aligned}\partial_t \rho^+ &= \partial_1\left(\rho^+[\partial_1 V * (\rho^+ - \rho^-) - F]\right)\\ \partial_t \rho^- &= \partial_1\left(\rho^-[\partial_1 V * (\rho^- - \rho^+) + F]\right)\end{aligned}$$

$(P_n)$

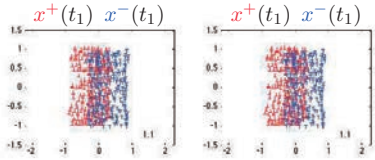


$(P)$

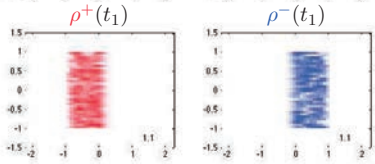




## Simulation with $F > 0$ at $t = t_2$

$(P_n)$

$$\frac{dx_i}{dt} = \left[F + \frac{1}{n}\sum_{j=1}^{n} b_j[-\partial_1 V](x_i - x_j)\right] b_i e_1$$

$(P)$

$$\begin{aligned}\partial_t \rho^+ &= \partial_1\left(\rho^+[\partial_1 V * (\rho^+ - \rho^-) - F]\right)\\ \partial_t \rho^- &= \partial_1\left(\rho^-[\partial_1 V * (\rho^- - \rho^+) + F]\right)\end{aligned}$$

$(P_n)$

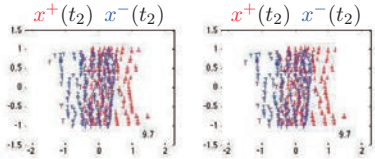


$(P)$

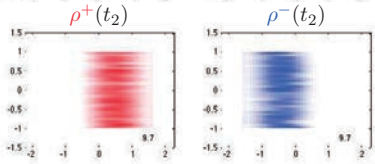




## Simulation with $F > 0$ at $t = t_3$ (boundaries at $\pm\frac{3}{2}e_1$)

$(P_n)$

$$\frac{dx_i}{dt} = \left[F + \frac{1}{n}\sum_{j=1}^{n} b_j[-\partial_1 V](x_i - x_j)\right] b_i e_1$$

$(P)$

$$\begin{aligned}\partial_t \rho^+ &= \partial_1\left(\rho^+[\partial_1 V * (\rho^+ - \rho^-) - F]\right)\\ \partial_t \rho^- &= \partial_1\left(\rho^-[\partial_1 V * (\rho^- - \rho^+) + F]\right)\end{aligned}$$

$(P_n)$

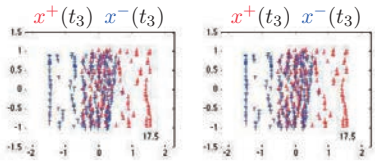


$(P)$

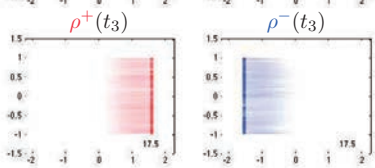

## Rigorous result on mismatch

$$\partial_t \rho^+ = \partial_1\big(\rho^+[\partial_1 V * (\rho^+ - \rho^-) - F]\big)$$
$$\partial_t \rho^- = \partial_1\big(\rho^-[\partial_1 V * (\rho^- - \rho^+) + F]\big)$$

With $F > 0$, $(P)$ is **not** stationary at

$$\rho_\circ^+ = \rho_\circ^- = \left\{ \begin{array}{ll} 1 & \text{on } (0,1)^2 \\ 0 & \text{otherwise} \end{array} \right\}.$$

Picture: $\exists x_\circ^\pm \approx \rho_\circ^\pm$ for which the solution $x(t)$ to $(P_n)$ is 'approximately stationary'

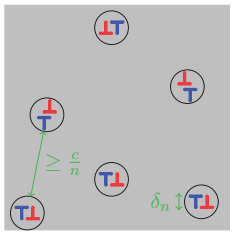


**Conclusion**: if $n^{3/2}\delta_n \to 0$, then $x^\pm(t) \not\approx \rho^\pm(t)$ for all $t > 0$

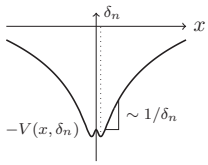




## How about our main question?

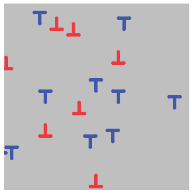

$(P_n)$

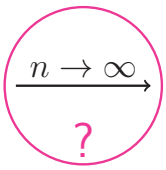


$(P)$

$$\frac{dx_i}{dt} = \left[F + \frac{1}{n}\sum_{j=1}^{n} b_j[-\partial_1 V](x_i - x_j)\right] b_i e_1$$

$$\partial_t \rho^+ = \partial_1\big(\rho^+[\partial_1 V * (\rho^+ - \rho^-) - F]\big)$$
$$\partial_t \rho^- = \partial_1\big(\rho^-[\partial_1 V * (\rho^- - \rho^+) + F]\big)$$

- Seemingly: no $(P)$ exists in terms of $\rho^+$, $\rho^-$ only!
- Statistical model of [Groma, Balogh; 1999] has limited applicability



## On the other hand...

$(P_n) \xrightarrow{n\to\infty} (P)$ holds when

- $\partial_1 V$ is **Lipschitz** [no singularity; next few slides], or
- all dislocation have the **same sign** (i.e., $\mu_n^- = 0 = \rho^-$), and
  - $V$ is **logarithmic** [Schochet; 1996]
  - $V(r,\theta) = |r|^{-\alpha}$ with $0 < \alpha < 1$ [Duerinckx; 2015]
  - $\Omega = (a,b)$ with $V$ **convex** [vM, Muntean; 2014]
  - $V(r,\theta) = |r|^{-\alpha}$ with $0 < \alpha < d-2$ and $\Omega \subset \mathbb{R}^d$ [Hauray; 2009]

  **Open problem**: which properties of $V$ are sufficient/necessary for $(P_n) \to (P)$ in the single-sign case?
  - It seems: the stronger the singularity of $V$, the more $(P)$ regularises $\rho^\pm$ over time, but the worse the control over $(P_n)$

## A different approach: regularising the dislocation core

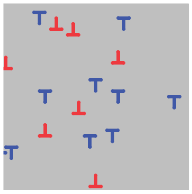

$$\xrightarrow{n \to \infty}$$

?

$(P_n)$ $\qquad$ $(P)$

$$\frac{dx_i}{dt} = \left[F + \frac{1}{n}\sum_{j=1}^{n} b_j[-\partial_1 V_{\delta_n}](x_i - x_j)\right] b_i e_1 \qquad \begin{aligned} \partial_t \rho^+ &= \partial_1\big(\rho^+[\partial_1 V * (\rho^+ - \rho^-) - F]\big) \\ \partial_t \rho^- &= \partial_1\big(\rho^-[\partial_1 V * (\rho^- - \rho^+) + F]\big) \end{aligned}$$

- For instance, $V_\delta := V * \eta_\delta$
- Other choices: cutting away balls, phase field
- $\delta_n$ is an atomic length-scale $\rightsquigarrow$ $\delta_n \xrightarrow{n\to\infty} 0$



## The auxiliary problem $(P^\delta)$

$$(P_n^\delta) \qquad \frac{dx_i}{dt} = \left[F + \frac{1}{n}\sum_{j=1}^{n} b_j[-\partial_1 V_\delta](x_i - x_j)\right] b_i e_1$$

$$(P^\delta) \qquad \begin{cases} \partial_t \rho_\delta^+ = \partial_1\big(\rho_\delta^+[\partial_1 V_\delta * (\rho_\delta^+ - \rho_\delta^-) - F]\big) \\ \partial_t \rho_\delta^- = \partial_1\big(\rho_\delta^-[\partial_1 V_\delta * (\rho_\delta^- - \rho_\delta^+) + F]\big) \end{cases}$$

$$(P) \qquad \begin{cases} \partial_t \rho^+ = \partial_1\big(\rho^+[\partial_1 V * (\rho^+ - \rho^-) - F]\big) \\ \partial_t \rho^- = \partial_1\big(\rho^-[\partial_1 V * (\rho^- - \rho^+) + F]\big) \end{cases}$$

$$\begin{array}{ccccc} (P_n^\delta) & & (P^\delta) & & (P) \\ x^{n,\pm} & \xrightarrow{n \to \infty} & \rho_\delta^\pm & \xrightarrow{\delta \to 0} & \rho^\pm \end{array}$$

For convenience, we set $F = 0$



## Standard approach: $(P_n^\delta) \to (P^\delta)$ as $n \to \infty$ (part 1)

- We assume:
  - $\partial_1 V_\delta$ **Lipschitz**, and
  - the solution trajectories $x_i(t)$ from $(P_n^\delta)$ remain in a **bounded domain** $\Omega \subset \mathbb{R}^2$
- We define the **empirical measures**

$$\mu_n^+ := \frac{1}{n}\sum_{i\,:\,b_i=+1} \delta_{x_i}, \quad \mu_n^- := \frac{1}{n}\sum_{i\,:\,b_i=-1} \delta_{x_i}$$

Note: $(\mu_n^+, \mu_n^-) \in \mathcal{P}\big(\overline{\Omega} \times \{+1, -1)\}\big) \ni (\rho^+, \rho^-)$

- **Weak topology**: $\mu_n^\pm \rightharpoonup \rho^\pm$ iff

$$\int_{\overline{\Omega}} \varphi \, d\mu_n^\pm \xrightarrow{n\to\infty} \int_{\overline{\Omega}} \varphi \, d\rho^\pm \qquad \forall \varphi \in C(\overline{\Omega})$$

## Standard approach: $(P_n^\delta) \to (P^\delta)$ as $n \to \infty$ (part 2)

Let $x(t)$ satisfy $(P_n^\delta)$, and let $\varphi \in C_c^\infty(\Omega \times (0,T))$. Then

$$\begin{aligned} 0 &= \int_0^T \frac{d}{dt}\varphi(x_i(t),t)\,dt = \dots \\ &= \int_0^T \partial_t\varphi(x_i,t) + \partial_1\varphi(x_i,t)\cdot\big[b_i\big(-\partial_1 V_\delta * (\mu_n^+ - \mu_n^-)\big)(x_i)\big]\,dt. \end{aligned}$$

Taking $\frac{1}{n}\sum_{i:b_i=+1}\dots$, we obtain

$$0 = \int_0^T\int_{\overline{\Omega}} \partial_t\varphi\,d\mu_n^+\,dt + \int_0^T\int_{\overline{\Omega}} \partial_1\varphi\cdot\big[-\partial_1 V_\delta * (\mu_n^+ - \mu_n^-)\big]\,d\mu_n^+\,dt \quad \forall\,\varphi \in C_c^\infty,$$

which is $\partial_t\mu_n^+ = \partial_1\big(\mu_n^+[\partial_1 V_\delta * (\mu_n^+ - \mu_n^-)]\big)$ in distributional sense.

**Conclusion**: $(\mu_n^+, \mu_n^-)$ satisfies $(P^\delta)$



## Standard approach: $(P_n^\delta) \to (P^\delta)$ as $n \to \infty$ (part 3)

$$0 = \int_0^T\int_{\overline{\Omega}} \partial_t\varphi\,d\mu_n^+\,dt + \int_0^T\int_{\overline{\Omega}} \partial_1\varphi\cdot\big[-\partial_1 V_\delta * (\mu_n^+ - \mu_n^-)\big]\,d\mu_n^+\,dt$$

- $\mathcal{P}(\overline{\Omega}\times\{+1,-1\})$ compact in weak topology
  $\Longrightarrow$ for a.e. $t$ $\exists\, n_k$ $\exists\,\rho^\pm(t) : \mu_{n_k}^\pm(t) \rightharpoonup \rho^\pm(t)$ as $k \to \infty$
- Arzelà-Ascoli: $n_k$ is $t$-independent
- With

$$\begin{aligned} &\int_{\overline{\Omega}} \partial_1\varphi\cdot\big[-\partial_1 V_\delta * (\mu_n^+ - \mu_n^-)\big]\,d\mu_n^+ \\ &\qquad = \iint_{\overline{\Omega}\times\overline{\Omega}} \partial_1\varphi(x)\,(-\partial_1 V_\delta)(x-y)\,d\big[(\mu_n^+ - \mu_n^-)\otimes\mu_n^+\big](y,x) \end{aligned}$$

we pass to the limit $n_k \to \infty$ in weak-$(P_n^\delta)$



## Standard approach: $(P_n^\delta) \to (P^\delta)$ as $n \to \infty$ (part 4)

We have proven $\boxed{\text{“}(P_n^\delta) \xrightarrow{n\to\infty} (P^\delta)\text{”}}$, i.e.,

- Let $\Omega \subset \mathbb{R}^2$ be a bounded domain, $T, \delta > 0$
- Then for all $(\rho_\circ^+, \rho_\circ^-) \in \mathcal{P}(\overline{\Omega}\times\{+1,-1\})$
- for all* $\mu_{n,\circ}^\pm \rightharpoonup \rho_\circ^\pm$
- there exists $n_k$ and $(\rho_\delta^+, \rho_\delta^-) \in AC(0,T;\mathcal{P}(\overline{\Omega}\times\{\pm\}))$ such that
  (i) $\mu_{n_k}^\pm(t) \rightharpoonup \rho_\delta^\pm(t)$ for a.e. $0 < t < T$
  (ii) $\rho_\delta^\pm(t)$ satisfies $(P^\delta)$ with $\rho_\delta^\pm(0) = \rho_\circ^\pm$

$$\begin{tikzcd} \mu_{n,\circ}^+ \arrow[r, "\partial_t\mu_n^+ = \partial_1\big(\mu_n^+[\partial_1 V_\delta * (\mu_n^+ - \mu_n^-)]\big)"] \arrow[d, "n\to\infty"'] & \mu_n^+(t) \arrow[d, "n_k\to\infty"] \\ \rho_\circ^+ \arrow[r, "\partial_t\rho_\delta^+ = \partial_1\big(\rho_\delta^+[\partial_1 V_\delta * (\rho_\delta^+ - \rho_\delta^-)]\big)"] & \rho_\delta^+(t) \end{tikzcd}$$

$(*)$ we assume $x_i(t) \in \Omega$ for all $i, n, t$

## Standard approach: $(P_n^\delta) \to (P^\delta)$ as $n \to \infty$ (part 5)

The following **Gronwall** estimate holds:

$$W_2\big(\mu_n^\pm(t), \rho_{n,\delta}^\pm(t)\big) \le e^{T\|\partial_1 V_\delta\|_{Lip}} W_2\big(\mu_{n,\circ}^\pm, \alpha_n \rho_\circ^\pm\big)$$

- $\alpha_n := \dfrac{\mu_{n,\circ}^\pm(\overline{\Omega})}{\rho_\circ^\pm(\overline{\Omega})}$ balances the total $\pm$-mass
- $\rho_{n,\delta}^\pm(t)$ satisfies $(P^\delta)$ with initial data $\alpha_n \rho_\circ^\pm$
- $W_2$: **Wasserstein distance**; metrises narrow topology
- Proof of estimate:
  - either by explicit computation, or
  - using that $(P_n^\delta)$ and $(P^\delta)$ are **gradient flows** with $-\boldsymbol{\lambda}$**-convex energies** $[\lambda = \|\partial_1 V_\delta\|_{Lip}]$



## Overview

$$\begin{array}{ccccc} (P_n^\delta) & & (P^\delta) & & (P) \\ \mu_n^\pm & \xleftrightarrow[\substack{W_2\big(\mu_n^\pm(t), \rho_{n,\delta}^\pm(t)\big) \le \\ \exp(T\|\partial_1 V_\delta\|_{Lip})\, W_2\big(\mu_{n,\circ}^\pm, \alpha_n \rho_\circ^\pm\big)}]{} & \alpha_n \rho_\circ^\pm & \xrightarrow[?]{} & \rho^\pm \end{array}$$



## Main challenge: $(P^\delta) \to (P)$?

$$(P^\delta) \qquad \begin{aligned} \partial_t \rho_\delta^+ &= \partial_1\big(\rho_\delta^+ [\partial_1 V_\delta * (\rho_\delta^+ - \rho_\delta^-)]\big) \\ \partial_t \rho_\delta^- &= \partial_1\big(\rho_\delta^- [\partial_1 V_\delta * (\rho_\delta^- - \rho_\delta^+)]\big) \end{aligned}$$

Weak-$(P^\delta)$ $$\int_0^T \int_{\overline{\Omega}} \partial_t \varphi \, d\rho_\delta^+ dt = \int_0^T \int_{\overline{\Omega}} \partial_1 \varphi \cdot \big[\partial_1 V_\delta * (\rho_\delta^+ - \rho_\delta^-)\big] \, d\rho_\delta^+ dt$$

- Interesting feature:
  $(P^\delta)$: $\partial_1 V_\delta * (\rho_\delta^+ - \rho_\delta^-)$ smooth, but $\rho_\delta^\pm$ may have delta-peaks
  $(P)$: singularity $V$ regularises $\rho^\pm$, but $\partial_1 V * (\rho^+ - \rho^-)$ rough
- Note: not clear why $(P)$ makes sense!
- [Monneau *et al.*; 2010]: $(P)$ is well-posed on $\mathbb{T}^2$
- Note: on $\mathbb{T}^2$, $f \in L^2(\mathbb{T}^2) \Longrightarrow \widehat{f} \in \ell^2(\mathbb{Z}^2)$
- Reason $\mathbb{T}^2$: $\exists C > 0 \; \forall k \in \mathbb{Z}^2 : 0 \le (1 + |k|^2)\widehat{V}_k \le C$
  We take $V_\delta \in W^{2,\infty}(\mathbb{T}^2)$ to satisfy the same bound
  We **define**: $\big[\widehat{\partial_1 V * f}\big]_k := 2\pi i k_1 \widehat{V}_k \widehat{f}_k$

## Improvement of Monneau's well-posedness of $(P)$

Key observation: if $\rho_\delta^\pm$ **smooth** solution to $(P^\delta)$, then $[\kappa_\delta := \rho_\delta^+ - \rho_\delta^-]$

$$\sum_\pm \partial_t \operatorname{Ent}(\rho_\delta^\pm) := \sum_\pm \partial_t \int_{\mathbb{T}^2} \rho_\delta^\pm \log \rho_\delta^\pm = \dots$$
$$= \int_{\mathbb{T}^2} [\partial_{11} V_\delta] * \kappa_\delta \, d\kappa_\delta \le -c \|\partial_1 V_\delta * \kappa_\delta\|^2_{H^1(\mathbb{T}^2)} \le 0.$$

Taking $\int_0^t \dots ds$, we obtain

$$\sum_\pm \operatorname{Ent}(\rho_\delta^\pm(t)) + c\|\partial_1 V_\delta * \kappa_\delta\|^2_{L^2(H^1)} \le \sum_\pm \operatorname{Ent}(\rho_{\delta,\circ}^\pm),$$

where $L^2(H^1) := L^2(0,T;H^1(\mathbb{T}^2))$. Hence, along a subsequence

$$\begin{aligned} \rho_\delta^\pm &\rightharpoonup \rho^\pm && \text{in } L^\infty(L\log L) \\ \partial_1 V_\delta * \kappa_\delta &\rightharpoonup \partial_1 V * \kappa && \text{in } L^2(H^1) \end{aligned}$$



## Passing to the limit in weak-$(P^\delta)$

$$\int_0^T \int_{\overline{\Omega}} \partial_t \varphi \, \rho_\delta^+ \, dxdt = \int_0^T \int_{\overline{\Omega}} \partial_1 \varphi \, [\partial_1 V_\delta * \kappa_\delta] \, \rho_\delta^+ \, dxdt$$

$$\begin{aligned} \rho_\delta^\pm &\rightharpoonup \rho^\pm && \text{in } L^\infty(L\log L) \\ \partial_1 V_\delta * \kappa_\delta &\rightharpoonup \partial_1 V * \kappa && \text{in } L^2(H^1) \end{aligned}$$

To get **strong** convergence of $(\partial_1 V_\delta * \kappa_\delta)_{\delta>0}$:

- Trudinger-Moser: $H^1(\mathbb{T}^2) \subset\subset Exp(\mathbb{T}^2) = (L\log L)(\mathbb{T}^2)^*$ $[f \in Exp(\mathbb{T}^2) \Rightarrow \int_{\mathbb{T}^2} e^{|f|} < \infty]$
- By Aubin-Lions-Simon: $\partial_1 V_\delta * \kappa_\delta \to \partial_1 V * \kappa$ in $L^2(Exp)$

**Conclusion**: the limit $\rho^\pm$ satisfies $(P)$



## Theorem: $(P_n^{\delta_n}) \to (P)$

$$\begin{array}{ccccc} (P_n^{\delta_n}) & & (P^{\delta_n}) & & (P) \\ \mu_n^\pm & \xleftrightarrow[\substack{W_2(\mu_n^\pm(t),\rho_{\delta_n}^\pm(t)) \le \\ \exp(T\|\partial_1 V_{\delta_n}\|_{Lip}) W_2(\mu_{n,\circ}^\pm, \alpha_n \rho_\circ^\pm)}]{} & \rho_{\delta_n}^\pm & \xrightarrow[L^\infty(L\log L)]{} & \rho^\pm \end{array}$$

**Theorem**: for $\begin{cases} V_\delta \in W^{2,\infty}(\mathbb{T}^2) \\ V_\delta \to V \text{ in } L^2(\mathbb{T}^2) \\ 0 \le (1+|k|^2)[\widehat{V}_\delta]_k \le C \ \forall \delta \end{cases}$

- $\forall T > 0 \ \ \exists \delta_n \to 0 \ \ \forall \rho_\circ^\pm \in L\log L(\mathbb{T}^2)$
- $\forall \mu_{n,\circ}^\pm \rightharpoonup \rho_\circ^\pm : \exp(T\|\partial_1 V_{\delta_n}\|_{Lip}) W_2(\mu_{n,\circ}^\pm, \alpha_n \rho_\circ^\pm) \xrightarrow{n\to\infty} 0$
- $\exists n_k \ \ \exists \rho^\pm \in L^\infty(L\log L)$ solution to $(P)$:
- $\mu_{n_k}^\pm(t) \rightharpoonup \rho^\pm(t)$ as $n_k \to \infty$ for a.e. $t \in (0,T)$

## $(P_n^{\delta_n}) \to (P)$: discussion

- Also works for $\nabla$ i.o. $\partial_1$; applies to **screw dislocations**
- Also works in $\mathbb{T}^d$ for all $d \geq 1$ with $V$ at most **logarithmic**
- Also works for given $F$ Lipschitz
- **Extends** [Monneau *et al.*; 2010]'s global existence result of $(P)$ to general $V$, and a larger class of initial data
- We do **not** use the **gradient flow** structure explicitly!
- Conditions on V:
  - $\widehat{V}_k \geq 0$: prevents 'negative-energy' micro-structures
  - $(1+|k|^2)\widehat{V}_k \leq C$: at most logarithmic singularities
- **Weak link**: Gronwall estimate on $W_2(\mu_n^{\pm}(t), \rho_{\delta_n}^{\pm}(t))$ requires at least $\delta_n > 2T/\log n$
- No uniqueness result on $(P)$



## How about counter-example to $(P_n^{\delta_n}) \to (P)$?

Counter example needs $n^{3/2}\delta_n \to 0$; incompatible with $\delta_n \to 0$ 'slowly'

**My current interpretation**:
$\delta_n \to 0$ slowly enough prevents dislocation to cluster in rigid dipole-structures

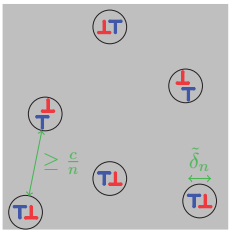


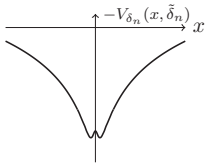




## Current answer to the main question

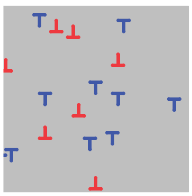

$(P_n)$

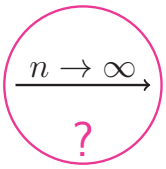


$(P)$

$$\frac{dx_i}{dt} = \left[F + \frac{1}{n}\sum_{j=1}^{n} b_j[-\partial_1 V_{\delta_n}](x_i - x_j)\right] b_i e_1$$

$$\begin{aligned} \partial_t \rho^+ &= \partial_1\left(\rho^+[\partial_1 V * (\rho^+ - \rho^-) - F]\right) \\ \partial_t \rho^- &= \partial_1\left(\rho^-[\partial_1 V * (\rho^- - \rho^+) + F]\right) \end{aligned}$$

- If $\delta_n \to 0$ very slowly: **yes**
- If $n^{3/2}\delta_n \to 0$: **no**
- [Groma, Balogh; 1999] uses no regularisation ($\approx \delta_n \to 0$ very fast)

# Anti-plane deformation model of screw dislocation and its related variational problem

**Masaaki Uesaka**
Hokkaido University

As a microscopic model of screw dislocation, Hudson and Ortner [1, 2] propose the lattice model based on anti-plane dislocation. They prove that in this model, the state corresponding to the screw dislocation is a globally stable equilibrium under appropriate conditions for the interaction energy. In this talk, we attempt to obtain the upscale model of the anti-plane deformation model in terms of $\Gamma$-convergence. The main point is that the discrete system which takes value in $S^1$ is naturally derived from the model. We also point out the mathematical difficulty of this discrete model.

## References

[1] Thomas Hudson and Christoph Ortner. Existence and stability of a screw dislocation under anti-plane deformation. *Arch. Ration. Mech. Anal*, 213 (2014) no. 3, 887-929.
[2] Thomas Hudson and Christoph Ortner. Analysis of stable screw dislocation configurations in an anti-plane lattice model. *SIAM J. Math. Anal.* 47-1 (2015), 291-320.

# Anti-plane deformation model of screw dislocation and its related variational problem

Masaaki Uesaka

Research Institute for Electronic Science, Hokkaido University

August 30, 2017
Mathematics in Interface, Dislocation and Structure of Crystals
at Nishijin Plaza, Kyushu University



## Crystallographic defect

- Crystallo-graphic defect
  - Point defect
    - Frenkel defect
    - Schottky defect
    - ...
  - Line defect =**Dislocation**
    - **Screw dislocation**
    - Edge dislocation
  - Planar defect
    - Twin boundary
    - Stacking fault
    - Grain boundary
    - ...



## Dislocations in crystal

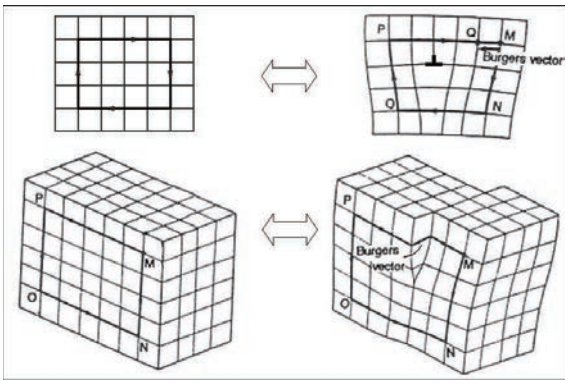


Figure: Edge dislocation & Screw dislocation (cited from wikipedia([4]))

## Importance of dislocation

**Dislocation is the origin of the plasticity of metals.**

- Dislocation can move with breaking and reforming a bond.
- As dislocations move, the crystal can be deformed by less energy.
- Dislocation = The carrier of plastic deformation

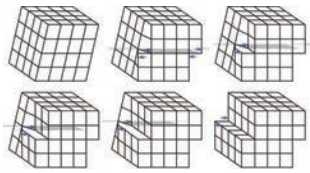

Figure: moving screw dislocation

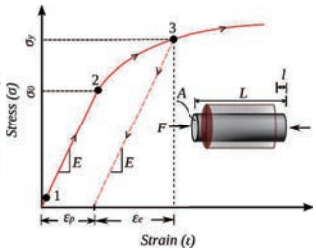


Figure: Plasticity



## Our Motivation

- How can we describe the atomic configuration when screw dislocation occurs?
  - (Not mention the detail today)We introduce the notion using **the concept of bundle** in topology.
    (Hamada, Matsutani, Nakagawa, Saeki, U. 2016, arXiv:1605.09550)
  - We find the algebraic method for any crystal structure to calculate
    - a bundle structure;
    - the corresponding description of a screw dislocation.

    by using the group theory.
- How can we introduce the energy of screw dislocation?
  - We propose the energy model with $S^1$**-valued function** (based on our description).
  - We consider the continuous limit (the $\Gamma$-limit) of an $S^1$-valued interacting particle system.



## Screw Dislocation is a displacement of $\mathbb{Z}$-lattice

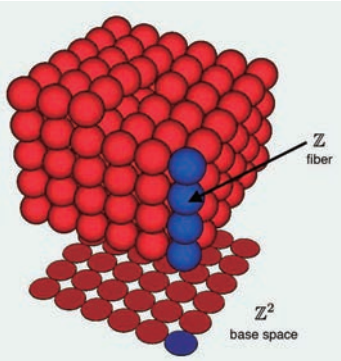


- We decompose the atomic configuration as a base space ($\mathbb{Z}^2$) and a fiber ($\mathbb{Z}$).
- We imagine that **the alignment of the atom is assigned for each lattice point in the base space**.
- Neighboring alignments possibly have the gap.
- From these description, **it is natural to consider the interaction between $\mathbb{Z}$-fiber**.

## Our observation

**Hamada, Matsutani, Nakagawa, Saeki, U. [7]**

1. We reveal the fiber structure of the screw dislocation:
   - Base space: the lattice in $\mathbb{Z}^2$;
   - Fiber: $\mathbb{Z}$ (possibly has discrepancy between neighbouring fibers).
2. We propose **the algebraic method of finding the fiber structure** for given crystal structure and Burger's vector.
3. The discrepancy between neighbouring fibers can be described by the value of $S^1$ if we consider the infinite dislocation line.



## Our model

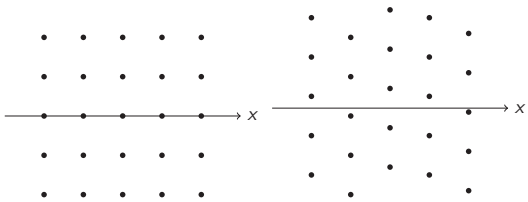


**Our System**

We consider **the discrete system where neighboring $\mathbb{Z}$-fiber interacts each other**.
$\Rightarrow$ the position of fiber is described as the value in $S^1$.



## Related Results (1/3: Discrete model of screw dislocation)

**Hudson and Ortner [8]:**

- $\Lambda := \begin{pmatrix} 1/6 \\ \sqrt{3}/6 \end{pmatrix} + \left\langle \begin{pmatrix} 1 \\ 0 \end{pmatrix}, \begin{pmatrix} 1/2 \\ \sqrt{3}/2 \end{pmatrix} \right\rangle_{\mathbb{Z}}$: triangular lattice
- $\Omega \subset \Lambda$: sublattice, $\mathcal{B}^{\Omega}$: all bonds of $\Omega$
- $\psi$: $C^4(\mathbb{R})$: 1-periodic, even at 0 and $1/2$ (interaction potential)
- For two forms $y, \widetilde{y} \colon \Omega \to \mathbb{R}$,

$$E^{\Omega}(y; \widetilde{y}) := \sum_{b \in \mathcal{B}^{\Omega}} \left( \psi(Dy(b)) - \psi(D\widetilde{y}(b)) \right),$$

where $Dy, D\widetilde{y} \colon \mathcal{B}^{\Omega} \to [-1/2, 1/2]$ are the differences of $y, \widetilde{y}$.

## Related Results (1/3: Discrete model of screw dislocation)

$$E^{\Omega}(y;\widetilde{y}) := \sum_{b\in\mathcal{B}^{\Omega}} \left(\psi(Dy(b)) - \psi(D\widetilde{y}(b))\right),$$

where $Dy, D\widetilde{y}\colon \mathcal{B}^{\Omega} \to [-1/2, 1/2]$ are the differences of $y, \widetilde{y}$.

**Theorem (Hudson, Ortner (2014))**

*Let $\psi$ satisfy $\psi''(0) > 0$ and $\psi(x) \geq \dfrac{\psi''(0)}{2}x^2$ in $[-1/2, 1/2]$.*
*Then for given centers of screw dislocations (which are sufficiently separated each other) and a given Burger's vector for each dislocation, There exists a locally stable equilibrium $y$ of $E^{\Omega}$ such that $y$ has given screw dislocations.*

Remark. $y$ is a locally stable equilibrium $\Leftarrow E(y+u;y) \geq 0$ for all perturbation $u$ with compact support.



## Our model

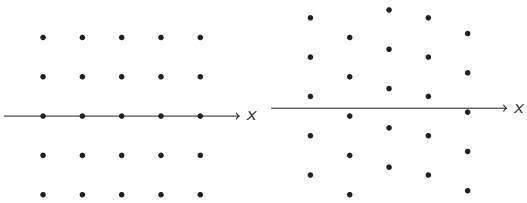


**Our System**

We consider **the discrete system where neighboring $\mathbb{Z}$ lattice interacts each other**.

*Remark.* We only consider the 1-dim. system. (multi-dim. case could be a future work.)



## Formulation in 1D

- $N \in \mathbb{N}$: large integer(number of points), $\varepsilon := 1/N$.
- $\varepsilon\mathbb{Z} := \{\varepsilon n | n \in \mathbb{Z}\}$.
- $S^1$ is parametrized by $\theta \in \mathbb{R}$ as $S^1 = \left\{ \begin{pmatrix} \cos 2\pi\theta \\ \sin 2\pi\theta \end{pmatrix} \middle| \theta \in \mathbb{R} \right\}$.
- $\iota\colon \mathbb{R} \to S^1$, $\iota(\theta) = \begin{pmatrix} \cos 2\pi\theta \\ \sin 2\pi\theta \end{pmatrix}$: covering map
- $u\colon \varepsilon\mathbb{Z} \to S^1$: displacement function. $u_j := u(j\varepsilon) = u(j/N)$
- $f_N\colon S^1 \to \mathbb{R}$: interaction potential s.t.
  - non-negative, $f_N\begin{pmatrix} 1 \\ 0 \end{pmatrix} = 0$
  - attain the unique minimum at 0.

  (We will add more assumptions later.)

**Energy**

$$E_N(u) = \sum_{j=1}^{N} f_N(\iota(\theta_j - \theta_{j-1}))$$

where we choose $\theta_j$ as $\iota(\theta_j) = u_j$. ($E_N(u)$ does not depend on the choice of $\theta_j$.)

## Problem: limit of the discrete system

**Energy**

$$E_N(u) = \sum_{j=1}^{N} f_N(\iota(\theta_j - \theta_{j-1}))$$

where we choose $\theta_j$ as $\iota(\theta_j) = u_j$. ($E_N(u)$ does not depend on the choice of $\theta_j$.)

**Problem**

What is the "limit problem" as $N \to \infty$?

**Problem in "Problem"**

What is the definition of "limit problem"?



## $\Gamma$-convergence

**Definition($\Gamma$-convergence)**

$X$:metric space. A sequence $F_j \colon X \to \mathbb{R} \cup \{\infty\}$ ($j \in \mathbb{N}$) $\Gamma$-converges to $F_\infty \colon X \to \mathbb{R} \cup \{\infty\}$ in $X$ if for any $x \in X$,

liminf inequality for every sequence $(x_j)$ converging to $x$,

$$F_\infty(x) \le \liminf_{j\to\infty} F_j(x_j);$$

limsup inequality there exists a sequence $(x_j)$ converging to $x$ such that

$$F_\infty(x) \ge \limsup_{j\to\infty} F_j(x_j).$$

**Theorem ([1])**

*If $(F_j)$ is equi-mildly coercive on $X$ and if $(x_j)$ is a precompact sequence such that each $x_j$ is a minimizer of $F_j$, then every limit of a subseq. of $(x_j)$ is a minimizer of $F_\infty$.*



## Problem: $\Gamma$-limit of the discrete system

**Energy**

$$E_N(u) = \sum_{j=1}^{N} f_N(\iota(\theta_j - \theta_{j-1}))$$

where we choose $\theta_j$ as $\iota(\theta_j) = u_j$. ($E_N(u)$ does not depend on the choice of $\theta_j$.)

**Problem**

**What is the $\Gamma$-limit as $N \to \infty$?**

## Related Results(2/3: $\Gamma$-convergence for dislocations)

**Garroni & Müller [5]**
$\Gamma$-convergence of the phase field type energy for dislocation pinning
**Ponsiglione [9]**

- $\{x_j\}_j$: centers of dislocations
- $\mu := \sum_j z_j \, |\mathbf{b}| \, \delta_{x_j}$ ($\mathbf{b}$:Burger's vector, $|\mathbf{b}| = 1$, $z_j \in \mathbb{Z}$)

$$E_\varepsilon(u) := \int_{\Omega \setminus \bigcup_j \overline{B_\varepsilon(x_j)}} |u(x)|^2 \, \mathrm{d}x$$

Then $\mathcal{F}_\varepsilon(\mu) := \frac{1}{|\log \varepsilon|} \left( \min_u E_\varepsilon(u) + |\mu|(\Omega) \right)$ $\Gamma$-converges to $\mathcal{F}(\mu) = \frac{1}{2\pi} |\mu|(\Omega)$ in a flat norm topology.



## Related Results(3/3: $\Gamma$-convergence for discrete system)

**If $u$ takes a value in $\mathbb{R}$, there are many previous results.**

$$E_N(u) = \sum_{j=1}^{N} f_N(u_j - u_{j-1}) =: \sum_{j=1}^{N} \frac{1}{N} \psi_N \left( \frac{u_j - u_{j-1}}{1/N} \right)$$

- Braides and Gelli [3]: Review on this topic
- Braides and Gelli [2]: Non-convex energies

  - $T_N^\pm \to \infty$ and $T_N^\pm / N \to 0$ as $N \to \infty$.
  - $\psi_N$: convex in $[T_N^-, T_N^+]$ and concave out of $[T_N^-, T_N^+]$.

$$\psi_N(z) := \begin{cases} F_N(z) & z \in [T_N^-, T_N^+] \\ N G_N \left( \dfrac{z - T_N^{\operatorname{sign} z}}{N} \right) & z \notin [T_N^-, T_N^+] \end{cases}$$

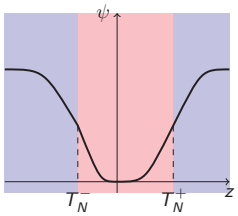




## Related Results(3/3: $\Gamma$-convergence for discrete system)

**Theorem (Braides and Gelli (2002))**

*With some assumptions on $F_N$ and $G_N$, the functionals $E_N$ $\Gamma$-converge w.r.t. the convergence in measure on $L^1(0,1)$ to*

$$E(u) = \begin{cases} \displaystyle\int_0^1 F(u'(x)) \, \mathrm{d}x + \sum_{t \in S(u)} G([u](t)) & u \in SBV(0,1), \\ +\infty & \text{otherwise}, \end{cases}$$

*where $S(u)$ is the jump set of $u$ and $[u]$ denote the jump, and $F := \lim_N F_N$ and $G := \lim_N G_N$.*

## Main Result: Assumptions

### Energy

$$E_N(u) = \sum_{j=1}^{N} f_N(\iota(\theta_j - \theta_{j-1}))$$

where we choose $\theta_j$ as $\iota(\theta_j) = u_j$.

Let $\psi_N \colon \mathbb{R} \to \mathbb{R}$ be a function defined by

$$\psi_N(z) = \begin{cases} N f_N(\iota(z/N)) & z \in [-N/2, N/2], \\ +\infty & \text{otherwise.} \end{cases}$$

By using $\psi_N$, we can write

$$E_N(u) = \sum_{j=1}^{N} \frac{1}{N} \psi_N\left(\frac{\theta_j - \theta_{j-1}}{1/N}\right),$$

where $(\theta_j)$ are chosen as $\iota(\theta_j) = u_j$ and as $\theta_j - \theta_{j-1} \in [-1/2, 1/2]$.



## Main Result: Assumptions(cont.)

- $\psi_N$ is convex in $[T_N^-, T_N^+]$ and concave out of $[T_N^-, T_N^+]$. Moreover,

$$\psi_N(z) := \begin{cases} F_N(z) & z \in [T_N^-, T_N^+], \\ N G_N\left(\frac{z}{N}\right) & z \notin [T_N^-, T_N^+]. \end{cases}$$

- $\exists p > 1$ s.t. $F_N(z) \geq |z|^p$ for $\forall z \in \mathbb{R}$.
- $G_n(z) \geq c > 0$ for $\forall z \neq 0$.
- We identify a discrete function $u \colon \varepsilon\mathbb{Z} \to S^1$ as a following piecewise constant function:

$$u(x) = u_j \text{ if } x \in \left[\frac{j}{N}, \frac{j+1}{N}\right), \; j = 0, 1, \ldots, N-1.$$



## Main result

### Theorem (U.)

*In addition to these assumptions, if $F = \lim_N F_N$ and $G = \lim_N G_N$ exists, then $E_N$ $\Gamma$-converges in $L^1$ to the following functional: for $u \in L^1(0,1)$, if there exists $\theta \in SBV(0,1)$ such that $\iota \circ \theta = u$, then*

$$E_\infty(u) = \int_0^1 F(u'(x))\,\mathrm{d}x + \sum_{t \in S(u)} \inf\left\{ G([\theta](t)) \,\middle|\, \begin{array}{l} \theta \in SBV(0,1) \\ \iota \circ \theta = u \end{array} \right\}$$

*and otherwise $E_\infty(u) = +\infty$.*

*Remark.*
$\theta_1, \theta_2 \colon (0,1) \to \mathbb{R}$ satisfies $\iota \circ \theta_1 = \iota \circ \theta_2 \Rightarrow \theta_1(x) - \theta_2(x) \in \mathbb{Z}$ for all $x \in (0,1)$.
Then the second term of the definition of $E_\infty$ can be written as follows:

$$\sum_{t \in S(\theta_0)} \inf_{n \in \mathbb{Z}} \{G([\theta_0](t) + n)\}$$

for fixed $\theta_0 \in SBV(0,1)$ with $\iota \circ \theta_0 = u$.

## The key point of proof: concentration

Example from Giaquinta, Modica and Souček [6]:

- Consider the following functions $u_n\colon [0,1] \to S^1$ ($n \in \mathbb{N}$):

$$u_n(t) := \begin{cases} (\cos 2\pi nt, \sin 2\pi nt) & t \in [0, 1/n], \\ (1,0) & \text{otherwise.} \end{cases}$$

- Total variation of $u_n$ is $2\pi$ for all $n \in \mathbb{N}$.
- $(u_n)$ converges in $L^1((0,1),\mathbb{R}^2)$ to the constant map $u_0\colon [0,1]$ with $u_0(t) = (1,0)$.
- This limit, however, does not conserve the total variation. ($\mathrm{Var}(u_0) = 0$.)
- The limit "forgets" how many times it goes around $S^1$.

By the theory of currents, we see that the corresponding graph current $G_{u_n}$ converges to

$$G_{u_0} + \delta_0 \times [\![S^1]\!]$$

where $\delta_0$ is a Dirac mass at zero.



## Brief Review on Cartesian current (1)

- $k$-dimensional current on a manifold $M$: a continuous linear functional on $k$-form space $\Omega^k(M)$.
- By defining $[[M]](\omega) := \int_M \omega$, we can regard $M$ as a current.
- Boundary of a current $T$:

$$(\partial T)(\omega) := T(d\omega).$$

- Graph current: Let $u \in BV(\Omega)$ where $\Omega \subset \mathbb{R}^n$.

$$G_u := (-1)^n \partial[[SG_u]]$$

where $SG_u$ is a subgraph of $u$ in $\mathbb{R}^{n+1}$.



## Brief Review on Cartesian current (2)

**Definition**

Let $\Omega \subset \mathbb{R}^{d_1}$ be an open set. Then $d_1 + d_2 - 1$-dimensional rectifiable current $T$ in $\Omega \times \mathbb{R}^{d_2}$ is called a Cartesian current if the following conditions hold:

$$\partial T \llcorner (\Omega \times \mathbb{R}^2) = 0;\ p_\# T = [[\Omega]]\,;\ T \llcorner dx \geq 0; \tag{1}$$

$$\|T\|_1 < \infty;\ \mathbf{M}(T) < \infty, \tag{2}$$

where

$$\|T\|_1 := \sup\left\{\langle T, \varphi(x,y)\,|y|\,dx\rangle\ ;\ \varphi \in C_0^\infty\left(\Omega \times \mathbb{R}^2\right) \text{ with } \|\varphi\| \leq 1\right\}. \tag{3}$$

We denote by $\mathrm{cart}\left(\Omega \times \mathbb{R}^{d_2}\right)$ by the set of Cartesian currents in $\Omega \times \mathbb{R}^{d_2}$.

## Brief Review on Cartesian current (3)

### Theorem ([6])

*We assume that $T$ is represented locally as $(\mathrm{id}_\Omega \times \iota)_\# G_u$ for some $BV(\Omega)$. Then*

$$\begin{aligned} \mathrm{JC}(T) &= J_u, \\ T^{(a)} &= (\mathrm{id}_\Omega \times \iota)_\# G_u^{(a)}, \\ T^{(C)} &= (\mathrm{id}_\Omega \times \iota)_\# G_u^{(C)}, \end{aligned} \tag{4}$$

*and for any form of type $\omega = \varphi(x,y)dx_1 \wedge \cdots \wedge dx_{j-1} \wedge dx_{j+1} \wedge dx_n \wedge dy$ for some $\varphi(x,y) \in C_0^\infty(\Omega \times \mathbb{R}^2)$, we have*

$$\begin{aligned} T^{(a)}(\omega) &= (-1)^{d-j} \int_\Omega \varphi(x, u_T(x))(D_i u_T)^{(a)} \, \mathrm{d}x, \\ T^{(C)}(\omega) &= (-1)^{d-j} \int_\Omega \varphi(x, u_T(x))(D_i u_T)^{(C)} \, \mathrm{d}x. \end{aligned} \tag{5}$$



### Theorem ([6], cont.)

*Moreover $T^{(Jc)}$ have a decomposition*

$$T^{(Jc)} = T^{(con)} + T^{(J)} \tag{6}$$

*which satisfies*

- *There exist a rectifiable $(n-1)$-current $L_T^{(con)}$ such that*

$$T^{(con)} = L_T^{(con)} \times [[S^1]];$$

- *For any form of type $\omega = \varphi(x,y)dx_1 \wedge \cdots \wedge dx_{j-1} \wedge dx_{j+1} \wedge dx_n \wedge dy$ for some $\varphi(x,y) \in C_0^\infty(\Omega \times \mathbb{R}^2)$,*

$$T^{(J)}(\omega) = (-1)^{d-j} \int_\Omega \left\{ \int_{\gamma_{u_-(x), u_+(x)}} \varphi(x,s) \, \mathrm{d}\ell_{S^1} \right\} \nu_{J_u}^{(j)}(x) \, \mathrm{d}\mathcal{H}^{d-1} \llcorner J_u,$$

*where $\gamma_{u_-(x), u_+(x)}$ is the oriented path in $S^1$ which connects $\iota(u_-(x))$ to $\iota(u_+(x))$.*



## Main result (Cartesian Current Ver.)

### Theorem (U.)

*In addition to these assumptions, suppose that $F = \lim_N F_N$ and $G = \lim_N G_N$ exists. Then $E_N$ $\Gamma$-converges in the space of Cartesian current to the following functional: for all the Cartesian current $G$ on $\Omega$, if $G$ has no Cantor part, then*

$$E_\infty(G) = \int_0^1 F(u') \, \mathrm{d}x + \sum_{t \in \mathcal{M}^{(Jc)}} [2\ell(t)] G\left(\frac{1}{2}\right) + G\left(\ell(t) - \frac{[2\ell(t)]}{2}\right).$$

*and otherwise $E_\infty(u) = +\infty$, where $u$ is a absolutely continuous part of $G$ and $\mathcal{M}^{Jc}$ is the jump and concentration part of $G$ and $\ell(t)$ is the jump and concentration length.*

Red part arises from the concentration phenomena.

## Summary & Future work

- From the topological description of screw dislocations, we can naturally imagine the model of the screw dislocation energy where **the intaraction between $\mathbb{Z}$-fiber exists**.
- In this model, **$S^1$-valued function** naturally appears.
- Our model is a discrete model and we consider the **$\Gamma$-limit** of this model.
- Our proof of the $\Gamma$-limit theorem is based on Cartesian currents and **the concentration phenomena** affects the limit functional.
- (Future work) Multi-dimensional base space
- (Future work) Periodic boundary constraints.
  - This corresponds to considering function from $S^1$ to $S^1$.
  - The mapping degree of this function needs to be prescribed.
- (Future work) Gradient Flow of our discrete model
  - (Related ongoing work) Numerical Scheme for total variation flow with a function valued in Lie group. (joint w/ Y. Giga, K. Sakakibara and K. Taguchi (Univ. of Tokyo).)



## Bibliography I


[1] Braides, A., $\Gamma$-convergence for beginners, Oxfor Lecture Series in Mathematics and it Applications, Vol. 22, 2002.

[2] Braides, A. & Gelli, M. S., Continuum limits of discrete systems without convexity hypotheses, *Math. Mech. Solids*, **6**, 395–414, 2002.

[3] Braides, A. & Gelli, M.S., From discrete systems to continuum variational problems: an introduction. In *Topics on Concentration Phenomena and Problems with Multiple Scales*, pp. 3 – 77, Lect. Notes Unione Mat. Ital. vol. 2. Springer, Berlin, 2006.

[4] "Vector de Burgers" by Javier Bartolomé Vílchez (Autor de la imagen original: David Gabriel García Andrade) - Modificación de una imagen subida al Commons. Licensed under CC BY-SA 3.0 via Commons - `https://commons.wikimedia.org/wiki/File:Vector_de_Burgers.PNG#/media/File:Vector_de_Burgers.PNG`.

[5] Garroni, A. and Müller, S., $\Gamma$-limit of a phase-field model of dislocations. *SIAM Math. Anal.*, 36(2005), no. 6, 1943-1964.




## Bibliography II


[6] Giaquinta, M., Modica, G. & Souček, J., Variational problems for maps of bounded variation with values in $S^1$, *Calc. Var. 1*, 87–121, 1993.

[7] Hamada, H., Matsutani, S., Nakagawa, J., Saeki, O., & Uesaka, M., An algebraic description of screw dislocations in SC and BCC crystal lattices, 2016, arXiv:1605.09550.

[8] Hudson, T. and Ortner, C., Existence and stability of a screw dislocation under anti-plane deformation. *Arch. Ration. Mech. Anal.*, 213 (2014) no. 3, 887-929.

[9] Ponsiglione, M., Elastic energy stored in a crystal induced by screw dislocations: from discrete to continuous. *SIAM J. Math. Anal.*, 39 (2007), no. 2, 449-469.

# Variational models of lattice defects

**Pierluigi Cesana**
IMI, Kyushu University

A martensitic phase-transformation is a first-order diffusionless transition occurring in elastic crystals and characterized by an abrupt change of shape of the underlying crystal lattice [1]. It is the basic activation mechanism for the so-called Shape-Memory effect. The re-organization of the crystalline structure is not only accompanied by the formation of sharp interfaces delimiting the various martensitic variants but also by presence of defects and mismatches. In this talk I will present a modeling approach for topological defects based on variational (energy-minimization) methods [3]. Considering disclinations (angular defects caused by the mismatch measured around a loop in a planar lattice) I will present a linearized theory based on a continuum model describing the formation of a nested hierarchical martensitic microstructure containing a disclination at the center [2]. The microstructure is described by the solution to a differential inclusion problem. I will then introduce the Gamma-Convergence approach to the description of dislocations (linear defects often observed in metal subject to shear stress). Comparisons are reported for numerical and analytical solutions and experimental observations.

## References

[1] Kaushik Bhattacharya. Microstructure of Martensite. Oxford University Press, Oxford (2003)
[2] Pierluigi Cesana, Marcel Porta, Turab Lookman. J. Mech. Phys. Sol. 72 (2014)
[3] Pierluigi Cesana Relaxation of an Energy Model for the Triangle-to-Centred Rectangle Transformation. In: Anderssen B. et al. (eds) The Role and Importance of Mathematics in Innovation. Mathematics for Industry, vol 25. Springer, Singapore (2017)

九州大学
KYUSHU UNIVERSITY

# Variational Models of Lattice Defects

Pierluigi Cesana

Institute of Mathematics for Industry

30 August, 2017



## Crystals vs. elastic crystals

We present continuum models of lattice defects observed in a class of Shape-Memory Alloys (SMAs).

The Shape-Memory effect is the capability of a material to recover large non-linear (although) elastic deformations.

The Shape-Memory Effect is the manifestation of a martensitic transformation, a first-order solid-to-solid transition characterized by a change of shape of the crystalline lattice driven by temperature or an applied mechanical stress.



## Crystal phases

By decreasing the temperature below a critical value $T_c$ a symmetry-break is induced in the crystal structure thus causing a transition from the high-temperature phase (austenite) to the low-temperature state called martensite. The low-symmetry and disordered phase usually appears in the form of a mixture of symmetry-related crystal variants, called martensitic microstructure.

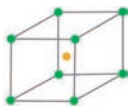

Austenite

1. "Parent" phase (cubic)
2. Stable at high temperatures

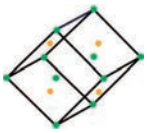

Martensite

1. "Product" phase
2. Stable at low temperatures

## Elasticity framework

We adopt a Landau-type approach by modeling the system with a multi-well energy density whose wells are represented by the martensitic variants

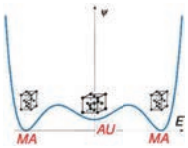


Figure : Energy density $\Psi$ at fixed temperature $T < T_c$.

In the regime of linearized elasticity:

- $E \in R^{3\times 3}$, $E = E^T$ mechanical strain gradient
- $Eu := \frac{1}{2}(\nabla u + \nabla^T u)$
- $\Psi(E)$ the free-energy density
- We apply this model to the Hexagonal-to-Orthorhombic transformation



## Hexagonal-to-Orthorhombic transformation

- Energy wells:

$$E_1 = \eta \begin{bmatrix} 1 & 0 \\ 0 & -1 \end{bmatrix}, E_2 = \eta \begin{bmatrix} -\frac{1}{2} & \frac{\sqrt{3}}{2} \\ \frac{\sqrt{3}}{2} & \frac{1}{2} \end{bmatrix}, E_3 = \eta \begin{bmatrix} -\frac{1}{2} & -\frac{\sqrt{3}}{2} \\ -\frac{\sqrt{3}}{2} & \frac{1}{2} \end{bmatrix}$$

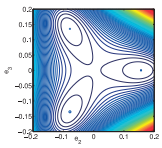

- $\Psi(Eu)$
- $E_1 \xrightarrow{2\pi/3} E_2 \xrightarrow{2\pi/3} E_3 \xrightarrow{2\pi/3} E_1$
- 3-state spin system
- $\eta \in \mathbb{R}^+$ material parameter

The energy model:

$$F_\varepsilon(u) = \begin{cases} \int_\Omega \Big[\varepsilon|\Delta u(x)|^2 + \Psi\big(Eu(x)\big)\Big]dx & \text{if div u} = 0 \\ +\infty & \text{otherwise} \end{cases}$$

Interfacial Energy + Bulk Energy



## Boundary Value Problem

$$\bullet F_\varepsilon(u) := \int_\Omega \Big[\varepsilon|\Delta u(x)|^2 + \Psi(Eu(x))\Big]dx$$

- The BVP problem (relaxation):


$min \to F_\varepsilon(u)$ with:
$u|_{\partial\Omega} = 0$

The homogeneous strain $E = 0$ is unstable: the material shows an energetic preference to develop spatially modulated deformations (shear bands) at fixed average deformation $E = 0$.

## Asymptotics

$$\bullet \min_{\mathcal{A}} \to F_\varepsilon(u) = \int_\Omega \left(\varepsilon|\Delta u(x)|^2 + \Psi(Eu(x))\right) dx \qquad (1)$$

$$\mathcal{A} = H_0^1(\Omega, \mathbb{R}^2) \cap H^2(\Omega, \mathbb{R}^2)$$

Denote with

1. $\overline{u}_\varepsilon$ the minimizers of Eq. (1)
2. $\{m_\varepsilon\} = \left\{\inf_{\mathcal{A}} F_\varepsilon(u)\right\} = \left\{F_\varepsilon(\overline{u}_\varepsilon)\right\}$ the minima of Eq. (1)

• The problem: to study the asymptotic behavior of minimizers and minima of the energy.
• We characterize the asymptotic behavior of the system by Γ-Convergence.



## Γ-convergence

Minimality:

- coercivity (compactness)
- lower semicontinuity

Let $\mathcal{F}_k, \mathcal{F}_\infty : X \to \mathbb{R} \cup \{+\infty\}$, $k \to \infty$. Compute:

1. $\inf_X \mathcal{F}_k(x) = \mathcal{F}_k(\overline{x}_k) := m_k$
2. $\inf_X \mathcal{F}_\infty(x) = \mathcal{F}_\infty(\overline{x}_\infty) := m_\infty$

We are interested in:

1. (convergence of minimum values) $m_k \to m_\infty$
2. (convergence of minimizers) $\overline{x}_k \to \overline{x}_\infty$ (in some topology...)

The result: $\Gamma\text{-}\lim_{k\to\infty} \mathcal{F}_k = \mathcal{F}_\infty$



## Definition (by sequences)

Let $(X, d)$ be a metric space, $\mathcal{F}_k : X \to \mathbb{R} \cup \{+\infty\}$. Define

$$\Gamma\text{-}\liminf_{k\to+\infty} \mathcal{F}(u) := \inf\left\{\liminf_{k\to+\infty} \mathcal{F}_k(u_k), \quad u_k \xrightarrow{d} u\right\}$$

$$\Gamma\text{-}\limsup_{k\to+\infty} \mathcal{F}(u) := \inf\left\{\limsup_{k\to+\infty} \mathcal{F}_k(u_k), \quad u_k \xrightarrow{d} u\right\}$$

If

$$\Gamma\text{-}\liminf_{k\to+\infty} \mathcal{F}_k = \Gamma\text{-}\limsup_{k\to+\infty} \mathcal{F}_k := \Gamma\text{-}\lim_{k\to+\infty} \mathcal{F}_k$$

## Compute the Γ-limit

Matching Upper and Lower Bound

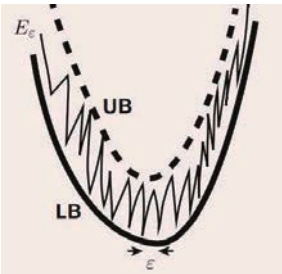


- Lower Bound: Stability
- Upper Bound: Optimality (+Kinematic Compatibility)



## Lower Bound

The lower bound is given by $\Psi^c$, the Convex envelope of $\Psi$

- $0 \leq \Psi$
- $\Psi^c \leq \Psi$ (convex envelope).

The (algebraic) inequality above holds at the level of the Γ-limit (in the weak-$H^1$ topology):

- $\int_\Omega \Psi^c(Eu)dx \leq \Gamma_{\varepsilon\to 0}\text{-}\lim F_\varepsilon$.



## Upper Bound

We have a chain of inequalities involving the concepts of partial convexity:

- $\Psi^c \leq \Psi^{pc} \leq \Psi^{qc} \leq \Psi^{rc}$.

Where $\Psi^{pc}$ denotes the polyconvex envelope, $\Psi^{qc}$ denotes the quasiconvex envelope, $\Psi^{pc}$ denotes the rank-1 convex envelope of $\Psi$.
The Upper bound is attained if we prove that:

- $\Psi^{rc} \leq \Psi^c$.

This is obtained via a lamination construction if we show all possible convex combinations of variants can be obtained by lamination (kinematically compatible rank-1 connections).

## Kinematic compatibility

Minimizing sequences of the problem

$$u : \Omega \to R^2, \qquad \inf_{u \in H^1_0(\Omega, R^2)} \to \int_\Omega \Psi(Eu(x))dx$$

have piecewise constant gradients oscillating at a very fine scale. Continuity is guaranteed by matching the tangential components of the gradients across each interface

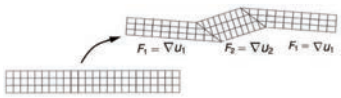


In turn this is an algebraic condition on matrices.
Conservation of tangential component of $\nabla u \to F_1 - F_2 = a \otimes n$

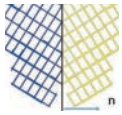




## Microstructure

A microstructure is the manifestation of a minimizing sequence of the infimum problem.

$$\inf_{u \in H^1_0(\Omega, R^2)} \to \int_\Omega \Psi(Eu(x))dx$$

For the Hexagonal-to-Orthorhombic transformation:

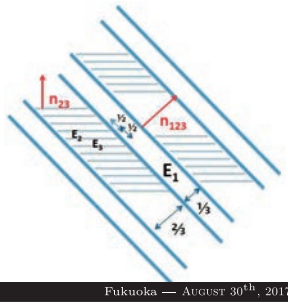


Volume fraction $E_i = \frac{1}{3}$

$\frac{1}{3}(E_1 + E_2 + E_3) = 0$

$\int_\Omega \Psi(Eu_k)dx \to \int_\Omega \Psi^c(0)dx = 0$



## Self-similar nested microstructure

Next, we show how to model a triple-star disclination occurring in a sample of $Pb_3(VO_4)_2$ undergoing the hexagonal-to-orthorhombic transformation in plane-strain geometry (find a picture of this structure in C. Manolikas, S. Amelinckx, Phys. Stat. Sol. 1980 ).

The triple-star disclination is a striking example of a Volterra's wedge disclination.

## Exact calculations

Consider the problem

$$\inf_{u\in\mathcal{A}} \to \int_\Omega \Big[\Psi\big(Eu\big) + |\nabla^2 u|^q\Big]\,dx, \tag{2}$$

with $q > 0$. Under the assumption that $\int_\Omega |\nabla^2 u|^p dx$ is small, we can study the simplified problem

$$\inf_{u\in H_0^1(\Omega,R^2)} \to \int_\Omega \Psi\big(Eu\big)\,dx. \tag{3}$$



## Kinematic Compatibility

We look for maps which minimize the integrand energy in (3) pointwise, that is, we solve

$$\inf_{E\in R^{2\times 2}_{sym}} \to \Psi\big(E\big)$$

with techniques from J. Ball, R. James, ARMA 1987. Indeed:

$$\inf_{E\in R^{2\times 2}_{sym}} \Psi\big(E\big) \Leftrightarrow \exists u : \frac{\nabla u + \nabla^T u}{2} \in \{E_1, E_2, E_3\}$$



## The result

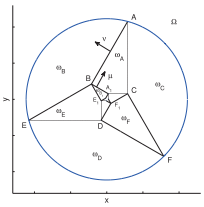


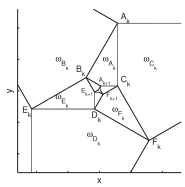


- It is possible to find an explicit formula for $u$
- $(\nabla u + \nabla^T u)/2 \in \{E_1, E_2, E_3\}$ for a.e. (x,y) in $\Omega$,
- volume ratio $E_i$ is 1/3
- $u \in W^{1,p}(\Omega, R^2), 1 \le p < \infty$, $|\nabla u| \to \infty$ as $(x, y) \to (0, 0)$

P.C., M. Porta, T. Lookman, JMPS 2014

## Level curves and graphs

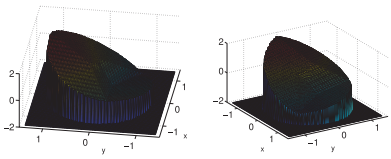

Figure : Plot of $u(x, y)$. (Here L=$\eta$=1).

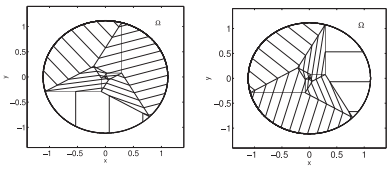

Figure : Level curves of $u(x, y)$. (Here L=$\eta$=1).



## Drawback of the linearized model

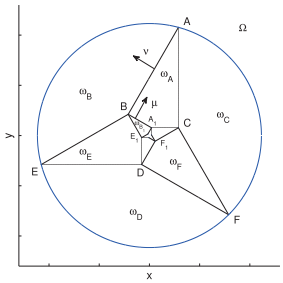


for $L \approx 0.07\mu m$ for $k = 3$ we are in the range $10^{-2} nm$



## Acknowledgments


- JSPS Research Category Grant-in-Aid for Young Scientists (B) 16K21213.


cesana@imi.kyushu-u.ac.jp

# Sequence representation of graph structure of crystal (Growth)

**Junichi Nakagawa**
Nippon Steel & Sumitomo Metal Co.

Growth is defined as a sequential representation of the graphical structure of crystal. The first growth corresponds to the coordination number of crystals which is used as a numerical index to describe the crystalline structure in material science.

We counted the number of growths in the case of eight crystals composed of two kinds of atoms and derived the numeric sequences. The numerical sequences have a cyclical property.

The generation functions can be derived from the numerical sequences. We show that the generating function has symmetrical properties which are derived from the cyclic property of the numerical sequence of the growth.

Mathematics in Interface, Dislocation and Structure of Crystals

# Sequential Representation of Graphical Structure of Crystals (Growth)

2017.8.28-8.30
Institute of Mathematics for Industry
Kyusyu University

Nippon Steel & Sumitomo Metal Corporation
Advanced Technology Research Laboratories
Mathematical Science & Technical Research Lab.

Junichi Nakagawa



新日鐵住金 NIPPON STEEL & SUMITOMO METAL

SG2013 in the University of Tokyo

## Application to Materials Informatics as Descriptors of Crystal Geometry

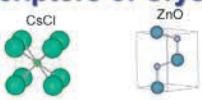


・different crystal lattice
・different configuration of atoms
etc.

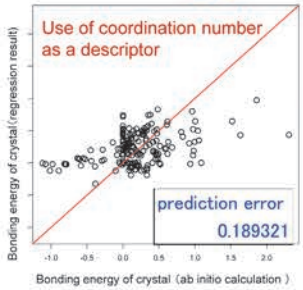


We would like to estimate the energy of compound from the information of atoms and crystal structure without ab initio calculation.

データは京都大学大学院工学系研究科材料工学専攻・田中功教授、世古准教授からのご提供



新日鐵住金 NIPPON STEEL & SUMITOMO METAL

SG2013 in the University of Tokyo

## Regression Method

- This problem can be viewed as a regression problem
  - Predictors: information of atoms and crystal structure
  - Response variable: energy of compound

regression model: $\boldsymbol{y} = \beta_1 \boldsymbol{x}_1 + \beta_2 \boldsymbol{x}_2 + \cdots + \beta_p \boldsymbol{x}_p + \varepsilon$

| Predictors $x_i$ | | Response variable $y$ |
|---|---|---|
| Atomic number | Position of periodic table | energy of compound |
| Electron affinity | Electronegativity | |
| Ionization Energy | Number of electrons | |
| Atomic mass | Coordination number | |
| Radius | Growth | |



新日鐵住金 NIPPON STEEL & SUMITOMO METAL

SG2013 in the University of Tokyo

## Concept of Growth

NaCl

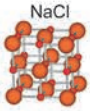

CsCl

β-BeO

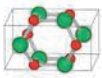

ZnS

| molecule | crystal lattice | order of group | # of Growth | | | |
|---|---|---|---|---|---|---|
| | | | 1st | 2nd | 3rd | 4th |
| NaCl | Cubic | 48 | 6 | 18 | 38 | 66 |
| CsCl | Cubic | 48 | 8 | 26 | 56 | 98 |
| β-BeO | Cubic | 16 | 4 | 11 | 18 | 41 |
| ZnS | Cubic | 24 | 4 | 12 | 24 | 42 |
| ZnO | Hexagonal | 12 | 4 | 12 | 25 | 44 |
| α-PbO | tetragonal | 16 | 4 | 8 | 12 | 16 |
| TlI | Orthorhombic | 8 | 7 | 22 | 47 | 82 |
| NiAs | Hexagonal | 24 | 6 | 20 | 42 | 74 |

The growth is generalization of the coordination number in material science.

ZnO

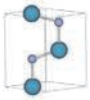

α-PbO

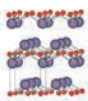

TlI

NiAs

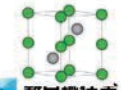



新日鐵住金 NIPPON STEEL & SUMITOMO METAL

## ZnO
## the 1st growth=4
(corresponding to coordination number)

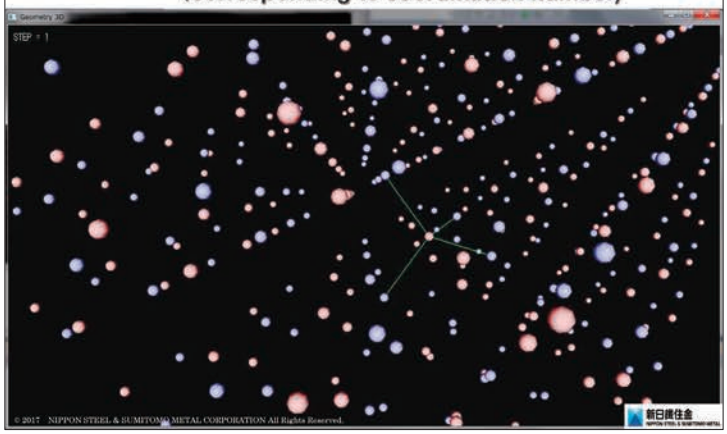


## ZnO
## the 2nd growth=12

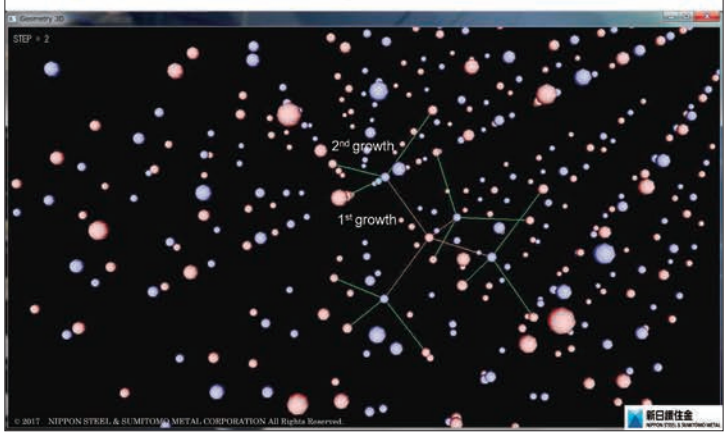

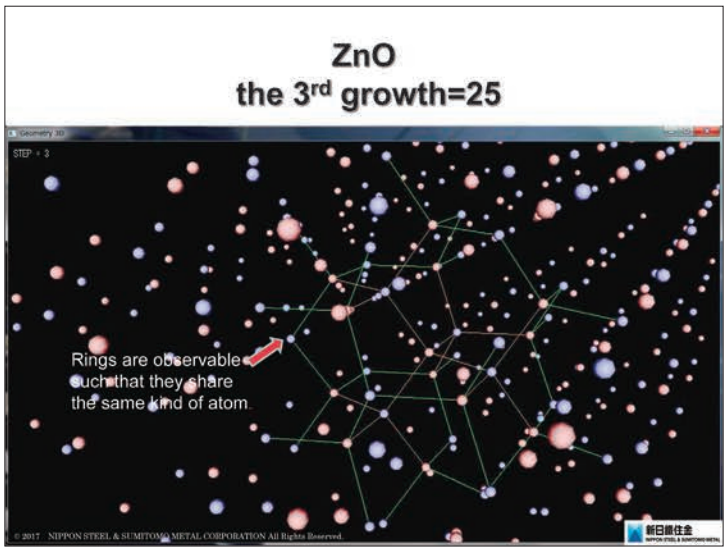
ZnO
the 3rd growth=25
STEP = 3
Rings are observable such that they share the same kind of atom
© 2017 NIPPON STEEL & SUMITOMO METAL CORPORATION All Rights Reserved.
新日鐵住金

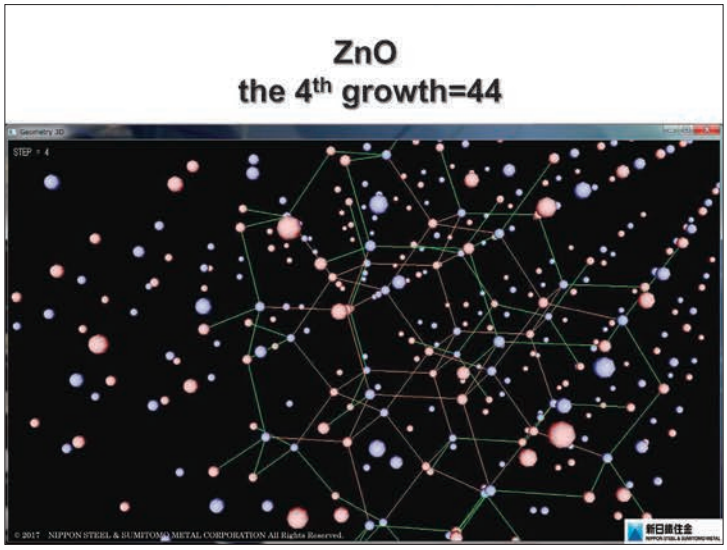
ZnO
the 4th growth=44
STEP = 4
© 2017 NIPPON STEEL & SUMITOMO METAL CORPORATION All Rights Reserved.
新日鐵住金

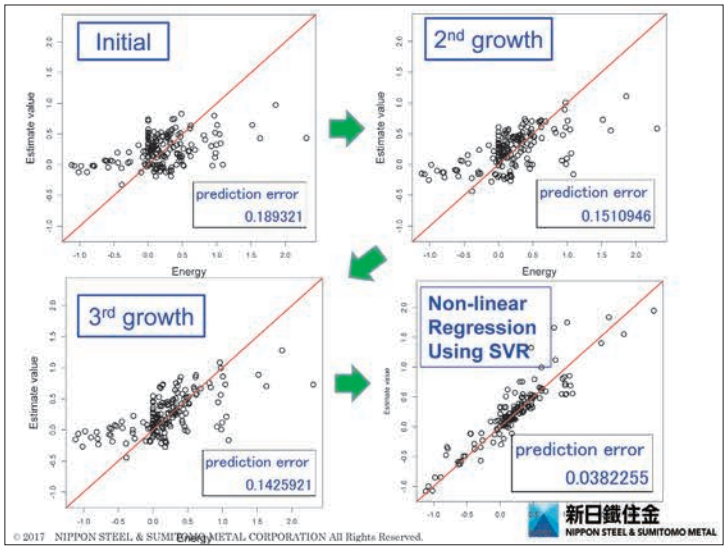
Initial
prediction error
0.189321
2nd growth
prediction error
0.1510946
3rd growth
prediction error
0.1425921
Non-linear Regression Using SVR
prediction error
0.0382255
Estimate value
Energy
© 2017 NIPPON STEEL & SUMITOMO METAL CORPORATION All Rights Reserved.
新日鐵住金
NIPPON STEEL & SUMITOMO METAL

SGW2014

## Counting Out of # Growth Using Computer

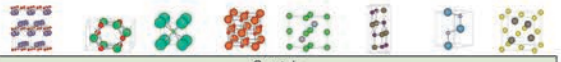

| Growth | Crystals | | | | | | | |
|---|---|---|---|---|---|---|---|---|
| | α -PbO | β -BeO | CsCl | NaCl | NiAs | TlI | ZnO | ZnS |
| g1 | 4 | 4 | 8 | 6 | 6 | 7 | 4 | 4 |
| g2 | 8 | 11 | 26 | 18 | 20 | 22 | 12 | 12 |
| g3 | 12 | 24 | 56 | 38 | 42 | 47 | 25 | 24 |
| g4 | 16 | 41 | 98 | 66 | 74 | 82 | 44 | 42 |
| g5 | 20 | 62 | 152 | 102 | 114 | 127 | 67 | 64 |
| g6 | 24 | 90 | 218 | 146 | 164 | 182 | 96 | 92 |
| g7 | 28 | 122 | 296 | 198 | 222 | 247 | 130 | 124 |
| g8 | 32 | 157 | 386 | 258 | 290 | 322 | 170 | 162 |
| g0 | 36 | 200 | 488 | 326 | 366 | 407 | 214 | 204 |
| g10 | 40 | 247 | 602 | 402 | 452 | 502 | 264 | 252 |
| g11 | 44 | 296 | 728 | 486 | 546 | 607 | 319 | 304 |
| g12 | 48 | 354 | 866 | 578 | 650 | 722 | 380 | 362 |
| g13 | 52 | 416 | 1016 | 678 | 762 | 847 | 445 | 424 |
| g14 | 56 | 479 | 1178 | 786 | 884 | 982 | 516 | 492 |
| g15 | 60 | 552 | 1352 | 902 | 1014 | 1127 | 592 | 564 |
| g16 | 64 | 629 | 1538 | 1026 | 1154 | 1282 | 674 | 642 |
| g17 | 68 | 706 | 1736 | 1158 | 1302 | 1447 | 760 | 724 |
| g18 | 72 | 794 | 1946 | 1298 | 1460 | 1622 | 852 | 812 |
| g19 | 76 | 886 | 2168 | 1446 | 1626 | 1807 | 949 | 904 |
| g20 | 80 | 977 | 2402 | 1602 | 1802 | 2002 | 1052 | 1002 |

Our interesting in mathematics is the $g_{\alpha\text{-}PbO}$.

新日鐵住金 NIPPON STEEL & SUMITOMO METAL



SGW2014

## Sequential Representation of # Growth

$$g_{\alpha\text{-}PbO}(n)=4n$$

$$g_{\beta\text{-}BeO}(n)=\begin{cases}\frac{22}{9}n^2+\frac{1}{9}n+\frac{13}{9} & (n\equiv 1 \mod 3)\\ \frac{22}{9}n^2-\frac{1}{9}n+\frac{13}{9} & (n\equiv 2 \mod 3)\\ \frac{22}{9}n^2+2 & (n\equiv 0 \mod 3)\end{cases}$$

$$g_{CsCl}(n)=6n^2+2$$

$$g_{ZnO}(n)=\begin{cases}\frac{21}{8}n^2+\frac{11}{8} & (n\equiv 1 \mod 3)\\ \frac{21}{8}n^2+\frac{3}{2} & (n\equiv 2 \mod 3)\\ \frac{21}{8}n^2+2 & (n\equiv 0 \mod 3)\end{cases}$$

$$g_{NaCl}(n)=4n^2+2$$

$$g_{TlI}(n)=5n^2+2$$

$$g_{NiAs}(n)=\begin{cases}\frac{9}{2}n^2+\frac{3}{2} & (n\equiv 1 \mod 2)\\ \frac{9}{2}n^2+2 & (n\equiv 0 \mod 2)\end{cases}$$

$$g_{ZnS}(n)=\begin{cases}\frac{5}{2}n^2+\frac{3}{2} & (n\equiv 1 \mod 2)\\ \frac{5}{2}n^2+2 & (n\equiv 0 \mod 2)\end{cases}$$

新日鐵住金 NIPPON STEEL & SUMITOMO METAL



## Generating Function of Growth

$$G(x):=1+\sum_{n=1}^{\infty} g_n x^n$$

H. Ochiai ※1
(2016.9.30)
※1 : Kyusyu University IMI

$$G_{\alpha\text{-}PbO}(x)=\frac{(1+x)^2}{(1-x)^2}$$

$$G_{\beta\text{-}BeO}(n)=\frac{(1+x)(1+2x+5x^2+6x^3+5x^4+2x^5+x^6)}{(1-x)(1-x^3)^2}$$

$$G_{CsCl}(x)=\frac{(1+x)(1+4x+x^2)}{(1-x)^3}$$

$$G_{ZnO}(x)=\frac{(1-x^3)(1+x+3x^2+x^3+x^4)}{(1-x)^3(1-x^4)}$$

$$G_{NaCl}(n)=\frac{(1+x)^3}{(1-x)^3}$$

$$G_{NiAs}(x)=\frac{1+4x+8x^2+4x^3+x^4}{(1-x)^2(1-x^2)}$$

$$G_{TlI}(x)=\frac{(1+x)(1+3x+x^2)}{(1-x)^3}$$

$$G_{ZnS}(x)=\frac{1+2x+4x^2+2x^3+x^4}{(1-x)^2(1-x^2)}$$

新日鐵住金 NIPPON STEEL & SUMITOMO METAL

## Symmetrical Properties of Generating Function (1)

Definition:

for $k, N, n_0 \in \mathbb{N}$, $N > 0,\ 0 \le n_0 \le N$

numerical sequence of growth

$$\left(g_k^{N,n_0}\right)_n = n^k \quad (n \equiv n_0 \bmod N)$$

$$\left(g_0^{N,n_0}\right)_0 = 1,\ \left(g_0^{N,N}\right)_0 = 0$$

generating function

$$G_k^{N,n_0}(x) := \sum_{n=0}^{\infty} \left(g_k^{N,n_0}\right)_n x^n$$

Proposition 1 (S. Wakatsuki)

(1) $G_{k+1}^{N,n_0}(x) = \left(x\dfrac{d}{dx}\right) G_k^{N,n_0}(x)$

(2) $G_k^{N,n_0}(x) = \dfrac{x^{n_0}}{\left(1-x^N\right)^{k+1}} \times (\textit{polynomial of degree } N_k)$

(3) $G_0^{N,0}(x) = G_0^{N,N}(x) + 1,\quad G_k^{N,N}(x) = G_k^{N,N} \quad \textit{for } k > 0$

Proposition 2 (S. Wakatsuki)

$$G_k^{N,n_0}\left(\frac{1}{x}\right) = (-1)^{k+1} G_k^{N,N-n_0}(x)$$



新日鐵住金 NIPPON STEEL & SUMITOMO METAL



## Symmetrical Properties of Generating Function (2)

For example, in the case of the numeric sequence of $\beta$-BeO

$$g_{\beta\text{-BeO}}(n) = \begin{cases} \dfrac{22}{9}n^2 + \dfrac{1}{9}n + \dfrac{13}{9} & (n \equiv 1 \mod 3) \\ \dfrac{22}{9}n^2 - \dfrac{1}{9}n + \dfrac{13}{9} & (n \equiv 2 \mod 3) \\ \dfrac{22}{9}n^2 + 2 & (n \equiv 0 \mod 3) \end{cases}$$

$$\left(g_k^{N,n_0}\right)_n = n^k \quad (n \equiv n_0 \bmod N)$$

$$G_{\beta\text{-BeO}}(x) = \frac{22}{9}G_2^{1,0}(x) + \frac{1}{9}G_1^{3,1}(x) - \frac{1}{9}G_1^{3,2}(x) + 2G_0^{3,3}(x) + \frac{13}{9}G_0^{3,1}(x) + \frac{13}{9}G_0^{3,2}(x) + 1$$

$$\begin{aligned} G_{\beta\text{-BeO}}\left(\frac{1}{x}\right) &= \frac{22}{9}G_2^{1,0}\left(\frac{1}{x}\right) + \frac{1}{9}G_1^{3,1}\left(\frac{1}{x}\right) - \frac{1}{9}G_1^{3,2}\left(\frac{1}{x}\right) + 2G_0^{3,3}\left(\frac{1}{x}\right) + \frac{13}{9}G_0^{3,1}\left(\frac{1}{x}\right) + \frac{13}{9}G_0^{3,2}\left(\frac{1}{x}\right) + 1 \\ &= -\frac{22}{9}G_2^{1,1}(x) + \frac{1}{9}G_1^{3,2}(x) - \frac{1}{9}G_1^{3,1}(x) - 2G_0^{3,0}(x) - \frac{13}{9}G_0^{3,2}(x) - \frac{13}{9}G_0^{3,1}(x) + 1 \\ &= -\frac{22}{9}G_2^{1,0}(x) + \frac{1}{9}G_1^{3,2}(x) - \frac{1}{9}G_1^{3,1}(x) - 2\left(G_0^{3,3}(x) + 1\right) - \frac{13}{9}G_0^{3,2} + 1 \\ &= -G_{\beta\text{-BeO}}(x) \end{aligned}$$





新日鐵住金 NIPPON STEEL & SUMITOMO METAL

## Summary and Future Works

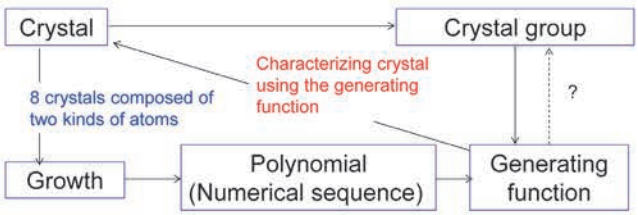


Cyclical property

e.g.

$$g_{\beta\text{-BeO}}(n) = \begin{cases} \dfrac{22}{9}n^2 + \dfrac{1}{9}n + \dfrac{13}{9} & (n \equiv 1 \mod 3) \\ \dfrac{22}{9}n^2 - \dfrac{1}{9}n + \dfrac{13}{9} & (n \equiv 2 \mod 3) \\ \dfrac{22}{9}n^2 + 2 & (n \equiv 0 \mod 3) \end{cases}$$

Symmetrical properties

$$G_{\beta\text{-BeO}}(n) = \frac{(1+x)\left(1+2x+5x^2+6x^3+5x^4+2x^5+x^6\right)}{(1-x)\left(1-x^3\right)^2}$$

$$G(x) = \mp G\left(\frac{1}{x}\right)$$





新日鐵住金 NIPPON STEEL & SUMITOMO METAL

Thank you for your attention!



16 新日鐵住金 NIPPON STEEL & SUMITOMO METAL

MI レクチャーノートシリーズ刊行にあたり

本レクチャーノートシリーズは、文部科学省 21 世紀 COE プログラム「機能数理学の構築と展開」(H.15-19 年度) において作成した COE Lecture Notes の続刊であり、文部科学省大学院教育改革支援プログラム「産業界が求める数学博士と新修士養成」(H19-21 年度) および、同グローバル COE プログラム「マス・フォア・インダストリ教育研究拠点」(H.20-24 年度) において行われた講義の講義録として出版されてきた。平成 23 年 4 月のマス・フォア・インダストリ研究所 (IMI) 設立と平成 25 年 4 月の IMI の文部科学省共同利用・共同研究拠点として「産業数学の先進的・基礎的共同研究拠点」の認定を受け、今後、レクチャーノートは、マス・フォア・インダストリに関わる国内外の研究者による講義の講義録、会議録等として出版し、マス・フォア・インダストリの本格的な展開に資するものとする。

平成 26 年 10 月
マス・フォア・インダストリ研究所
所長　福本康秀

# 平成29年度　九州大学マス・フォア・インダストリ研究所 共同利用研究集会 (I) 結晶の界面，転位，構造の数理

発　行　2017年12月20日
編　集　松谷茂樹, 佐伯修, 中川淳一, 田上大助, 上坂正晃, Pierluigi Cesana, 濵田裕康
発　行　九州大学マス・フォア・インダストリ研究所
九州大学大学院数理学府
〒819-0395 福岡市西区元岡744
九州大学数理・IMI 事務室
TEL 092-802-4402　FAX 092-802-4405
URL http://www.imi.kyushu-u.ac.jp/

印　刷　城島印刷株式会社
〒810-0012 福岡市中央区白金 2 丁目 9 番 6 号
TEL 092-531-7102　FAX 092-524-4411

## シリーズ既刊

| Issue | Author／Editor | Title | Published |
|---|---|---|---|
| COE Lecture Note | Mitsuhiro T. NAKAO<br>Kazuhiro YOKOYAMA | Computer Assisted Proofs - Numeric and Symbolic Approaches - 199pages | August 22, 2006 |
| COE Lecture Note | M.J.Shai HARAN | Arithmetical Investigations - Representation theory, Orthogonal polynomials and Quantum interpolations- 174pages | August 22, 2006 |
| COE Lecture Note Vol.3 | Michal BENES<br>Masato KIMURA<br>Tatsuyuki NAKAKI | Proceedings of Czech-Japanese Seminar in Applied Mathematics 2005 155pages | October 13, 2006 |
| COE Lecture Note Vol.4 | 宮田　健治 | 辺要素有限要素法による磁界解析 - 機能数理学特別講義 21pages | May 15, 2007 |
| COE Lecture Note Vol.5 | Francois APERY | Univariate Elimination Subresultants - Bezout formula, Laurent series and vanishing conditions - 89pages | September 25, 2007 |
| COE Lecture Note Vol.6 | Michal BENES<br>Masato KIMURA<br>Tatsuyuki NAKAKI | Proceedings of Czech-Japanese Seminar in Applied Mathematics 2006 209pages | October 12, 2007 |
| COE Lecture Note Vol.7 | 若山　正人<br>中尾　充宏 | 九州大学産業技術数理研究センター キックオフミーティング 138pages | October 15, 2007 |
| COE Lecture Note Vol.8 | Alberto PARMEGGIANI | Introduction to the Spectral Theory of Non-Commutative Harmonic Oscillators 233pages | January 31, 2008 |
| COE Lecture Note Vol.9 | Michael I.TRIBELSKY | Introduction to Mathematical modeling 23pages | February 15, 2008 |
| COE Lecture Note Vol.10 | Jacques FARAUT | Infinite Dimensional Spherical Analysis 74pages | March 14, 2008 |
| COE Lecture Note Vol.11 | Gerrit van DIJK | Gelfand Pairs And Beyond 60pages | August 25, 2008 |
| COE Lecture Note Vol.12 | Faculty of Mathematics,<br>Kyushu University | Consortium “MATH for INDUSTRY” First Forum 87pages | September 16, 2008 |
| COE Lecture Note Vol.13 | 九州大学大学院<br>数理学研究院 | プロシーディング「損保数理に現れる確率モデル」<br>— 日新火災・九州大学 共同研究 2008 年 11 月 研究会 — 82pages | February 6, 2009 |

## シリーズ既刊

| Issue | Author／Editor | Title | Published |
|---|---|---|---|
| COE Lecture Note Vol.14 | Michal Beneš,<br>Tohru Tsujikawa<br>Shigetoshi Yazaki | Proceedings of Czech-Japanese Seminar in Applied Mathematics 2008<br>77pages | February 12, 2009 |
| COE Lecture Note Vol.15 | Faculty of Mathematics,<br>Kyushu University | International Workshop on Verified Computations and Related Topics<br>129pages | February 23, 2009 |
| COE Lecture Note Vol.16 | Alexander Samokhin | Volume Integral Equation Method in Problems of Mathematical Physics<br>50pages | February 24, 2009 |
| COE Lecture Note Vol.17 | 矢嶋　　徹<br>及川　正行<br>梶原　健司<br>辻　　英一<br>福本　康秀 | 非線形波動の数理と物理 66pages | February 27, 2009 |
| COE Lecture Note Vol.18 | Tim Hoffmann | Discrete Differential Geometry of Curves and Surfaces 75pages | April 21, 2009 |
| COE Lecture Note Vol.19 | Ichiro Suzuki | The Pattern Formation Problem for Autonomous Mobile Robots<br>—Special Lecture in Functional Mathematics— 23pages | April 30, 2009 |
| COE Lecture Note Vol.20 | Yasuhide Fukumoto<br>Yasunori Maekawa | Math-for-Industry Tutorial: Spectral theories of non-Hermitian operators and their application 184pages | June 19, 2009 |
| COE Lecture Note Vol.21 | Faculty of Mathematics,<br>Kyushu University | Forum “Math-for-Industry”<br>Casimir Force, Casimir Operators and the Riemann Hypothesis<br>95pages | November 9, 2009 |
| COE Lecture Note Vol.22 | Masakazu Suzuki<br>Hoon Hong<br>Hirokazu Anai<br>Chee Yap<br>Yousuke Sato<br>Hiroshi Yoshida | The Joint Conference of ASCM 2009 and MACIS 2009:<br>Asian Symposium on Computer Mathematics Mathematical Aspects of Computer and Information Sciences 436pages | December 14, 2009 |
| COE Lecture Note Vol.23 | 荒川　恒男<br>金子　昌信 | 多重ゼータ値入門 111pages | February 15, 2010 |
| COE Lecture Note Vol.24 | Fulton B.Gonzalez | Notes on Integral Geometry and Harmonic Analysis 125pages | March 12, 2010 |
| COE Lecture Note Vol.25 | Wayne Rossman | Discrete Constant Mean Curvature Surfaces via Conserved Quantities<br>130pages | May 31, 2010 |
| COE Lecture Note Vol.26 | Mihai Ciucu | Perfect Matchings and Applications 66pages | July 2, 2010 |

# シリーズ既刊

| Issue | Author／Editor | Title | Published |
|---|---|---|---|
| COE Lecture Note Vol.27 | 九州大学大学院<br>数理学研究院 | Forum “Math-for-Industry” and Study Group Workshop<br>Information security, visualization, and inverse problems, on the basis of optimization techniques　100pages | October 21, 2010 |
| COE Lecture Note Vol.28 | ANDREAS LANGER | MODULAR FORMS, ELLIPTIC AND MODULAR CURVES<br>LECTURES AT KYUSHU UNIVERSITY 2010　62pages | November 26, 2010 |
| COE Lecture Note Vol.29 | 木田　雅成<br>原田　昌晃<br>横山　俊一 | Magma で広がる数学の世界　157pages | December 27, 2010 |
| COE Lecture Note Vol.30 | 原　　隆<br>松井　　卓<br>廣島　文生 | Mathematical Quantum Field Theory and Renormalization Theory<br>201pages | January 31, 2011 |
| COE Lecture Note Vol.31 | 若山　正人<br>福本　康秀<br>高木　　剛<br>山本　昌宏 | Study Group Workshop 2010 Lecture & Report　128pages | February 8, 2011 |
| COE Lecture Note Vol.32 | Institute of Mathematics for Industry,<br>Kyushu University | Forum “Math-for-Industry” 2011<br>“TSUNAMI-Mathematical Modelling”<br>Using Mathematics for Natural Disaster Prediction, Recovery and Provision for the Future　90pages | September 30, 2011 |
| COE Lecture Note Vol.33 | 若山　正人<br>福本　康秀<br>高木　　剛<br>山本　昌宏 | Study Group Workshop 2011 Lecture & Report　140pages | October 27, 2011 |
| COE Lecture Note Vol.34 | Adrian Muntean<br>Vladimír Chalupecký | Homogenization Method and Multiscale Modeling　72pages | October 28, 2011 |
| COE Lecture Note Vol.35 | 横山　俊一<br>夫　　紀恵<br>林　　卓也 | 計算機代数システムの進展　210pages | November 30, 2011 |
| COE Lecture Note Vol.36 | Michal Beneš<br>Masato Kimura<br>Shigetoshi Yazaki | Proceedings of Czech-Japanese Seminar in Applied Mathematics 2010<br>107pages | January 27, 2012 |
| COE Lecture Note Vol.37 | 若山　正人<br>高木　　剛<br>Kirill Morozov<br>平岡　裕章<br>木村　正人<br>白井　朋之<br>西井　龍映<br>栄　伸一郎<br>穴井　宏和<br>福本　康秀 | 平成 23 年度 数学・数理科学と諸科学・産業との連携研究ワークショップ　拡がっていく数学　～期待される “見えない力” ～<br>154pages | February 20, 2012 |

# シリーズ既刊

| Issue | Author／Editor | Title | Published |
|---|---|---|---|
| COE Lecture Note Vol.38 | Fumio Hiroshima<br>Itaru Sasaki<br>Herbert Spohn<br>Akito Suzuki | Enhanced Binding in Quantum Field Theory　204pages | March 12, 2012 |
| COE Lecture Note Vol.39 | Institute of Mathematics for Industry, Kyushu University | Multiscale Mathematics; Hierarchy of collective phenomena and interrelations between hierarchical structures　180pages | March 13, 2012 |
| COE Lecture Note Vol.40 | 井ノ口順一<br>太田　泰広<br>筧　　三郎<br>梶原　健司<br>松浦　　望 | 離散可積分系・離散微分幾何チュートリアル 2012　152pages | March 15, 2012 |
| COE Lecture Note Vol.41 | Institute of Mathematics for Industry, Kyushu University | Forum “Math-for-Industry” 2012<br>“Information Recovery and Discovery”　91pages | October 22, 2012 |
| COE Lecture Note Vol.42 | 佐伯　　修<br>若山　正人<br>山本　昌宏 | Study Group Workshop 2012 Abstract, Lecture & Report　178pages | November 19, 2012 |
| COE Lecture Note Vol.43 | Institute of Mathematics for Industry, Kyushu University | Combinatorics and Numerical Analysis Joint Workshop　103pages | December 27, 2012 |
| COE Lecture Note Vol.44 | 萩原　　学 | モダン符号理論からポストモダン符号理論への展望　107pages | January 30, 2013 |
| COE Lecture Note Vol.45 | 金山　　寛 | Joint Research Workshop of Institute of Mathematics for Industry (IMI), Kyushu University<br>“Propagation of Ultra-large-scale Computation by the Domain-decomposition-method for Industrial Problems (PUCDIP 2012)”<br>121pages | February 19, 2013 |
| COE Lecture Note Vol.46 | 西井　龍映<br>栄　伸一郎<br>岡田　勘三<br>落合　啓之<br>小磯　深幸<br>斎藤　新悟<br>白井　朋之 | 科学・技術の研究課題への数学アプローチ<br>―数学モデリングの基礎と展開―　325pages | February 28, 2013 |
| COE Lecture Note Vol.47 | SOO TECK LEE | BRANCHING RULES AND BRANCHING ALGEBRAS FOR THE COMPLEX CLASSICAL GROUPS　40pages | March 8, 2013 |
| COE Lecture Note Vol.48 | 溝口　佳寛<br>脇　　隼人<br>平坂　　貢<br>谷口　哲至<br>島袋　　修 | 博多ワークショップ「組み合わせとその応用」　124pages | March 28, 2013 |

# シリーズ既刊

| Issue | Author／Editor | Title | Published |
|---|---|---|---|
| COE Lecture Note Vol.49 | 照井　　章<br>小原　功任<br>濱田　龍義<br>横山　俊一<br>穴井　宏和<br>横田　博史 | マス・フォア・インダストリ研究所　共同利用研究集会 II<br>数式処理研究と産学連携の新たな発展　137pages | August 9, 2013 |
| MI Lecture Note Vol.50 | Ken Anjyo<br>Hiroyuki Ochiai<br>Yoshinori Dobashi<br>Yoshihiro Mizoguchi<br>Shizuo Kaji | Symposium MEIS2013:<br>Mathematical Progress in Expressive Image Synthesis　154pages | October 21, 2013 |
| MI Lecture Note Vol.51 | Institute of Mathematics for Industry, Kyushu University | Forum “Math-for-Industry” 2013<br>“The Impact of Applications on Mathematics”　97pages | October 30, 2013 |
| MI Lecture Note Vol.52 | 佐伯　　修<br>岡田　勘三<br>髙木　　剛<br>若山　正人<br>山本　昌宏 | Study Group Workshop 2013 Abstract, Lecture & Report<br>142pages | November 15, 2013 |
| MI Lecture Note Vol.53 | 四方　義啓<br>櫻井　幸一<br>安田　貴徳<br>Xavier Dahan | 平成25年度　九州大学マス・フォア・インダストリ研究所<br>共同利用研究集会　安全・安心社会基盤構築のための代数構造<br>～サイバー社会の信頼性確保のための数理学～　158pages | December 26, 2013 |
| MI Lecture Note Vol.54 | Takashi Takiguchi<br>Hiroshi Fujiwara | Inverse problems for practice, the present and the future　93pages | January 30, 2014 |
| MI Lecture Note Vol.55 | 栄　伸一郎<br>溝口　佳寛<br>脇　　隼人<br>渋田　敬史 | Study Group Workshop 2013 数学協働プログラム Lecture & Report<br>98pages | February 10, 2014 |
| MI Lecture Note Vol.56 | Yoshihiro Mizoguchi<br>Hayato Waki<br>Takafumi Shibuta<br>Tetsuji Taniguchi<br>Osamu Shimabukuro<br>Makoto Tagami<br>Hirotake Kurihara<br>Shuya Chiba | Hakata Workshop 2014<br>~ Discrete Mathematics and its Applications ~　141pages | March 28, 2014 |
| MI Lecture Note Vol.57 | Institute of Mathematics for Industry, Kyushu University | Forum “Math-for-Industry” 2014:<br>“Applications + Practical Conceptualization + Mathematics = fruitful Innovation”　93pages | October 23, 2014 |
| MI Lecture Note Vol.58 | 安生健一<br>落合啓之 | Symposium MEIS2014:<br>Mathematical Progress in Expressive Image Synthesis　135pages | November 12, 2014 |

# シリーズ既刊

| Issue | Author／Editor | Title | Published |
|---|---|---|---|
| MI Lecture Note Vol.59 | 西井　龍映<br>岡田　勘三<br>梶原　健司<br>髙木　　剛<br>若山　正人<br>脇　　隼人<br>山本　昌宏 | Study Group Workshop 2014 数学協働プログラム<br>Abstract, Lecture & Report　196pages | November 14, 2014 |
| MI Lecture Note Vol.60 | 西浦　　博 | 平成 26 年度九州大学 IMI 共同利用研究・研究集会（I）<br>感染症数理モデルの実用化と産業及び政策での活用のための新たな展開　120pages | November 28, 2014 |
| MI Lecture Note Vol.61 | 溝口　佳寛<br>Jacques Garrigue<br>萩原　　学<br>Reynald Affeldt | 研究集会<br>高信頼な理論と実装のための定理証明および定理証明器<br>Theorem proving and provers for reliable theory and implementations (TPP2014)　138pages | February 26, 2015 |
| MI Lecture Note Vol.62 | 白井　朋之 | Workshop on “β-transformation and related topics”　59pages | March 10, 2015 |
| MI Lecture Note Vol.63 | 白井　朋之 | Workshop on “Probabilistic models with determinantal structure”<br>107pages | August 20, 2015 |
| MI Lecture Note Vol.64 | 落合　啓之<br>土橋　宜典 | Symposium MEIS2015:<br>Mathematical Progress in Expressive Image Synthesis　124pages | September 18, 2015 |
| MI Lecture Note Vol.65 | Institute of Mathematics for Industry, Kyushu University | Forum “Math-for-Industry” 2015<br>“The Role and Importance of Mathematics in Innovation”　74pages | October 23, 2015 |
| MI Lecture Note Vol.66 | 岡田　勘三<br>藤澤　克己<br>白井　朋之<br>若山　正人<br>脇　　隼人<br>Philip Broadbridge<br>山本　昌宏 | Study Group Workshop 2015 Abstract, Lecture & Report<br>156pages | November 5, 2015 |
| MI Lecture Note Vol.67 | Institute of Mathematics for Industry, Kyushu University | IMI-La Trobe Joint Conference<br>“Mathematics for Materials Science and Processing”<br>66pages | February 5, 2016 |
| MI Lecture Note Vol.68 | 古庄　英和<br>小谷　久寿<br>新甫　洋史 | 結び目と Grothendieck-Teichmüller 群<br>116pages | February 22, 2016 |
| MI Lecture Note Vol.69 | 土橋　宜典<br>鍛治　静雄 | Symposium MEIS2016:<br>Mathematical Progress in Expressive Image Synthesis　82pages | October 24, 2016 |
| MI Lecture Note Vol.70 | Institute of Mathematics for Industry, Kyushu University | Forum “Math-for-Industry” 2016<br>“Agriculture as a metaphor for creativity in all human endeavors”<br>98pages | November 2, 2016 |
| MI Lecture Note Vol.71 | 小磯　深幸<br>二宮　嘉行<br>山本　昌宏 | Study Group Workshop 2016 Abstract, Lecture & Report　143pages | November 21, 2016 |

## シリーズ既刊

| Issue | Author／Editor | Title | Published |
|---|---|---|---|
| MI Lecture Note Vol.72 | 新井　朝雄<br>小嶋　　泉<br>廣島　文生 | Mathematical quantum field theory and related topics　133pages | January 27, 2017 |
| MI Lecture Note Vol.73 | 穴田　啓晃<br>Kirill Morozov<br>須賀　祐治<br>奥村　伸也<br>櫻井　幸一 | Secret Sharing for Dependability, Usability and Security of Network Storage and Its Mathematical Modeling　211pages | March 15, 2017 |
| MI Lecture Note Vol.74 | QUISPEL, G. Reinout W.<br>BADER, Philipp<br>MCLAREN, David I.<br>TAGAMI, Daisuke | IMI-La Trobe Joint Conference<br>Geometric Numerical Integration and its Applications　71pages | March 31, 2017 |
| MI Lecture Note Vol.75 | 手塚　　集<br>田上　大助<br>山本　昌宏 | Study Group Workshop 2017 Abstract, Lecture & Report　118pages | October 20, 2017 |
| MI Lecture Note Vol.76 | 宇田川誠一 | Tzitzéica 方程式の有限間隙解に付随した極小曲面の構成理論<br>―Tzitzéica 方程式の楕円関数解を出発点として―　68pages | August 4, 2017 |

Institute of Mathematics for Industry
Kyushu University

九州大学マス・フォア・インダストリ研究所
九州大学大学院 数理学府
〒819-0395 福岡市西区元岡744　TEL 092-802-4402　FAX 092-802-4405
URL http://www.imi.kyushu-u.ac.jp/